

UNIVERSITI TEKNOLOGI PETRONAS
THERMOPHYSICAL PROPERTIES AND CARBON DIOXIDE SOLUBILITY
OF NOVEL ROOM TEMPERATURE IONIC LIQUIDS

By

ABOBAKR KHIDIR ZIYADA TAHA

The undersigned certify that they have read, and recommend to the Postgraduate Studies Programme for acceptance this thesis for the fulfillment of the requirements for the degree stated.

Signature: _____

Main Supervisor: Assoc. Prof. Dr. Cecilia Devi Wilfred

Signature: _____

Co-Supervisor: Assoc. Prof. Dr. Mohamad Azmi Bustam

Signature: _____

Head of Department: Assoc. Prof. Dr. Shuhaimi Mahadzir

Date: _____

THERMOPHYSICAL PROPERTIES AND CARBON DIOXIDE SOLUBILITY
OF NOVEL ROOM TEMPERATURE IONIC LIQUIDS

By

ABOBAKR KHIDIR ZIYADA TAHA

A Thesis

Submitted to the Postgraduate Studies Programme
as a Requirement for the Degree of

DOCTOR OF PHILOSOPHY

CHEMICAL ENGINEERING DEPARTMENT

UNIVERSITI TEKNOLOGI PETRONAS

BANDAR SRI ISKANDAR

PERAK

AUGUST 2011

ACKNOWLEDGEMENTS

For first and for most, I thank ALLAH for the strength that keeps me standing and for the hope that keeps me believing that this affiliation would be possible and more interesting. There are many who have contributed in small and large ways to the completion of this thesis and to whom I give special thanks for what they have given and what I have learned from them.

I would like to express my genuine appreciation to my supervisors, AP. Dr. Cecilia Devi Wilfred and AP. Dr. Mohamad Azmi Bustam, for their excellent guidance, motivation and support throughout the course of my study at Universiti Teknologi PETRONAS. I appreciate their patience, insightful comments and for giving me the opportunity to think and learn independently and for giving me the freedom in performing the research. I am very fortunate to have a wonderful mentors and advisors guiding and assisting me.

I would like to thank Universiti Teknologi PETRONAS and PETRONAS IONIC LIQUIDS CENTRE at Universiti Teknologi PETRONAS for the facilities provided in this work. I am indebted for the PETRONAS Company Bhd, University of Gezira and Ministry of Higher Education (SUDAN) for my sponsorship.

I express my warmest gratitude to my wife, Dena, for her dedication, encouragement, and love during my hectic time in research. Heartfelt thanks to my family, especially to my dear mother, my brothers and sisters, for their love, prayers, sincerity and unconditional support at every stage of my life.

I extend my thanks and grateful to all my friends, near and far, who gave me friendship, prayers, and support and who share a great and memorable time during my research and thesis work.

Finally, for all, I love you and I thank you for being in my life.

DEDICATION

To My Mother, Bakhita, and My Wife, Dena,

For their love, encouragement and patience

To My Daughter, Neam, and My Son, Akram,

Who still did not understand what I do

To my brothers and sisters for their support and encouragement

This work would not exist without them

&

To The Soul of My Father

ABSTRACT

In the present work, a novel series of 1-alkyl-3-propanenitrile imidazolium-based room temperature ionic liquids (RTILs) ($[C_2CN\text{ Rim}]^+$, where R = butyl, hexyl, octyl, decyl, allyl, ethoxyl, benzyl, incorporating sulfonate-based anions (dioctylsulfosuccinate (DOSS), dodecylsulfate (DDS), sulfobenzoic acid (SBA), benzenesulfonate (BS) and trifluoromethanesulfonate (TFMS)) were synthesized. Trialkylphosphonium-based monocationic and dicationic RTILs incorporating dioctylsulfosuccinate anion ($[P_{n,n,n,14}][\text{dioctylsulfosuccinate}]$ where $n = 6, 8$ and $[P_{8,8,8}C_y P_{8,8,8}][\text{dioctylsulfosuccinate}]$ where $y = 6, 10$) were also synthesized. The molecular structures of the thirty four RTILs synthesized were confirmed using 1H and ^{13}C NMR, FTIR and elemental analysis.

The densities and viscosities of the present RTILs were measured at atmospheric pressure at $T = 293.15$ to 353.15 K, refractive index was measured at $T = 293.15$ to 333.15 K, whereas, the start and decomposition temperatures were determined at heating rate $10\text{ }^\circ\text{C}\cdot\text{min}^{-1}$. The thermal expansion coefficient, densities at range of temperatures and pressures, molecular volume, molar refraction, standard entropy and lattice energy of these RTILs were also estimated. The present RTILs showed lower densities, similar refractive indices and higher viscosities compared to the other imidazolium and phosphonium-based RTILs. The thermogravimetric results exhibited short-term thermal stability in the range between 470 to 670 K. These RTILs showed a weak temperature dependency on the thermal expansion coefficients, $\alpha_p = 5.0 \times 10^{-4}$ to $7.50 \times 10^{-4}\text{ K}^{-1}$. Empirical correlations were proposed to represent the present data on the physical properties. The densities of the present imidazolium-based RTILs are highest when paired with TFMS anion followed by SBA, BS and DDS anion. The lowest densities was observed with DOSS anion. The measured viscosities are higher for the RTILs with DOSS anion, while it was the lowest with TFMS anion.

The solubility of CO₂ in the synthesized RTILs was measured using gravimetric measurement technique (magnetic suspension balance) at $T = 298$ to 343 K and pressures $P = 1$ to 20 bar. The results showed that CO₂ solubility is influenced by the alkyl chain, functional group and nature of the cation and anion. The solubility of CO₂ increases with an increase in pressure and decreases with increasing temperature. The solubility of the present RTILs is described using the Henry's law constant along with some thermodynamic properties such as molar enthalpy, entropy and Gibb's free energy.

The ILs with the DOSS anion has a considerably higher affinity for CO₂ compared with the ILs incorporating DDS, TFMS, SBA and BS anions. The [C₂CNDim]DOSS, [C₂CNHeim]DOSS and [P_{8,8,8,14}]DOSS ILs have a higher solubility capacity among the studied imidazolium-based nitrile functionalized ILs, imidazolium-based dual functionalized ILs and phosphonium-based ILs respectively. Moreover, [C₂CNDim]DOSS IL shows the highest CO₂ solubility. The magnitude of ΔH^0 decreases from that for moderately strong acid-base bonds at 298 K to that for weak acid-base bonds at 343 K for [C₂CNHeim]DOSS and [P_{8,8,8,14}]DOSS ILs while [C₂CNDim]DOSS shows a very small decrease. [C₂CNHeim]DOSS shows greater IL/CO₂ interactions compare to [C₂CNDim]DOSS and [P_{8,8,8,14}]DOSS but the effect of temperature on this interaction was lower for [C₂CNDim]DOSS. There was a considerable increase in CO₂/CH₄ solubility selectivity relative to the corresponding non functionalized imidazolium-based ILs. The highest selectivity obtained with non functionalized ILs ([APMim]BF₄) is around 47 while for the nitrile functionalized IL ([C₂CNDim]DOSS) is 82.7 . The CO₂/CH₄ selectivity for the nitrile functionalized IL ([C₂CNDim]DOSS) was approximately four times higher than that of the [bmim]BF₄, [emim]NTf₂ and Sulfolane. Moreover, the recyclability studies indicated that the CO₂ solubility capacity of the studied IL could be maintained for several cycles.

ABSTRAK

Kajian terbaru menunjukkan cecair ion bersuhu bilik (RTILs) 1-alkyl-3-propanenitril berdasarkan-imidazolium cecair ion bersuhu bilik (RTILs) ($[\text{C}_2\text{CN Rim}]^+$, di mana R = butil, hexil, octil, decil, allil, ethoxil, benzil, mengandungi anion asas-sulfonat (dioctilsulfosuccinat (DOSS), dodecilsulfat (DDS), benzenesulfonat (BS) dan triflourometanasulfonat (TFMS)) telah disintesis. Monokationik dan dikationik trialkilfosfonium RTILs mengandungi anion dioctilsulfosuccinat ($[\text{P}_{n,n,n,14}][\text{dioctilsulfosuccinat}]$ di mana $n = 6, 8$ dan $[\text{P}_{8,8,8} \text{C}_y \text{P}_{8,8,8}][\text{dioctilsulfosuccinat}]$ di mana $y = 6, 10$) juga berjaya disintesis. Struktur molekul tiga puluh empat RTILs yang disintesis telah dikenalpasti menggunakan ^1H dan ^{13}C NMR, FTIR dan analisis elemen.

Ketumpatan dan kepekatan RTILs yang telah disintesis dianalisis pada tekanan atmosfera 1 atm dan suhu diantara $T = 293.15$ ke 353.15 K. Manakala, indeks biasan telah dicerap pada suhu $T = 293.15$ ke 333.15 K. Kestabilan cecair ionik telah ditentukan dengan menganalisis haba penguraian bahan berkenaan. Ini dilakukan dengan menggunakan alat Thermal Gravimetric Analyzer (TGA) pada kadar pemanasan $10 \text{ }^\circ\text{C}\cdot\text{min}^{-1}$ bermula dari $50 \text{ }^\circ\text{C}$ sehingga $600 \text{ }^\circ\text{C}$. Pemalar suhu pengembangan, ketumpatan pada julat suhu dan tekanan yang berbeza, isipadu molekul, pecahan molar, entropi mol piawai dan tenaga kekisi kesemua RTILs telah dianggarkan. RTILs ini didapati mempunyai ketumpatan yang lebih rendah, indeks biasan yang sama dan kelikatan yang lebih tinggi berbanding cecair ionik imidazolium dan fosfonium yang lain. Daripada eksperimen yang dijalankan, didapati cecair ionik yang dikaji mempunyai julat haba penguraian yang pendek iaitu diantara 470 K ke 670 K sahaja. Pemalar pengembangan yang diperolehi adalah sangat rendah iaitu di antara $\alpha_p = 5.0 \times 10^{-4}$ ke $7.50 \times 10^{-4} \text{ K}^{-1}$ mempamerkan sifat pengembangan cecair ionik ini yang kurang bergantung pada suhu. Persamaan empirikal dicadangkan

untuk mewakili data-data fizikal yang diperolehi. Didapati ketumpatan RTILs yang berasaskan imidazolium adalah tertinggi apabila digabungkan dengan anion TFMS diikuti oleh SBA, BS dan anion DDS. Nilai ketumpatan yang terendah adalah bagi cecair ionik imidazolium yang terdiri daripada anion DOSS. Bagi faktor kelikatan

pula, cecair ionik dengan anion DOSS menunjukkan kelikatan tertinggi, manakala cecair ionic dengan anion TFMS mempunyai kelikatan terendah.

Keterlarutan gas CO₂ di dalam cecair ionik yang telah disintesis ditentukan dengan menggunakan teknik penimbangan graviti (penimbangimbangan magnetik) pada julat suhu diantara T= 298 ke 343 k dan pada tekanan diantara P=1 ke 20 bar. Hasil kajian menunjukkan keterlarutan CO₂ di dalam cecair ionic ini dipengaruhi oleh panjang rantai alkil, kumpulan berfungsi dan sifat semulajadi anion dan cation cecair ionik itu sendiri. Keterlarutan gas CO₂ meningkat sejajar dengan pertumbuhan tekanan, manakala akan berkurang dengan peningkatan suhu. Nilai keterlarutan ini diperjelaskan dengan lebih lanjut dengan menggunakan Hukum Henry dan juga berdasarkan beberapa parameter termodinamik seperti perubahan entalpi pengatoman, entropi dan tenaga bebas Gibbs.

Cecair ionik dengan anion DOSS, memaparkan keafinan yang tinggi terhadap CO₂ berbanding cecair ionic yang terdiri daripada anion DDS, TFMS, SBA and BS.

Cecair ionik [C₂CNDim]DOSS, [C₂CNHeim]DOSS dan [P_{8,8,8,14}]DOSS mengandungi kelarutan CO₂ yang tinggi di antara semua jenis cecair ionik samada cecair ionik berasaskan imidazolium dengan kumpulan berfungsi nitril, imidazolium dengan dua kumpulan berfungsi atau cecair ionik fosfonium. Tambahan lagi, [C₂CNDim]DOSS RTIL menunjukkan kelarutan CO₂ yang tertinggi. Magnitud ΔH^0 menurun daripada ikatan asid kuat 298 K kepada ikatan asid lemah 343 K untuk [C₂CNHeim]DOSS dan [P_{8,8,8,14}]DOSS RTILs manakala [C₂CNDim]DOSS menunjukkan penurunan yang sangat rendah. [C₂CNHeim]DOSS menunjukkan interaksi diantara IL/CO₂ yang kuat berbanding dengan [C₂CNDim]DOSS dan [P_{8,8,8,14}]DOSS tetapi kesan suhu ke atas interaksi ini adalah lemah untuk [C₂CNDim]DOSS. Kajian kitar semula penggunaan cecair ionik ini menunjukkan kapasiti keterlarutan CO₂ yang tinggi membolehkan ia digunakan beberapa kali dalam satu proses.

In compliance with the terms of the Copyright Act 1987 and the IP Policy of the university, the copyright of this thesis has been reassigned by the author to the legal entity of the university,

Institute of Technology PETRONAS Sdn Bhd.

Due acknowledgement shall always be made of the use of any material contained in, or derived from, this thesis.

© ABOBAKR KHIDIR ZIYADA TAHA, 2011
Institute of Technology PETRONAS Sdn Bhd.
All rights reserve

TABLE OF CONTENTS

ACKNOWLEDGEMENTS.....	V
DEDICATION	VI
ABSTRACT	VII
ABSTRAK	IX
LIST OF FIGURES	XVI
LIST OF TABLES	XXII
NOMENCLATURE.....	XXIV
CHAPTER 1.....	1
INTRODUCTION	1
1.1 IMPORTANCE OF CO ₂ REMOVAL FROM NATURAL GAS	1
1.2 OVERVIEW OF ILS	3
1.2.1 Definition and history of ILS	3
1.2.2 Structures of ILS	5
1.2.3 Preparation of ILS	6
1.2.4 Properties and applications.....	8
1.3 PROBLEM STATEMENT.....	13
1.4 RESEARCH OBJECTIVES	14
1.5 SCOPE OF STUDY	16
1.6 THESIS OUTLINE	17
CHAPTER 2.....	19
LITERATURE REVIEW.....	19
2.1 INTRODUCTION.....	19
2.2 NATURAL GAS.....	19
2.3 THERMOPHYSICAL PROPERTIES OF RTILS.....	23
2.3.1 Introduction.....	23
2.3.2 Density	25
2.3.3 Viscosity	27
2.3.4 Refractive index.....	29
2.3.5 Thermal stability.....	30

2.3.6 Derived thermodynamic properties	31
2.4 SOLUBILITY OF CO ₂ IN ILS	34
2.4.1 Introduction	34
2.4.2 Methods for measuring Solubility of CO ₂ in ILS	36
2.4.3 Effects of ILS structures on CO ₂ solubility	36
2.4.3.1 Effect of the cation	37
2.4.3.2 Effect of the anion	41
2.4.3.3 Effect of functional group	44
CHAPTER 3	49
RESEARCH METHODOLOGY	49
3.1 INTRODUCTION	49
3.2 MATERIALS	50
3.3 SYNTHESIS OF RTILS	50
3.3.1 Synthesis of nitrile functionalized imidazolium-based RTILs	50
3.3.1.1 Synthesis of 1-alkyl-3-propanenitrile imidazolium bromide	51
3.3.1.2 Synthesis of 1-alkyl-3-propanenitrile imidazolium chloride	52
3.3.1.3 Synthesis of 1-alkyl-3-propanenitrile Imidazolium dioctylsulfosuccinate	52
3.3.1.4 Synthesis of 1-alkyl-3-propanenitrile imidazolium dodecylsulfate ..	53
3.3.1.5 Synthesis of 1-alkyl-3-propanenitrile imidazolium sulfobenzoic acid	54
3.3.1.6 Synthesis of 1-alkyl-3-propanenitrile imidazolium benzenesulfonate	55
3.3.1.7 Synthesis of 1-alkyl-3-propanenitrile imidazolium trifluoromethanesulfonate	55
3.3.2 Synthesis of imidazolium-based dual functionalized RTILs	56
3.3.3 Synthesis of phosphonium-based monocationic RTILs	57
3.3.3.1 Synthesis of trihexyltetradecylphosphonium dioctylsulfosuccinate ..	57
3.3.3.2 Synthesis of trioctyltetradecylphosphonium dioctylsulfosuccinate ..	58
3.3.4 Synthesis of phosphonium-based dicationic RTILs	59
3.4 CHARACTERIZATION OF RTILS	60
3.4.1 NMR, FTIR and elemental analysis	61

3.4.2 Water and halide contents.....	61
3.5 THERMOPHYSICAL PROPERTIES OF RTILS.....	62
3.5.1 Density and viscosity	62
3.5.2 Refractive index	65
3.5.3 Thermogravimetric analysis.....	66
3.5.4 Derived thermodynamic properties	67
3.6 SOLUBILITY OF CO ₂ IN ILS USING MAGNETIC SUSPENSION BALANCE	69
3.6.1 Blank measurement	71
3.6.2 Drying.....	72
3.6.3 Buoyancy measurement	73
3.6.4 Solubility measurement.....	74
CHAPTER 4.....	79
CHARACTERIZATION AND THERMOPHYSICAL PROPERTIES	79
4.1 CHARACTERIZATION OF ILS	79
4.2 THERMOPHYSICAL PROPERTIES	100
4.2.1 Density	100
4.2.2 Viscosity	110
4.2.3 Refractive index	120
4.2.4 Thermal stability	124
4.3 DERIVED THERMODYNAMIC PROPERTIES	130
4.3.1 Thermal expansion coefficient.....	130
4.3.2 Lattice energy.....	131
4.3.3 Molar refraction.....	132
4.3.4 Standard molar entropy	134
CHAPTER 5.....	137
CARBON DIOXIDE SOLUBILITY	137
5.1 INTRODUCTION.....	137
5.2 EFFECT OF THE ILS ANIONS ON CO ₂ SOLUBILITY	138
5.3 EFFECT OF THE ILS CATIONS ON CO ₂ SOLUBILITY.....	143
5.3.1 Imidazolium-based nitrile functionalized ILS.....	143
5.3.2 Imidazolium-based dual functionalized ILS	147

5.3.3 Phosphonium-based ILs.....	151
5.4 THERMODYNAMIC PARAMETERS	157
5.4.1 Henry's constant	157
5.4.2 Enthalpy, entropy and Gibbs free energy	163
5.5 IDEAL CO ₂ /CH ₄ SOLUBILITY SELECTIVITY	166
5.6 RECYCLABILITY OF IL.....	169
CHAPTER 6.....	173
CONCLUSIONS AND RECOMMENDATIONS.....	173
6.1 CONCLUSIONS	173
6.2 RECOMMENDATIONS	177
REFERENCES	179
PUBLICATIONS.....	206
APPENDIX A.....	210
EXPERIMENTAL DATA FOR CHARACTERIZATION AND THERMOPHYSICAL PROPERTIES.	210
APPENDIX B	237
EXPERIMENTAL SOLUBILITY DATA FOR CO ₂ IN ILs.....	237

LIST OF FIGURES

Fig 1-1: Trends in Atmospheric Concentrations and Anthropogenic Emissions of Carbon Dioxide	2
Fig 1-2 Structures of common cations and anions.....	4
Fig 1-3 General synthetic scheme for preparation of alkylammonium ILs	7
Fig 1-4 Typical preparation routes for imidazoium ILs.....	8
Fig 1-5 Synthesis route of ammonium ILs by acid/base neutralization reaction.....	8
Fig 1-6 Selection of applications where ILs have been used	9
Fig 2-1 Structure of methane	21
Fig 2-2 Structure of carbon dioxide	22
Fig 2-3 Carbon dioxide solubility in 1-alkyl-3-methylimidazolium bis(trifluoro methyl sulfonyl)amide ionic liquids as a function of the number of carbon atoms, <i>n</i> , in the alkyl-side chain..	38
Fig 2-4 Absorption amount of CO ₂ in aqueous solution of IL +MDEA with 30% total amines	39
Fig 2-5 Effect of the partial fluorination of the cation on the carbon dioxide solubility in 1-methyl-3-octylimidazolium bis(trifluoromethylsulfonyl) amide ionic liquids as a function of temperature expressed as mole fraction of carbon dioxide at a partial pressure of 1 bar	41
Fig 2-6 Comparison and correlation of the solubility of CO ₂ in hydroxyl ammonium ionic liquids at 303 K	43
Fig 2-7 CO ₂ absorption in NH ₂ -cation functionalized RTILs at 303 K.....	46
Fig 3-1 Synthesis route of the RTILs [C ₂ CN C _n im]X	51
Fig 3-2 Synthesis route of the RTILs [C ₂ CN C _n im]DOSS	53
Fig 3-3 Synthesis route of the RTILs [C ₂ CN C _n im]DDS	53
Fig 3-4 Synthesis route of the RTILs [C ₂ CN C _n im]SBA	54
Fig 3-5 Synthesis route of the RTILs [C ₂ CN C _n im]BS	55
Fig 3-6 Synthesis route of the RTILs [C ₂ CN C _n im]TFMS.....	55
Fig 3-7 Synthesis route of imidazolium-based dual functionalized RTILs	56

Fig 3-8 Synthesis route of trihexyltetradecylphosphonium dioctylsulfosuccinate IL	58
Fig 3-9 Synthesis route of trioctyltetradecylphosphonium-based ILs	59
Fig 3-10 Synthesis route of phosphonium-based dicationic RTILs	60
Fig 3-11 T_{onset} (intersection of baseline weight and the tangent of weight vs temperature curve (---))	67
Fig 3-12 Schematic of magnetic suspension balance for solubility measurements	71
Fig 3-13 Example for result of the blank measurement	72
Fig 3-14 Example for the results of the drying process at 100 °C	73
Fig 3-15 Example for the results of the buoyancy measurement	74
Fig 3-16 Example for the results of the solubility measurement	75
Fig 3-17 Flowchart for the procedure performed to measure gases solubility in ILs using MSB	78
Fig 4-1 Structure of [C ₂ CN Bim]Br	80
Fig 4-2 Structure of [C ₂ CN Him]Br	81
Fig 4-3 Structure of [C ₂ CN Oim]Br	81
Fig 4-4 Structure of [C ₂ CN Dim]Br	81
Fig 4-5 Structure of [C ₂ CN Bim]Cl	82
Fig 4-6 Structure of [C ₂ CN Him]Cl	82
Fig 4-7 Structure of [C ₂ CN Oim]Cl	83
Fig 4-8 Structure of [C ₂ CN Bim]DOSS	83
Fig 4-9 Structure of [C ₂ CN Him]DOSS	84
Fig 4-10 Structure of [C ₂ CN Oim]DOSS	84
Fig 4-11 Structure of [C ₂ CN Dim]DOSS	85
Fig 4-12 Structure of [C ₂ CN Bim]DDS	85
Fig 4-13 Structure of [C ₂ CN Him]DDS	86
Fig 4-14 Structure of [C ₂ CN Oim]DDS	86
Fig 4-15 Structure of [C ₂ CN Dim]DDS	87
Fig 4-16 Structure of [C ₂ CN Him]SBA	87
Fig 4-17 Structure of [C ₂ CN Oim]SBA	88
Fig 4-18 Structure of [C ₂ CN Dim]SBA	88
Fig 4-19 Structure of [C ₂ CN Bim]BS	89
Fig 4-20 Structure of [C ₂ CN Him]BS	89

Fig 4-21 Structure of [C ₂ CN Oim]BS.....	90
Fig 4-22 Structure of [C ₂ CN Bim]TFMS	90
Fig 4-23 Structure of [C ₂ CN Him]TFMS	91
Fig 4-24 Structure of [C ₂ CN Oim]TFMS	91
Fig 4-25 Structure of [C ₂ CN Heim]DOSS.....	92
Fig 4-26 Structure of [C ₂ CN Bzim]DOSS.....	92
Fig 4-27 Structure of [C ₂ CN Ayim]DOSS	93
Fig 4-28 Structure of [P _{8,8,8,14}]Cl.....	94
Fig 4-29 Structure of [P _{8,8,8} C ₆ P _{8,8,8}]Cl ₂	94
Fig 4-30 Structure of [P _{8,8,8} C ₁₀ P _{8,8,8}]Cl ₂	94
Fig 4-31 Structure of [P _{6,6,6,14}]DOSS	95
Fig 4-32 Structure of [P _{8,8,8,14}]DOSS	95
Fig 4-33 Structure of [P _{8,8,8} C ₆ P _{8,8,8}]DOSS ₂	96
Fig 4-34 Structure of [P _{8,8,8} C ₁₀ P _{8,8,8}]DOSS ₂	96
Fig 4-35 FTIR spectra of [CNC ₂ Him]DOSS, [CNC ₂ Him]DDS, [CNC ₂ Him]BS, [CNC ₂ Him]SBA and [CNC ₂ Him]TFMS.....	100
Fig 4-36 Densities ρ (g.cm ⁻³) of [C ₂ CN Bim] ILs as a function of temperature with a linear correlation of the data	101
Fig 4-37 Densities ρ (g.cm ⁻³) of [C ₂ CN Him] ILs as a function temperature with a linear correlation of the data.....	101
Fig 4-38 Densities ρ (g.cm ⁻³) of [C ₂ CN Oim] ILs as a function temperature with a linear correlation of the data	102
Fig 4-39 Densities ρ (g.cm ⁻³) of [C ₂ CN Dim] ILs as a function temperature with a linear correlation of the data	102
Fig 4-40 Densities ρ (g.cm ⁻³) of imidazolium and phosphonium-based ILs incorporating DOSS anion as a function of temperature.....	103
Fig 4-41 Densities ρ (g.cm ⁻³) of chloride-based ILs as a function of temperature....	105
Fig 4-42 Densities ρ (g.cm ⁻³) of [C ₂ CN C _n im]DDS ILs as a function of temperature	105
Fig 4-43 Densities ρ (g.cm ⁻³) of [C ₂ CN C _n im]SBA ILs as a function of temperature	106

Fig 4-44 Densities ρ (g.cm ⁻³) of [C ₂ CN C _n im]BS ILs as a function of temperature .	106
Fig 4-45 Densities ρ (g.cm ⁻³) of [C ₂ CN C _n im]TFMS ILs as a function of temperature	106
Fig 4-46 Densities ρ (g.cm ⁻³) of [C ₂ CN C _n im]Br ILs as a function of temperature ..	107
Fig 4-47 Plot of Molar volumes (V_m) versus the number of carbon (n_C).....	108
Fig 4-48 Effect of pressure on the densities of [C ₂ CN C _n im]Br, [C ₂ CN C _n im]Cl, [C ₂ CN C _n im]DOSS, [C ₂ CN C _n im]DDS and [C ₂ CN C _n im]SBA ILs at 298.15 K	110
Fig 4-49 Effect of pressure on the densities of [C ₂ CN C _n im]BS, [C ₂ CN C _n im] TFMS, [C ₂ CN Ayim]DOSS,[C ₂ CN Bzim]DOSS,[C ₂ CNHeim]DOSS, [P _{6,6,6,14}]DOSS [P _{8,8,8,14}]X and [P _{8,8,8} C _n P _{8,8,8}]X ₂ ILs at 298.15 K.	110
Fig 4-50 Structures of DOSS, DDS, SBA, BS and TFMS anions.....	112
Fig 4-51 Viscosities as a function of temperature for [C ₂ CN Bim]X.....	112
Fig 4-52 Viscosities as a function of temperature for [C ₂ CN Him]X.....	113
Fig 4-53 Viscosities as a function of temperature for [C ₂ CN Oim]X.....	113
Fig 4-54 Viscosities as a function of temperature for [C ₂ CN Dim]X.....	114
Fig 4-55 Viscosities for the DOSS-based ILs as a function of temperature	116
Fig 4-56 Arrhenius plot of viscosity for [C ₂ CN C _n m]Br and [C ₂ CN C _n m]Cl ILs	117
Fig 4-57 Arrhenius plot of viscosity for [C ₂ CN C _n m]DOSS and [C ₂ CN C _n m]DDS ILs	118
Fig 4-58 Arrhenius plot of viscosity for [C ₂ CN C _n m]SBA and [C ₂ CN C _n m]TFMS ILs	118
Fig 4-59 Arrhenius plot of viscosity for [C ₂ CN C _n m]BS and dual functionalized ILs	118
Fig 4-60 Arrhenius plot of viscosity for phosphonium-based ILs.....	119
Fig 4-61 Experimental values of refractive index.....	121
Fig 4-62 Experimental values of refractive index n_D , against T for imidazolium and phosphonium-based ILs incorporating DOSS anion.....	122
Fig 4-63 Experimental values of refractive index n_D , against T for [C ₂ CN C _n im]Br	122
Fig 4-64 Experimental values of refractive index n_D , against T for the ILs incorporating chloride anion	123

Fig 4-65 Experimental values of refractive index n_D , against T for [C ₂ CN C _n im]BS and [C ₂ CN C _n im]TFMS	123
Fig 4-66 Experimental values of refractive index n_D , against against T for [C ₂ CN C _n im]DDS and [C ₂ CN C _n im]SBA	123
Fig 4-67 Thermogravimetric traces of imidazolium and phosphonium- based ILs incorporating DOSS anion	124
Fig 4-68 Thermogravimetric traces of [C ₂ CN Him]-based ILs	125
Fig 4-69 Thermogravimetric traces of [C ₂ CN C _n im]DDS and [C ₂ CN C _n im]SBA ILs	126
Fig 1-1 Thermogravimetric traces of [C ₂ CN C _n im]BS and [C ₂ CN C _n im]TFMS ILs	126
Fig 4-71 Thermogravimetric traces of [C ₂ CN C _n im]Cl ILs.....	127
Fig 4-72 Thermogravimetric traces of [C ₂ CN C _n im]Br.....	128
Fig 5-1 CO ₂ solubility in [C ₂ CN Him]DOSS as a function of time at 298.15 K.....	139
Fig 5-2 CO ₂ solubility in [C ₂ CN Him]TFMS as a function of time at 298.15 K	139
Fig 5-3 CO ₂ solubility in [C ₂ CN Him]DDS as a function of time at 298.15 K.....	139
Fig 5-4 CO ₂ solubility in [C ₂ CN Him]SBA as a function of time at 298.15 K.....	140
Fig 5-5 CO ₂ solubility in [C ₂ CN Him]BS as a function of time at 298.15 K.....	140
Fig 5-6 CO ₂ solubility in [C ₂ CN Him]-based ILs incorporating DOSS, DDS, TFMS, SBA and BS anions at 298.15 K	141
Fig 5-7 CO ₂ solubility in [C ₂ CNBim]DOSS ILs as a function of time at 298.15 K .	144
Fig 5-8 CO ₂ solubility in [C ₂ CNOim]DOSS ILs as a function of time at 298.15 K .	144
Fig 5-9 CO ₂ solubility in [C ₂ CNDim]DOSS ILs as a function of time at 298.15 K .	145
Fig 5-10 Solubility of CO ₂ in [C ₂ CNC _n im]DOSS ILs at 298.15 K as a fuction of pressure.....	147
Fig 5-11 CO ₂ solubility in [C ₂ CN Heim]DOSS as a function of time at 298.15 K...	148
Fig 5-12 CO ₂ solubility in [C ₂ CN Bzeim]DOSS as a function of time at 298.15 K .	148
Fig 5-13 CO ₂ solubility in [C ₂ CN Ayim]DOSS as a function of time at 298.15 K...	148
Fig 5-14 Solubility of CO ₂ in imidazolium-based dual functionalized ILs at 298.15 K as a fuction of pressure	150
Fig 5-15 CO ₂ solubility in [P _{6,6,6,14}]DOSS as a function of time at 298.15 K	151
Fig 5-16 CO ₂ solubility in [P _{8,8,8,14}]DOSS as a function of time at 298.15 K	152

Fig 5-17 CO ₂ solubility in [P _{8,8,8} C ₆ P _{8,8,8}]DOSS ₂ as a function of time at 298.15 K.	152
Fig 5-18 CO ₂ solubility in [P _{8,8,8} C ₁₀ P _{8,8,8}]DOSS ₂ as a function of time at 298.15 K	152
Fig 5-19 Solubility of CO ₂ in phosphonium-based ILs at 298.15 K as a function of pressure.....	155
Fig 5-20 Solubility of CO ₂ in [C ₂ CNDim]DOSS, [C ₂ CNHeim]DOSS and [P _{8,8,8,14}]DOSS ILs at 298.15 K as a function of pressure.....	156
Fig 5-21 Solubility of CO ₂ in [C ₂ CNHim]-based ILs as a function of pressure.....	159
Fig 5-22 Solubility of CO ₂ in [C ₂ CNC _n im]DOSS ILs as a function of pressure.....	159
Fig 5-23 Solubility of CO ₂ in dual functionalized-based ILs as a function of pressure	159
Fig 5-24 Solubility of CO ₂ in phosphonium-based ILs as a function of pressure	160
Fig 5-25 Solubility of CO ₂ in [C ₂ CNDim]DOSS, [C ₂ CNHeim]DOSS	163
Fig 5-26 Solubility selectivity of [C ₂ CNDim]DOSS RTIL.....	168
Fig 5-27 CO ₂ /CH ₄ selectivity of physical solvents and ionic liquids at 10 bar. Selectivity at 333 K in physical solvents was taken from available literature:	168
Fig 5-28 Solubility of CO ₂ in recycled [C ₂ CNDim]DOSS.....	170

LIST OF TABLES

Table 2-1 Typical composition of natural gas	20
Table 2-2 Properties of carbon dioxide.....	22
Table 2-3 Measured solubilities of carbon dioxide in ionic liquids at 298.15K [162]	42
Table 2-4 Studied anions and cations for CO ₂ capture	48
Table 4-1 Schematic representation of the relation between cations and anions for the synthesized ILs	80
Table 4-2 Start and onset temperatures of the studied ILs.....	129
Table 4-3 Molar volume (V_m), Molecular volume ($V_{molecular}$), molar standard entropy (S^0) and lattice energy (U_{POT}) of the studied ILs.....	133
Table 4-4 Molar free volumes (V_f) of the synthesized ILs	135
Table 5-1 Experimental solubility data for CO ₂ in [C ₂ CN C _n im]X at 298 K	142
Table 5-2 Experimental solubility data for CO ₂ in [C ₂ CN C _n im]DOSS at 298 K.....	146
Table 5-3 Experimental solubility data for CO ₂ in imidazolium.....	149
Table 5-4 Experimental solubility data for CO ₂ in phosphonium-based ILs at 298 K.....	153
Table 5-5 Henry's law constant and correlation coefficients for the studied ILs	161
Table 5-6 Experimental solubility data for CO ₂ in [C ₂ CN Dim]DOSS, [C ₂ CN Heim]DOSS and [P _{8,8,8,14}]DOSS at 313 K.....	162
Table 5-7 Experimental solubility data for CO ₂ in [C ₂ CN Dim]DOSS, [C ₂ CN Heim]DOSS and [P _{8,8,8,14}]DOSS at 343 K.....	162
Table 5-8 Thermodynamic properties for the solution of CO ₂ in selected ILs.....	165

LIST OF ABBREVIATIONS

η	Dynamic viscosity
ν	Kinematic viscosity
ρ	Density
U_{POT}	Lattice energy
R_{M}	Molar refraction
N_{A}	Avogadro's number
α_{e}	Mean molecular polarizability
ϵ_0	Permittivity of free space
V_{f}	Molar free volume
V_{m}	Molar volume
m_{SC}	Mass of the empty container
v_{SC}	Volume of the empty container
m_{S}	Mass of sample
m_{CO_2}	Mass of carbon dioxide
<i>ppm</i>	Part per million
E_{η}	Activation energy
k_{H}	Henry's law constant
P_{CO_2}	Partial pressure of the gas
x	Mole fraction
R^2	Coefficient of determination of regression
ΔH^0	Standard enthalpy
ΔS^0	Standard entropy
ΔG^0	Gibbs free energy

NOMENCLATURE

[Ala	Alanine
[B(CN) ₄	Tetracyanoborate
[BEpyr]	Butylethylpyridinium
[Bmim]	1-butyl-3-methylimidazolium
[C ₁₀ mim]	1-decyl-3-methylimidazolium
[C ₁₂ H ₂₅ PhSO ₃]	Dodecylbenzenesulfonate
[C ₁₂ mim]	1-dodecyl-3-methylimidazolium
[C ₁ C ₄ pyrr]	1-butyl-1-methylpyrrolidinium
[C ₂ CN Bim]	1-butyl-3-propanenitrile imidazolium
[C ₂ CN Bzim]	1-benzyl-3-propanenitrileonitrile imidazolium
[C ₂ CN C _n im]	1-alkyl-3-propanenitrile imidazolium
[C ₂ CN Dim]	1-decyl-3-propanenitrile imidazolium
[C ₂ CN Heim]	1-(2-hydroxyethyl)-3-propanenitrile imidazolium
[C ₂ CN Him]	1-hexyl-3-propanenitrile imidazolium
[C ₂ CN Mim]	1-propylnitrile-3-methylimidazolium
[C ₂ CN Oim]	1-octyl-3-propanenitrile imidazolium
[C ₂ mim]	1-ethyl-3-methylimidazolium
[C ₂ mim]	1-ethyl-3-methylimidazolium
[C ₃ CN Mim]	1-butylnitrile-3-methylimidazolium
[C ₃ CNdmim]	1-alkylnitrile-2,3-dimethylimidazolium
[C ₃ CNMMIm]	1-butylnitrile-2,3-dimethylimidazolium
[C ₃ CNPy]	Butylnitrilepyridinium
[C ₄ CN Mim]	1-pentylnitrile-3-methylimidazolium
[C ₄ mim]	1-butyl-3-methylimidazolium
[C ₆ mim]	1-hexyl-3-methylimidazolium
[C ₈ H ₄ F ₁₃ mim]	1-(3,3,4,4,5,5,6,6,7,7,8,8,8-tridecafluorooctyl)-3-methylimidazolium
[C ₈ mim]	1-octyl-3-methylimidazolium
[CF ₃ SO ₂] ₂ N	Bis(trifluoromethylsulfonyl)imide
[C ₂ F ₅ SO ₂] ₂ N	Bis(perfluoromethylsulfonyl)imide
[CF ₃ SO ₂] ₂ N	Bis(trifluoromethylsulfonyl)imide

[CH ₃ SO ₄]	Methylsulfate
[C _n CNmim]	1-alkylnitrile-3-methylimidazolium
[C _n mim]	1-alkyl-3-methylimidazolium
[DCA]	Dicyanamide
[DEP]	Diethylphosphate
[DMFH]	N,N-dimethylformamidium
eFAP	Tris(pentafluoroethyl)trifluorophosphate
[Emim]	1-ethyl-3-methylimidazolium
[EMpyr]	ethylmethylpyridinium
[EtNH ₃]	Ethyl ammonium
EtSO ₄	Ethylsulfate
[Hemim]	1-(2-hydroxyethyl)-3-methylimidazolium
[Hmim]	1-hexyl-3-methylimidazolium
Lys	Lysinate
[MDEA]	N-methyldiethanolamine
[N _{1,1,1,1}]	Tetramethylammonium
[N _{1,1,1,10}]	Trimethyldecylammonium
[N _{1,1,1,4}]	Trioctylmethylammonium
[N _{1,1,3,10}]	Decylpropyldimethylammonium
[N _{1,8,8,8}]	Trioctylmethylammonium
[N ₁₁₃₂ -OH]	Propylcholinium
[N _{2,2,2,2}]	Tetraethylammonium
[N _{2,2,2,6}]	Triethylhexylammonium
[N _{4,4,4,4}]DOSS]	Tetrabutylammonium dioctylsulfosuccinate
[n-C ₁₆ H ₃₃ COO]	1-butyl-3-methylimidazolium palmitate
[n-C ₁₈ H ₃₅ COO]	1-butyl-3-methylimidazolium stearate
[Omim]	1-octyl-3-methylimidazolium
OTf	Trifluoromethanesulfonate
[P _{2,2,2,12}]	Triethyldodecylphosphonium
[P _{2,2,2,8}]	Triethyloctylphosphonium
[P _{6,6,6,14}]	Trihexyltetradecylphosphonium
[P _{8,8,8,14}]	Trioctyltetradecylphosphonium
[P _{8,8,8,8}]	Tetraoctylphosphonium
[P _{8,8,8} C ₁₀ P _{8,8} , 8]	1,10-bis(trioctylphosphonium)decane
[P _{8,8,8} C ₆ P _{8,8} , 8]	1,6-bis(trioctylphosphonium)hexane

BS	Benzenesulfonate
C ₁₂ (mim) ₂	1,12-bis(3-methylimidazolium)dodecane
C ₃ (mim) ₂	1,3-bis(3-methylimidazolium)propane
C ₆ (mim) ₂	1,6-bis(3-methylimidazolium)hexane
C ₉ (mim) ₂	1,9-bis(3-methylimidazolium)nonane
Cpmim	1-butyronitrile-3-methylimidazolium
Cpmmim	1-butyronitrile-2,3-dimethylimidazolium
DCILs	Dicationic ionic liquids
DDS	Dodecylsulfate
DOSS	Dioctylsulfosuccinate
Gly	Glycine
HEA	2-hydroxy ethylammonium acetate
HEAA	2-(2-hydroxy ethoxy)-ammonium acetate
HEAF	2-(2-hydroxy ethoxy)-ammonium formate
HEAL	2-(2-hydroxy ethoxy)-ammonium lactate
HEF	2-hydroxy ethylammonium formate
HEL	2-hydroxy ethylammonium lactate
ILs	Ionic liquids
Met	Methionine
N(CN) ₂	Dicyanamide
NTf ₂	Bis(trifluoromethylsulfonyl) imide
OAc	Acetate
Pro	Proline
SBA	Sulfobenzoic acid
TFMS	Trifluoromethanesulfonate
THEAA	Tri-(2-hydroxy ethyl)-ammonium acetate
THEAL	Tri-(2-hydroxy ethyl)-ammonium lactate
B(CN) ₄	Tetracyanoborate
Et ₂ PO ₄	Diethylphosphate
[TMGH]	1,1,3,3-tetramethylguanidinium
MP	Methylphosphonate
pFAP	Tris(heptafluoropropyl)trifluorophosphate
[N ₂₂₂₄]	Butyltriethylammonium
[N ₄₄₄₄]	Tetrabutylammonium
[N ₁₈₈₈]	Trioctylmethylammonium

[NH ₂ C _n mim]	Alkylaminemethylimidazolium
FEP	Tris(pentafluoroethyl)trifluorophosphate
[ETO] ₂ im]	1,3-diethoxyimidazolium
TFA	Trifluoroacetate
Bu ₂ PO ₄	Dibutylphosphate
C ₇ F ₁₅ CO ₂	Pentadecafluoroacetate
[P ₄₄₄₃]	tributylpropylphosphonium
[AA]	Amino acid
L	Lactate
[Hmpy]	1-hexyl-3-methylpyrinium
[Bmpy]	1-butyl-3-methylpyrinium
[C ₆ H ₄ F ₉ mim]	1-methyl-3-(3,3,4,4,5,5,6,6,6-nonafluorohexyl)imidazolium

CHAPTER 1

INTRODUCTION

1.1 Importance of CO₂ removal from natural gas

The high world demands for energy to meet the multiplex human consumption and the multitudinous industrial needs have aided the search for alternative sources of primary energy even to the remote part of the globe [1]. The major alternative source discovered some decades ago is energy from natural gas. The high demand of the world for energy leads to the increase of the importance of the natural gas and make them play an important role in the national economy of the producing countries.

Natural gas is a vital energy source expected to be the fastest growing primary energy source in the coming decades [1]. Natural gas at its geological conditions in some deposits contain some complex contaminants such as nitrogen, carbon dioxide, carbon monoxide and sulfur compounds [2], which constitutes great environmental hazards when released to the atmosphere and also hinders natural gas processes [3].

Even though the natural gas has lower content of CO₂ compared to coal and oil, approximately twenty percent of natural gas contains excess CO₂ which has several disadvantages including the lowering of calorific value, corrosion of pipelines and process equipments [4]. Due to the large volume of natural gas produced annually (world production in 2009 was 106.453 Billion cubic feet), even small improvements in CO₂ removal efficiency could lead to considerable cost reduction [5].

In contrast, the atmospheric concentration of CO₂ has increased unabated by about 25 percent since large- scale industrialization began around 150 years ago as shown in Fig 1-1 [6]. The relatively constant concentration of CO₂ in the atmosphere prior to

the industrial revolution implied that the amounts of CO₂ generated by natural processes are almost equal to the amount absorbed by natural processes [7]

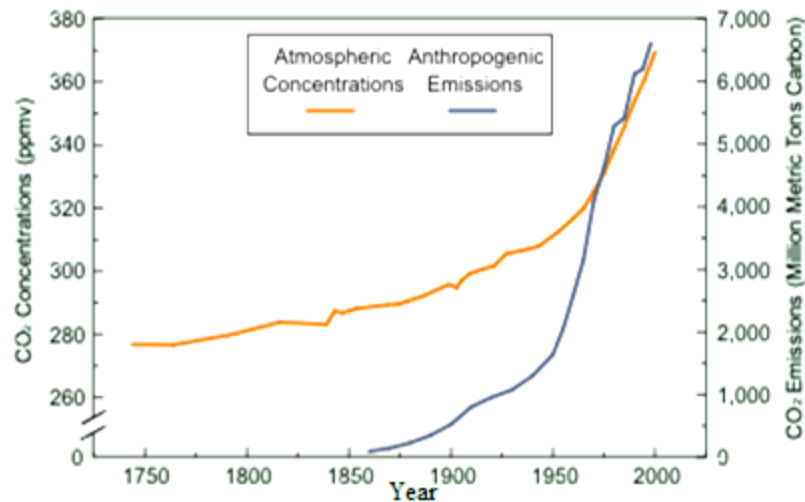


Fig 1-1: Trends in Atmospheric Concentrations and Anthropogenic Emissions of Carbon Dioxide
(Source: Oak Ridge National Laboratory Carbon Dioxide Information Analysis Centre. <http://cdiac.esd.ornl.gov>)

During the past 20 years, more than three-quarters of human-made CO₂ emissions were from natural gas. This growing carbon burden has significant implications for the global climate (CO₂ is the largest contributor in regard of its amount present in the atmosphere contributing to 60 percent of global warming effects) [8, 9]. Moreover, the relatively high production rate and the human body's relatively low tolerance will frequently make CO₂ removal the foremost concern [7]. Furthermore, the issue of environmental pollution has become a significant threat to the world in which we live and the environmental regulations to restrict CO₂ emission are increasingly stringent every year [10].

The high demand for capture and separation of carbon dioxide for fuel, medical and environmental applications is speedily growing as more nations have become industrialized [11]. Therefore, CO₂ capture and reduction of the CO₂ concentration in the atmosphere are needed during the next several decades. Theoretically we can remove CO₂ from the air by enhancing natural sinks, such as growing more algae by ocean fertilization, planting trees, and greening the desert [7]. These ideas have long-term significance, but are not practicable at present; therefore it is commercially

important and environmentally desirable to develop new materials to capture CO₂. ILs could be designed for the specific needs of the CO₂ separation, showing great potential and would provide improvements in absorption capacity and selectivity of CO₂ by making use of their designing character and choosing appropriate combination of cation and anion [12-15].

1.2 Overview of ILs

1.2.1 Definition and history of ILs

Ionic liquids (ILs) are typically defined as a new class of organic salts comprised of large delocalized ions and having very low melting points (below 100 °C) or even at room temperature (room temperature ILs, RTILs). This melting point restriction distinguishes ILs from their higher melting counterparts, molten salts with negligible vapor pressure [16, 17].

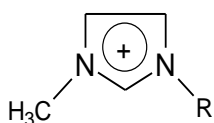
The date of discovery, as well as the discoverer, the "first" IL is disputed. However, one of the earlier known RTILs was ethyl ammonium nitrate ([EtNH₃]⁺ [NO₃]⁻), which was synthesized and published in 1914. However, this discovery of a new class of liquids did not prompt any significant interest at that time. Today, this is widely recognized as the start of the field of ILs, and it has left an important inheritance [18]. Hereafter, Hurley and Weir (1951), Robinson *et al.*(1979), Wilkes *et al.* (1982), Seddon *et al.* (1983) and Appleby *et al.*(1986) directed extensive research works towards new aluminum chloride-based ILs. The first investigation to use the chloroaluminate ILs as nonaqueous, polar solvent, reaction media and catalyst was at the end of 1980s [19]. ILs did not find many practical applications due to their hydroscopic nature which required both preparation and handling to take place in an inert gas atmosphere [19, 20].

In the early 90's, the concept of water immiscible ILs (1-ethyl-3-methylimidazolium-based ILs) was introduced by Zaworotko, Wilkes, Cooper and O'Sullivan in separate works. Contrary to chloroaluminates salts, these ILs can be

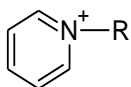
prepared on the bench. However, they can absorb water from the atmosphere, and they do not react with water [21].

The development of more hydrophobic ILs started (1996) when Bonhôte *et al.* reported the synthesis and characterization of ILs containing hydrophobic anions such as trifluoromethane sulfonate, tris (trifluoromethylsulfonyl) methanide and bis (trifluoromethylsulfonyl) imide. Nowadays, around 10^{18} ILs have been predicted and could be synthesized by combining different ions (as shown in Fig 1-2) [18, 20].

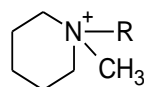
Most commonly used cations



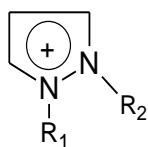
1-alkyl-3-methyl imidazolium



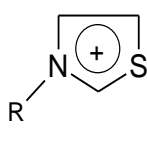
N-alkyl pyridinium



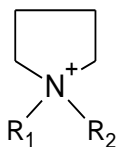
N-alkyl-N-methyl piperidinium



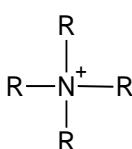
N,N-dialkyl pyrazolium



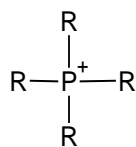
N-alkyl thiazolium



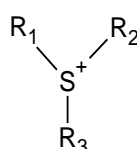
N-alkyl-N-methyl pyrrolidinium



Tetraalkyl ammonium



Tetraalkyl phosphonium



Trialkylsulfonium

Most commonly used anions



Bromide



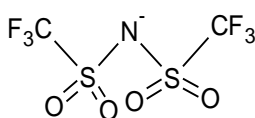
Chloride



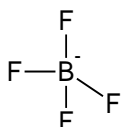
Acetate



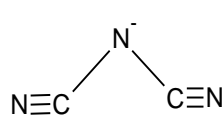
Nitrate



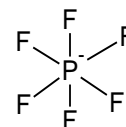
Bis(trifluoromethane) sulfonimide (NTf₂)



Tetrafluoroborate (BF₄⁻)



Dicyanamide (dca)



Hexafluorophosphate (PF₆⁻)

Fig 1-2 Structures of common cations and anions used in the formation of ILs

1.2.2 Structures of ILs

ILs are exclusively composed of weakly coordinating organic cations with low symmetry and inorganic or organic anions (making them markedly different from ionic solutions, which contain ions dissolved in a molecular medium), with different molecular sizes. They can either be hydrophilic or hydrophobic, depending on the nature of ionic combinations [22, 23].

The cations are generally bulky possessing organic components with low symmetry. Those described until now are based on ammonium, sulfonium, phosphonium, imidazolium, pyridinium, pyrrolidinium, thiazolium, triazolium, oxazolium, and pyrazolium differently substituted. Of particular interest are the salts based on the *N,N*-dialkylimidazolium cation because of the wide spectrum of physicochemical properties available in that class. Concerning the anions, they can be classified in two parts: the first are those that give polynuclear anions (Al_2Cl_7 , $\text{Al}_3\text{Cl}_{10}$, Fe_2Cl_7). The second class of anions corresponds to mononuclear anions which lead to neutral, stoichiometric ILs (BF_4 , PF_6 , $\text{N}(\text{CF}_3\text{SO}_2)_2$, $\text{N}(\text{C}_2\text{F}_5\text{SO}_2)_2$, $\text{N}(\text{FSO}_2)_2$, $\text{C}(\text{CF}_3\text{SO}_2)_3$, CF_3CO_2 , CF_3SO_3 , CH_3SO_3) [24].

Cations and anions that are widely studied are shown in Fig 1-2. Recently, people have been moving away from $[\text{PF}_6]^-$ and $[\text{BF}_4]^-$ since they are highly toxic, and lean towards new anions such as bistriflimide $[(\text{CF}_3\text{SO}_2)_2\text{N}]^-$, CF_3COO^- , alkylsulfate, carboxylates (acetate, formate), dialkylphosphates, amino acids [25-27], acesulfamate and saccharinate [28]. Moves towards less toxic cations have also been growing, with compounds like ammonium salts (choline) and 3-alkoxymethyl-1-methylimidazolium salts [29-32]. Zwitterions ILs (cation and anion tethered by covalent bond) were also prepared [33]. In addition, many amino acid-based ionic liquids have been prepared including amino acids as anions, amino acids as cations or amino acid derivatives [34].

As the use of RTILs becomes more widespread, the design of tailored, “task-specific” ILs (TSILs) also known as functionalized ILs is becoming more common [14, 35, 36]. TSIL are ILs in which the functional group is cation and anion-tethered [37]. The functionalized ion of a TSIL can be regarded as possessing two segments.

The first is a core that bears the ionic charge and serves as the locus for the second segment, the substitution group. Many researchers have been able to meet the demands of their applications by synthesizing RTILs with specific functional groups (carboxyl-functionalized ILs for solubilizing metal oxides, amine-appended IL for, CO₂ capture)[13, 14, 38, 39]. Recently, a series of new task-specific ILs (TSILs) have been introduced by incorporating additional functional group, to impart specific properties or reactivities. Replacing the CH₂ group in the side chain in the imidazolium-based ILs with an oxygen atom resulted in the repulsive interactions between neighboring oxygen atoms or anions. This leads to significant ion pairing in the solid phase. As a results there are notable differences in the thermal properties of the salts) [35, 40-42]. Incorporation of a functional group (such as amine [43-45], sulfonic acid [44, 46], ether, alcohol [40, 47], carboxylic and fluoruous chains [38, 48]) facilitates the choice of ILs for interaction with dissolved substrates in specific ways resulting in a wide range of applications [49].

A relatively new class of ILs called dicationic ILs (DCILs) has emerged recently. DCILs are molecules containing two head groups linked by a rigid or flexible spacer; they have special properties and potential applications in many areas such as lubricants and electrolyte components. An advantage of DCILs over monocationic ILs is that their properties can be “tuned”, controlled, or altered to a greater extent than the more conventional RTILs [50, 51].

ILs can be fine-tuned to optimize the chemistry, the chemical engineering, and the cost of the system. Consequently ILs can rightfully be called “designer” solvents, and offer a flexibility for process design previously unknown [18].

1.2.3 Preparation of ILs

The most common salts in use are those with alkylammonium, alkylphosphonium, *N*-alkylpyridinium, *N,N'*-dialkylimidazolium cations. Generally the preparation of these ILs can be broadly divided into two steps [52]:

1. The formation of the desired cation.
2. Anion exchange in order to form the final desired product.

The formation of the cations may be carried out either by protonation with a free acid or by quaternization of an amine, phosphine or sulphide. In all cases it is recommended that the addition of acid is carried out with cooling of the amine solution, as the reaction can be quite exothermic [37, 52]. The removal of the starting materials (haloalkanes) and reaction solvents is generally not a problem, especially for the relatively volatile shorter chain haloalkanes. In the case of longer chain haloalkanes, their boiling points are higher than shorter ones, and they are removed in the washing (recrystallization) cycles [53].

The anion exchange reactions of ILs can be divided into two divergent categories: direct reaction of the haloalkane with Lewis acids and anion metathesis [37]. Fig 1-3 and Fig 1-4 show a typical synthetic paths for preparation of ILs based on alkylammonium and *N,N*-dialkylimidazolium cations respectively [54, 55]. Moreover, some ammonium ILs are also prepared by acid/base neutralization reaction as shown in Fig 1-5 (monoalkylammonium nitrate salts are best prepared by the neutralization of aqueous solutions of the amine with nitric acid and tetraalkylammonium sulfonate are prepared by mixing equimolar amounts of the sulfonic acid and the tetraalkylammonium hydroxide).

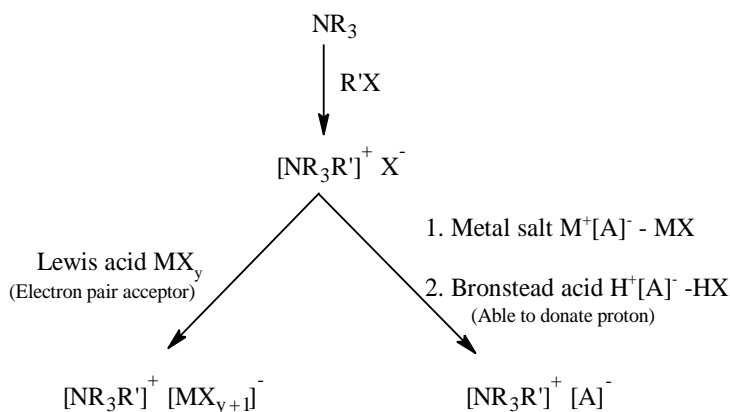


Fig 1-3 General synthetic scheme for preparation of alkylammonium ILs

The alkylation process possesses a number of advantages that makes it attractive such as a wide range of relatively inexpensive haloalkanes are readily available and the substitution reactions generally occur smoothly under mild reaction conditions [36, 56].

- Low or reduced flammability hazards.
- Tunable properties, such as the polarity and hydrophilicity. Hence the ILs can be tailored to be immiscible with some organic solvents and can be used in two-phase systems. In a similar manner, hydrophobic ILs are suitable for use in aqueous biphasic systems. In addition, some ILs can operate un triphasic system which is a very advantageous property for the extraction of the products.
- Excellent solvation capacity for both polar and non polar compounds.
- High thermal stability (up to 450 ° C) [51, 61] and wide liquid range which offers distinct advantages over the traditional solvent systems.
- High electrical conductivity and wide electrochemical window ($> 15 \text{ mScm}^{-1}$) which make them attractive materials in numerous applications in the electrochemical applications [62].

Although ILs are generally known as safe and benign compounds, some of them are flammable and others are volatile [63, 64].

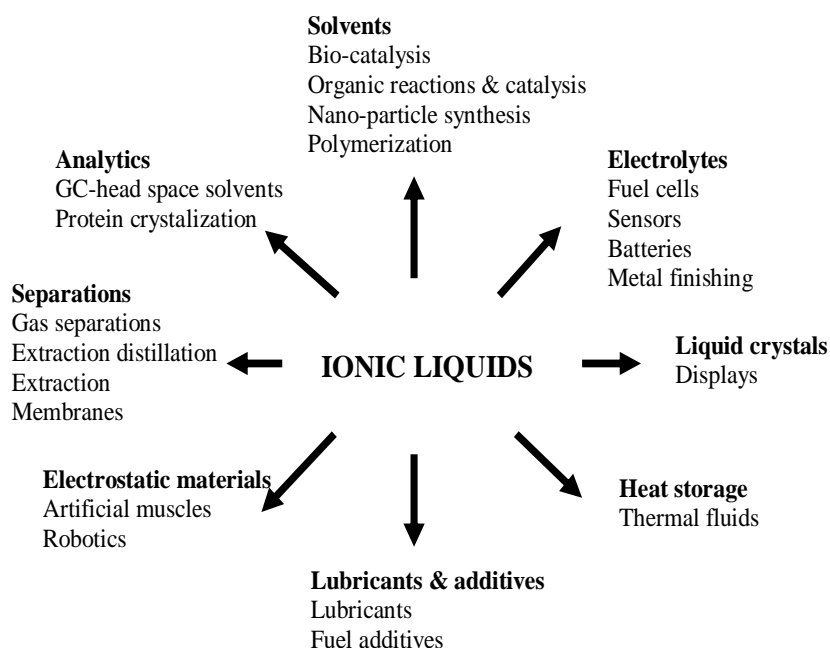


Fig 1-6 Selection of applications where ILs have been used [65]

The distinctive properties of these compounds enhanced their capabilities over some traditionally used volatile solvents and make them useful in many important areas of commercial applications such as: solvents for reactions, absorption media for gas separations, separating agent in extractive distillation, heat transfer fluids,

biomass processing, working fluid in a variety of electrochemical applications [66] (batteries, capacitors, solar cells, etc.), lubricants [56, 67] and in biocatalysts with unique advantages [68]. Fig 1-6 shows a selection of applications where ILs have been used [65].

Both cationic and anionic components of ILs can be varied and modified for specific application with desirable properties. The versatility of these unique solvents also benefits other areas of chemical research. Among the latest successes, ILs were used in recovery of biofuels, in deep desulfurization of diesel fuel and also as versatile lubricants [27, 69].

Recently, the interest of the application of ILs in separations has increased, typically as replacements for the organic diluents employed in traditional liquid-liquid extraction or in membrane-based separations of organic solutes, metal ions, and gases. Some of the studied applications are outlined below [70]:

- Liquid extraction:

1. Extraction of organics from aqueous solution

RTILs having a miscibility gap with water have been shown to be effective solvents for a range of organic compounds [71]. Furthermore, the pH-dependent distribution of certain solutes can provide a route for reverse extraction [71, 72].

2. Metals extraction from aqueous solution

RTILs provide unique solvation environment for ionic species and have been shown to be highly effective as replacements for conventional organic solvents in the liquid-liquid extraction of metal ions. The partitioning of metal ions from aqueous solutions into ILs containing extractants far exceeds that obtainable with most conventional solvent [35, 72]. In addition, “Task-specific” ILs (TSIL), incorporating a metal ion-ligand functional group into one of the ions of an RTIL functions as both the hydrophobic solvent and the extractants in liquid-liquid separations of metal ions [73, 74].

- Hydrocarbon Processing

1. Sulfur removal from hydrocarbon fuels, including extraction of organosulfur compounds by selective solubilization, removal of mercaptans, and electrochemical oxidation [37, 75].

2. Hydrocarbon separations based on interaction of metal salts dissolved in ILs [76].
 3. Extractive distillation is an apparent processing application for ILs, given the possibility for selective solubility and no volatility of RTILs for separation of azeotropic mixtures (azeotrope is a special class of liquid mixture of two or more liquids in such a ratio that its composition cannot be changed by simple distillation). This occurs because, when an azeotrope is boiled, the resulting vapor has the same ratio of constituents as the original mixture) and in multiple hydrocarbon separation processes (separation of hydrocarbons with close boiling points, such as C₄ mixtures) [76].
- Membrane separations
 1. Supported liquid membrane system employing ILs as carriers utilize the characteristics of selective solubility and low volatility, while minimizing volume of potentially costly solvent [77].
 2. Method for separating substances from solutions containing ILs by means of a membrane. The main function of this method is to perform fine separation of undesirable constituents from the catalytic system after phase decantation has already performed the coarse separation of the catalyst from the products [37].
 - Metals separation by electrorefining

IL processes developed for production, refining, and recycling of metals, including aluminum processing and spent nuclear fuel treatment. The metal ion extraction in the ionic liquid/aqueous two phase system indicated high efficiency and selectivity that expelled most of the organic solvents. The metal ion partitioning always rely on the species of the ionic liquid, metal ion and ligand. In addition, it has been demonstrated that room-temperature ionic liquids can be used for solvent extraction of metal species from aqueous media; this is an area of great significance to the nuclear industry which currently uses solvent extraction in the process for reprocessing spent nuclear fuel. [78].
 - Analytical/small-scale separations
 1. Stationary phases for gas chromatography: ILs coated onto fused silica capillaries exhibit a dual behaviour, acting as low-polarity phases with

nonpolar compounds and in the opposite manner for compounds bearing strong proton-donor groups. The chromatographic properties of these materials can be readily tuned by minor changes in the cationic or anionic constituent of the IL. ILs appear to act as a low-polarity stationary phase to nonpolar compounds. However, molecules with strong proton donor groups, in particular, are tenaciously retained. The nature of the anion can have a significant effect on both the solubilizing ability and the selectivity of ionic liquid stationary phases. [79].

2. Electrolytes in capillary electrophoresis: RTILs have been shown to be suitable as running electrolytes in capillary electrophoresis for compounds such as basic proteins and polyphenols [80].

- Gas Separation

Selective solubility of specific gases in ILs has been measured, leading to the possibility for gas separations. Carbon dioxide exhibits a relatively high solubility in imidazolium-based ILs; oxygen, nitrogen, hydrogen, carbon monoxide, argon have low solubility (the solubility of CO₂ in [bmim]PF₆ is greater than 0.2 mol fraction while that of O₂ and Ar in the same IL is less than 0.02 mol fraction) [81].

The solubility of CO₂ in the conventional ionic liquids, such as imidazolium, phosphonium and sulfonate based ILs is relatively higher than the solubility of CO₂ in some conventional organic solvents such as heptane, ethanol, benzene, cyclohexane. The equilibrium solubility of CO₂ in conventional ILs ([bmim]PF₆ and [bmim]BF₄) is about 0.10-0.15 wt% at room temperature and atmospheric pressure, which is obviously too low for industrial application for CO₂ capture [61].

Task-specific ILs have been demonstrated for selective gas solubility and the incorporation of functional groups to ILs was adopted to increase the solubility of CO₂ in ILs [82]. Increasing the free volume (unoccupied part of the molar volume of a substance [83]) also can enhance the CO₂ solubility capacity. The structure of an imidazolium-based cation was modified by appending an amine substituent, yielding an IL with elevated carbon dioxide capture from gas mixtures [14]. In addition, 1-alkyl-3-fluoroalkylimidazolium-based ILs such as 1-methyl-3-(nonafluorohexyl)imidazolium bis[(trifluoromethyl)sulfonyl]imide ([C₆H₄F₉mim][NTf₂]) and 1-methyl-

3-(tridecafluorooctyl)imidazolium bis[(trifluoromethyl)sulfonyl]imide [$C_8H_4F_{13}mim$] [NTf₂] have a high solubility capacity for CO₂ compared to the conventional ILs [82].

1.3 Problem statement

The composition of natural gas contains a mixture of inorganic compounds such as CO₂, SO₂ and N₂. Separation of CO₂ will be crucial to the realization of the everyday use of natural gas. The political issues coupled with growing social concern and desire for clean, sustainable technologies will drive research to find or develop new materials for CO₂ separation. The presence of CO₂ in natural gas constitutes great environmental hazards when it gets to the atmosphere. In addition, CO₂ must be removed from natural gas in order to increase the heating value of the gas, prevent corrosion of gas process equipment and crystallization of CO₂ during the cryogenic process (liquefaction process) and to meet pipeline specifications. Moreover, due to the large volume of natural gas produced annually even small improvements in CO₂ removal efficiency could lead to considerable cost production. Thus it is environmentally and commercially important and desirable to remove CO₂ from natural gas.

Recently, RTILs have been proposed as promising alternative or next-generation CO₂-selective separation media. Unlike organic solvents, both the solubility and the selectivity of CO₂ in RTILs can be readily “tuned” by tailoring the structures of the cation and/or anion. This highly attractive feature, coupled with their negligible vapour pressure, low or reduced flammability and high thermal stability of the RTILs, has made CO₂ separations one of the most prominent areas for the development of RTILs. In spite of all recent advantages in the field of RTILs, there are many gaps to be filled. The main impediment is the deficient of comprehensive knowledge about the factors that govern their physical properties and solubility of CO₂. Therefore, in addition to gathering the property data of the RTILs to assess their potential uses and dangers, a detailed understanding of how a structure affects properties and CO₂ solubility is needed to understand the relationships between RTILs structure, the resulting physical properties and the solubility of CO₂. This is especially important for RTILs because there can be a considerable amount of structural variation results from

varying the basic cation and anion types, in addition to side chains and functional groups.

In order to enhance the CO₂ solubility and gas separation factors in RTILs, new materials must be designed. While both the anion and cation can be specified, chemical modifications are best suited to the cation. Anions have been typically chosen from species with multiple resonance structures. The introduction of new RTILs (other than fluorinated RTILs) with unique structures (incorporating functional groups and/or long alkyl chains that could enhance the CO₂ solubility) having high CO₂-philic property and free volume are expected to have significant performance in the solubility of CO₂.

Long alkyl chain and functional group have a significant effect in the thermophysical properties, CO₂ solubility and selectivity. Imidazolium-based RTILs incorporating either long alkyl chain or functional group in the third position of the imidazolium ring are studied (only alkylimidazoles with short alkyl chains (methyl, ethyl and butyl) are often commercially available) while incorporating long alkyl chains and functional group. In addition, phosphonium-based RTILs incorporating long alkyl chain such as octyl in both the cation and anion was studied.

1.4 Research objectives

Gas absorption is generally the technology favored for the CO₂/CH₄ separation and cryogenic separation, although highly energy demanding is normally applied to separations. The CO₂/CH₄ separation by gas absorption can be improved by finding low volatile solvents that require less energy for regeneration, exhibit a high stability and having a higher solubility capacity without degradation or loss of the separating agent. Based on their properties, it is expected that Room Temperature Ionic liquids (RTILs) can be used as improved solvents in the targeted gas separations. RTILs are liquid organic salts, which generally consist of an organic cation and either an inorganic or organic anion. Among other properties, the RTILs are non volatile and can be considered as designer solvents. The nature of the cation and the anion determine the physical and chemical properties of the ionic liquid. As result of the

existing dependence of properties on the nature of the constituent ions, it is possible to achieve specific properties by choosing the right combination of anion and cation. Using this tailoring process, functional groups can be added to the structure to provide a better performance of the RTIL when chemical reaction or specific affinity and selectivity are required.

The potential of the standard room temperature ionic liquids as absorption solvents for the CO₂ separation can be expanded due to their designer capability together with their wider range of polarities, low lattice energy and especially their dual organic and ionic character. At the same time, ionic liquids may overcome the drawbacks of the available solvents.

The overall goals of this project are to obtain a fundamental understanding and increase the solubility of CO₂ in RTILs. These goals have been made through a combination of synthesis of new RTILs and experimental measurements of thermophysical properties and CO₂ solubility of these RTILs. The specific objectives of this study are as follows:

- To synthesize and characterize a novel series of imidazolium-based nitrile functionalized and phosphonium-based RTILs incorporating sulfonate-base anions with systematic structural variations of the cations and anions.
- To explore the effects of the structures variations of the present RTILs on the thermophysical properties.
- To investigate the effect of alkyl chain length and functional group of the cation and anion type on the derived thermophysical properties (thermal expansion coefficient, molar entropy, crystal energy) to understand the underlying relationships between the IL structure and the resulting physical properties.
- To explore the solubility of CO₂ in the synthesized RTILs using magnetic suspension balance. The experimental data is then used to estimate Henry's constant, enthalpy, entropy and Gibbs free energy of the RTILs.
- To investigate the effects of the cation, alkyl chain, functional group, anion, temperature and pressure on the solubility of CO₂ in the RTILs.

1.5 Scope of study

The principal scope of this research is to investigate and understand systematically how the structure variations of the imidazolium and phosphonium-based RTILs affect their properties and solubility of CO₂ based on the experimental outcome of the synthesized RTILs. Thus, the structures of the synthesized RTILs were varied systematically to understand the effect on thermophysical properties and solubility of CO₂.

To pursue this scope, this study has been divided into three stages. The first is taking the advantages of the existing information regarding CO₂ solubility in RTILs to synthesize (design) new generation of RTILs with increased CO₂-philic property and free volume. The designed RTILs are planned to have the most promising combination of ions in the liquid structure and incorporate the identified specific functionalities. Then as a result of the structural composition and chemical functionalization of the RTILs, the performance of solubility agent is expected to be improved. The second is the study of the structure-property relationship using the experimental data to construct structure-property relationships. These relationships serve the dual purpose of providing predictive relationships for new compounds and elucidating the structural features that most influence a given property. The third is the study of the property-solubility relationship, which used the experimental data to construct property-solubility relationships. These relationships serve the purpose of providing predictive relationships for new compounds and elucidating the property that most influence the solubility. Moreover, the experimental data could be used to develop the process for CO₂ removal using RTILs. The second and third stages are especially important for RTILs because there are a considerable amount of structural variation resulting from varying the basic cation and anion types, in addition to the modifications of the side chains and functional groups.

The present study involves the synthesis of novel imidazolium-based RTILs with nitrile functionality ([CNC₂C_nim] where n = 4, 6, 8, 10) and incorporating sulfonate-based anions such as; dioctylsulfosuccinate (DOSS), dodecylsulfate (DDS), sulfobenzoic acid (SBA), benzenesulfonate (BS) and trifluoromethanesulfonate (TFMS). Trialkylphosphonium-based monocationic and dicationic RTILs

([P_{n,n,n,14}][dioctylsulfosuccinate] where n = 6, 8 and [P_{8,8,8} C_y P_{8,8,8}][dioctylsulfosuccinate] where y = 6, 10) were also synthesized. The molecular structures of the synthesized RTILs were confirmed using ¹H and ¹³H NMR, FTIR and elemental analysis. The densities and viscosities of the present RTILs were measured at atmospheric pressure at $T = 293.15$ to 353.15 K, refractive index was measured at $T = 293.15$ to 333.15 K, whereas, the start and decomposition temperatures were determined at heating rate $10\text{ }^{\circ}\text{C}\cdot\text{min}^{-1}$. The thermal expansion coefficient, molecular volume, molar refraction, standard entropy and crystal energy of these RTILs were also estimated.

The solubility of CO₂ in the synthesized RTILs was measured using gravimetric measurement technique (magnetic suspension balance) at $T = 298$ to 343 K and pressures $P = 1$ to 20 bar. The influence caused by the alkyl chain, functional group, nature of the cation and anion were studied. The solubility of the present RTILs is described using the Henry constant along with some thermodynamic properties such as molar enthalpy and entropy. The CO₂/CH₄ selectivity was estimated from the single gas solubility and the recyclability was investigated. The structures of the RTILs and the solubility relationships were studied using the experimental data to construct structure-property and structure-solubility relationships.

1.6 Thesis outline

A brief description and overview of the thermophysical properties of RTILs will be presented in Chapter 2. Furthermore, a detailed literature review and the progress of the solubility of CO₂ in RTILs will be addresses.

Chapter 3 present the design and characterization of imidazolium-based RTILs with nitrile and either butyl or hexyl, octyl, decyl, benzyl, allyl, 2-hydroxyethyl substituents tethered to the cation and incorporating either bromide or chloride, dioctylsulfosuccinate, dodecylsulfate, sulfobenzoic acid, benzene sulfonate, trifluoromethane sulfonate as anions. Trihexyl and trioctyl phosphonium-based RTILs incorporating dioctylsulfosuccinate were also synthesized and characterized. The synthesis and characterizations of each of these types of RTILs are presented to

illustrate the multitudes of design possibilities and their performance in target solubility. The details, calibration techniques and experimental procedures of the instruments used to study the thermophysical properties and CO₂ solubility are also given in this chapter along with the basis for the solubility calculations. Furthermore, the CO₂ solubility in the present RTILs was measured at pressures and temperatures up to 20 bar and 343 K respectively.

Chapter 4 focuses on the thermophysical properties since it is needed in order to relate the properties and the structure of the synthesized RTILs. The values of density, viscosity and refractive index of the present RTILs were reported at temperatures up to 353.15 K and the dependency with temperature of the measured properties is included. The data obtained were used to estimate the thermal expansion coefficient, molar refraction, crystal energy and entropy. Correlations were proposed to represent the experimental results. The results were compared with other imidazolium and phosphonium-based RTILs.

In chapter 5, the results of the CO₂ solubility in the synthesized RTILs were presented. First the effects of the RTILs anions were studied to select the optimum one, then the cation, alkyl chain length and functional group effects were discussed along with the effects of temperature and pressure. Moreover, The CO₂ solubility in recycled RTILs is also presented. The solubility of CO₂ in the RTILs was expressed in terms of Henry's coefficient, which is used along with the Peng-Robinson equation of state to estimate some thermodynamic properties (molar enthalpy and entropy). The results were compared with the available literature.

Finally, the achievements and recommendations for designing RTILs as absorption solvents are discussed and summarized in chapter 6 along with the conclusions and recommendations for future work.

CHAPTER 2

LITERATURE REVIEW

2.1 Introduction

This chapter divided into two main parts; thermophysical properties and CO₂ solubility of RTILs. The thermophysical properties part provides a review on related work in the field of density, viscosity, refractive index, thermal stability, thermal expansion coefficient, molar refraction, entropy and crystal energy of imidazolium and phosphonium-based ILs. The second part provides a review on related research work in the field of the solubility of CO₂ in the imidazolium and phosphonium-based ILs. Furthermore, the effect of different factors such as alkyl chain and functional groups on the CO₂ solubility is reported.

2.2 Natural gas

Natural gas is a mixture of many compounds which can be classified into three major groups--hydrocarbons, inerts, and miscellaneous trace compounds. Most of the hydrocarbons in natural gas are saturated. This group of compounds is also known as alkanes, paraffins, and aliphatics. The most abundant alkane in natural gas is methane, commonly referred to as C1 because it contains one carbon atom. Next is ethane (C2) with two carbons, followed by propane (C3), iso-butane and normal butane (C4), iso-pentane and normal pentane (C5), and hexanes and heavier hydrocarbons (C6+). The C6+ fraction can contain up to 100 or more compounds including aromatics such as benzene, toluene, ethylbenzene and xylenes [84].

In addition to hydrocarbons, the other components of natural gas such as nitrogen and carbon dioxide are not combust. Therefore, they do not contribute to the heating value of the gas, making them undesirable. Trace components commonly include water vapor, hydrogen sulfide, carbon dioxide, nitrogen, and helium (Table). Hydrogen sulfide is highly toxic and is characterized by a very strong foul odor. It is also referred to as sour gas. Helium is a true inert gas that is nonreactive with other compounds. Most of the nation’s helium production comes from natural gas deposits. Other less common trace components include oxygen, hydrogen, and carbon monoxide[84].

Table 2-1 Typical composition of natural gas

Methane	CH ₄	70-90%
Ethane	C ₂ H ₆	
Propane	C ₃ H ₈	0-20%
Butane	C ₄ H ₁₀	
Carbon Dioxide	CO ₂	0-8%
Oxygen	O ₂	0-0.2%
Nitrogen	N ₂	0-5%
Hydrogen sulphide	H ₂ S	0-5%
Rare gases	Ar, He, Ne, Xe	trace

In its purest form, such as the natural gas that is for cooking, it is almost pure methane. Methane is a molecule made up of one carbon atom and four hydrogen atoms, and is referred to as CH₄. The distinctive “rotten egg” smell that we often associate with natural gas is actually an odorant called mercaptan that is added to the gas before it is delivered to the end-user. Mercaptan aids in detecting any leaks [85]. Ethane, propane, and the other hydrocarbons commonly associated with natural gas have slightly different chemical formulas. Natural gas is considered 'dry' when it is almost pure methane, having had most of the other commonly associated hydrocarbons removed [85].

Natural gas has many uses, residentially, commercially, and industrially. Found in reservoirs underneath the earth, natural gas is often associated with oil deposits. Production companies search for evidence of these reservoirs by using sophisticated

technology that helps to find the location of the natural gas, and drill wells in the earth where it is likely to be found. Once brought from underground, the natural gas is refined to remove impurities such as water, other gases, sand, and other compounds. Some hydrocarbons are removed and sold separately, including propane and butane. Other impurities are also removed, such as hydrogen sulfide (the refining of which can produce sulfur, which is then also sold separately). After refining, the clean natural gas is transmitted through a network of pipelines. From these pipelines, natural gas is delivered to its point of use [85].

Methane is the major constituent of natural gas, consists of one carbon and four hydrogen atoms (CH_4). In methane C-atom is Sp^3 -hybridized. One s-orbital and three p-orbitals ($2p_x, 2p_y, 2p_z$) of carbon atom undergo Sp^3 -hybridization to produce four Sp_3 -hybrid orbitals. Methane molecule is tetrahedral in structure in which carbon is central atom and four H-atoms are surrounding it in three-dimensions (Fig 2-1). Methane is a colorless, odourless and non-poisonous gas having melting point = -182.5°C , boiling point = -169.5°C , its molecule is symmetrical. It is lighter than air, virtually insoluble in water, but it will dissolve in organic solvents [86].

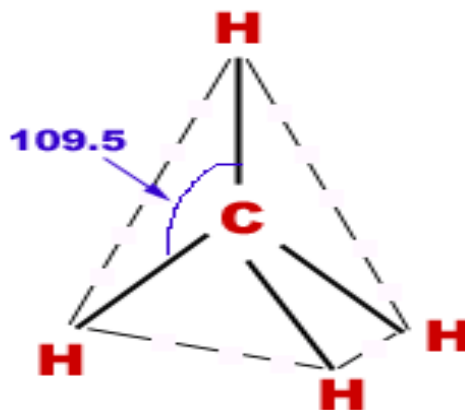


Fig 2-1 Structure of methane

Carbon dioxide is a molecule with the molecular formula CO_2 . The linear molecule consists of a carbon atom that is doubly bonded to two oxygen atoms, $\text{O}=\text{C}=\text{O}$ (Fig 2-2).

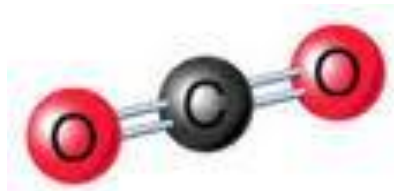


Fig 2-2 Structure of carbon dioxide

Although carbon dioxide mainly consists in the gaseous form, it also has a solid and a liquid form. It can only be solid when temperatures are below $-78\text{ }^{\circ}\text{C}$. Liquid carbon dioxide mainly exists when carbon dioxide is dissolved in water. Carbon dioxide is only water-soluble, when pressure is maintained. After pressure drops the CO_2 gas will try to escape to air. This event is characterized by the CO_2 bubbles forming into water.

Table 2-2 Properties of carbon dioxide

Property	Value
Molecular weight	44.01
Specific gravity	1.53 at $21\text{ }^{\circ}\text{C}$
Critical density	468 kg/m^3
Concentration in air	$370,3 * 10^7\text{ ppm}$
Stability	High
Liquid	Pressure $< 415.8\text{ kPa}$
Solid	Temperature $< -78\text{ }^{\circ}\text{C}$
Henry constant for solubility	$298.15\text{ mol/ kg * bar}$
Water solubility	$0.9\text{ vol/vol at } 20\text{ }^{\circ}\text{C}$

Carbon dioxide, CO_2 , is one of the gases in our atmosphere, being uniformly distributed over the earth's surface at a concentration of about 0.033% or 330 ppm. Commercially, CO_2 finds uses as a refrigerant (dry ice is solid CO_2), in beverage carbonation, and in fire extinguishers. Because the concentration of carbon dioxide in the atmosphere is low, it is not practical to obtain the gas by extracting it from air. Most commercial carbon dioxide is recovered as a by-product of other processes, such as the production of ethanol by fermentation and the manufacture of ammonia. Some CO_2 is obtained from the combustion of coke or other carbon-containing fuels.

Carbon dioxide is released into our atmosphere when carbon-containing fossil fuels such as oil, natural gas, and coal are burned in air. As a result of the tremendous world-wide consumption of such fossil fuels, the amount of CO₂ in the atmosphere has increased over the past century, now rising at a rate of about 1 ppm per year. Major changes in global climate could result from a continued increase in CO₂ concentration. In addition to being a component of the atmosphere, carbon dioxide also dissolves in the water of the oceans. At room temperature, the solubility of carbon dioxide is about 90 cm³ of CO₂ per 100 mL of water [2].

2.3 Thermophysical properties of RTILs

2.3.1 Introduction

Knowing the thermophysical properties of organic chemicals is a prerequisite for many tasks met by chemical engineers and scientists; they have many applications in the chemical industry and, essentially, cover all aspects of chemical plant operation as well as product lifecycle [87]. An example of such a task includes behavior in chemical separation, distribution between environmental compartments, predicting a chemical's bioactivity and bioavailability [88]. Industrial uses of thermophysical properties have been motivated by the definite or anticipated need. If improved properties can help avoid steps in the development of a new chemical process or product, they can have an enormous impact not only in terms of reduced development costs but also in terms of faster sales and higher profit margins[87]. Thermophysical properties affect all aspects of the chemical industry. As well as having impact in the design and operation of processes, the importance of thermophysical properties in product design, green and environmental engineering, applied nanotechnology/material science, and biotechnology was recently elucidated. The increasing importance for accurate thermophysical properties data due to increasing capability and complexity of chemical process simulation software, trends in process simulation applications, and nontraditional applications of thermophysical properties [87, 89]. The requirement for reliability and accuracy varies depending on the

application. For instance, for the design of separation processes the issue is sensitive, as often more than 40 % of the process cost is related to the separation units [89]. Due to the diversity of products and applications, the need for accurate and reliable thermophysical properties and transport property data, over a wide range of mixtures and conditions, is apparent [89].

Utilizing RTILs is one of the goals of green chemistry because they create a cleaner and more sustainable chemistry and are receiving growing attention as environmental friendly solvents for many synthetic and catalytic processes [90]. A fascinating characteristic is to fine tune the thermophysical properties by suitable choice of cations and anions [91]. Therefore, RTILs have been known as “designer-solvents” [90]. To optimize the use of and design the desirable RTILs, knowledge of the thermophysical properties of RTILs is essentially important. From the industrial viewpoint, a fundamental understanding of the thermophysical properties of RTILs should be known before its industrial application.

Thermophysical properties such as melting point, density, and viscosity, are related to the mechanical and engineering components associated with a process [92]. For academic research, thermophysical properties are also essential to validate the theoretical models or select proper RTILs. For example, densities and viscosities determine important parameters including rates of liquid-liquid phase separation, mass transfer, power requirements of mixing, and pumping. Other thermophysical properties, such as refractive index, are related to certain chemical properties despite providing a bulk property description [92]. Most of the recent work with RTILs has focused on the characterization and application of certain kinds of RTILs, and provided a large amount of useful data as well as regulations. However, there is not a comprehensive database publicly available for researchers to consult. Although there are some data of RTILs from some databases, the data are limited and most of them are Br^- , Cl^- , BF_4^- and PF_6^- . There are also IL databases developed by companies such as Merck, but these are not complete and most of them are products of company [90]. The establishment of the thermophysical properties database will definitely promote the research and development of ILs. It was reported that there is a demonstrable lack of the thermophysical properties data and some entries listed several data reported

from different sources with great deviations [90]. So, more attention should be paid on the measurement of thermophysical properties RTILs.

2.3.2 Density

The density, ρ , is elementary physical property of matter. For a homogeneous object it is defined as the ratio of its mass to its volume, numerically it represents the mass per unit volume of matter. The volume of an object increases with increasing temperature, because of the matter's volumetric thermal expansion. Therefore, the density of an object depends on its temperature, higher temperature resulting in lower density [93].

Density has probably been the most widely studied thermophysical property of RTILs because of its high significance and experimental accessibility [94, 95]. The molar volumes, standard entropy and crystal energy values of RTILs could be estimated using the density values [96-99]. Early attempts to measure density of RTILs resulted in large differences among the results obtained by other researchers, which have been accounted for by an unusually strong influence of impurities on density [100]. The magnitude of density, in the case of RTILs depends on the constituent cation and anion. For instance, the densities of RTILs vary with the alkyl chain length and also depend upon the nature of the anion. As a thumb rule, the density of comparable RTILs decreases with the increase in the bulkiness of the organic cation and the choice of the anion [101]. Further, density of RTILs decreases linearly with increasing temperature but at a rate less than that for molecular organic solvents [90].

Recently, Tariq, M. *et al.*[102] present the density of several ILs such as 1-alkyl-3-methylimidazolium bis(trifluoromethylsulfonyl) imide $[C_n\text{mim}]\text{NTf}_2$ ILs (with $n = 2, 4, 6, 8, 10, 12, 14$; where n is the number of carbon atoms of the alkyl chain); 1-alkyl-3-methylimidazolium hexafluorophosphate $[C_n\text{mim}]\text{PF}_6$ ILs (with $n = 4, 6, 8$); trihexyl(tetradecyl) phosphonium $[\text{P}_{6,6,6,14}]$ -based ILs (with the anions bis(trifluoromethylsulfonyl)amide $[\text{NTf}_2]$, acetate $[\text{OAc}]$, and triflate $[\text{OTf}]$); and $[\text{C}_4\text{mim}]$ -based ILs (with anions $[\text{OAc}]$, $[\text{OTf}]$, methylsulfate $[\text{MeSO}_4]$, and tetrafluoroborate $[\text{BF}_4]$). The data obtained were analysed to determine the effect of

temperature, the role of the alkyl side-chain length of the $[C_n\text{mim}]$ cation, and the influence of the nature of the anion.

Density data sets of ILs formed by imidazolium cations paired with dicyanamide (DCA^-), tetrafluoroborate (BF_4^-), thiocyanate (SCN^-), methylsulfate (MeSO_4^-) and trifluoroacetate (TFA^-) anions were reported by Sanchez, L. G. *et al.* [103]. The methylsulfate anion showed highest density followed by tetrafluoroborate and then by the thiocyanate anion. The lowest densities were observed with the dicyanamide anion. The densities increase with increasing molecular weight of the anion. However, the density of the ILs with thiocyanate as anion is higher than that of the ILs with the dicyanamide anion. Similar behavior was reported for other imidazolium cations, where the increase of the liquid density does not directly correspond to a rise in the molecular weight of the anion [104]. The density of the $[C_n\text{mim}]$ -based ILs decreases when the alkyl chain length on the imidazolium cation increases [103, 105].

A density data for a series of imidazolium salts with the nitrile functional group attached to the alkyl side chain, $[C_n\text{CNmim}][X]$ (where $C_n\text{CNmim}$ is the 1-alkylnitrile-3-methylimidazolium cation and $C_n = (\text{CH}_2)_n$, $n = 1-4$; $X = \text{Cl}$, PF_6 , and BF_4) and $[C_3\text{CNdmim}]X$ (where $C_3\text{CNdmim}$ is the 1-alkylnitrile-2,3-dimethylimidazolium cation and $C_n = (\text{CH}_2)_n$, $n = 3$; $X = \text{Cl}$, PF_6 , and BF_4), have been reported by Zhao, D. [41]. The densities of the alkylnitrile ILs are higher than those of the nonfunctionalized analogues. Incorporating the nitrile group serves to increase the density of the IL [41, 106]. The densities of the nitrile-functionalized ILs decreases as the alkyl chain linking the nitrile group and the imidazolium ring increases; the densities of $[C_2\text{CN Mim}]\text{BF}_4$, $[C_3\text{CN Mim}]\text{BF}_4$ and $[C_4\text{CN Mim}]\text{Cl}$ are (2.15, 1.87 and 1.61) $\text{g}\cdot\text{cm}^{-3}$ respectively [41]. The densities of a series of ILs based on nitrile-functionalized imidazolium and pyridinium as cations and chlorides, tetrafluoroborate, hexafluorophosphate, dicyanamide, and bis-(trifluoromethanesulfonyl)imide as anions has been reported by Zhang, Q. *et al.*[106]. The densities of these ILs showed that the density of $[C_3\text{CNMIm}]\text{NTf}_2$ ($1.519 \text{ g}\cdot\text{cm}^{-3}$) is much higher than that of $[C_3\text{CNMIm}]\text{N}(\text{CN})_2$ ($1.165 \text{ g}\cdot\text{cm}^{-3}$); the densities of $[C_3\text{CNMIm}]\text{N}(\text{CN})_2$, $[C_3\text{CNMMIm}]\text{N}(\text{CN})_2$, and $[C_3\text{CNPy}]\text{N}(\text{CN})_2$ ranged from

1.165 to 1.168 g·cm⁻³, indicating that the impact of the anions on density is stronger than that of cations [106].

The densities of the dicationic phosphonium-based ILs are highest when compare with the monocationic phosphonium-based IL. The decrease in density with increasing spacer alkyl chain length has been reported for a large series of dicationic ILs (DILs) [50].

Tariq, M. *et al.* [102] reported the density data for [P_{6,6,6,14}]⁺NTf₂⁻ and [P_{6,6,6,14}]⁺OTf₂⁻; (1.0654 and 0.9823) g·cm⁻³ respectively, while Yua, G. *et al.* [50] reported the density of the trioctylphosphonium-based monocationic ILs; density for [P_{8,8,8,8}]⁺NTf₂⁻ and [P_{8,8,8,8}]⁺dithiomalenitrile is (1.07 and 0.946) g·cm⁻³ respectively [50]. The densities of trioctylphosphonium and triethylphosphonium-based monocationic are lower compared to the phosphonium ILs with short alkyl chains due to the increasing of free volume which resulted from alkyl chain length; the density of [P_{2,2,2,8}]⁺NTf₂⁻ and [P_{2,2,2,12}]⁺NTf₂⁻ are (1.26 and 1.21) g·cm⁻³ respectively [102].

2.3.3 Viscosity

Viscosity is an important physical property for a number of processes. For instance, it determines the force and energy required to transfer and mix the IL with other substances. It appears in many dimensionless groups used in mass- and heat-transfer correlations [107, 108]. The viscosities of a variety of RTILs based on the imidazolium cation with a series of anions were reported [108, 109]. Most ILs are more viscous than common molecular solvents, the viscosity behaviour was attributed to the types of interaction between the ions in the RTIL and influenced by hydrogen bonding and Van der Waals interactions, which in turn is strongly dependent on the type of anion present [109]. Watanabe and coworkers [110] hypothesized that some of the differences observed in the transport properties of the RTILs may be due to different levels of “ionicity” (association/disassociation) that they elucidated from diffusion and ionic conductivity data [108].

Zhao and coworkers [41] reported the viscosities of methylimidazolium-based ILs with nitrile functionality such as; [C₂CNmim]BF₄, [C₃CNmim]BF₄, [C₄CNmim]Cl, [C₄CNmim]PF₆ and [C₄CNmim]BF₄ (the viscosity is (65, 230, 5222, 2181 and 552.9) mPa·s). Furthermore, Zhang, Q. *et al.* [106] reported the viscosities of methylimidazolium/1,2-dimethylimidazolium/pyridinium-based ILs incorporating the nitrile functionality and BF₄, NTf₂ and N(CN)₂ anions (the viscosity of [C₃CNMIIm]BF₄, [C₃CNMIIm]NTf₂, [C₃CNMIIm]N(CN)₂, [C₃CNMMIIm]NTf₂, [C₃CNMMIIm]N(CN)₂, [C₃CNPy]NTf₂ and [C₃CNPy]N(CN)₂ is 352, 286, 206, 506, 5255, 409 and 152 mPa·s respectively). Torrecilla, J. S. *et al.* [105] reported that the viscosity values of [C_nmim]CH₃SO₄ ILs with *n* = 1, 4 and 6 are 75.5, 213 and 383 mPa·s, respectively. Also reported that the viscosity decreases as temperature increases, rises with the alkyl chain length of the cation and ILs based on higher anion sizes present higher viscosity values.

The viscosity values of the imidazolium-based RTILs incorporating the nitrile functionality are higher than those of the corresponding ILs without nitrile group [41] and these values increase as the alkyl chain of the cation increases as observed by Tokuda *et al.* [111]. Even though the viscosities are high, the effect of shear rate on viscosities was investigated and the ILs is classified as either Newtonian fluid or a thixotropic fluid. For the present ILs the shear rate has no difference in the viscosity but longer alkyl chains show non-Newtonian behavior [92].

Phosphonium based ILs tend to have viscosities somewhat higher than their ammonium counterparts [112]. Furthermore, quaternary phosphonium cations themselves also contributed to reducing viscosity [113]. Sesto and coworkers [114] reported the viscosity values of [P_{6,6,6,14}], [P_{8,8,8,14}] and [P_{4,4,4,14}] incorporating NTf₂ anion; 450, 418 and 464 cP and also incorporating dithiomaleonitrile anion 4780, 5590 and 7480 cP. The viscosity values of the DCILs are much higher comparable to monocationic ILs and phosphonium-based monocationic ILs; the viscosities of [P_{6,6,6,14}]NTf₂, [P_{2,2,2,5}]NTf₂ and [P_{2,2,2,12}]NTf₂ is 450, 88 and 180 mPa·s respectively [111]. For the DCILs, the viscosity values increases as the spacer alkyl chain length increase as observed by Tokuda *et al.* [115]. The high viscosity of the DCILs was attributed to an increase in van der Waals forces, hydrogen bonding between cationic

protons and anionic halides the symmetry of the cations and anions [92]. Jared and coworkers [51] also reported the effect of spacer alkyl chain on the viscosity of $C_3(\text{mim})_2\text{-NTf}_2$, $C_6(\text{mim})_2\text{-NTf}_2$, $C_9(\text{mim})_2\text{-NTf}_2$ and $C_{12}(\text{mim})_2\text{-NTf}_2$ (the viscosity values are 249, 362, 443, and 606 cP). The viscosities of a series of DCILs range from (241 to 1217) cSt were reported by Payagala, T. *et al.*[116]. The viscosities of some DCILs lie within the general monocationic ILs range and some extend beyond the commonly observed values. The viscosities are exceptionally high for DCILs incorporating benzyl groups, probably because of the added intermolecular π - π interactions [116].

2.3.4 Refractive index

The refractive index is related to the excess molar refraction which is used in the least squares energy relationships (LSERs) as a predictor of solute distribution [50]. Also, the relation between the refractive index and the polarizability constitute a measure of the importance of the dispersion forces to the cohesion of the liquid (solvents with a large index of refraction should be capable of enjoying strong dispersion forces). In addition, the values of refractive index are regarded as a measure of the relative extent of the polar domains in the IL [102]. Brocos, P. *et al.* and Deetlefs, M. *et al.*[117, 118] studied the relation between the molar free volume and refractive index and reported that the unoccupied part of the molar volume of a substance, has smaller refractive index.

Hasse, and coworkers [119] measured the refractive index for the ILs $[\text{Emim}]\text{MeSO}_3$ and $[\text{Emim}]\text{OcSO}_4$ in the temperature range from 283.15 to 313.15 K at atmospheric pressure. The results showed that increasing the alkyl chain of the anion decrease the refractive index. Tariq, M. *et al.* [102] reported that the refractive index of $[\text{P}_{6,6,6,14}]\text{OTf}$ and $[\text{P}_{6,6,6,14}]\text{NTf}_2$ is 1.4585 and 1.4587. As expected, the refractive index values decrease almost linearly with increasing temperature and also decrease with increasing the spacer alkyl chain length. The refractive index values are depend on the anion and the results follow the trend: $[\text{PF}_6] < [\text{BF}_4] < [\text{NTf}_2] < [\text{OTf}] < [\text{MeSO}_4] < [\text{OAc}]$ both in the $[\text{C}_4\text{mim}]^+$ based ILs and in the $[\text{P}_{6,6,6,14}]^+$ based liquids [83, 102].

Zhang *et al.* [106] presented the refractive index for nitrile functionalized ILs; for $[\text{C}_3\text{CN Mim}]\text{NTf}_2$ and $[\text{C}_3\text{CN Mim}]\text{BF}_4$ are 1.4398 and 1.4349 respectively. The refractive index values are increases after the incorporation of nitrile group. Breitbach, Z. S and Armstrong D. W.[120] showed that the refractive indices of $[\text{P}_{6,6,6,14}]$ incorporating the anions Cl, BF_4 , TfO, NTf_2 and $\text{N}(\text{CN})_2$ 1.4841, 1.4564, 1.4585, 1.4507 and 1.4840 respectively. They also reported the refractive index of dicationic ILs such as; $[\text{C}_{12}(\text{P}_{3,3,3})_2]\text{NTf}_2$ and $[\text{C}_{12}(\text{mim})_2]\text{NTf}_2$ are 1.4514 and 1.443 respectively.

2.3.5 Thermal stability

Thermal stability is a significant factor that determines the applicability of ILs for specific applications. Onset and decomposition temperatures of several ILs determined using scanning thermogravimetric analysis method were reported [121, 122]. The long-term isothermal stabilities of $[\text{C}_4\text{mim}]\text{NTf}_2$, $[\text{C}_6\text{mim}]\text{PF}_6$ and $[\text{C}_8\text{mim}]\text{PF}_6$ were investigated and the results showed that these IL's decompose at a faster rate with increasing temperature [123]. Additionally, thermal decomposition is strongly dependent on the structure of ILs.

Different from organic solvents, many kinds of ILs can be kept in the liquid state above 400 K with decomposition temperature ranging from 600 to 700 K, which make them have excellent catalytic activity. Generally, the imidazolium cations tend to be thermally more stable than the tetra-alkyl ammonium cations. For common anions, the onset of thermal decompositions is $\text{NTf}_2 > \text{BF}_4 > \text{PF}_6 > \text{halides}$, with a large effect on going to ILs containing halides anions [124]. High thermal stability is provided by certain kinds of anions such as $(\text{CF}_3\text{SO}_2)_2\text{N}$ and $(\text{C}_2\text{F}_5\text{SO}_2)_2\text{N}$ [90]. Large onsets for the decomposition temperatures were also reported for pyridinium or tetraalkylphosphonium based ILs. The onset of thermal decomposition for the common ILs based in the alkylimidazolium cation showed that the nature of the anion has great effect in this property, whereas the effect of the cation is much lower [124].

Thermal stabilities of RTILs are affected slightly by the size of the alkyl chain of the cation and the nitrile group; the decomposition temperature decreases as the alkyl

chain increases (the decomposition temperatures of $[P_{2,2,2,8}]NTf_2$ and $[P_{2,2,2,12}]NTf_2$ are 380 and 400 °C respectively) and also with incorporation of a CN group [51, 106, 113]. However, the incorporation of a CN group made the ILs more reactive than the ILs without a CN group. The decomposition temperatures of ILs incorporating CN group were less in comparison with the corresponding ILs without a CN group (T_d of $[C_4Mim]Cl$, $[C_6Mim]Cl$ and $[C_8Mim]Cl$ is 254, 253 and 243°C respectively) [92].

Breitbach, Z. S. and Armstrong, D. W. [120] reported the thermal stability for many ILs. The results showed that phosphonium-based ILs are more stable compare with nitrogen-based ILs whether it is mono or dicationic ILs. The dicationic phosphonium ILs showed increasing of thermal stability possessing decomposition temperatures up to 425 °C and liquid ranges well over 400 °C.

2.3.6 Derived thermodynamic properties

The high-precision measurement of density over extended range of temperatures allowed estimating thermal expansion coefficients. In spite of the volumetric “good-behavior” of RTILs, different ILs exhibit different rates of expansion as temperature is progressively distanced from ambient conditions [125]. Moreover, according to Glasser [98, 99] the standard entropy and crystal energy for RTILs can be estimated from the experimental values of density and molecular weight.

The thermal expansion coefficient of the RTILs is lower than most of the molecular organic liquids. For the alkyimidazolium tetrafluoroborate liquids, the thermal expansion coefficient decreases as the length of the substitute chain on the cation decreases. Additionally when comparing the ILs with the same anion and with a butyl and methyl-alkyl chain appended to the cation, the thermal expansion coefficient increases as follows: $BMIM^+ > BMPy^+ > BMPyrr^+$ [126].

Thermal expansion coefficients of $[C_4mim]NTf_2$, $[C_4mim]dca$ and $[C_2mim]EtSO_4$ ILs in temperature range of 293.15 to 363.15 K⁻¹ are in the range of 4.8 to 6.6×10^{-4} K⁻¹ as presented by Carlos and coworkers [126]. Kilaru, P. and coworkers [127] presented the thermal expansion coefficients of the phosphonium-based ILs, for

[P_{6,6,6,14}NTf₂, [P_{6,6,6,14}DBS and [P_{6,6,6,14}DEP are 5.71, 5.77 and 6.03·10⁻⁴ K⁻¹ respectively, and ammonium-based ILs, for [N_{4,1,1,3}NTf₂, [N_{6,1,1,3}NTf₂ and [N_{10,1,1,3}NTf₂ are 5.79, 5.88. 5.82 × 10⁻⁴ K⁻¹ respectively. In the case of [Bmpy]NTf₂ the thermal expansion coefficient varies between 6.32·10⁻⁴ and 6.34 × 10⁻⁴ K while for [P_{6,6,6,14}DCA the variation is between 6.51· 10⁻⁴ and 6.29 × 10⁻⁴ K⁻¹ in the working temperature range [128]. The values of thermal expansion coefficient for a series of imidazolium-, pyridinium-, phosphonium- and ammonium – based ILs was reported in the range of 5.0 × 10⁻⁴ to 6.5 × 10⁻⁴ K⁻¹ [94, 127]. Moreover, Guan, W. and coworkers [125] reported the thermal expansion coefficient of the amino acid IL [C₃mim]Glu was 3.28 × 10⁻⁴ K⁻¹.

Absolute standard entropy represents thermodynamic data of special significance, forging the link between enthalpy and Gibbs energy, which is the true arbiter of chemical equilibrium and stability in processes whose outcome is determined by thermodynamic (as opposed to kinetic) considerations[98]. Standard absolute entropies of many materials are unknown which precludes a full understanding of their thermodynamic stabilities. It is useful to estimate standard entropy data for several reasons. First, there is a paucity of standard entropy data for inorganic materials in standard thermochemical tables. Second, experimental determination of absolute entropy calorimetry is both a lengthy and nontrivial procedure; such measurements are no longer fashionable science and, for this reason, increasing reliance has to be placed on estimation techniques for thermochemical data [98]. Glasser, L. and Jenkins, H. D. B. [98, 99] showed that formula unit volume, V_m, can be employed for the general estimation of standard entropy values for materials of varying stoichiometry, through a simple linear correlation between entropy and molar volume. Few literatures are available for the standard entropy of RTILs.

Guan, W. and coworkers [125] reported that the standard molar entropy of the amino acid ILs, [C_nmim][Glu] where n = 1-6, are in varied from 417.9 to 589.3 J·K⁻¹·mol⁻¹, the value was increased with the increase of the alkyl chain length. The standard entropy values for a series of ILs based on, [C_nmim] (where n = 2,3,4,5,6) incorporating alanine and glycine anions were reported by Fang, D. W. and

coworkers [97]. The values range from 396.9 to 535.5 $\text{J}\cdot\text{K}^{-1}\cdot\text{mol}^{-1}$ and (360.2 to 498.8) $\text{J}\cdot\text{K}^{-1}\cdot\text{mol}^{-1}$ for $[\text{C}_n\text{mim}]\text{Ala}$ and $[\text{C}_n\text{mim}]\text{Gly}$ respectively.

Glasser, L. [99] illustrate that the lattice energy of RTILs can be expressed in terms of the density. It was presented that the densities of the condensed melt and solid phases are very similar, and so the calculated lattice potential energies may well be applied to phase of the material, with the difference between the values generated resulting from the change in density and corresponding to the energy of the phase transition.

The lattice energy for fused CsI is $602.5 \text{ kJ}\cdot\text{mol}^{-1}$ which is the lowest crystal energy among alkali-chlorides[97], the low crystal energy is the underlying reason for forming ILs at room temperature as pointed by Krossing [129]. Only few researchers report the crystal energy of the RTILs. Guan, W. and coworkers [125] reported that the crystal energy of the amino acid ILs, $[\text{C}_n\text{mim}][\text{Glu}]$ where $n = 1-6$, are in varied from 410 to 450 $\text{kJ}\cdot\text{mol}^{-1}$, the value was decreased with increasing the alkyl chain length. Fang, D. W. and coworkers [97] presented the crystal energy values for a series of ILs based on, $[\text{C}_n\text{mim}]$ (where $n = 2,3,4,5,6$) incorporating alanine and glycine anions The values range from (421 to 456) $\text{kJ}\cdot\text{mol}^{-1}$ and (429 to 469) $\text{kJ}\cdot\text{mol}^{-1}$ for $[\text{C}_n\text{mim}]\text{Ala}$ and $[\text{C}_n\text{mim}]\text{Gly}$ respectively. All the reported crystal energy values of the RTILs were lower than the lowest crystal energy values among alkali-chlorides.

Molar refraction is a measure of the total polarizability of a mole of a substance and is dependent on the temperature, the refractive index and the pressure, it can be interpreted as the hard-core volume, i.e., an approximate measure of the total volume (without free space) of molecules in one mole of the compound [130]. The molar refraction values for RTILs is generally estimated using Lorentz–Lorenz relationships [102].

The molar refraction of few ILs was reported, for $[\text{C}_4\text{Mim}]\text{PF}_6$, $[\text{C}_6\text{Mim}]\text{PF}_6$, $[\text{C}_8\text{Mim}]\text{PF}_6$, $[\text{C}_4\text{mim}]\text{BF}_4$ and $[\text{C}_8\text{mim}]\text{Cl}$ the molar refraction is 51.46, 60.69, 70.29, 47.84 and 67.91 $\text{cm}^3\cdot\text{mol}^{-1}$ respectively [102, 131]. The results showed that an increase in the alkyl chain length ($[\text{BEpyr}]\text{ESO}_4$, $[\text{EMpyr}]\text{ESO}_4$ means a slight increase in the values of the molar refractions and the anion effect was in order of Cl^{-1}

> [PF₆⁻ > BF₄⁻ [132]. Tariq, M. *et al.* [102] reported the molar refraction of a number of imidazolium and phosphonium-based ILs. They showed the molar refraction of [C_nmim] incorporating different anions, the effect of these anions is in the order NTf₂ > OTf > PF₆ > MeSO₄ > BF₄ > OAc and the molar refraction values increased from 74.91 ([C₂mim]NTf₂) to 112.02 ([C₁₂mim] NTf₂). Moreover, the molar refraction values of the phosphonium-based ILs [P_{6,6,6,14}] incorporating NTf₂, OTf and OAc are 192.57, 175.69 and 173.57 cm³·mol⁻¹ respectively.

2.4 Solubility of CO₂ in ILs

2.4.1 Introduction

The world consumption of natural gas has grown significantly over the last years and it is considered as the most environmentally friendly fossil fuel, because burning of it leads to negligible SO₂ emissions, low nitrous oxide levels, and less than half of the CO₂ emissions in comparison to coal or oil [12]. However, the remarkable challenge is that raw natural gas is contaminated with undesired components, such as hydrogen sulfide and carbon dioxide. Removal of contaminants from raw natural gases has to be performed not only because of environmental restrictions but also considering technological problems during gas transportation and commercialization [12]. Development of solvents that contribute to the process economy as well as production sustainability by lowering the solvent inventory and reducing the discharges of volatile chemicals to the atmosphere is required for the improvement of gas absorption processes [39].

Physical and chemical absorption processes are extensively used for the removal of CO₂ from natural gas, petroleum and chemical industries. Physical absorption is preferred when acid gases (H₂S, CO₂) are present at high concentration in the gas stream. Physical solvents are non-reactive polar organic compounds with an acid gas affinity such as methanol, propylene carbonate, sulfolane, N-formyl morpholine, N-methylpyrrolidone which are used as solvents in physical absorption processes. For chemical absorption processes, aqueous solutions of primary, secondary, tertiary,

hindered amines and amine mixtures are the most widely used solvents. Moreover, about 75–90% of the CO₂ is captured using a monoethanolamine (MEA)-based technology [133].

The major drawbacks of the traditional gas absorption separation processes are mainly caused by the nature of the solvent, and the type of interactions given between the solute and the solvent. In an industrial gas absorption process, it is desirable to achieve fast absorption rates and high solute capacities into a solvent that is easily regenerated with minimized volume make-up [133]. There are some disadvantages in commercial use of these amine solutions [9], including high energy consumption during regeneration, degradation of amine reagents to form corrosive byproducts, loss of amine reagents and transfer of water into the gas stream during the desorption stage, and as well as insufficient carbon dioxide capture capacity [9, 134]

A promising alternative for CO₂ capture from natural gas is the use of ILs (ILs) as absorbents [14, 135]. Considering that IL properties can be tailor-designed to satisfy the specific application requirements, the use of ILs for CO₂ capture has received enormous interest in the last few years because of their unique characteristics and high solubility of CO₂ (in terms of mole fractions) [12, 136]. ILs have adjustable physicochemical properties, negligible vapor pressure, wide liquid range, and are stable at temperatures up to several hundred degrees centigrade, which make them suitable candidates for CO₂ capture [12, 137]. Most of the ILs-CO₂ interaction is due to its quadrupole moment and dispersion forces (in the case of physisorption), with a weak Lewis acid-base which results in decreasing the heat required for the regeneration process [12]. In addition, recent studies reported a better performance for ILs in comparison to amine-based absorption processes at selected constant process parameters. Additionally, ILs performance could be improved through the suitable selection of anion/cation combinations and functional group that would lead to better absorption ability [12, 138]. It was reported that the engineering design estimation indicate that the investment for the IL process will be 11% lower than the amine based process and provide a 12% reduction in equipment footprint. A parametric study examined four improvements in the IL technology, which may reduce even further the energy and cost required for CO₂ capture.

2.4.2 Methods for measuring Solubility of CO₂ in ILs

There are many techniques can be uses to measure the solubility of a gas in a liquid, the most important are the volumetric, the gravimetric and the NMR spectroscopic methods [4, 37].

In the volumetric method, large amount of solvent is required compare to the gravimetric method and the amount of dissolved gas is determined volumetrically either during absorption or desorption. There are many high-precision gas solubility studies known where this method was applied [4]. The gravimetric method needs only small amounts of the solvent, and it can provide data of excellent quality, in particular when the gas solubility is sufficiently high and the volume expansion of the liquid remains small, in this method a high-resolution balance is applied to determine the increase of mass when a gas is dissolved in a liquid at preset temperature and pressure. A very fast, but less accurate technique is the NMR-spectroscopic method; it is mostly used to screen solvents for gases [139].

2.4.3 Effects of ILs structures on CO₂ solubility

The first measurement of high physical CO₂ solubility in an IL was reported in 1999 [140]. Subsequently, there have been numerous studies of the solubility of CO₂ in a wide variety of ILs.

Solubility data of CO₂ in different imidazolium-based ILs are the most often found in literature especially the case for [Bmim]BF₄ and [Bmim]PF₆ because those ILs were among the first ones commercially available [39] and their observed affinity toward CO₂ [12]. Many attempts to improve the solubility of CO₂ in the imidazolium ILs were results in using different anions, different alkyl chains and functionalized cations. The solubility of CO₂ and other light gases in [C_nmim]X RTIL solvents has been under investigation for several years [141]. Moreover, the origin of interaction between CO₂ and imidazolium groups was investigated [12].

Imidazolium-based RTILs at their core are derived from imidazole, an inexpensive and highly versatile starting material. A large number of imidazole

derivatives are commercially available, and the chemistry to customize and transform imidazoles into different imidazolium-based RTILs is usually straightforward [141]. The possibility to increase the carbon dioxide uptake by an IL relying on physical interactions only was proven by Almantariotis, D. and coworkers [142].

2.4.3.1 Effect of the cation

Experimental and molecular modeling studies to investigate the underlying mechanisms for the high solubility of CO₂ in imidazolium-based ILs was conducted by Cadena, C. *et al.* [143]. The CO₂ absorption in six different ILs at 10, 25, and 50 °C are reported, two different cations differ only in the nature of the “acidic” site at the 2-position on the imidazolium ring and NTf₂, PF₆ and BF₄ anions were used. The simulation results are consistent with the experimental finding that, for a given anion, there are only small differences in CO₂ solubility for the two cations [143]. Moreover, Huang, J. and Ruether, T. [144] reported that CO₂ is absorbed in ILs by occupying the free space between the ions through physical absorption mechanisms. Moreover, the overall absorption capacity could be improve by attaching functional group to the ions.

The solubility of CO₂ in imidazolium-based ILs incorporating alkyl chains varied between ethyl and octyl was tested [142, 145]. It was observed that Henry’s constant for the studied ILs decrease gradually from (39 to 30) bar. Also, Peters *et al.* showed that the solubility of CO₂ in [Hmim] is higher than that in [Emim] salt [146]. The solubilities of CO₂ in n-alkyl-3-methyl-imidazolium bis(trifluoromethylsulfonyl) imide ILs (n = 2, 6, 10) were measured in a temperature range from (298.15 to 343.15) K and pressure up to 25 MPa. The effects of the cation on the phase behavior and CO₂ solubility showed that the longer alkyl chain lengths increase the CO₂ solubility (Fig 2-3) [142, 147]. Moreover, other studies showed that CO₂ is more soluble in PF₆ - salt of the [Bmim] compound than that of the [Emim] derivative [146].

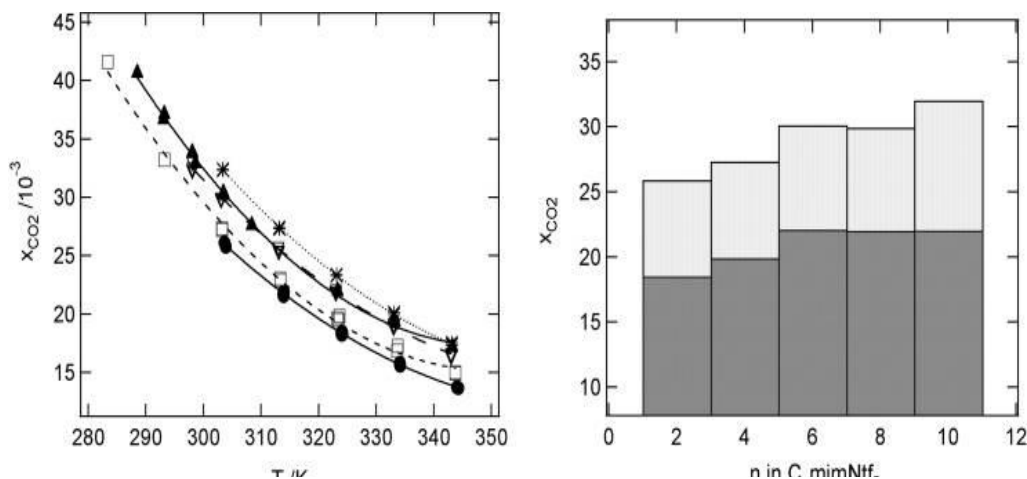


Fig 2-3 Carbon dioxide solubility in 1-alkyl-3-methylimidazolium bis(trifluoromethyl sulfonyl)amide ionic liquids as a function of the number of carbon atoms, n , in the alkyl-side chain. On the right: carbon dioxide solubility at 303 K in light gray and carbon dioxide solubility at 323 K in dark gray [142].

Cadena, *et al.* studied a series of imidazolium-based ILs incorporating methyl group at the C2 atom to investigate the responsibility of the acidic proton of the imidazolium ring located at C2 in the CO₂- IL interaction [143]. The modification of the structure of the cation leads to a small decrease (1-3 kJ/mol) in the enthalpy of absorption [12]. The influence of changing the cation of the IL (IL) on CO₂ solubility was also studied by G. Hong, G. and coworkers [148]. The solubility of carbon dioxide in three ILs based on the [NTf₂] anion and 1-ethyl-3-methylimidazolium [C₁C₂mim], 1-butyl-1-methylpyrrolidinium [C₁C₄pyrr] and propylcholinium [N₁₁₃₂-OH] was investigated experimentally between 300 and 345 K. The effect of changing the cation is small but significant. The solubility of CO₂ in imidazolium-, and ammonium-based RTILs incorporating the [NTf₂] anion were studied by Kilaru, P. and Scovazzo, P. [149]. The results showed that the solubility increases in the order; [C₆mim] > [Emim] for imidazolium, and [N_{1,8,8,8}] > [N_{1,1,3,10}] > [N_{1,1,1,10}] > [N_{2,2,2,6}] > [N_{1,1,1,4}] for ammonium. In addition, the solubility of CO₂ in a Brønsted acid-base IL, [DMFH][NTf₂] was investigated at high pressures and at different temperatures. The results showed that the mole fraction solubility of CO₂ in [DMFH]NTf₂ was a slight higher than [Bmim]NTf₂ [150].

Fenga and coworkers [151] studied the solubility of CO₂ in a new type of solvents constitute of tetramethylammonium glycinate ([N_{1,1,1,1}]Gly), tetraethylammonium

glycinate ($[N_{2,2,2,2}]\text{Gly}$), tetramethylammonium lysinate ($[N_{1,1,1,1}]\text{Lys}$) and tetraethylammonium lysinate ($[N_{2,2,2,2}]\text{Lys}$) mixed with N-methyldiethanolamine (MDEA) for the uptake of CO_2 (Fig 2-4).

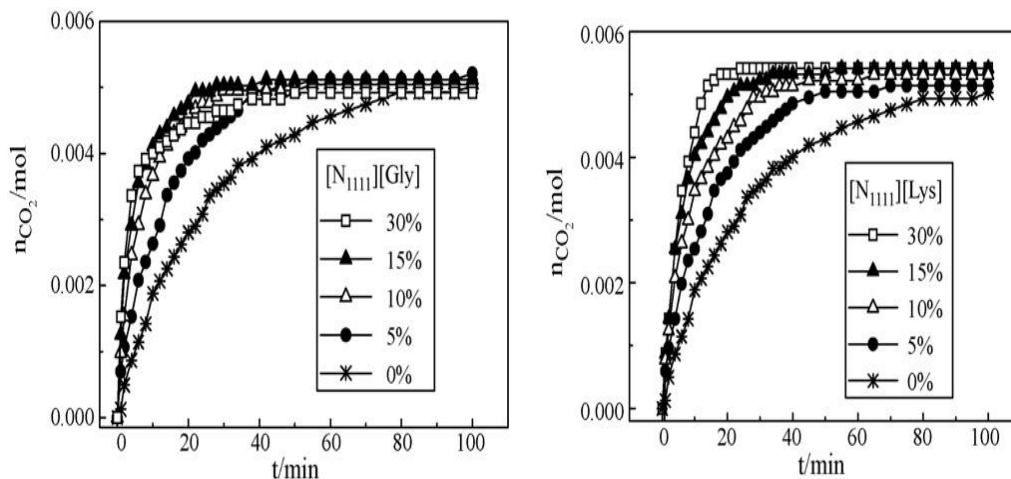


Fig 2-4 Absorption amount of CO_2 in aqueous solution of IL +MDEA with 30% total amines [151]

The solubility of CO_2 in these IL+MDEA aqueous solutions was investigated over a wide range of IL concentrations (5-100%), temperature (298–318 K) and partial pressure of CO_2 (4–400 kPa). It was found that the aqueous solutions of 15% IL and 15% MDEA had higher absorption rate and larger uptake than other IL + MDEA solutions of 30% total amines. The results indicated that IL could greatly enhance the absorption and increased the absorption rate of CO_2 in MDEA aqueous solutions. Noticeably, due to the two amino groups in a molecular, the mole absorption of the 30% lysine based ILs aqueous solutions was 0.98 ($[N_{1,1,1,1}]\text{Lys}$) and 1.21 ($[N_{2,2,2,2}]\text{Lys}$) mole CO_2 , being about 2–3 times the absorption capacity of MDEA under the same condition. Regeneration under the condition of temperature 353 K, 4 kPa for 240 min showed significant regeneration efficiency (over 98%).

The solubility of carbon dioxide in room temperature ILs (RTILs), dialkylimidazolium dialkylphosphates, was measured at temperature range of 313–333 K and at pressures close to atmospheric pressure, from which Henry's law coefficients, standard Gibbs free energy, enthalpy, and entropy changes of solvation

were derived. The CO₂ solubility in dialkylimidazolium dialkylphosphate was found to increase with increasing chain length of the alkyl groups on the cation and/or the anion as was similarly found in other RTILs [152], the solubility capacities were lower than that of 1-butyl-3-methylimidazolium bis(trifluoromethylsulfonyl)imide ([Bmim][NTf₂]) [152]. In addition, the solubilities of carbon dioxide, ethylene, ethane, methane, argon, oxygen, carbon monoxide, hydrogen, and nitrogen gases in 1-n-butyl-3-methylimidazolium hexafluorophosphate were presented. The results indicated that carbon dioxide have the highest solubility and strongest interactions with the IL, followed by ethylene and ethane. The solubilities exhibited a nonlinear trend as the CO₂ pressure was increased [81].

The solubility of CO₂ in phosphonium-based ILs has received little attention in spite of their interesting characteristics. The gas–liquid equilibrium of two ILs, trihexyltetradecylphosphonium bis(trifluoromethylsulfonyl)imide and trihexyltetradecylphosphonium chloride, in a wide range of temperatures, pressures showed that phosphonium ILs can dissolve even larger amounts of CO₂ (on a molar fraction basis) than the corresponding imidazolium-based ILs [153]. Furthermore, the solubility of CO₂ in sulfonate ILs (ILs), such as trihexyltetradecylphosphonium dodecylbenzenesulfonate ([P_{6,6,6,14}]C₁₂H₂₅PhSO₃) and trihexyltetradecylphosphonium methylsulfonate ([P_{6,6,6,14}]MeSO₃) was determined at temperatures ranging from (305 to 325) K and pressures ranging from 4 to 9 MPa. It was found that the different solubility of CO₂ in the two kinds of sulfonate ILs is not dramatic on the basis of molality. The solubility of CO₂ in [P_{6,6,6,14}]MeSO₃ is higher than in [P_{6,6,6,14}]C₁₂H₂₅PhSO₃. The Henry's law constant for CO₂ in all the investigated ILs increases with increasing temperature [154]. Furthermore, Ferguson, L. and Scovazzo, P. [155] presented the solubility, diffusivity, and permeability data for carbon dioxide, ethylene, propylene, butene, and 1,3-butadiene gases in five phosphonium-based ILs at 30 °C. The gas solubilities and diffusivities of the phosphonium-based ILs are of the same magnitude as the gas solubilities for the more familiar imidazolium-based liquids [155].

One of the common ways to increase the solubility of CO₂ in ILs is use of fluorinated cations [12]. The solubility of carbon dioxide in the IL 1-

(3,3,4,4,5,5,6,6,7,7,8,8,8-tridecafluorooctyl)-3-methylimidazolium bis(trifluoromethyl-sulfonyl) amide $[C_8H_4F_{13}mim][NTf_2]$ was studied (Fig 2-5).

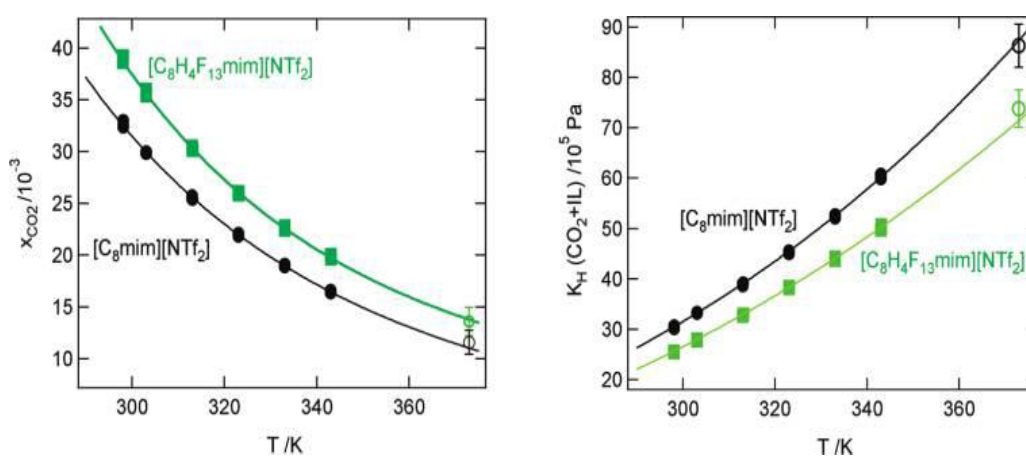


Fig 2-5 Effect of the partial fluorination of the cation on the carbon dioxide solubility in 1-methyl-3-octylimidazolium bis(trifluoromethylsulfonyl) amide ionic liquids as a function of temperature expressed as mole fraction of carbon dioxide at a partial pressure of 1 bar [142]

It was reported that the solubility increases as the fluorinated alkyl chain length increases, IL with longest fluoroalkyl chain exhibit highest CO₂ solubility [82, 142]. In addition, they reported that increasing the fluorinated alkyl chain in the imidazolium cation does not lead to a steady rise of the gaseous uptake by the liquid which may due to the increase of the nonpolar domains of the IL, carbon dioxide being solvated preferentially in the charged regions of the solvent [142]. Even though fluorination of cation and anion is a proven method of increasing the CO₂-philicity of compounds but the disadvantages associated with these fluorinated ILs are that they are very costly and environmentally less benign (high stability and low reactivity of the fluorinated compounds lead them to being poorly biodegradable and persistent in the environment [61, 156]).

2.4.3.2 Effect of the anion

It was reported that the anion has a dramatic effect in CO₂ solubility, which suggests that the nature of the anion has the key role in CO₂-IL interactions [143]. Some theoretical studies focusing on understanding the interactions between CO₂ and the anion suggested that there is an interaction between the CO₂ and the IL [157, 158].

The solubility of CO₂ in Emim-based ILs with different anions was studied to investigate the effect of the anion nature [159]. The results showed that the solubility decreases in the following order: Tf₂N⁻, dca⁻, OTf⁻, and Cl⁻. [159]. Moreover, The solubility of CO₂ in a series of 1-(2-hydroxyethyl)-3-methylimidazolium ([Hemim]⁺) based ILs (ILs) with different anions such as, PF₆⁻, OTf⁻, BF₄⁻ and NTf₂⁻ at temperatures ranging from 303.15 K to 353.15 K and pressures up to 1.3 MPa were determined. The results showed that the solubility of CO₂ in these ILs follows the order [Hemim]NTf₂⁻ > [Hemim]OTf⁻ > [Hemim]PF₆⁻ > [Hemim]BF₄⁻ [160].

The performance of a series of ILs that incorporate a nitrile- containing anion paired to 1-alkyl-3-methylimidazolium cations was studied by Mahurin, S. [161]. The results showed that the solubility, selectivity, and performance can be optimized for CO₂/N₂ separation through controlled introduction of the nitrile functionality into the anion, 1-ethyl-3-methylimidazolium tetracyanoborate, [Emim]B(CN)₄⁻, showed the highest performance with a magnitude 30% higher than that of the popular IL [Emim]NTf₂⁻. This same nitrile-bearing IL also exhibited a high CO₂/N₂ selectivity. The solubilities of carbon dioxide in the ILs with 1-alkyl-3-methylimidazolium cations and [PF₆]⁻, [BF₄]⁻ and [NTf₂]⁻ anions were experimentally studied (Table 2-3) by many researchers (the most studied ILs) at a large range of temperatures and pressures [162-165].

Table 2-3 Measured solubilities of carbon dioxide in ionic liquids at 298.15K [162]

[C ₆ mim]PF ₆		[emim]BF ₄		[C ₆ mim]BF ₄		[emim]Tf ₂ N		[C ₆ mim]Tf ₂ N	
<i>P</i> (MPa)	Mole fraction	<i>P</i> (MPa)	Mole fraction	<i>P</i> (MPa)	Mole fraction	<i>P</i> (MPa)	Mole fraction	<i>P</i> (MPa)	Mole fraction
0.296	0.058	0.251	0.033	0.312	0.071	0.213	0.050	0.164	0.069
0.347	0.063	0.349	0.046	0.406	0.085	0.298	0.070	0.242	0.093
0.408	0.078	0.436	0.056	0.504	0.103	0.397	0.100	0.337	0.118
0.470	0.091	0.531	0.068	0.597	0.119	0.503	0.122	0.433	0.142
0.520	0.100	0.598	0.077	0.692	0.131	0.604	0.146	0.518	0.163
0.562	0.106	0.674	0.085	0.783	0.147	0.704	0.168	0.609	0.187
0.606	0.113	0.732	0.091	0.863	0.158	0.801	0.191	0.693	0.206
0.648	0.119	0.818	0.101	0.899	0.163	0.903	0.209	0.786	0.222
0.697	0.129	0.875	0.106					0.859	0.236
0.746	0.137								
0.794	0.146								
0.831	0.150								
0.881	0.158								
0.927	0.167								

The solubilities of CO₂ in a series of hydroxyl ammonium-based ILs were investigated by Yuan, Z. and coworkers[166]. 2-hydroxy ethylammonium (HE) and tri-(2-hydroxy ethyl)-ammonium acetate (THE), incorporating formate (F), acetate (A) and lactate (L) anions were studied at the temperatures ranging from (303 to 323) K and pressures ranging from (0 to 11) MPa (Fig 2-6). Results showed that the solubility of CO₂ in these ILs was in sequence: THEAL >HEAA>HEA> HEF > HEAL >THEAA≈HEL > HEAF [166].

The solubility phenomena of the CO₂ in phosphonium-based RTILs incorporating different anions were studied by Kilaru, P. and Scovazzo, P. [149]. The results showed that the solubility increases in the order; [P_{6,6,6,14}]DCA > [P_{6,6,6,14}]Cl > [P_{6,6,6,14}]NTf₂ > [P_{6,6,6,14}]DEP [149].

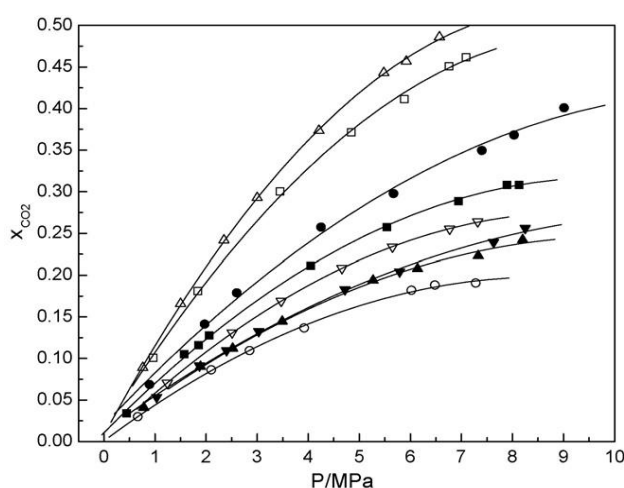


Fig 2-6 Comparison and correlation of the solubility of CO₂ in hydroxyl ammonium ionic liquids at 303 K: (■) HEF; (●) HEA; (▲) HEL; (▼) THEAA; (□) THEAL; (○) HEAF; (Δ) HEAA; (▽), HEAL [166]

One of the common ways to increase the solubility of CO₂ in ILs is use of fluorinated anions [12]. The solubility of carbon dioxide in the ILs [C₈mim]NTf₂ and [C₁₀mim]NTf₂, were studied experimentally in a temperature range from (298 to 343) K and at pressures close to atmospheric. The results showed that the solubility of carbon dioxide is significantly higher in the fluorine-substituted IL with Henry's law

constants of 33.3 and 30.7 for [C₈mim]NTf₂, and [C₁₀mim]NTf₂ respectively at 303 K [142]. Moreover, other studies showed the effect of other fluorinated anions on the CO₂ solubility in the following order; [CF₃SO₃] < [(CF₃SO₂)₂N] [82].

Muldoon, *et al.* [82] reported that [N_{4,4,4,4}]DOSS which contains an anion of known low toxicity, has several features that lead to good solubility of CO₂ the highest pressures. The solubility of CO₂ in [N_{4,4,4,4}]DOSS was nearly identical to that in [hmim]eFAP [82], one of the best performing fluorinated ILs.

2.4.3.3 Effect of functional group

One of the common ways to increase the solubility of CO₂ in ILs is fluorination of the IL's cation due to the well known affinity of CO₂ to fluoroalkyl groups. It should be noted that insertion of the fluorine atom to the cationic part of IL leads to a small increase in CO₂ solubility [12]. Considering that the anion-CO₂ interaction plays a significant role in CO₂ solubility, one expects a higher CO₂ solubility when fluorinated derivatives of the anionic part are used. The effect of fluorinated anion was studied by Brennecke *et al.* [82]. The derivatives of the PF₆⁻ anion where three fluorine atoms are replaced with pentafluoroethyl, heptafluoropropyl, and nonafluorobutyl groups were studied and the results showed an increase in CO₂ solubility as the length of the fluoroalkyl group increases. However other studies reported that the contribution of fluorination increases the CO₂ solubility not more than 10% [12, 167].

The higher solubility of CO₂ in ILs with fluorinated substituents could be attributed to the following factors [12]:

- (i) Fluorinated complexes have weaker self-interactions which lead to higher miscibility with CO₂.
- (ii) Lewis acid-base interaction between electronegative fluorine atoms and the electron-poor carbon atom of CO₂.
- (iii) A hydrogen-bonding interaction between oxygen atoms of CO₂ and relatively more acidic protons of IL because of the presence of neighboring fluorine atoms.

The fluorinated compounds are less environmentally friendly because of their high toxicity values which weaken their potential use as green solvents [12]. Additionally, they contribute significantly to the cost of CO₂ capture because it increases the experimental cost.

Incorporation of oxygen-containing functional (ether and ester groups) to the cation or anion to increase the solubility of CO₂ in ILs received much attention because the electron-poor carbon atom of CO₂ has an affinity toward electronegative atoms [167, 168]. The ideal solubility selectivities of CO₂, N₂, and CH₄ in a series of imidazolium-based room-temperature ILs (RTILs) with one, two, or three oligo(ethylene glycol) substituents were investigated [169]. The results showed that these RTILs reveal similar levels of CO₂ solubility but lower solubilities of N₂ and CH₄. As a consequence, RTILs with oligo(ethylene glycol) substituents were observed to have 30-75% higher ideal solubility selectivities for CO₂/N₂ and CO₂/CH₄. Additionally, Yuan and co-workers [166] studied the solubility of CO₂ in a group of hydroxyl ammonium ILs and obtained similar solubility values to those for imidazolium-based ILs. One of the clear applications of the design of task-specific ILs (TSILs) is the incorporation of amine functional groups to ILs because they are specifically designed to increase the CO₂-IL interaction [170]. The absorption of CO₂ in the amine functionalized ILs is carried out through chemisorption, and the experimental results showed that the mole ratio of CO₂/TSIL approaches a maximum of 0.5 (Fig 2-7) [14].

Increasing the number of potential sites for the CO₂ interaction by obtaining ILs with more than one specific functional group is another approach to obtain a low Henry's law constant. Amino-acid-based ILs possess both carboxyl and amine functional groups, it was found that they react with CO₂ in a 1:1 stoichiometric ratio [171]; [P₆₆₆₁₄]Met and [P₆₆₆₁₄]Pro were used for this study and the absorption is in good agreement with the results obtained from IR spectroscopy and CO₂ absorption studies. A developed (3-aminopropyl)tributylphosphonium amino acid ILs for CO₂ capture, leading to 1 mol of CO₂ captured/1 mol of IL, and the ILs can be repeatedly recycled for CO₂ uptake [172]. Nevertheless, the high viscosities of these compounds, which are even larger upon complexation with CO₂, would hinder the

CO₂ diffusion and uptake rate. Furthermore, the ability of 1,1,3,3-tetramethylguanidinium-based ILs to reversibly absorb gaseous was investigated. It was found the gas almost completely desorbed by heating or lowering of the pressure and no change in absorbing capacity of the ILs was observed after several cycles [173].

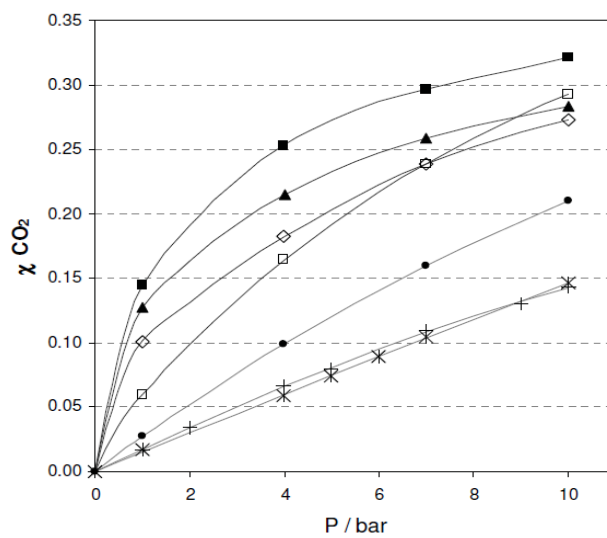


Fig 2-7 CO₂ absorption in NH₂-cation functionalized RTILs at 303 K. Lines plotted as view aid. Points represent experimental measurements: (■) APMim[BF₄], (□) APMim[DCA], (▲) AEMPyrr[BF₄] and (◇) APMim[NTf₂]. Standard Ionic liquids: (●) emim[NTf₂], (+) bmim[BF₄] and (×) bmim[DCA].

Zhang, J. and coworkers [174] studied the solubilities of CO₂ and the interactions of polar and nonpolar solutes with the ILs 1-butyronitrile-3-methylimidazolium bis(trifluoromethylsulfonyl) imidate [Cpmim]NTf₂, 1-butyronitrile-2,3-dimethylimidazolium bis(trifluoromethylsulfonyl) imidate [Cpmmim]NTf₂, 1-butyronitrile-3-methylimidazolium dicyanamide [Cpmim]N(CN)₂, 1-butyronitrile-2,3-dimethylimidazolium dicyanamide [Cpmmim]N(CN)₂, 1-butyl-3-methylimidazolium palmitate [Bmim][n-C₁₆H₃₃COO], and 1-butyl-3-methylimidazolium stearate [Bmim][n-C₁₈H₃₅COO] at T = (303.15, 313.15, 323.15, and 333.15) K. The incorporation of the cyano functional group substitution on the alkyl chain results in a remarkable decrease of the interactions of hydrocarbons compared with the 1,3-dialkylimidazolium ILs [174, 175].

To design IL-based processes, knowledge of the solubilities of gases in ILs is needed. However, only limited information about these properties is available in the literature. CO₂ has been used in many previous studies of solubility in ionic liquids, because it is of interest for a variety of ILs applications. Therefore, it was a convenient solute choice for many studies [176]. Several cations and anions were studied at different temperatures and pressure also several binary systems for these compounds were investigated. Table 2-4 present examples of cations, anions, functionalized cations and functionalized anions that have been studied for CO₂ capture.

Table 2-4 Studied anions and cations for CO₂ capture

Cation	Anion	Reference	Cation	Anion	Reference
[Emim]	[NTf ₂]	[177]	[N _{113 10}]	[NTf ₂]	[159]
[Emim]	[OTf]	[178]	[N _{111 10}]	[NTf ₂]	[159]
[Emim]	[dca]	[178]	[N ₂₂₂₆]	[NTf ₂]	[159]
[Emim]	[BF ₄]	[163]	[Hmpy]	[NTf ₂]	[173]
[Emim]	[B(CN) ₄]	[161]	[Bmpy]	[NTf ₂]	[143]
[Emim]	[Et ₂ PO ₄]	[152]	[Hmpy]	[NTf ₂]	[143]
[C ₃ mim]	[BF ₄]	[145]	[P _{666 14}]	[NTf ₂]	[153]
[Bmim]	[NTf ₂]	[177]	[P _{666 14}]	[OTf]	[153]
[Bmim]	[SCN]	[179]	[P _{666 14}]	[PF ₆]	[153]
[Bmim]	[PF ₆]	[12]	[P ₄₄₄₃]	[AA]	[172]
[Bmim]	Acetate	[180]	[HEF]	Formate	[166]
[Bmim]	[NO ₃]	[82]	[HEA]	Lactate	[166]
[Bmim]	[DCA]	[82]	[THEA]	Acetate	[166]
[Bmim]	[OTf]	[82]	[THEA]	Lactate	[166]
[Bmim]	[TFA]	[82]	[HEA]	Formate	[166]
[Bmim]	[Bu ₂ PO ₄]	[152]	[HEA]	Acetate	[166]
[Bmim]	[C ₇ F ₁₅ CO ₂]	[82]	[Hemim]	[NTf ₂]	[166]
[Bmim]	Palmitate	[174]	[Hemim]	[OTf]	[166]
[Bmim]	Stearate	[174]	[Hemim]	[PF ₆]	[166]
[Hmim]	[BF ₄]	[145]	[C ₆ H ₄ F ₉ mim]	[NTf ₂]	[8]
[Hmim]	[PF ₆]	[4]	[C ₈ H ₄ F ₁₃ mim]	[NTf ₂]	[8]
[Hmim]	[NTf ₂]	[143]	[TMGH]	L	[173]
[Omim]	[BF ₄]	[145]	[CpMIm]	[NTf ₂]	[174]
[Omim]	[NTf ₂]	[142]	[CpMMIm]	[Dca]	[174]
[Dmim]	[NTf ₂]	[147]	[CpMIm]	[NTf ₂]	[174]
[Dmim]	[MP]	[179]	[CpMMIm]	[Dca]	[174]
[N ₁₁₁₁]	[Gly]	[151]	[NH ₂ C _n mim]	[NTf ₂]	[39]
[N ₁₁₁₁]	[Lys]	[151]	[NH ₂ C _n mim]	[SCN]	[39]
[N ₂₂₂₂]	[Gly]	[151]	[NH ₂ C _n mim]	[TFA]	[39]
[N ₂₂₂₂]	[Lys]	[151]	[NH ₂ C _n mim]	[CH ₃ SO ₄]	[39]
[N ₄₁₁₁]	[NTf ₂]	[177]	[Hmim]	[eFAP]	[143]
[N ₂₂₂₄]	[CH ₃ COO]	[181]	[Hmim]	[pFAP]	[143]
[N ₄₄₄₄]	Doc	[82]	[Etoim]	[NTf ₂]	[179]
[N ₁₈₈₈]	[NTf ₂]	[159]			

CHAPTER 3

RESEARCH METHODOLOGY

3.1 Introduction

One of the potential applications of ILs that several research groups along with our group have examined is the separation of CO₂ from gas mixtures [4, 82, 159]. A number of investigations have shown that CO₂ is remarkably soluble in ILs. More detailed studies showed that the anion and substituents on the cation did affect the CO₂ solubility [82]. Designer RTILs were used as solvents for the separation of CO₂ to improve the absorption of CO₂ and increase the CO₂ selectivity over CH₄. Given the “designer” nature of the ILs, functional groups are incorporated into the structure of IL to promote the selective absorption of CO₂.

To design and optimize processes using ILs, it is crucial to understand the important factors that affect the solubility of the CO₂ in the ILs to produce ILs that have high potential CO₂-philic ILs. It was found that there were a number of factors that controlled the CO₂ solubility in the chosen ILs. Anions and cations that contain fluoroalkyl groups were found to have some of the highest CO₂ solubilities, and as the quantity of fluoroalkyl groups increased, the CO₂ solubility also increased [82]. Additionally, increasing alkyl chain length on the cation also increases the CO₂ solubility [82]. In an effort to improve the CO₂ solubility in ILs, we decided to concentrate on ILs that possess many CO₂-philic functionalities in one structure. This can be achieved by the addition of nitrile, carbonyl groups, sulfonate, branching the alkyl chain and long alkyl chain in one structure. In some cases we systematically changed the IL structures to allow direct comparisons to be made.

The details related to the material, preparation, purification and characterization of

the designed ILs have been included in this chapter. Thermophysical properties measurements (density, viscosity, refractive index and thermal stability) and CO₂ solubilities measurement of the ILs also will be described in this chapter.

3.2 Materials

Chemicals of analytical grade were used for the synthesis of ILs. The CAS (Chemical Abstracts Service) number, source and grades of the chemicals used are: Imidazole, acrylonitrile, 1-bromohexane, 1-bromooctane, 1-bromodecane, 1-chlorohexane, 1-chlorooctane, 1-chlorotetradecane, allyl chloride, benzyl chloride, 2-chloroethanol, 1,6-dichlorohexane, 1,10-dichlorodecane, sodium dioctylsulfosuccinate, sodium dodecylsulfate, sodium benzenesulfonate, 3-sulfobenzoic acid sodium salt and lithium trifluoromethanesulfonate of 98 -99.99 % purity were purchased from Aldrich. 1-bromobutane of 98 % purity was purchased from Merck. 1-chlorobutane, anhydrous methanol, anhydrous ethylacetate, acetone and anhydrous diethyl ether of 98 -99.9 % purity were purchased from Sigma-Aldrich. Trihexyltetradecylphosphonium chloride and trioctylphosphine of 95 % and 90 % purity respectively, were purchased from Aldrich. All the chemicals were used without further purification.

Purified gases supplied by MOX-Linde Gases Sdn Bhd, Malaysia were used for the CO₂ solubilities measurement. The grades of gases used are: carbon dioxide (CO₂) with purity 99.9% minimum (moisture < 10 ppm, hydrocarbon < 1 ppm), Methane (CH₄) with purity > 99.995%, Nitrogen (N₂) with purity 99.99% and Helium (He) with purity 99.99%).

3.3 Synthesis of RTILs

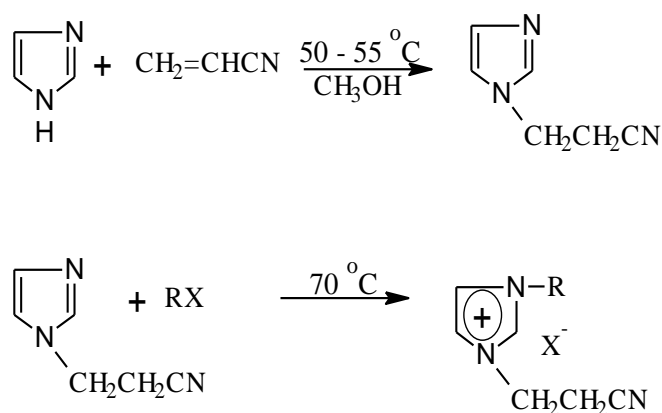
3.3.1 Synthesis of nitrile functionalized imidazolium-based RTILs

A new series of propanenitrile imidazolium-based ILs incorporating different sulfonate based anions such as; dioctylsulfosuccinate (DOSS), dodecylsulfate (DDS),

benzenesulfonate (BS), and trifluoromethanesulfonate (TFMS) were synthesized. They were prepared by reacting imidazole with acrylonitrile which was then brought to react with 1-haloalkane. After the reaction was completed, metathesis reaction was carried out using (DOSS), (DDS), (BS) and (TFMS) metal anions.

3.3.1.1 Synthesis of 1-alkyl-3-propanenitrile imidazolium bromide

1-alkyl-3-propanenitrile imidazolium bromide ILs were synthesized by following the method shown in Fig 3-1.



R = butyl, hexyl, octyl, decyl

X = Br, Cl

Fig 3-1 Synthesis route of the RTILs [C₂CN C_nim]⁺X⁻

A 250 mL, round-bottomed flask equipped with a heating oil bath, a nitrogen inlet adapter, magnetic stirrer, reflux condenser is flushed with dry nitrogen. The flask was charged with imidazole (34.04g, 0.5 mol) in methanol (43 mL, 1.0 mol) and mixed with acrylonitrile (39.5 mL, 0.6 mol). The solution was heated under reflux and under nitrogen atmosphere at 50-55 °C for 10 hr and then cooled to room temperature. The volatile materials were removed from the mixture under *vacuo* at 70°C. The viscous liquid left was propanenitrile imidazole. Nitrile functionalized IL was synthesized by direct quaternization reaction of the propanenitrile imidazole with 1-bromobutane [182]. 1-bromobutane (53.9 ml, 0.5 mol) was added to the propanenitrile. The resulting compound was cooled to room temperature and washed with ethyl acetate for three

times and the remaining solvent was removed at 80°C in *vacuo*. It was then dried in a vacuum oven for 72 h to produce 1-butyl-3-propanenitrile imidazolium bromide [C₂CN Bim]Br.

Similar procedure was repeated to synthesize 1-hexyl-3-propanenitrile imidazolium bromide [C₂CN Him]Br, 1-octyl-3-propanenitrile imidazolium bromide [C₂CN Oim]Br and 1-decyl-3-propanenitrile imidazolium bromide [C₂CN Dim]Br by replacing 1-bromobutane with 1-bromohexane, 1-bromooctane and 1-bromodecane, respectively.

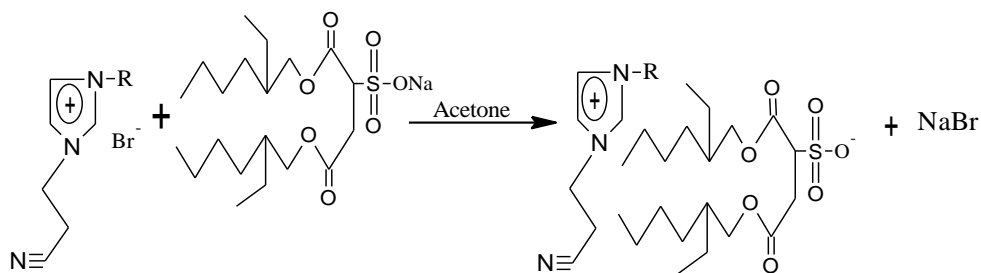
3.3.1.2 Synthesis of 1-alkyl-3-propanenitrile imidazolium chloride

Similar procedure as that described in 3.3.1.1 was adopted to synthesize 1-butyl-3-propanenitrile imidazolium chloride [C₂CN Bim]Cl, 1-hexyl-3-propanenitrile imidazolium chloride [C₂CN Him]Cl and 1-octyl-3-propanenitrile imidazolium chloride [C₂CN Oim]Cl by replacing 1-bromobutane, 1-bromohexane and 1-bromooctane with 1-chlorobutane, 1-chlorohexane and 1-chlorooctane, respectively.

3.3.1.3 Synthesis of 1-alkyl-3-propanenitrile imidazolium dioctylsulfosuccinate

1-alkyl-3-propanenitrile imidazolium dioctylsulfosuccinate [C₂CN C_nim]DOSS ILs were synthesized by following the method shown in Fig 3-2.

1-butyl-3-propanenitrile imidazolium dioctylsulfosuccinate [C₂CN Bim]DOSS was synthesized by mixing 7.74 g, 0.03 mol of [C₂CN Bim]Br and sodium dioctylsulfosuccinate (13.34 g, 0.03 mol) in 50 ml of acetone in a 250-mL round-bottomed flask. The mixture was stirred at room temperature for 48 h. The solid precipitate formed was separated and the solvent removed in *vacuo*. The resulting pale yellow viscous compound was washed with ethyl acetate and diethyl ether. It was then dried in a vacuum oven for 48 h to give 1-butyl-3-propanenitrile imidazolium dioctylsulfosuccinate [C₂CN Bim]DOSS.



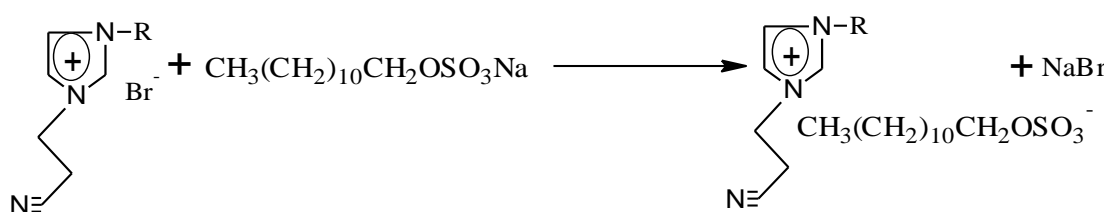
R = butyl, hexyl, octyl, decyl

Fig 3-2 Synthesis route of the RTILs [C₂CN C_nim]DOSS

Similar procedure was repeated to synthesize 1-hexyl-3-propanenitrile imidazolium dioctylsulfosuccinate [C₂CN Him]DOSS, 1-octyl-3-propanenitrile imidazolium dioctylsulfosuccinate [C₂CN Oim]DOSS and 1-decyl-3-propanenitrile imidazolium dioctylsulfosuccinate [C₂CN Dim]DOSS by replacing [C₂CN Bim]Br with equivalent moles of [C₂CN Him]Br, [C₂CN Oim]Br and [C₂CN Dim]Br, respectively.

3.3.1.4 Synthesis of 1-alkyl-3-propanenitrile imidazolium dodecylsulfate

1-alkyl-3-propanenitrile imidazolium dodecylsulfate [C₂CN C_nim]DDS ILs were synthesized by the method shown in Fig 3-3.



R = butyl, hexyl, octyl, decyl

Fig 3-3 Synthesis route of the RTILs [C₂CN C_nim]DDS

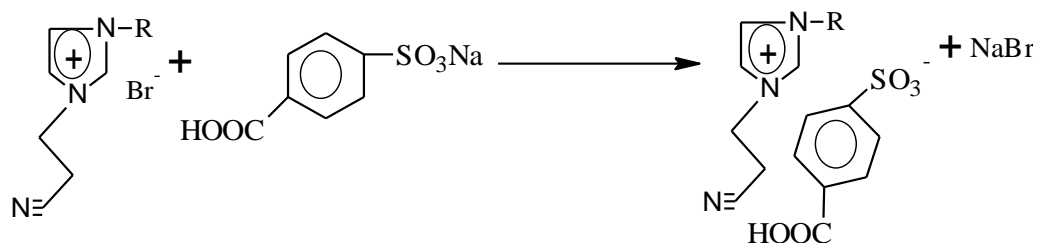
1-butyl-3-propanenitrile imidazolium dodecylsulfate [C₂CN Bim]DDS was synthesized by mixing [C₂CN Bim]Br (10.33 g, 0.04 mol) and sodium dodecyl sulfate C₁₂H₂₅OSO₃Na (11.54 g, 0.04 mol) in 40 ml of hot dionized water (60 °C). The

mixture was stirred at room temperature for 48 h. The water was slowly removed under *vacuo* at 80 °C. CH₂Cl₂ was added to the precipitate out the salt and the mixture was filtered. The viscous extract was then washed with deionized water and the washing was repeated until it was bromide-free. The remaining solvent was removed at 80°C in *vacuo* and then dried in a vacuum oven for 48 h to produce the viscous gel product, 1-butyl-3-propanenitrile imidazolium dodecylsulfate [C₂CN Bim]DDS.

Similar procedure was repeated to synthesize 1-hexyl-3-propanenitrile imidazolium dodecylsulfate [C₂CN Him]DDS, 1-octyl-3-propanenitrile imidazolium dodecylsulfate [C₂CN Oim]DDS and 1-decyl-3-propanenitrile imidazolium dodecylsulfate [C₂CN Dim]DDS by replacing [C₂CN Bim]Br with equivalent moles of [C₂CN Him]Br, [C₂CN Oim]Br and [C₂CN Dim]Br, respectively.

3.3.1.5 Synthesis of 1-alkyl-3-propanenitrile imidazolium sulfobenzoic acid

1-alkyl-3-propanenitrile imidazolium sulfobenzoic acid [C₂CN C_nim]SBA ILs were synthesized by following the method shown in Fig 3-4.



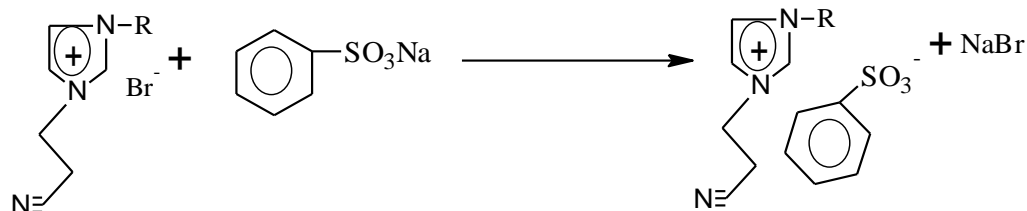
R = hexyl, octyl, decyl

Fig 3-4 Synthesis route of the RTILs [C₂CN C_nim]SBA

1-hexyl-3-propanenitrile imidazolium sulfobenzoic acid [C₂CN Him]SBA, 1-octyl-3-propanenitrile imidazolium sulfobenzoic acid [C₂CN Oim]SBA and 1-decyl-3-propanenitrile imidazolium sulfobenzoic acid [C₂CN Dim]SBA were synthesized by following the same procedure as that described in 3.3.1.4 by adding equivalent moles of sodium sulfobenzoic acid HOOC-C₆H₄-SO₃Na to [C₂CN Him]Br, [C₂CN Oim]Br and [C₂CN Dim]Br, respectively.

3.3.1.6 Synthesis of 1-alkyl-3-propanenitrile imidazolium benzenesulfonate

1-alkyl-3-propanenitrile imidazolium benzenesulfonate [C₂CN C_nim]BS ILs were synthesized by following the method shown in Fig 3-5.



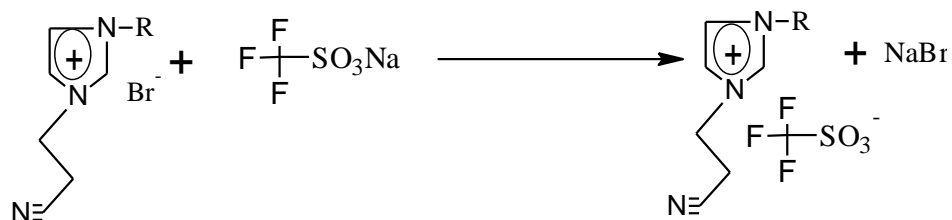
R = butyl, hexyl, octyl

Fig 3-5 Synthesis route of the RTILs [C₂CN C_nim]BS

1-butyl-3-propanenitrile imidazolium benzenesulfonate [C₂CN Bim]BS, 1-hexyl-3-propanenitrile imidazolium benzenesulfonate [C₂CN Him]BS and 1-octyl-3-propanenitrile imidazolium benzenesulfonate [C₂CN Oim]BS were synthesized by following the same procedure as that described in 3.3.1.4 by adding equivalent moles of sodium benzenesulfonate C₆H₅SO₃Na to [C₂CN Bim]Br, [C₂CN Him]Br and [C₂CN Oim]Br, respectively.

3.3.1.7 Synthesis of 1-alkyl-3-propanenitrile imidazolium trifluoromethanesulfonate

1-butyl-3-propanenitrile imidazolium trifluoromethanesulfonate [C₂CN C_nim]TFMS ILs were synthesized by following the method as shown in Fig 3-6.



R = butyl, hexyl, octyl

Fig 3-6 Synthesis route of the RTILs [C₂CN C_nim]TFMS

1-butyl-3-propanenitrile imidazolium trifluoromethanesulfonate [C_2CN Bim]TFMS, 1-hexyl-3-propanenitrile imidazolium trifluoromethanesulfonate [C_2CN Him]TFMS and 1-decyl-3-propanenitrile imidazolium trifluoromethanesulfonate [C_2CN Oim]TFMS were synthesized by following the same procedure as that described in 3.3.1.4 by adding equivalent moles of lithium trifluoromethanesulfonate CF_3SO_3Li to [C_2CN Bim]Br, [C_2CN Him]Br and [C_2CN Oim]Br, respectively

3.3.2 Synthesis of imidazolium-based dual functionalized RTILs

A new series of imidazolium-based dual functionalized ILs incorporating dioctylsulfosuccinate (DOSS) anion were synthesized as shown in Fig 3-7.

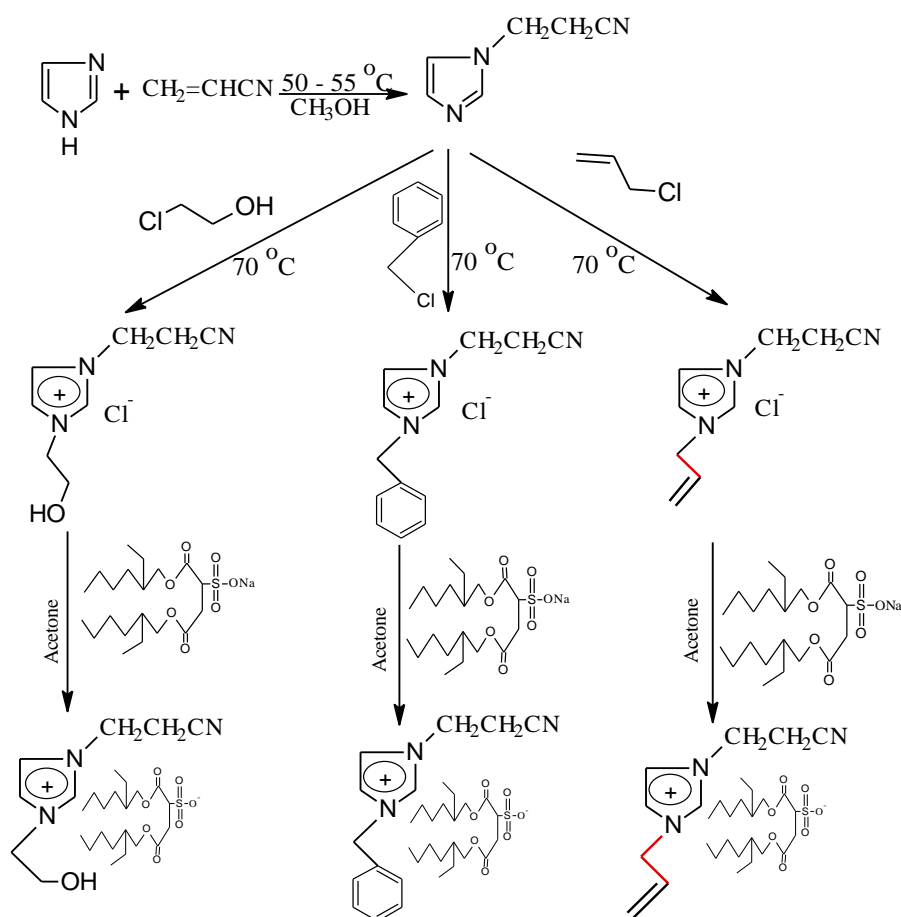


Fig 3-7 Synthesis route of imidazolium-based dual functionalized RTILs

They are prepared by reacting imidazole with acrylonitrile and then reacting the product with allyl chloride, 2-chloroethanol and benzyl chloride. After the reaction was completed, metathesis reaction was carried out using (DOSS) metal anion.

A 100-mL, round-bottomed flask equipped with a heating oil bath, a nitrogen inlet adapter, magnetic stirrer, reflux condenser is flushed with dry nitrogen. The flask was charged with imidazole (6.81 g, 0.1 mol) in methanol (8.6 mL, 0.2 mol) and mixed with acrylonitrile (7.9 mL, 0.12 mol). The solution was heated under reflux and nitrogen atmosphere at 50-55 °C for 10 hr and then cooled to room temperature. The volatile materials were removed from the mixture under *vacuo* at 70 °C. Then, 8.1 mL, 0.1 mol of allyl chloride was added and the mixture was stirred and maintained at 70°C under nitrogen atmosphere for 48 hr. The resulting compound was cooled to room temperature and washed with ethyl acetate and the remaining solvent was removed at 80°C under *vacuo*. The product was mixed with 44.46 g, 0.1 mol, of sodium dioctylsulfosuccinate in 60 mL of acetone in a 250-mL round-bottomed flask. The mixture was stirred at room temperature for 24 h. The solid precipitate formed was separated and the solvent removed in vacuum. The resulting viscous compound was washed with ethyl acetate and diethyl ether. It was then dried in a vacuum oven for 48 h to give 1-allyl-3-propanenitrile imidazolium dioctylsulfosuccinate [C₂CN Ayim]DOSS.

Similar procedure was repeated to synthesise 1-benzyl-3-propanenitrileonitrile imidazolium dioctylsulfosuccinate [C₂CN Bzim]DOSS and 1-(2-hydroxyethyl)-3-propanenitrile imidazolium dioctylsulfosuccinate [C₂CN Heim]DOSS by substituting allyl chloride with equivalent moles of benzyl chloride and 2-chloroethanol, respectively.

3.3.3 Synthesis of phosphonium-based monocationic RTILs

3.3.3.1 Synthesis of trihexyltetradecylphosphonium dioctylsulfosuccinate

Trihexyltetradecylphosphonium dioctylsulfosuccinate was synthesized by mixing stoichiometric amounts of trihexyltetradecylphosphonium chloride and sodium dioctylsulfosuccinate (as shown in Fig 3-8) in diethyl ether and stirred for 48 h followed by separation of the solid. The product was washed with acetone and the remaining solvent was removed at 70 °C under vacuum and then dried in a

vacuum oven for at 80 °C for 48 h to afford the clear viscous gel product trihexyltetradecylphosphonium dioctylsulfosuccinate [P_{6,6,6,14}]DOSS.

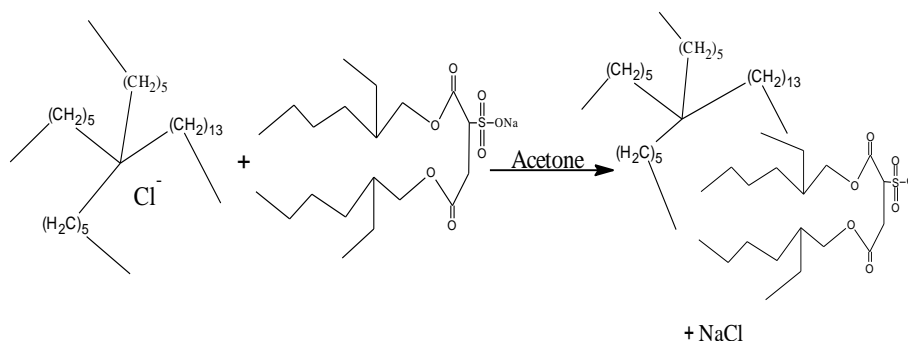


Fig 3-8 Synthesis route of trihexyltetradecylphosphonium dioctylsulfosuccinate IL

3.3.3.2 Synthesis of trioctyltetradecylphosphonium dioctylsulfosuccinate

Trioctyltetradecylphosphonium-based ILs were synthesized by following the method as shown in Fig 3-9.

Trioctyltetradecylphosphonium docusate [P_{8,8,8,14}]DOSS was synthesized from trioctyltetradecylphosphonium chloride [P_{8,8,8,14}]Cl. The synthesis was performed using a three-necked round bottom flask immersed in an oil bath with nitrogen flow. The flask is connected to a reflux condenser. The flask is flushed with dry nitrogen before trioctylphosphine (17.8 mL, 0.04 mol) and 1-chlorotetradecane (11.4 mL, 0.042 mol) were added (Fig 3-9). The reaction was carried out at 80 °C and stirred for 48 h under nitrogen atmosphere. The product was washed with ethyl acetate and the remaining solvent was removed under vacuum then dried in vacuum oven at 80 °C for 48 h to form a clear viscous gel product [P_{8,8,8,14}]Cl. Then, [P_{8,8,8,14}]Cl was dissolved in 30 mL of acetone and mixed with 0.04 mol sodium dioctylsulfosuccinate (Fig 3-9). The mixture was stirred at room temperature for 48 h followed by filtration of the solid. The product was washed with ethyl ether and the remaining solvent was removed under vacuum and then dried in a vacuum oven for 48 h to afford the clear viscous gel product [P_{8,8,8,14}]DOSS.

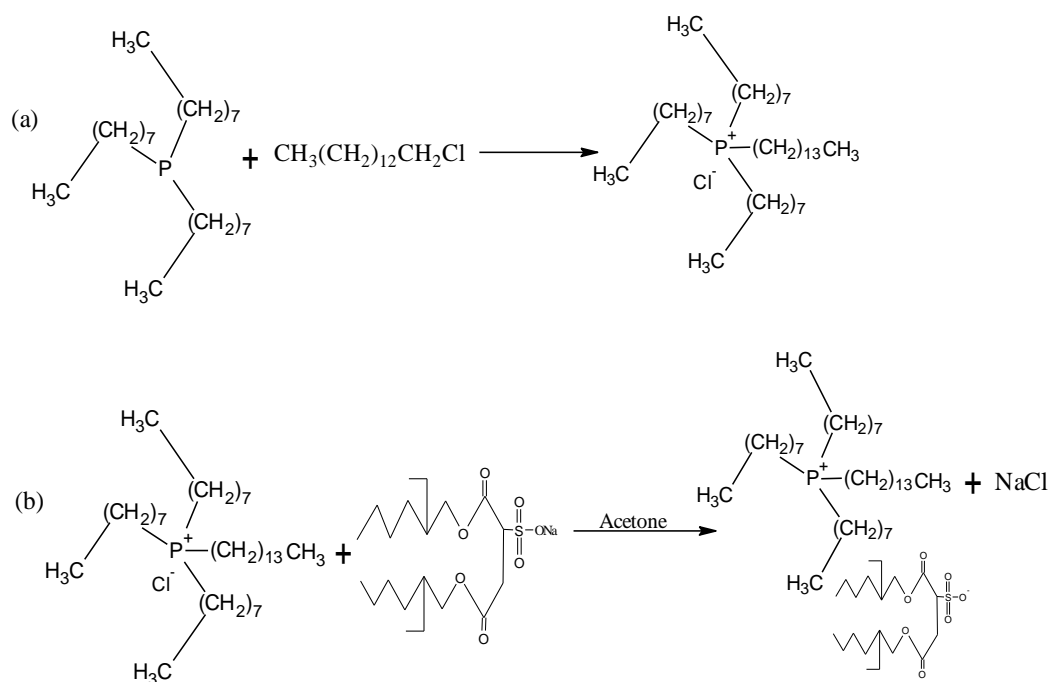


Fig 3-9 Synthesis route of trioctyltetradecylphosphonium-based ILs

3.3.4 Synthesis of phosphonium-based dicationic RTILs

Phosphonium-based dicationic ILs were synthesized by following the method shown in Fig 3-10. 1,6-bis(trioctylphosphonium)hexane dioctylsulfosuccinate; $[\text{P}_{8,8,8}\text{C}_6\text{P}_{8,8,8}]\text{DOSS}_2$ was synthesized in two steps as shown in Fig 3-10. First, 1,6-bis(trioctylphosphonium)hexane chloride was added into a three-necked round bottom flask equipped with a heating oil bath, a nitrogen inlet adapter, magnetic stirrer, and a reflux condenser. Trioctylphosphine (18.7 mL, 0.041 mol) and 1,6-dichlorohexane (3.3 mL, 0.02 mol) were added. The system was heated to 120 °C and stirred for 24 h under nitrogen atmosphere then placed under *vacuo* at 100 °C to remove any volatile components. The product was then cooled to room temperature and washed with acetone. Then remaining solvent was removed at 80 °C under *vacuo* and then dried in a vacuum oven for 48 h to afford the clear viscous gel product 1,6-bis(trioctylphosphonium)hexane chloride $[\text{P}_{8,8,8}\text{C}_6\text{P}_{8,8,8}]\text{Cl}_2$.

In the second step, stoichiometric amounts of $[\text{P}_{8,8,8}\text{C}_6\text{P}_{8,8,8}]\text{Cl}_2$ and sodium dioctylsulfosuccinate (Fig 3-10) were mixed in diethyl ether and stirred for 48 h followed by separation of the solid. The product was washed with acetone and the

remaining solvent was removed at 70 °C under vacuum and then dried in a vacuum oven at 80 °C for 48 h to afford the clear viscous gel product [P_{8,8,8}C₆P_{8,8,8}] DOSS₂.

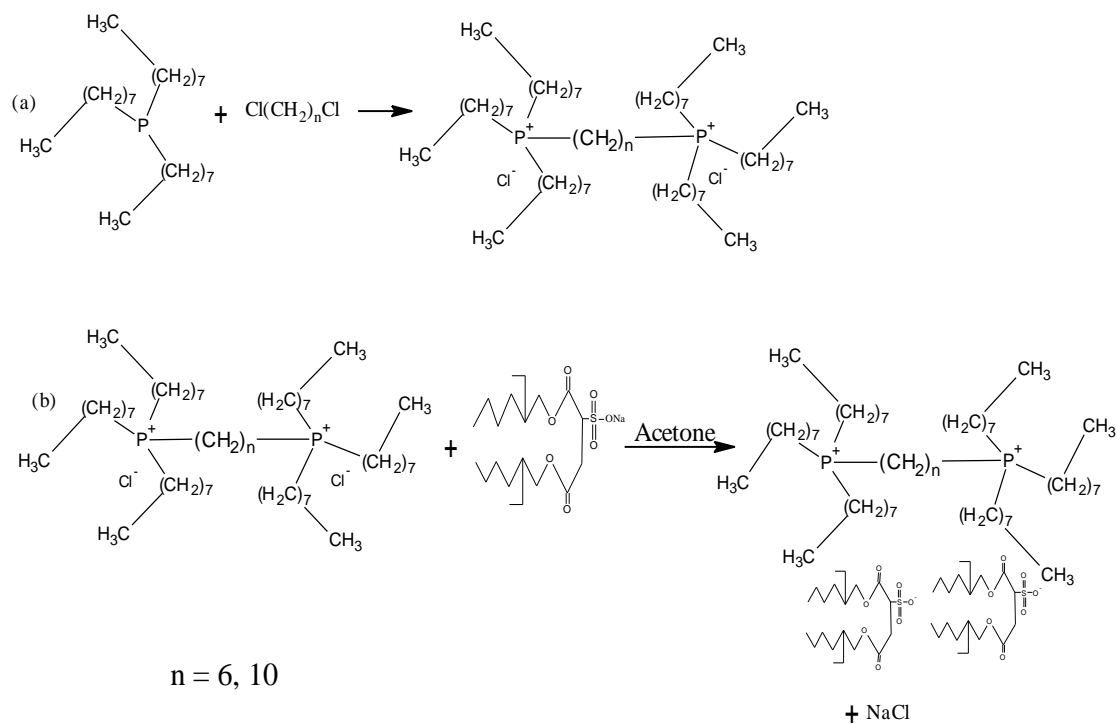


Fig 3-10 Synthesis route of phosphonium-based dicationic RTILs

1,10-bis(trioctylphosphonium)decane dioctylsulfosuccinate [P_{8,8,8}C₆P_{8,8,8}]DOSS₂ was synthesized in a similar manner as [P_{8,8,8}C₆P_{8,8,8}]Cl₂ except, 1,10-dichlorodecane was used instead of 1,6-dichlorohexane.

3.4 Characterization of RTILs

The structure of all ILs synthesized in the present study was characterized using FTIR, NMR and elemental analysis (CHNS). Water and halide contents were determined using coulometric Karl Fischer titrator and ion chromatography, respectively.

It is of the utmost importance to assess the purity of ILs. Water and halides are known to influence the physical properties of ILs considerably. The presence of halide contamination, for example increases the viscosity of ILs, whereas the presence

of water or other cosolvents, reduces the viscosity. Another point, which will be important to the process engineers, is the corrosive nature of halide ions in ILs [100].

3.4.1 NMR, FTIR and elemental analysis

The ILs of the present study were characterized using Fourier transform infrared (FTIR) spectroscopy. The spectra were recorded in a Shimadzu FTIR-8400S Fourier Transform Infrared Spectrometer (FTIR) in the mid region ($4000\text{--}400\text{ cm}^{-1}$) using the Attenuated Total Reflectance ((MIRacle ATR) measurement mode.

The individual percentage of carbon, hydrogen, nitrogen and sulfur of the synthesized ILs were determined using CHNS-932 (LECO instruments) elemental analyzer. The instrument was calibrated using standard calibration sample with known chemical composition provided by supplier before each measurement. Samples of less than 2 mg each were covered in silver capsule containing sorbit pad and then analyzed. The measurements were made under the following conditions: oxygen dose 20 cc, oxidation furnace temperature $1000\text{ }^{\circ}\text{C}$, reduction furnace temperature $650\text{ }^{\circ}\text{C}$, and helium was used as the carrier gas for the measurement. The measurement for each IL was made in triplicate and the average values were reported.

A Burcher Avance 300 and JEOL JNM-ECA400 nuclear magnetic resonance spectrophotometers were used to determine the ^1H and ^{13}C NMR spectra of the present ILs using D_2O or CDCl_3 as solvents. 5-10 mg of sample was dissolved in 0.7 mL of deuterated solvent. The chemical shifts were reported downfield at room temperature in parts per million (ppm, δ) from a tetramethylsilane (TMS) reference. Multiplicities are abbreviated as *s*, singlet; *d*, doublet; *t*, triplet; and *m*, multiplet.

3.4.2 Water and halide contents

A coulometric Karl Fischer titrator, DL 39 (Mettler Toledo) with CombiCoulomat fritless Karl Fischer reagent (Merck) was used to determine the water content of the synthesized ILs, using Hydranal coulomat AG reagent (Riedel-de Haen). The measurement for each IL was made in triplicate and the average values were reported.

Bromide and chloride measurements were conducted by ion chromatography (Metrohm Model 761 Compact IC) with (150 X 4.0) mm analytical column (Metrosep A Supp 5-150) and (5.0 X 4.0) mm guard column (Metrosep A Supp 4/5). The samples were diluted by dissolving 0.5 cm³ of each IL in 10 cm³ of acetonitrile then the volume was completed to 50 cm³ with deionized water. The analysis of the results was made using Metrodata IC Net 2.3 software.

3.5 Thermophysical properties of RTILs

Thermophysical properties such as density, viscosity and refractive index of the synthesized ILs are measured and reported over a wide temperature range and at atmospheric pressure. Empirical correlations were proposed to represent the present experimental results.

3.5.1 Density and viscosity

There are serious disagreements in the published literature for a number of the properties of ILs, especially viscosity and density. It was reported that these disagreements resulted from a number of factors, including the purities of the ILs, with the main impurities being water and halide ions, as well as the use of inappropriate measurement methods. To avoid the disagreements in thermophysical data, [C₆mim]NTF₂ was recommended as reference IL. The reference-quality measurements on selected thermophysical properties of this IL were reported by IUPAC team. Moreover, recommended values for the properties measured were established accordingly with recommendations on measurement methods [183].

Density is defined as the concentration of matter, measured by the mass per unit volume. The molar volume, V_M , is defined as the volume occupied by 1 mol of a substance [88]. Information on solvent density values is important. It is particularly used in fluid flow calculations and for the design of liquid/liquid two phase mixer settler units. Density can be considered as a fundamental data for developing equations of state, which are the main tool used for thermophysical properties

prediction for process design purposes, and solution theories for ILs. It is also required for many relevant industrial problems such as liquid metering applications or for the design of different types of equipment such as condensers, separation trains, or even storage vessels [124]. Uses of density data include conversion of kinematic into dynamic viscosity and vice versa, calculation of molar refraction with the Lorentz-Lorenz equation, derive cohesion parameters, estimation of liquid viscosity and to decide if an immiscible compound floats in water or sinks to the bottom [88].

The viscosity of a fluid arises from the internal friction of the fluid. It might be described as an internal resistance of a gas or a liquid to flow [37, 88]. There are two broad classes of fluids, Newtonian and non-Newtonian. Newtonian fluids have a constant viscosity regardless of strain rate (low molecular weight pure liquids are examples of Newtonian fluids). Non-Newtonian fluids do not have a constant viscosity and will either thicken or thin when strain is applied (Recently, new data have been published to indicate that there are ILs that are non-Newtonian [37, 184]).

Viscosity data are reported as dynamic viscosity, η , or as kinematic viscosities, ν , which are related through density, ρ , by the following equation:

$$\eta = \nu \cdot \rho \quad 3-1$$

Viscosity is an important physical property for a number of processes. For instance, it determines the force and energy required to transfer and mix the IL with other substances. It appears in many dimensionless groups used in mass- and heat-transfer correlations. Applications that occur at high temperatures and/or pressures require reliable and accurate experimental data and mathematical models. This is especially pertinent for engineering applications as hydraulic fluids. ILs cover a wide range of viscosity [108].

The viscosities of ILs have normally been measured using one of three methods: falling or rolling ball, capillary, or rotational. The disadvantage of the falling or rolling ball viscometer is that it needs to be calibrated with a standard fluid that is similar in viscosity to the fluid of interest. Capillary viscometers measure the kinematic viscosity directly. In order to convert to absolute viscosity, the kinematic

viscosity must be multiplied by the fluid density which requires additional experiments to determine fluid density so that the absolute viscosity can be calculated.

The last type of widely used viscometer is the rotational viscometer. These can adopt a variety of geometries including concentric cylinders, cone and plate, and parallel disks. Of the three geometries, a concentric cylinder is well suited for low viscosity fluids. All the three methods appear to provide equally high quality IL viscosity data. Most of IL viscosity data found in the literature were generated using the capillary method that is probably due to its low cost and relative ease of use. However, the rotational viscometer has the potential to provide additional information by the Newtonian behavior of the ILs [37].

The density and viscosity measurements of the present synthesized ILs were carried out over a temperature range 293.15 to 353.15 K using Anton Paar viscometer (Model SVM3000). A built-in density measurement based on the oscillating U-tube principle allows the determination of kinematic viscosity from the measured dynamic viscosity. The measuring ranges for this instrument are as follows: dynamic viscosity 0.2-20000 mPa·s, kinematic viscosity 0.2-20000 mm²/s, density 0.65-3.0 g·cm³, temperature range 20-105 °C (with cooling from -40 °C). The temperature was controlled to within ±0.01 °C. The reproducibility of the measurements were 0.35 % and ± 5×10⁻⁴ g·cm⁻³ for viscosity and density respectively. The uncertainties of the viscosity and density were ±0.5 % and ±0.0004 g·cm⁻³ respectively. Required sample volume for both measuring cells is 2.5 ml. The instrument was calibrated before each series of measurements and checked using pure organic solvents with known viscosity and density and also by measuring the densities of atmospheric air. During the measurements the IL was transferred to a syringe and injected into the instrument. To prevent any air bubble, the tube was first filled with some of the contents and the first measurement was taken (after the temperature set point was reached). Another measurement followed after the liquid of the vibrating tube was replaced with the one that remained in the syringe. The agreement between both values is a measure of the effectiveness of the method.

3.5.2 Refractive index

Physical properties such as refractive index are related to certain chemical properties along with other bulk property [92]. The refractive index of a medium or a compound is defined as the ratio of the velocity of light in vacuum to the velocity of light in the medium or compound [88]. The refractive index can be used to assess the purity of compound, to calculate the molecular electronic polarizability, to estimate the boiling point and to estimate liquid viscosity.

The refractive index is related to the polarizability/dipolarity of the medium and the excess molar refraction is used in the least squares energy relationships (LSERs) as a predictor of solute distribution. It can also provide useful information when studying the forces between molecules or their behaviour in solution [92, 102].

The relation between the refractive index and the polarizability offers significant information about the behaviour of a liquid as a solvent media. The electronic polarizability constitutes a measure of the importance of the dispersion forces to the cohesion of the liquid. Therefore, solvents with a large index of refraction, and hence large polarizability, should be capable of enjoying particularly strong dispersion forces, being also good solvents for species possessing high polarizabilities [102]. Additionally, the refractive index can be used to estimate the molar refractions which often considered as a measure of the hard-core molecular volumes, the molar refraction can be used to calculate the molar free volumes for the ILs [102].

ATAGO programmable digital refractometer (RX-5000 alpha) with measuring accuracy of $\pm 4 \times 10^{-5}$ and a controlled temperature to within ± 0.05 °C was used to measure the refractive index of the synthesized IL in the temperature range (298.15 to 333.15) K. Dried samples kept in desiccators were directly placed into the measuring cell. The apparatus was calibrated by measuring the refractive index of Millipore quality water and pure organic solvents with known refractive indices. Samples were directly introduced in the cell (prism assembly) using a syringe. At least three independent measurements were taken for each sample at each temperature to assure the effectiveness of the measurement.

3.5.3 Thermogravimetric analysis

Thermogravimetric analysis (TGA) is a technique in which changes in weight of a specimen are recorded as a function of temperature. It is achieved by heating the specimen in air or in a controlled atmosphere such as nitrogen [185]. TGA is one of the most common techniques to investigate a material's thermal stability by monitoring the weight change that occurs as the specimen is heated. The analysis involves heating a known mass of sample in an inert gas or oxidizing atmosphere and measuring the mass change over specific temperature ranges to provide indications of the sample thermal stability. There are many factors influence the form of the TGA curve, the primary factors are heating rate and sample size, an increase in either of which tends to increase the temperature at which sample decomposition occurs.

IL stability is known to be a function of temperature but the presence of nucleophiles/bases and the water content also have to be considered [37]. Most ILs exhibit extremely low vapor pressure. The reduced coulombic interactions between ions energetically restrict the ion pair formation required for volatilization of ILs, leading to low vapor pressures. This leads to high upper temperature limits, defined in many cases by decomposition of the IL rather than vaporization. The nature of the ILs, containing organic cations generally restricts the upper stability temperatures and in most cases, decomposition occurs with complete mass loss and volatilization of the component fragments [37]. Thermal stability is a significant factor that determines the applicability of ILs for high temperature applications [123].

Thermal stability of the synthesized ILs was investigated using a thermogravimetric analyzer (TGA, Perkin-Elmer, Pyris V-3.81) at temperatures range (50 - 500) °C, heating rate of 10 °C·min⁻¹ (with a temperature accuracy better than 2 °C) and under a nitrogen atmosphere supplied at the rate of 20 mL·min⁻¹. The values for thermal decomposition of all samples are reported in terms of T_{start} and T_{onset} . The onset temperature is defined as the intersection of the baseline weight and the tangent of the weight vs temperature curve obtained from TGA analysis as decomposition occurs. The start temperature is the temperature at which the decomposition of the sample begins (Fig 3-11). Prior to the analysis, the instrument was calibrated to ensure accurate weight and temperature measurement and the sample was dried in

vacuum oven for 72 h. TGA furnace was purged with N₂ for at least 10 minutes to eliminate moisture from the system. About 10 mg of the IL was placed into an aluminum crucible inside a programmable furnace, hold for 1 minute at 50 °C with continuous purging of N₂. TGA was carried out with a heating rate of 10 °C·min⁻¹ and heating the IL from 50-500 °C.

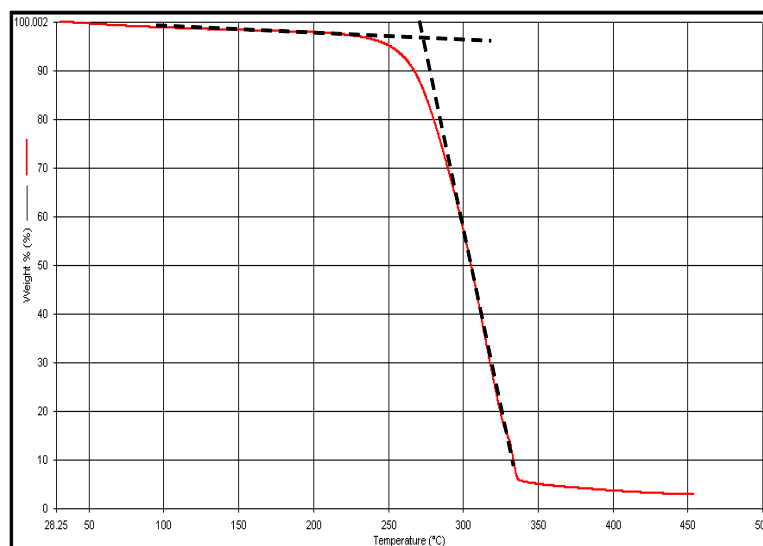


Fig 3-11 T_{onset} (intersection of baseline weight and the tangent of weight vs temperature curve (---))

3.5.4 Derived thermodynamic properties

The density and refractive index data obtained were used to estimate other properties such as, the lattice energy, molar refraction, free volume and the standard entropy.

Lattice energy of IL is the surface excess energy which is reliant on interaction energy between ions. Moreover, the low crystal energy is the underlying reason for forming the IL at room temperature [97]. Lattice energies of ILs were estimated according to Glasser theory [99] using the following equation:

$$U_{POT} = 1981.2 \left(\frac{\rho}{M} \right)^{\frac{1}{3}} + 103.8 \quad 3-2$$

where U_{POT} is the crystal lattice energy in kJ.mol⁻¹, ρ is density and M is molecular weight.

The refractive index and molar refraction provide useful information about the behavior of the molecules in the solution and the forces between these molecules. It uses the relation with the electronic polarizability of the molecule (this relation can be expressed in terms of molar polarizability or molar refraction) which is known as Lorenz–Lorentz equation [102]. The Lorenz–Lorentz equation can provide important information concerning the performance of a liquid as a solvent media since α_e represents the effect of the dispersion forces in the cohesion of the liquid [102]. This equation was used to estimate the molar refraction of the present IL. The equation takes the form:

$$R_M = \frac{N_A \alpha_e}{3\epsilon_0} = \frac{M}{\rho} \left(\frac{n_D^2 - 1}{n_D^2 + 1} \right) \quad 3-3$$

where, R_M is the molar refraction in $\text{cm}^3 \cdot \text{mol}^{-1}$, N_A is the Avogadro's number in mol^{-1} , α_e is the mean molecular polarizability (electronic polarizability), ϵ_0 is the permittivity of free space, M is the molecular weight in $\text{g} \cdot \text{mol}^{-1}$, N_A is the Avogadro's number in mol^{-1} , ρ is the density in $\text{g} \cdot \text{cm}^{-3}$ and n_D is refractive index. Molar refractions are also often considered as a measure of the hard-core molecular volumes because the electronic polarizability can be related to the spherical molecular radius [102]. The molar refraction was used to estimate the free volume of the molecule using the following equation[102]:

$$V_f = V_m - R_M \quad 3-4$$

Where V_f is the molar free volume in $\text{cm}^3 \cdot \text{mol}^{-1}$, V_m is the molar volume and .

The standard entropy for the synthesized ILs was estimated using the relation suggested by Glasser and Jenkins [97, 98]:

$$S^0 = 12465(V_{\text{molecular}}) + 29.5 \quad 3-5$$

$$V_{\text{molecular}} = \frac{M}{N_A \rho} \quad 3-6$$

where S^0 is the standard entropy at 298.15 K in $\text{J} \cdot \text{K}^{-1} \cdot \text{mol}^{-1}$, $V_{\text{molecular}}$ is the molecular volume in nm^3 , M is the molecular weight in $\text{g} \cdot \text{mol}^{-1}$, N_A is the Avogadro's number in mol^{-1} ρ is the density in $\text{g} \cdot \text{cm}^{-3}$ [96, 97].

3.6 Solubility of CO₂ in ILs using Magnetic Suspension Balance

The accurate determination of sorption represents a scientific and technical challenge. Four types of sorption measuring instruments are available: volumetric/manometric, gravimetric, carrier gas and calorimetric. With respect to dangers in handling of radioactive material the determination of the adsorbed amount by measuring the dose of radioactive radiation from radioactive isotopes of xenon or krypton is out of practice. A calorimetric measurement requires a highly sensitive calorimeter and complicated measuring techniques. Specialized instruments are not available and thus are restricted to special cases. The two most popular techniques to measure the adsorption of pure fluids are the volumetric and the gravimetric methods [186-189].

In comparison to gravimetric apparatus the volumetric are simpler in design and easier to operate. Because samples of any size can be investigated using a suitable sample bulbs, a high sensitivity can be achieved. The relative sensitivity of both methods is equivalent. The most serious error in volumetric is the error in the calibration of the dead space; the difference between the volume of sorptive gas consumed and the gas remaining in the dead space. The two variables: pressure and adsorbed amount are determined by one instrument: the manometer and by calibrated volumes and this may result in a slightly larger measuring error which is added up at each step of the adsorption isotherm [189, 190]. Favorably with the gravimetric method all variables: temperature, pressure and adsorbed mass are measured separately. The sorptive pressure is controlled at each step. Sample preparation is registered and thus optimum degassing conditions (temperature, pressure and time) can be found out and the mass of the dry sample can be determined. The gravimetric apparatus is more complicated and more expensive on account of the additional vacuum microbalance. Balance operating requires some skills [189].

The solubility of carbon dioxide in ILs was measured using a magnetic suspension balance (Rubotherm, Präzisionsmesstechnik GmbH, Bochum, Germany), also referred to as the MSB (Fig 3-12). The MSB employs a magnetic suspension coupling consisting of an electromagnet and a suspension magnet, which maintains freely suspended contactless balance connections. This ensures the safety of the microbalance during the measurement of corrosive or noxious gases. For the software

unit, MessPro was the software used to control a Rubotherm magnetic suspension balance and it is also the software for the data capture. Additionally, the temperature control in an overlapping controller consists of the direct temperature controller (JUMO IMAGO 5000 and /or JULABO F-25ME) and a software-controlled on the computer.

The MSB makes it possible to weigh samples contactlessly in almost all environments with a balance maintained at ambient conditions. The sample was located in the measuring cell and can be (un)coupled specifically (from) to the balance with a contactless magnetic suspension coupling. An electromagnet was attached to the bottom of the balance. It lifts the suspension magnet, which consists of a permanent magnet, a sensor core and a measuring load decoupling cage. The electromagnet, which was attached to the underfloor weighing hook of the weighing cell, maintained a freely suspension state of the suspension magnet via an electronic control unit. Thereby, different vertical positions were possible. First the zero-point position (ZP) in which the suspension part suspends alone and contactlessly and thus represented the unburdened balance. And second the measuring point position (MP), in which the suspension part reaches a higher vertical position, thereby couples the sample to the balance and transmits the weight of the sample to the balance. In addition to the off point position (OP) in which the sample is resting on landing. The precision of the microbalance was reported to be 0.001 mg. The temperature and pressure in the measuring cell were controlled to within ± 0.2 °C and ± 0.05 bar respectively. The reproducibility of the machine was ± 0.020 mg. The experiment was conducted three times to obtain repeatability of the data.

To perform highly accurate weight measurements all potential disturbances caused by the environment of the sample were reduced as much as possible and determined. The buoyancy effect cannot be reduced or prohibited, thus this effect was quantified and corrected. Additionally, the density of the atmosphere surrounding the sample was determined to perform the buoyancy effect; the density of the gas phase at the specific condition (temperature, pressure) was calculated using Peng-Robinson equation of state (PR-EOS). Helium was used as a measuring gas for volume determination since it was reported that it was much better than any other gas. The

solubility measurement was performed in four main consequence steps namely, blank measurement, drying, buoyancy and solubility measurements. The principle and purposes of these steps are briefly described below.

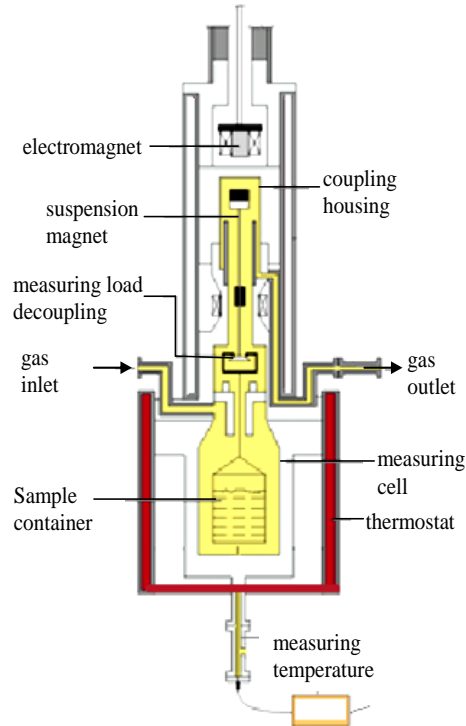


Fig 3-12 Schematic of magnetic suspension balance for solubility measurements

3.6.1 Blank measurement

The blank measurement was performed only once (for the first sample) to measure the absorption isotherm without sample in the MSB and the data obtained were used to determine the mass and volume of the empty sample container. Starting from vacuum the pressure was increased stepwise with nitrogen (also helium can be used). The recorded data during the blank measurement were the balance reading (m_{BAL}), the temperature (T) and pressure (P) of the gas. The temperature and pressure data were used to calculate the density of the gas using Peng-Robinson equation of state (PR-EOS). The weigh of the empty sample container decreases with increasing pressure of the gas due to the buoyancy effect acting on the sample container. The buoyancy effect (B) acts on anybody located in the gas atmosphere with density ρ . It is

proportional to the density and described as the product of the density and the volume (V) of the body as in 3-7 equation 3-7.

$$B = \rho \cdot V \tag{3-7}$$

The balance reading was plotted against the density, ρ , of the gas (Fig 3-13) to estimate the mass and volume of the empty sample container, (m_{SC} and V_{SC}), (the negative slope).

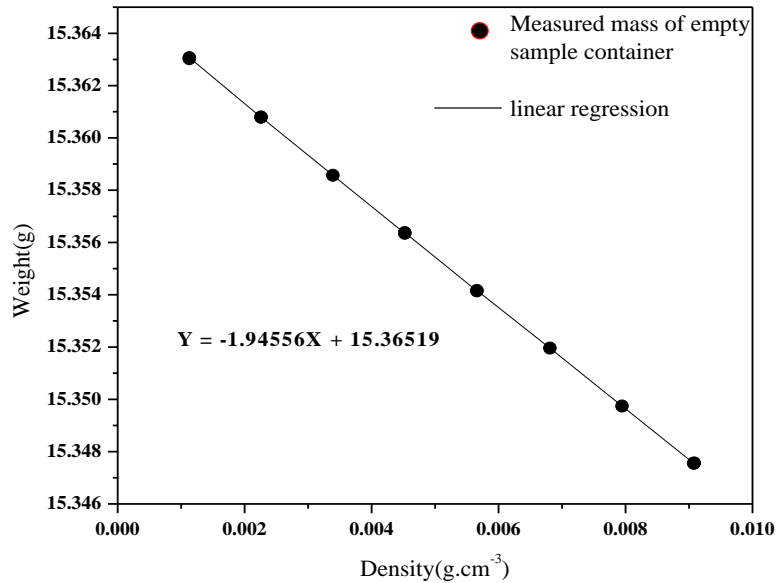


Fig 3-13 Example for result of the blank measurement

The linear regression of the measured masses can be written as:

$$m_{BAL} = m_{SC} - \rho \cdot V_{SC} \tag{3-8}$$

The values of the parameters of this linear function are the weight and volume of the empty sample container.

3.6.2 Drying

Each IL was dried before the CO₂ solubility measurement to ensure maximum removal of water and volatile matter. The sample was distributed in the three discs of the liquid sample container (0.8-1.0 g) in the MSB and the measuring cell was closed. Leak test was performed by purging helium to the specific pressure, then the pressure

controller was turned off and the pressure reading was monitored for some time to ensure that there is no gas leak. The sample was heated gradually until 100 °C under evacuation and the weight reading was monitored by the MSB until there was no further mass change of the sample (Fig 3-14) then the drying was considered completed. After that the sample was cooled down to the measurement temperature. At the end of the drying this mass was measured in vacuum.

$$m_{SC+S} = m_{BAL} \quad (P = 0, \rho = 0) \quad 3-9$$

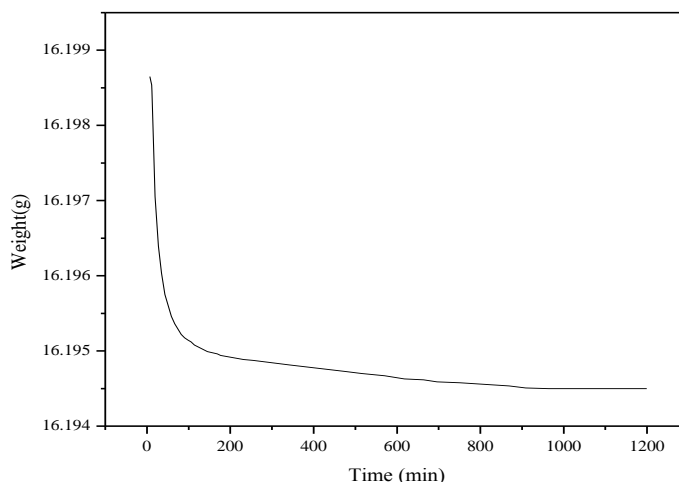


Fig 3-14 Example for the results of the drying process at 100 °C

3.6.3 Buoyancy measurement

Usually the volume of the sample was not known accurately. In order to determine the volume of the sample located in the sample container of the MSB a buoyancy measurement was carried out for each sample. The buoyancy measurement was performed to correct the mass of the sample weight with the MSB during the solubility measurement due to the buoyancy effect acting on it in the gas phase (equation 3-7).

The measurement was performed by stepwise increase of pressure at constant temperature using helium gas (helium is almost not absorbing and it does not change the mass of the sample). Peng-Robinson equation of state (PR-EOS) was used to calculate the density of gas at the specific temperatures and pressures. Then, the

balance reading (m_{BAL}) was plotted as a function of the density of the gas and a straight line with negative slope was obtained (Fig 3-15).

The decrease of the measured masses of the sample container (loaded with sample) with increasing pressure of the gas was due to the buoyancy acting on the sample container and the sample. The linear regression of the measured masses was performed (Fig 3-15).

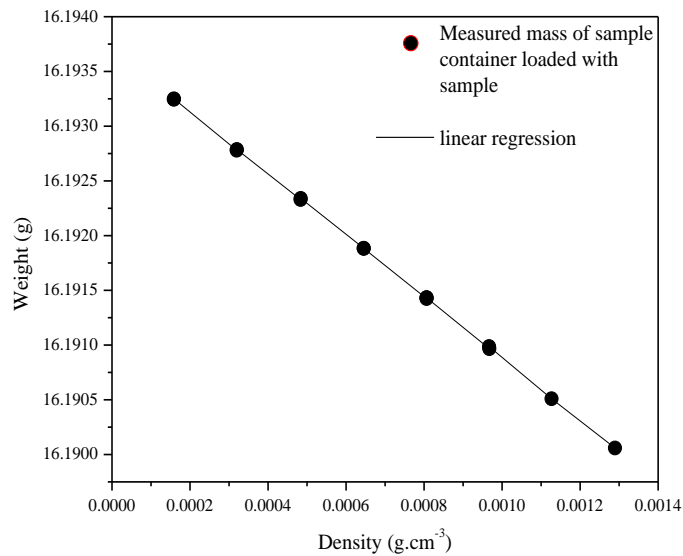


Fig 3-15 Example for the results of the buoyancy measurement

The linear function is the mass of the sample container plus sample in vacuum (m_{SC+S}) minus the buoyancy effect. The buoyancy effect is due to the volume of empty sample container plus the volume of the sample (V_{SC+S}). This gas determined by subtraction of the volume of the empty sample container (V_{SC} determined from the blank measurement). The volume of the sample was then obtained:

$$m_{BAL} = m_{SC+S} - \rho \cdot V_{SC+S} \quad 3-10$$

The regression is shown in Fig 3-15. By completing the buoyancy measurements, the mass and volume of the sample were determined.

3.6.4 Solubility measurement

Before performing the solubility measurement and after the buoyancy measurement was completed, the MSB was evacuated. The solubility measurement was commenced at constant temperature and the pressure of the gas in the cell was increased stepwise until it reaches the desire pressure. The process was then continuously monitored until the MSB shows no further mass increase of the reading (or negligible increases) or the solubility measurement shows no further increase (Fig 3-16) then the solubility measurement was considered completed.

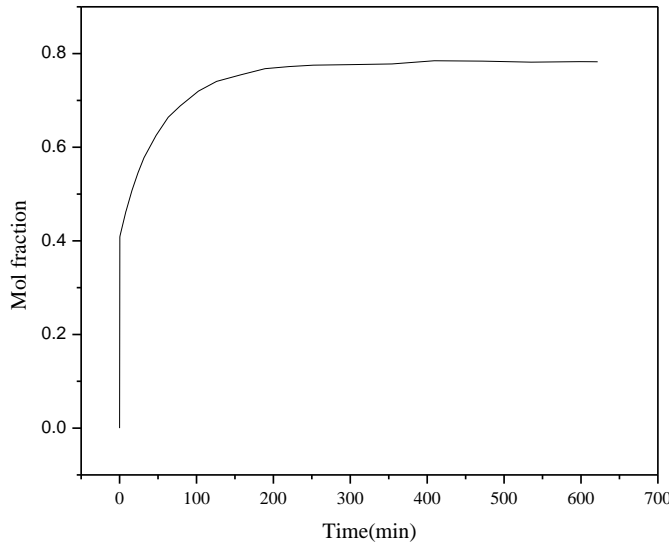


Fig 3-16 Example for the results of the solubility measurement

The data recorded in the solubility measurement was the balance reading (m_{BAL}), the temperature (T) and the pressure of the gas (P). From these data the density of the gas was calculated using PR-EOS. The recorded balance reading (m_{BAL}) in the solubility measurement was corrected for the buoyancy effect acting on the sample and sample container. The correction was done by adding the density of the gas (ρ , calculated before) and the volume of the sample container (V_{SC+S} determined in the buoyancy measurement before) to the balance reading as shown in equation 3-11.

$$m_{BAL.CORR} = m_{BAL} + \rho \cdot V_{SC+S} \quad 3-11$$

The buoyancy corrected mass is the mass of the sample and the sample container, and then the mass of the sample is the product of subtracting the mass of the empty container from this.

$$m_S = m_{BAL.CORR} - m_{SC} \quad 3-12$$

The mass of the sample with CO₂ was determined. The mass of the CO₂ absorbed by the sample was then determined as follows:

$$m_{CO_2} = m_{S+SC} - m_S \quad 3-13$$

In a typical experiment the following steps were followed:

1. The liquids sample container (with three stainless steel discs) was suspended in the place of the measuring cell in the MSB and it was verified that the zero point and measuring point are stable. The measuring cell was sealed by securing the bolts on the flange (ensure that the bolts do not protrude outside the diameter of the measuring cell so that the heating jacket will slide on with ease). Then, it was verified that the zero point and measuring point are stable. An o-ring was inserted. The gas delivery system was connected to the measuring cell. The heating jacket was installed around the measuring cell and again it was verified that the zero point and measuring point are stable. Then, a high-pressure (helium) was fed to the measuring cell to leak test the system. The measuring cell was evacuated using a vacuum pump.
2. A blank measurement was made using nitrogen gas at 25 °C at pressures of 1, 2, 3, 4, 5, 6, 7 and 8 bars (see blank measurement).
3. Then, the measuring cell was opened and 0.8-1.0 g of the IL was placed in the liquid sample container (the sample distributed in the three stainless steel discs of the liquid sample container).
4. Step 1 was repeated.
5. The IL was dried (to ensure removal of moisture) at 100 °C (see drying), the temperature was controlled using JUMO IMAGO 5000 heater for heating and JULABO F-25ME for cooling.
6. The effect of the buoyancy was determined using helium gas at 25 °C in pressures 1, 2, 3, 4, 5, 6, 7 and 8 bars (see buoyancy measurement).
7. The measuring cell was evacuated to remove the helium gas.
8. The sample chamber was pressurized with the gas at constant temperature to a given pressure and the system was allowed to reach thermodynamic

equilibrium. Once stabilized, a measurement was taken and the system advanced to the next higher pressure. Additional CO₂ was added in increments and the corresponding equilibrium weight of the IL sample was recorded at each pressure interval. To ensure equilibrium and reversibility, a desorption isotherm was measured by incrementally evacuating the gas from the chamber. The solubility at a given pressure and temperature was determined by measuring the mass uptake and corrected for buoyancy effects. The solubility measurements were performed and selected samples were measured at different temperatures (25, 40 and 70 °C).

9. The recyclability of selected IL sample was determined at 20 bar for 5 times. After the solubility measurement, the measuring cell was evacuated and heated to 100 C° until there was no further mass change of the sample then a new solubility measurement was made.

The liquid sample container was cleaned using suitable solvent and dried after each gas solubility measurement. A schematic flow chart for the procedure to measure the solubility of a gas in IL using MSB was shown in Fig 3-17.

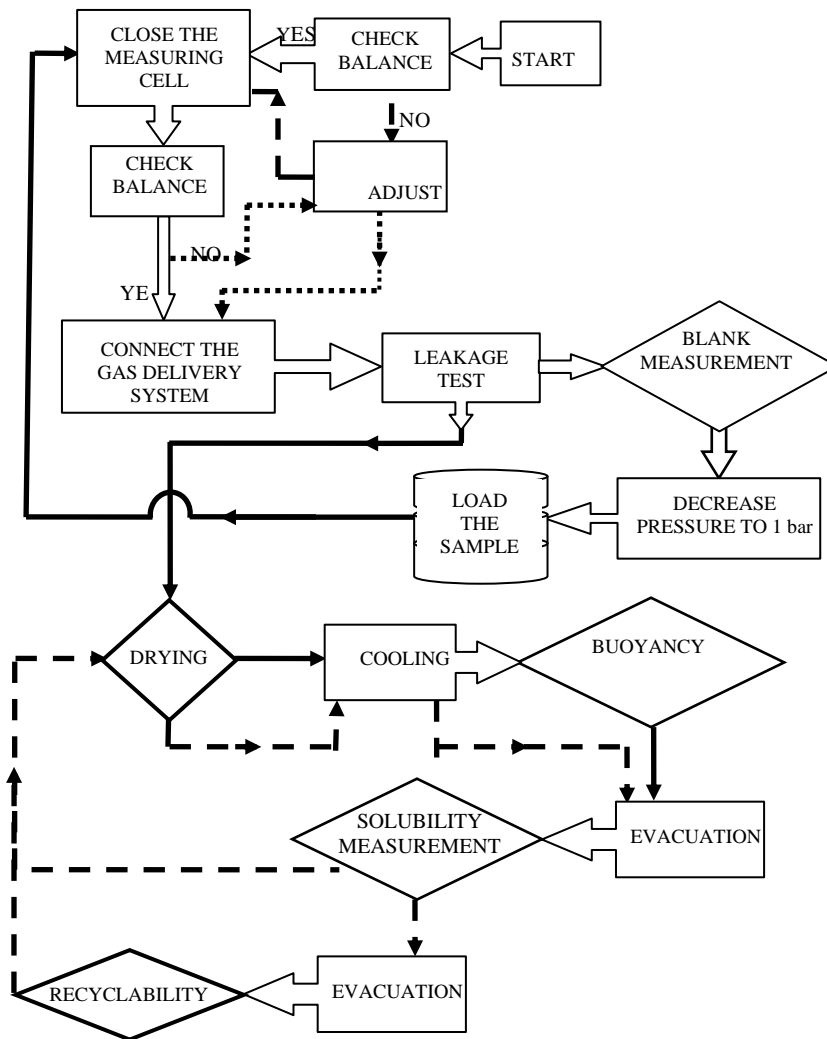


Fig 3-17 Flowchart for the procedure performed to measure gases solubility in ILs using MSB

CHAPTER 4

CHARACTERIZATION AND THERMOPHYSICAL PROPERTIES

4.1 Characterization of ILs

The imidazolium-based ILs were prepared by the quaternization of n-propanenitrile imidazole with the respective alkyl bromide, alkyl chloride, allyl chloride, benzyl chloride and 2-chloroethanol resulting in the bromo or chloro ILs. The phosphonium-based ILs were prepared by reacting the trialkylphosphine with alkylchloride or dialkyl chloride. These ILs were converted into (DOSS), (DDS), (SBA), (BS) and (TFMS) salts by metathesis reaction with sodium salts of (DOSS), (DDS), (SBA), (BS) and (TFMS). Propanenitrile imidazole was obtained by the reaction of imidazole with acrylonitrile. A very viscous liquid was obtained with a yellowish colour. Schematic representation of the relation between cations and anions for the synthesized ILs is shown in Table 4-1.

The purity of an IL is of paramount importance, since impurities influence its chemical and physical properties [74]. Prior to use, ILs were carefully characterized using several methods, such as NMR, FTIR and elemental analysis. ILs have a very low vapour pressure and, therefore, cannot be purified by distillation. It is important to use purified starting materials in their preparation in order to get a pure IL. The main contaminants of ILs are halides, water, organic compounds or inorganic salts. The level of purity of the IL determines the application where an IL will be used.

Table 4-1 Schematic representation of the relation between cations and anions for the synthesized ILs

Cations	Anions						
	Cl	Br	DOSS	DDS	SBA	BS	TFMS
[CNC ₂ Bim]	•	•	•	•		•	•
[CNC ₂ Him]	•	•	•	•	•	•	•
[CNC ₂ Oim]	•	•	•	•	•	•	•
[CNC ₂ Dim]		•	•	•	•		
[P _{6,6,6,14}]			•				
[P _{8,8,8,14}]	•		•				
[P _{8,8,8,14}]	•		•				
[P _{8,8,8} C ₁₀ P _{8,8,8}]	•		•				
[P _{8,8,8} C ₆ P _{8,8,8}]	•		•				
[CNC ₂ Heim]			•				
[CNC ₂ Bzim]			•				
[CNC ₂ Ayim]			•				

The ¹H NMR of the synthesized RTILs is shown in Fig A-1 to Fig A-5. The ¹H and ¹³C NMR, FTIR, elemental analysis (% actual % theoretical), water content and halide contents results for the present ILs are as follows:

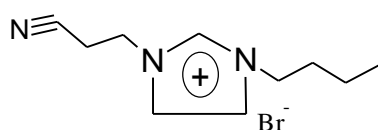


Fig 4-1 Structure of [C₂CN Bim]Br

[C₂CN Bim]Br; δ_H(300 MHz; CDCl₃): = 9.24 (s, 1H, N-CH-N), 7.79 (s, 1H, N-CH-CH), 7.75 (s, 1H, 1H, N-CH-CH), 4.60 (t, 2H, N-CH₂- (CH₂)₂- CH₃), 4.29 (t, 2H, 2H, N-CH₂-CH₂- CN), 3.21 (t, 2H, N-CH₂-CH₂- CN), 1.90 (m, 2H, N-CH₂-CH₂-CH₂-), 1.38 (m, 2H, CH₂-CH₂-CH₃), 0.98 (t, 3H, CH₂-CH₃). ¹³C NMR (75 MHz; CDCl₃) = 136.80, 121.54, 120.58, 117.28, 48.22, 42.96, 30.02, 19.08, 17.99, 11.43. FTIR-ATR ν_{max}/cm⁻¹: 2246 and 1562 (C≡N), 2923, 2854 and 1461 (C-H).

Elemental analysis: % actual C, 46.62; H, 6.01; N, 16.97. $C_{10}H_{16}N_3Br$ % theoretical C, 46.52; H, 6.26; N, 16.28; mass fraction of water 406×10^{-6} .

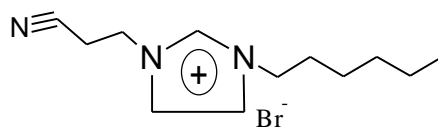


Fig 4-2 Structure of $[C_2CN \text{ Him}]Br$

$[C_2CN \text{ Him}]Br$; $\delta_H(300 \text{ MHz}; CDCl_3)$: = 9.77 (s, 1H, N-CH-N), 7.82 (s, 1H, N-CH-CH), 7.26 (s, 1H, 1H, N-CH-CH), 4.49 (t, 2H, N-CH₂- (CH₂)₂- CH₃), 3.88 (t, 2H, 2H, N-CH₂-CH₂- CN), 3.00 (t, 2H, N-CH₂-CH₂- CN), 1.48, (m, 2H, N-CH₂-CH₂-CH₂-),), 0.87 (m, 6H, CH₂), 0.43 (t, 3H, CH₂-CH₃). $^{13}C \text{ NMR}$ (75 MHz; $CDCl_3$) = 128.87, 120.25, 117.39, 106.71, 53.43, 41.24, 32.97, 30.77. 28.58, 20.15, 16.62, 12.24. FTIR-ATR ν_{max}/cm^{-1} : 2245 and 1558 (C≡N), 2929, 2863 and 1458 (C-H).

Elemental analysis: % actual C, 50.56; H, 6.90; N, 13.98. $C_{12}H_{20}N_3 Br$ % theoretical C, 50.35; H, 7.06; N, 14.68; mass fraction of water 385×10^{-6} .

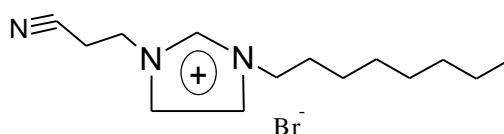


Fig 4-3 Structure of $[C_2CN \text{ Oim}]Br$

$[C_2CN \text{ Oim}]Br$; $\delta_H(300 \text{ MHz}; CDCl_3)$: = 9.80 (s, 1H, NCHN), 8.05 (s, 1H, CHN), 7.39 (s, 1H, CHN), 4.75 (t, 2H, NCH₂), 4.10 (t, 2H, CNCH₂), 3.24 (t, 2H, CH₂CH₂CN), 1.72 (t, 2H, CH₂CH₂N), 1.14 (br, 8H, CH₂), 0.68 (t, 3H, CH₃CH₂). $^{13}C \text{ NMR}$ (75 MHz; $CDCl_3$) = 130.83, 123.71, 120.73, 107.89, 52.92, 42.57, 33.16, 30.58. 29.13, 26.93, 24.58, 20.63, 17.41, 13.22. FTIR-ATR ν_{max}/cm^{-1} : 2245 and 1561 (C≡N), 2925, 2858 and 1458 (C-H).

Elemental analysis: % actual C, 52.20; H, 7.43; N, 12.93; S, 5.41. $C_{14}H_{24}N_3 Br$ % theoretical C, 53.49; H, 7.71; N, 13.37; mass fraction of water 369×10^{-6} .

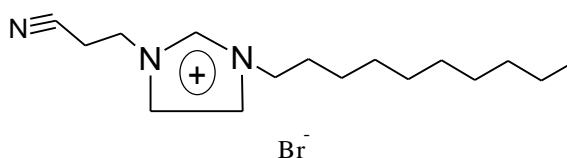


Fig 4-4 Structure of $[C_2CN \text{ Dim}]Br$

$[C_2CN \text{ Dim}]Br$; $\delta_H(300 \text{ MHz}; CDCl_3)$: = 9.82 (s, 1H, NCHN), 7.88(s, 1H, CHN), 7.27(s, 1H, CHN), 4.54 (t, 2H, NCH₂), 3.92 (t, 2H, CNCH₂), 3.05 (t, 2H,

CH_2CH_2CN), 1.54 (t, 2H, CH_2CH_2N), 0.93 (br, 12H, CH_2), 0.47 (t, 3H, CH_3CH_2). ^{13}C NMR (75 MHz; $CDCl_3$) = 137.02, 122.95, 121.13, 116.87, 49.61, 45.9, 31.23, 29.68, 28.21, 23.12, 22.65, 18.97, 13.42. FTIR-ATR ν_{max}/cm^{-1} : 2244 and 1562 ($C\equiv N$), 2921, 2852 and 1461 (C-H).

Elemental analysis: % actual C, 56.22; H, 8.04; N, 12.59. $C_{16}H_{28}N_3Br$ % theoretical C, 56.13; H, 8.26; N, 12.28; mass fraction of water 341×10^{-6} .

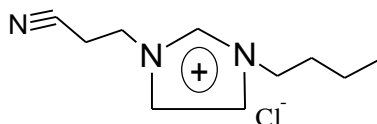


Fig 4-5 Structure of $[C_2CN \text{ Bim}]Cl$

$[C_2CN \text{ Bim}]Cl$; δ_H (300 MHz; $CDCl_3$): = 7.92 (s, 1H, N-CH-N), 7.80 (s, 1H, N-CH-CH), 7.70 (s, 1H, N-CH-CH), 4.61 (t, 2H, N- CH_2 - $(CH_2)_2$ - CH_3), 4.31 (t, 2H, N- CH_2 - CH_2 -CN), 3.22 (t, 2H, N- CH_2 - CH_2 -CN), 1.92 (m, 2H, N- CH_2 - CH_2 - CH_2 -), 1.37 (m, 2H, CH_2 - CH_2 - CH_3), 0.93 (t, 3H, CH_2 - CH_3). FTIR-ATR ν_{max}/cm^{-1} : 2252 and 1562 ($C\equiv N$), 2958, 2833 and 1460 (C-H).

Elemental analysis: % actual C, 54.28; H, 10.16; N, 19.31. $C_{10}H_{16}N_3Cl$ % theoretical C, 54.39; H, 10.98; N, 19.03; mass fraction of water 471×10^{-6} .

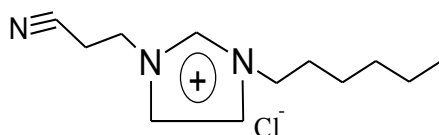


Fig 4-6 Structure of $[C_2CN \text{ Him}]Cl$

$[C_2CN \text{ Him}]Cl$; δ_H (300 MHz; $CDCl_3$): = 9.60 (s, 1H, N-CH-N), 7.48 (s, 1H, N-CH-CH), 6.83 (s, 1H, N-CH-CH), 4.07 (t, 2H, N- CH_2 - $(CH_2)_4$ - CH_3), 3.67 (t, 2H, N- CH_2 - CH_2 -CN), 3.45 (t, 2H, N- CH_2 - CH_2 -CN), 2.60 (m, 2H, - CH_2 - CH_2 - CH_3), 2.29 (m, 2H, N- CH_2 - CH_2 - CH_2 -), 1.08 (m, 2H, N- $(CH_2)_2$ - CH_2 -), 0.92 (m, 2H, - CH_2 - CH_2 - CH_3), 0.61 (t, 3H, - CH_2 - CH_2 - CH_3). FTIR-ATR ν_{max}/cm^{-1} : 2250 and 1562 ($C\equiv N$), 2954, 2858 and 1458 (C-H).

Elemental analysis: % actual C, 59.14; H, 8.03; N, 17.67. $C_{12}H_{20}N_3Cl$ % theoretical C, 59.85; H, 8.39; N, 17.45; mass fraction of water 428×10^{-6} .

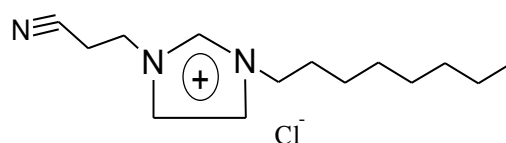


Fig 4-7 Structure of [C₂CN Oim]Cl

[C₂CN Oim]Cl; δ_{H} (300 MHz; CDCl₃): = 9.99 (s, 1H, N-CH-N), 7.90 (s, 1H, N-CH-CH), 7.19 (s, 1H, N-CH-CH), 4.48 (t, 2H, N-CH₂-(CH₂)₆-CH₃), 3.85 (t, 2H, N-CH₂-CH₂-CN), 3.02 (t, 2H, N-CH₂-CH₂-CN), 2.98 (m, 2H, N-CH₂-CH₂-CH₂), 1.48 (m, 2H, N-CH₂-CH₂-CH₂-), 0.87 (m, 2H, N-(CH₂)₃-CH₂-), 0.80 (m, 6H, -N-(CH₂)₄-(CH₂)₃-), 0.48 (t, 3H, -CH₂-CH₃). FTIR-ATR $\nu_{\text{max}}/\text{cm}^{-1}$: 2246 and 1562 (C≡N), 2925, 2854 and 1460 (C-H).

Elemental analysis: % actual C, 64.78; H, 6.32; N, 16.53. C₁₄H₂₄N₃Cl % theoretical C, 64.48; H, 6.20; N, 16.12; mass fraction of water 459×10⁻⁶.

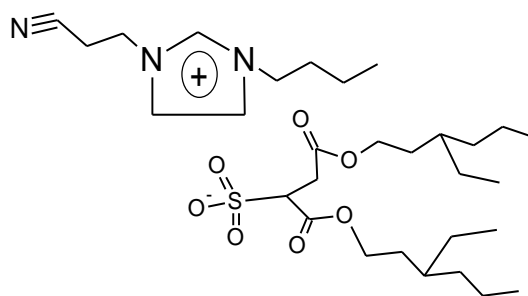


Fig 4-8 Structure of [C₂CN Bim]DOSS

[C₂CN Bim]DOSS; δ_{H} (300 MHz; CDCl₃): = 9.95 (s, 1 H, NCHN), 7.80 (s, 1 H, CHN), 7.34 (1 H, s, CHN), 4.71 (t, 1 H, CHSO₃), 4.28 (t, 2 H, NCH₂), 4.05 (d, 4 H, OCH₂CH), 3.98 (t, 2 H, CNCH₂), 3.19 (t, 2 H, CH₂CH₂CN), 1.91 (d, 2 H, COCH₂CH), 1.62 (t, 2 H, CH₂CH₂N), 1.38 (d, 4 H, OCH₂CH), 1.24 (br m, 16 H, CH₂), 0.84 (t, 15 H, CH₃CH₂). ¹³C NMR (75 MHz; CDCl₃) = 171.26, 168.56, 136.68, 122.64, 116.67, 67.53, 66.92, 62.06, 48.21, 48.00, 47.78, 47.57, 47.36, 30.21, 28.81, 22.75, 19.15, 13.24, 13.20. FTIR-ATR $\nu_{\text{max}}/\text{cm}^{-1}$: 2248 and 1564 (C≡N), 2929, 2871 and 1460 (C-H), 1213 and 1035 (SO₃), 1730 (C=O), 1161 (C-O-C).

Elemental analysis: % actual C, 59.89; H, 9.15; N, 6.90; S, 5.41. C₃₀H₅₄N₃O₇S % theoretical C, 59.97; H, 9.06; N, 6.99; S, 5.34; mass fraction of water 198×10⁻⁶, mass fraction of bromide 78×10⁻⁶.

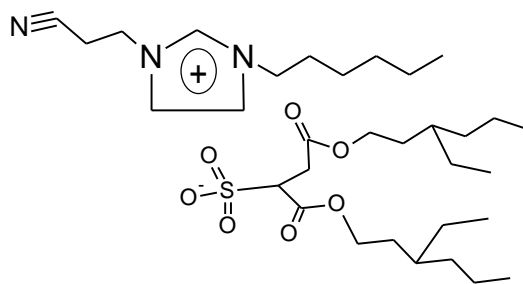


Fig 4-9 Structure of [C₂CN Him]DOSS

[CNC₂Him]DOSS: δ_{H} (300 MHz; CDCl₃): = 9.83 (s, 1 H, NCHN), 7.80 (s, 1 H, CHN), 7.30 (s, 1 H, CHN), 4.71 (t, 1 H, CHSO₃), 4.25 (t, 2 H, NCH₂), 4.16 (d, 4 H, OCH₂CH), 4.01 (t, 2 H, CNCH₂), 3.17 (t, 2 H, CH₂CH₂CN), 2.30 (d, 2 H, COCH₂CH), 1.92 (t, 2 H, CH₂CH₂N), 1.59 (d, 4 H, OCH₂CH), 1.28 (br m, 24 H, CH₂), 0.88(t, 15 H, CH₃CH₂). ¹³C NMR (75 MHz; CDCl₃) = 171.44, 169.22, 137.68, 123.22, 121.78, 116.96, 76.70, 67.23, 62.05, 50.27, 45.39, 38.56, 34.24, 31.03, 28.88, 25.87, 22.93, 19.62, 14.00, 10.93, 10.78. FTIR-ATR ν_{max} /cm⁻¹: 2252 and 1562 (C≡N), 2929, 2870 and 1460 (C-H), 1213 and 1037 (SO₃), 1730 (C=O), 1159 (C-O-C).

Elemental analysis: % actual C, 61.03; H, 9.41; N, 6.52; S, 5.13. C₃₂H₅₈N₃O₇S

% theoretical C, 61.12; H, 9.30; N, 6.52; S, 5.10; mass fraction of water 219×10⁻⁶, mass fraction of bromide 65×10⁻⁶.

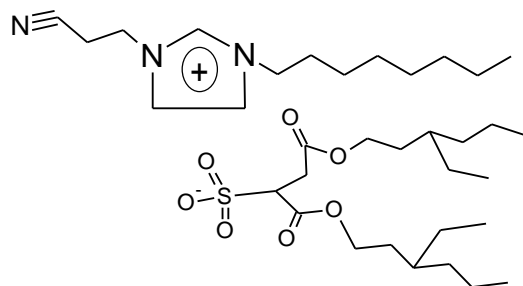


Fig 4-10 Structure of [C₂CN Oim]DOSS

[C₂CN Oim]DOSS: δ_{H} (300 MHz; CDCl₃): = 9.72 (s, 1 H, NCHN), 7.86 (s, 1 H, CHN), 7.33 (s, 1 H, CHN), 4.73 (t, 1 H, CHSO₃), 4.24 (t, 2 H, NCH₂), 4.13 (d, 4 H, OCH₂CH), 3.98 (t, 2 H, CNCH₂), 3.19 (t, 2 H, CH₂CH₂CN), 3.11 (d, 2 H, COCH₂CH), 1.89 (t, 2 H, CH₂CH₂N), 1.62 (d, 4 H, OCH₂CH), 1.27 (br m, 24 H, CH₂), 0.89 (15 H, t, CH₃CH₂). ¹³C NMR (75 MHz; CDCl₃) = 171.41, 169.31, 137.44, 123.30, 121.88, 117.01, 77.35, 67.95, 61.98, 50.25, 45.34, 38.67, 34.09, 31.65, 28.99, 26.25, 23.63, 22.93, 19.66, 14.03, 10.91, 10.85. FTIR-ATR ν_{max} /cm⁻¹: 2250 and

1564 (C≡N), 2929, 2860 and 1461 (C-H), 1215 and 1035 (SO₃), 1730 (C=O), 1159 (C-O-C).

Elemental analysis: % actual C, 62.18; H, 9.44; N, 6.47; S, 4.82. C₃₄H₆₂N₃O₇S

% theoretical C, 62.10; H, 9.51; N, 6.47; S, 4.88; mass fraction of water 152×10⁻⁶, mass fraction of bromide 67×10⁻⁶.

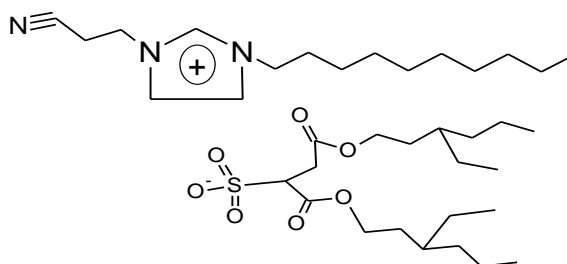


Fig 4-11 Structure of [C₂CN Dim]DOSS

[C₂CN Dim]DOSS: δ_H(300 MHz; CDCl₃): = 9.62 (s, 1 H, NCHN), 7.88(s, 1 H, CHN), 7.34 (s, 1 H, CHN), 4.72 (t, 1 H, CHSO₃), 4.24 (t, 2 H, NCH₂), 4.17 (d, 4 H, OCH₂CH), 3.96 (t, 2 H, CNCH₂), 3.21 (t, 2 H, CH₂CH₂CN), 2.83 (d, 2 H, COCH₂CH), 1.87 (t, 2 H, CH₂CH₂N), 1.55 (d, 4 H, OCH₂CH), 1.32 (br m, 28 H, CH₂), 0.88 (15 H, t, CH₃CH₂). ¹³C NMR (75 MHz; CDCl₃) = 171.40, 169.37, 137.32, 123.31, 121.93, 117.05, 68.01, 50.23, 45.32, 38.58, 31.82, 30.03, 29.22, 28.84, 26.26, 23.39, 22.90, 19.67, 13.99, 10.83. FTIR-ATR ν_{max}/cm⁻¹: 2250 and 1564 (C≡N), 2925, 2873 and 1460 (C-H), 1223 and 1037 (SO₃), 1731 (C=O), 1159 (C-O-C).

Elemental analysis: % actual C, 63.03; H, 9.65; N, 6.04; S, 4.73. C₃₆H₆₆N₃O₇S

% theoretical C, 63.12; H, 9.71; N, 6.13; S, 4.68; mass fraction of water 184×10⁻⁶, mass fraction of bromide 83×10⁻⁶.

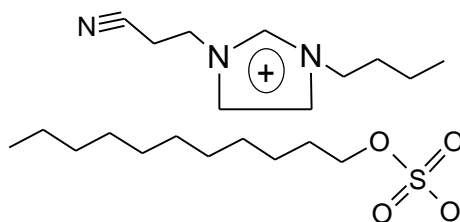


Fig 4-12 Structure of [C₂CN Bim]DDS

[C₂CN Bim]DDS; δ_H(300 MHz; D₂O): = 7.81 (s, 1 H, NCHN), 7.75 (s, 2 H, CHN), 4.79 (t, 2 H, NCH₂CH₂), 4.70 (t, 2 H, OCH₂CH₂), 4.39 (t, 2 H, CNCH₂), 3.33 (t, 2 H,

CH_2CH_2CN), 3.30 (t, 2 H, CH_2CH_2N), 1.98 (t, 2 H, CH_2CH_2O), 1.45 (br m, 20 H, CH_2), 1.01 (t, 6 H, CH_3CH_2). ^{13}C NMR (75 MHz; D_2O) = 136.29, 123.32, 122.79, 118.04, 68.45, 49.8386, 45.12, 43.64, 32.23, 31.68, 30.13, 26.16, 22.87, 19.96, 19.59, 19.20, 14.05, 13.25. FTIR-ATR ν_{max}/cm^{-1} : 2252 and 1564 ($C\equiv N$), 2923, 2865 and 1461 (C-H), 1215 and 1163 (SO_3).

Elemental analysis: % actual C, 59.35; H, 9.61; N, 9.49; S, 7.15. $C_{22}H_{42}N_3O_4S$

% theoretical C, 59.43; H, 9.52; N, 9.49; S, 7.15; mass fraction of water 170×10^{-6} , mass fraction of bromide 66×10^{-6} .

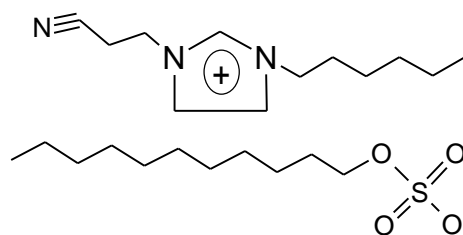


Fig 4-13 Structure of $[C_2CN \text{ Him}]DDS$

$[CNC_2Him]DDS$: δ_H (300 MHz; D_2O): = 9.92 (s, 1 H, $NCHN$), 7.75 (s, 2 H, CHN), 7.51 (t, 2 H, NCH_2CH_2), 4.57 (t, 2 H, OCH_2CH_2), 4.63 (t, 2 H, $CNCH_2$), 4.19 (t, 2 H, CH_2CH_2CN), 3.18 (t, 2 H, CH_2CH_2N), 1.93 (t, 2 H, CH_2CH_2O), 1.81 (br m, 4 H, CH_2), 1.30 (br m, 20 H, CH_2), 0.87 (t, 6 H, CH_3CH_2). FTIR-ATR ν_{max}/cm^{-1} : 2250 and 1564 ($C\equiv N$), 2923, 2854 and 1461 (C-H), 1217 and 1163 (SO_3).

Elemental analysis: % actual C, 61.09; H, 9.92; N, 8.81; S, 6.73. $C_{24}H_{46}N_3O_4S$

% theoretical C, 60.98; H, 9.81; N, 8.89; S, 6.78; mass fraction of water 198×10^{-6} , mass fraction of bromide 83×10^{-6} .

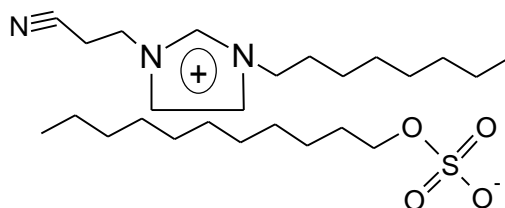


Fig 4-14 Structure of $[C_2CN \text{ Oim}]DDS$

$[C_2CN \text{ Oim}]DDS$: δ_H (300 MHz; D_2O): = 7.77 (s, 1 H, $NCHN$), 7.75 (s, 2 H, CHN), 4.81 (t, 2 H, NCH_2CH_2), 4.57 (t, 2 H, OCH_2CH_2), 4.27 (t, 2 H, $CNCH_2$), 3.98 (t, 2 H, CH_2CH_2CN), 3.18 (t, 2 H, CH_2CH_2N), 1.93 (t, 2 H, CH_2CH_2O), 1.63 (br m, 8 H, CH_2), 1.32 (br m, 20 H, CH_2), 0.89 (t, 6 H, CH_3CH_2). FTIR-ATR ν_{max}/cm^{-1} : 2250 and 1564 (CN), 2921, 2852 and 1461 (C-H), 1218 and 1163 (SO_3).

Elemental analysis: % actual C, 62.45; H, 10.05; N, 8.35; S, 6.36. $C_{26}H_{50}N_3O_4S$
 % theoretical C, 62.36; H, 10.06; N, 8.39; S, 6.40; mass fraction of water 137×10^{-6} ,
 mass fraction of bromide 53×10^{-6} .

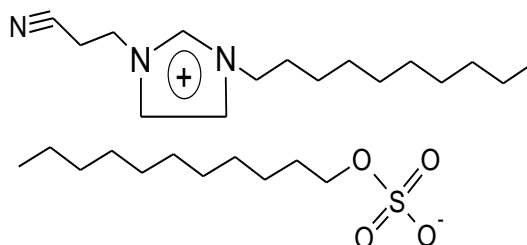


Fig 4-15 Structure of [C₂CN Dim]DDS

[C₂CN Dim]DDS: δ_H (300 MHz; D₂O): = 7.77 (s, 1 H, NCHN), 7.75 (s, 2 H, CHN), 4.58 (t, 2 H, NCH₂CH₂), 4.25 (t, 2 H, OCH₂CH₂), 3.98 (t, 2 H, CNCH₂), 3.20 (t, 2 H, CH₂CH₂CN), 3.17 (t, 2 H, CH₂CH₂N), 1.90 (t, 2 H, CH₂CH₂O), 1.36 (br m, 12 H, CH₂), 1.29 (br m, 20 H, CH₂), 0.88 (t, 6 H, CH₃CH₂). ¹³C NMR (75 MHz; D₂O) = 122.96, 122.53, 116.5245, 109.39, 67.84, 48.37, 47.7243, 45.07, 31.74, 29.49, 29.45, 29.23, 28.19, 25.94, 25.66, 22.43, 18.62, 13.17. FTIR-ATR ν_{max}/cm^{-1} : 2250 and 1564 (C≡N), 2921, 2872 and 1455 (C-H), 1218 and 1163 (SO₃).

Elemental analysis: % actual C, 63.68; H, 10.37; N, 7.98; S, 6.01. $C_{28}H_{54}N_3O_4S$
 % theoretical C, 63.60; H, 10.29; N, 7.95; S, 6.06; mass fraction of water 235×10^{-6} ,
 mass fraction of bromide 62×10^{-6} .

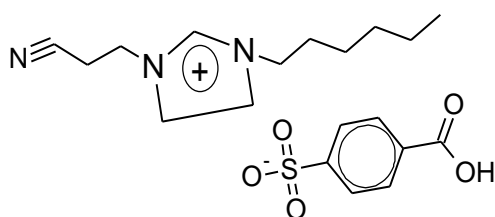


Fig 4-16 Structure of [C₂CN Him]SBA

[CNC₂Him]SBA: δ_H (300 MHz; D₂O): = 9.93 (s, 1 H, NCHN), 8.27 (br, 2 H, C(CH₂)₂SO₃), 8.06 (s, 1 H, OH), 7.96 (d, 2 H, C(CH₂)₂COOH), 7.59 (s, 1 H, NCHCHN), 7.53 (s, 1 H, NCHCHN), 4.53 (t, 2 H, NCH₂(CH₂)₄), 4.16 (t, 2 H, CNCH₂CH₂), 3.13 (t, 2 H, CH₂CH₂CN), 1.80, (t, 2 H, NCH₂CH₂(CH₂)₃), 1.21 (br m, 6H, CH₂), 0.77 (t, 3 H, CH₃CH₂). ¹³C NMR (75 MHz; D₂O) = 135.79, 132.08, 129.63,

129.46, 126.31, 123.14, 122.46, 117.88, 49.99, 44.84, 30.34, 29.08, 25.00, 21.81, 19.33, 13.30. FTIR-ATR $\nu_{\max}/\text{cm}^{-1}$: 2250 and 1558 (C≡N), 2921, 2859 and 1461(C-H), 1158 and 1026 (SO₃), 1632 (C=O), 3417 (-OH).

Elemental analysis: % actual C, 55.93, H, 6.45; N, 10.35; S, 7.89. C₁₉H₂₆N₃O₅S
% theoretical C, 56.00; H, 6.18; N, 10.31; S, 7.87; mass fraction of water 233×10⁻⁶, mass fraction of bromide 74×10⁻⁶.

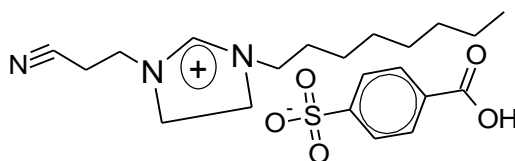


Fig 4-17 Structure of [C₂CN Oim]SBA

[C₂CN Oim]SBA: δ_{H} (300 MHz; D₂O): = 9.02 (s, 1 H, NCHN), 7.64 (br, 2 H, C(CH₂)₂SO₃), 7.85 (s, 1 H, OH), 4.70 (d, 2 H, C(CH₂)₂COOH), 4.57 (s, 1 H, NCHCHN), 3.16 (s, 1 H, NCHCHN), 2.19 (t, 2 H, NCH₂ (CH₂)₄), 1.86 (t, 2 H, CNCH₂CH₂), 1.25 (t, 2 H, CH₂CH₂CN), 1.21, (t, 2 H, NCH₂CH₂ (CH₂)₃), 1.19 (br m, 6H, CH₂), 0.79 (t, 3 H, CH₃CH₂). ¹³C NMR (75 MHz; D₂O) = 135.90, 123.12, 122.55, 117.86, 50.00, 44.89, 31.17, 29.25, 28.40, 25.44, 22.14, 19.42, 13.57. FTIR-ATR $\nu_{\max}/\text{cm}^{-1}$: 2254 and 1562 (C≡N), 2925, 2854 and 1460 (C-H), 1161 and 1030 (SO₃), 1629 (C=O), 3413 (-OH).

Elemental analysis: % actual C, 57.72; H, 6.99; N, 9.57; S, 7.30. C₂₁H₃₀N₃O₅S % theoretical C, 57.91; H, 6.71; N, 9.65; S, 7.36; mass fraction of water 145×10⁻⁶, mass fraction of bromide 59×10⁻⁶.

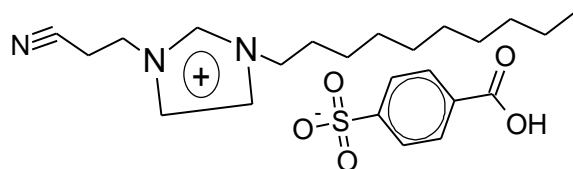


Fig 4-18 Structure of [C₂CN Dim]SBA

[C₂CN Dim]SBA: δ_{H} (300 MHz; D₂O): = 9.03 (s, 1 H, NCHN), 8.29 (br, 2 H, C(CH₂)₂SO₃), 7.93 (s, 1 H, OH), 7.62 (d, 2 H, C(CH₂)₂COOH), 7.49 (s, 1 H, NCHCHN), 4.54 (s, 1 H, NCHCHN), 4.11 (t, 2 H, NCH₂ (CH₂)₄), 3.11 (t, 2 H, CNCH₂CH₂), 2.16 (t, 2 H, CH₂CH₂CN), 1.67, (t, 2 H, NCH₂CH₂ (CH₂)₃), 1.09 (br m,

6H, CH_2), 0.76 (t, 3 H, CH_3CH_2). ^{13}C NMR (75 MHz; D_2O) = 144.78, 136.01, 132.66, 129.44, 128.44, 122.94, 117.74, 49.79, 44.97, 31.85, 29.27, 28.91, 25.88, 22.56, 19.42, 13.81. FTIR-ATR ν_{max}/cm^{-1} : 2252 and 1562 ($C\equiv N$), 2923, 2852 and 1458 (C-H), 1218 and 1031 (SO_3), 1710 ($C=O$), 3408 (-OH).

Elemental analysis: % actual C, 59.40; H, 7.25; N, 9.15; S, 6.84. $C_{23}H_{34}N_3O_5S$

% theoretical C, 59.59; H, 7.17; N, 9.06; S, 6.92; mass fraction of water 212×10^{-6} , mass fraction of bromide 74×10^{-6} .

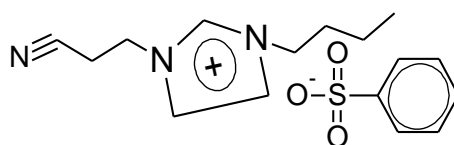


Fig 4-19 Structure of $[C_2CN \text{ Bim}]BS$

$[C_2CN \text{ Bim}]BS$; δ_H (300 MHz; D_2O): = 8.98 (br, 2 H, $CHCSO_3$), 7.78 (s, 1 H, $NCHN$), 7.63 (s, 1 H, CHN), 7.58 (s, 1 H, CHN), 7.54 (d, 3 H, $CHCHCH$), 4.57 (t, 2 H, NCH_2CH_2), 4.23 (t, 2 H, $CNCH_2CH_2$), 3.17 (t, 2 H, CH_2CH_2CN), 1.87 (t, 2 H, CH_2CH_2N), 1.28 (t, 2H, CH_2CH_3), 0.83 (t, 3 H, CH_3CH_2). ^{13}C NMR (75 MHz; D_2O) = 135.82, 131.53, 129.04, 125.41, 123.12, 117.93, 50.00, 44.84, 30.38, 29.10, 25.01, 21.82, 19.36, 13.32. FTIR-ATR ν_{max}/cm^{-1} : 2242 and 1562 (CN), 2963, 2861 and 1460 (C-H), 1184 and 1028 (SO_3).

Elemental analysis: % actual C, 57.22; H, 6.54; N, 12.57; S, 9.48. $C_{16}H_{22}N_3O_3S$

% theoretical C, 57.12; H, 6.59; N, 12.49; S, 9.53; mass fraction of water 182×10^{-6} , mass fraction of bromide 73×10^{-6} .

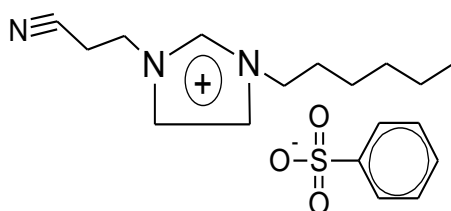


Fig 4-20 Structure of $[C_2CN \text{ Him}]BS$

$[CNC_2\text{Him}] \text{ BS}$: δ_H (300 MHz; D_2O): = 8.96 (br, 2 H, $CHCSO_3$), 7.75 (s, 1 H, $NCHN$), 7.61 (s, 1 H, CHN), 7.57 (s, 1 H, CHN), 7.50 (d, 3 H, $CHCHCH$), 4.56 (t, 2 H, NCH_2CH_2), 4.19 (t, 2 H, $CNCH_2CH_2$), 3.15 (t, 2 H, CH_2CH_2CN), 1.84 (t, 2 H,

CH_2CH_2N), 1.26 (br m, 6H, CH_2), 0.81 (t, 3 H, CH_3CH_2). ^{13}C NMR (75 MHz; D_2O) = 135.83, 129.03, 125.40, 123.17, 123.11, 122.48, 122.43, 117.92, 50.02, 49.99, 44.86, 44.83, 30.35, 29.10, 25.01, 21.81, 19.36, 13.31. FTIR-ATR ν_{max}/cm^{-1} : 2250 and 1562 ($C\equiv N$), 2927, 2858 and 1458 (C-H), 1190 and 1016 (SO_3).

Elemental analysis: % actual C, 51.35, H, 7.14; N, 11.57; S, 8.72. $C_{18}H_{26}N_3O_3S$
 % theoretical C, 59.31; H, 7.19; N, 11.53; S, 8.80; mass fraction of water 206×10^{-6} ,
 mass fraction of bromide 52×10^{-6} .

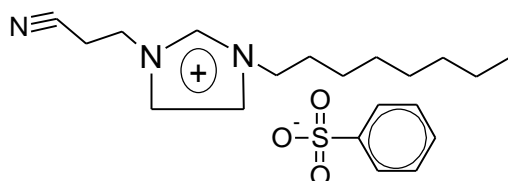


Fig 4-21 Structure of $[C_2CN \text{ Oim}]BS$

$[C_2CN \text{ Oim}]BS$: δ_H (300 MHz; D_2O): = 9.01 (br, 2 H, $CHCSO_3$), 7.77 (s, 1 H, $NCHN$), 7.62 (s, 1 H, CHN), 7.39 (s, 1 H, CHN), 7.54 (d, 3 H, $CHCHCH$), 4.54 (t, 2 H, NCH_2CH_2), 4.20 (t, 2 H, $CNCH_2CH_2$), 3.13 (t, 2 H, CH_2CH_2CN), 1.86 (t, 2 H, CH_2CH_2N), 1.22 (br m, 6H, CH_2), 0.77 (t, 3 H, CH_3CH_2). ^{13}C NMR (75 MHz; D_2O) = 135.92, 128.74, 125.60, 123.06, 122.54, 117.85, 49.96, 44.89, 31.25, 29.31, 28.49, 28.33, 25.52, 22.20, 19.43, 13.62. FTIR-ATR ν_{max}/cm^{-1} : 2248 and 1562 ($C\equiv N$), 2960, 2871 and 1460 (C-H), 1190 and 1031 (SO_3).

Elemental analysis: % actual C, C 61.12; H, 7.78; N, 10.61; S, 8.20. $C_{20}H_{30}N_3O_3S$
 % theoretical C, 61.20; H, 7.70; N, 10.70; S, 8.17; mass fraction of water 184×10^{-6} ,
 mass fraction of bromide 71×10^{-6} .

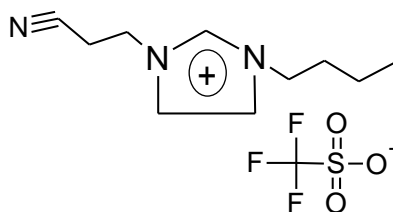


Fig 4-22 Structure of $[C_2CN \text{ Bim}]TFMS$

$[C_2CN \text{ Bim}]TFMS$: δ_H (300 MHz; D_2O): = 8.94 (s, 1 H, $NCHN$), 7.61 (s, 1 H, CHN), 7.54 (s, 1 H, CHN), 4.56 (t, 2 H, NCH_2CH_2), 4.23 (t, 2 H, $CNCH_2CH_2$), 3.15 (t, 2 H, CH_2CH_2CN), 1.85 (t, 2H, CH_2CH_2N), 1.29 (t, 2 H, CH_2CH_3), 0.90 (t, 3 H, CH_3CH_2). ^{13}C NMR (75 MHz; D_2O) = 135.73, 123.04, 122.33, 121.34, 117.92, 49.71, 44.80,

31.17, 19.24, 18.77, 12.66. FTIR-ATR $\nu_{\max}/\text{cm}^{-1}$: 2254 and 1564 (C≡N), 2964, 2875 and 1460 (C-H), 1249 and 1029 (SO₃), 1226 and 1159 (CF₃).

Elemental analysis: % actual C, 40.29, H, 4.94; N, 12.79; S, 9.73. C₁₁H₁₆F₃N₃O₃S
 % theoretical C, 40.36; H, 4.93; N, 12.84; S, 9.80; mass fraction of water 179×10^{-6} ,
 mass fraction of bromide 103×10^{-6} .

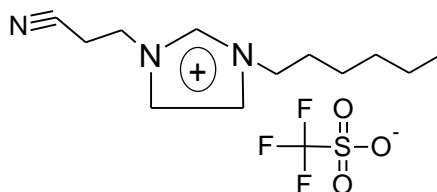


Fig 4-23 Structure of [C₂CN Him]TFMS

[CNC₂Him] TFMS: δ_{H} (300 MHz; D₂O): = 7.92 (s, 1 H, NCHN), 7.60 (s, 1 H, CHN), 7.56 (s, 1 H, CHN), 4.55 (t, 2 H, NCH₂CH₂), 4.21 (t, 2 H, CNCH₂CH₂), 3.14 (t, 2 H, CH₂CH₂CN), 1.84 (m, 6H, CH₂), 1.26 (t, 2 H, CH₂CH₃), 0.81 (t, 3 H, CH₃CH₂). ¹³C NMR (75 MHz; D₂O) = 181.60, 169.11, 161.62, 137.72, 135.79, 127.34, 123.11, 120.29, 117.89, 115.00, 106.15, 49.98, 44.80, 42.59, 30.33, 24.98, 21.78, 9.27, 13.26, 11.93. FTIR-ATR $\nu_{\max}/\text{cm}^{-1}$: 2256 and 1564 (CN), 2933, 2864 and 1458 (C-H), 1249 and 1031 (SO₃), 1228 and 1159 (CF₃).

Elemental analysis: % actual C, 43.98, H, 5.78; N, 11.70; S, 9.13. C₁₃H₂₀F₃N₃O₃S
 % theoretical C, 43.94; H, 5.67; N, 11.82; S, 9.02; mass fraction of water 243×10^{-6} ,
 mass fraction of bromide 91×10^{-6} .

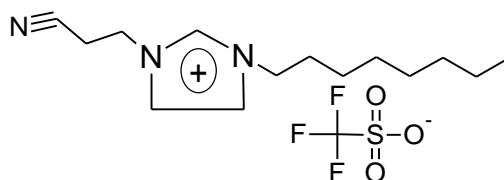


Fig 4-24 Structure of [C₂CN Oim]TFMS

[C₂CN Oim]TFMS: δ_{H} (300 MHz; D₂O): = 8.06 (s, 1 H, NCHN), 7.67 (s, 1 H, CHN), 7.55 (s, 1 H, CHN), 4.42 (t, 2 H, NCH₂CH₂), 4.18 (t, 2 H, CNCH₂CH₂), 3.12 (t, 2 H, CH₂CH₂CN), 1.85 (m, 10H, CH₂), 1.21 (m, 2 H, CH₂CH₃), 0.81 (t, 3 H, CH₃CH₂). ¹³C NMR (75 MHz; D₂O) = 172.00, 165.62, 157.89, 154.98, 137.03, 135.63, 125.94,

122.79, 120.21, 118.43, 114.67, 106.72, 99.17, 91.88, 77.63, 67.27, 49.68, 44.65, 31.28, 28.74, 24.96, 22.11, 19.40, 13.30. FTIR-ATR $\nu_{\max}/\text{cm}^{-1}$: 2254 and 1562 (C≡N), 2927, 2858 and 1460 (C-H), 1249 and 1029 (SO₃), 1226 and 1159 (CF₃).

Elemental analysis: % actual C, 47.01; H, 6.43; N, 10.89; S, 8.42. C₁₅H₂₄F₃N₃O₃S
% theoretical C, 46.99; H, 6.31; N, 10.96; S, 8.36; mass fraction of water 197×10^{-6} ,
mass fraction of bromide 62×10^{-6} .

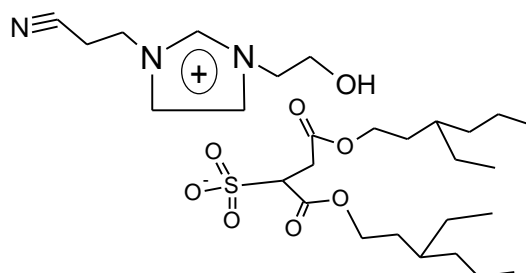


Fig 4-25 Structure of [C₂CN Heim]DOSS

[C₂CN Heim]DOSS; δ_{H} (300 MHz; CD₃OD): = 9.18 (s, 1 H, NCHN), 7.77 (s, 1 H, CHN), 7.75 (1 H, s, CHN), 7.01 (t, 1 H, CHSO₃), 4.65 (t, 2 H, NCH₂CH₂OH), 4.30 (t, 2 H, NCH₂CH₂OH), 4.08 (d, 4 H, OCH₂CH(CH₂)₂), 3.95 (t, 2 H, CNCH₂CH₂N), 3.40 (t, 2 H, CNCH₂CH₂N), 3.15 (d, 2 H, COCH(SO₃)CH₂), 3.06 (t, 4 H, CH(CH₂)CH₂CH₂), 1.32 (br m, 15 H, CH₂CH₂), 0.95 (t, 12 H, CH₃CH₂). ¹³C NMR (75 MHz; CD₃OD) = 171.58, 168.80, 137.39, 123.66, 122.67, 116.93, 67.77, 62.36, 60.16, 60.04, 52.54, 45.36, 39.18, 33.91, 30.51, 29.10, 23.74, 23.05, 13.49, 10.42. FTIR-ATR $\nu_{\max}/\text{cm}^{-1}$: 2251 and 1566 (C≡N), 2921, 2874 and 1458 (C-H), 1220 and 1032 (SO₃), 1728 (C=O), 1156 (C-O-C), 3428 (OH).

Elemental analysis: % actual C, 48.71; H, 10.23; N, 8.39; S, 6.41. C₂₀H₄₉N₃O₈S
% theoretical C, 48.86; H, 10.04; N, 8.55; S, 6.52; mass fraction of water 283×10^{-6} ,
mass fraction of bromide 62×10^{-6} .

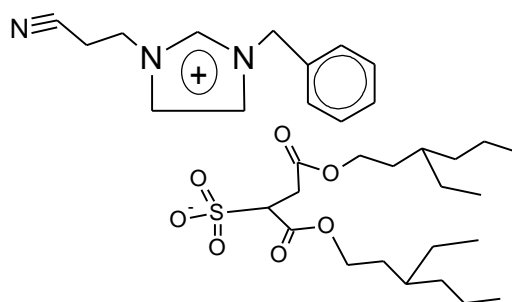


Fig 4-26 Structure of [C₂CN Bzim]DOSS

[C₂CN Bzim]DOSS; δ_{H} (300 MHz; CD₃OD): = 9.27 (s, 1 H, NCHN), 7.79 (t, 2 H, Ar (CH), 7.72 (t, 2 H, Ar (CH), 7.64 (d, 1 H, Ar (CH), 5.50 (s, 1 H, CHCHN), 5.48 (1 H, s, CHCHN), 7.01 (t, 1 H, CHSO₃), 4.60 (t, 2 H, NCH₂C₆H₅), 4.11 (d, 4 H, OCH₂CH(CH₂)₂), 3.33 (t, 2 H, CNCH₂CH₂N), 3.20 (t, 2 H, CNCH₂CH₂N), 3.05 (d, 2 H, COCH(SO₃)CH₂), 1.59 (t, 4 H, CH(CH₂)CH₂CH₂), 1.32 (br m, 14 H, CH₂), 0.91 (t, 12 H, CH₃CH₂). ¹³C NMR (75 MHz; CD₃OD) = 171.59, 168.81, 137.13, 134.30, 129.46, 128.77, 123.21, 116.86, 67.83, 67.21, 62.37, 53.34, 47.61, 39.10, 33.93, 30.38, 29.10, 23.03, 18.87, 13.47, 10.35. FTIR-ATR ν_{max} /cm⁻¹: 2246 and 1557 (C≡N), 2928, 2864 and 1460 (C-H), 1220 and 1031 (SO₃), 1726 (C=O), 1152 (C-O-C).

Elemental analysis: % actual C, 62.71; H, 8.26; N, 6.57; S, 5.11. C₃₃H₅₁N₃O₇S

% theoretical C, 62.53; H, 8.11; N, 6.63; S, 5.06. mass fraction of water 204×10⁻⁶, mass fraction of bromide 78×10⁻⁶.

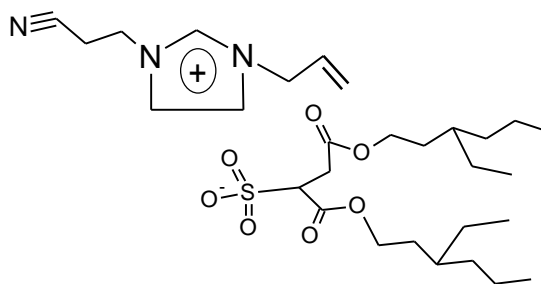


Fig 4-27 Structure of [C₂CN Ayim]DOSS

[C₂CN Ayim]DOSS; δ_{H} (300 MHz; CD₃OD): = 9.18 (s, 1 H, NCHN), 7.81 (s, 1 H, CHCHN), 7.80 (1 H, s, CHCHN), 7.71 (t, 1 H, N-CH=CH₂), 5.48 (t, 1 H, CHSO₃), 4.95 (d, 2 H, N-CH=CH₂), 4.62 (d, 4 H, OCH₂CH(CH₂)₂), 4.07 (t, 2 H, CNCH₂CH₂), 3.34 (t, 2 H, CNCH₂CH₂), 3.23 (d, 2 H, COCH(SO₃)CH₂), 3.01 (t, 4 H, CH(CH₂)CH₂CH₂), 1.61 (d, 4 H, CH(CH₂)CH₂CH₃), 1.34 (br m, 12 H, CH₂), 0.92 (t, 12 H, CH₃CH₂). ¹³C NMR (75 MHz; CD₃OD) = 171.57, 168.85, 137.50, 131.03, 123.76, 121.07, 123.21, 116.97, 67.21, 62.81, 52.01, 48.07, 39.14, 33.94, 30.52, 23.06, 18.91, 13.33, 10.24. FTIR-ATR ν_{max} /cm⁻¹: 2247 and 1568 (CN), 2926, 2879 and 1461 (C-H), 1223 and 1027 (SO₃), 1724 (C=O), 1152 (C-O-C), 1645 (C=C).

Elemental analysis: % actual C, 59.71; H, 8.51; N, 7.44; S, 5.56. C₂₈H₄₇N₃O₇S

% theoretical C, 59.03; H, 8.31; N, 7.38; S, 5.63 mass fraction of water 229×10⁻⁶, mass fraction of bromide 59×10⁻⁶.

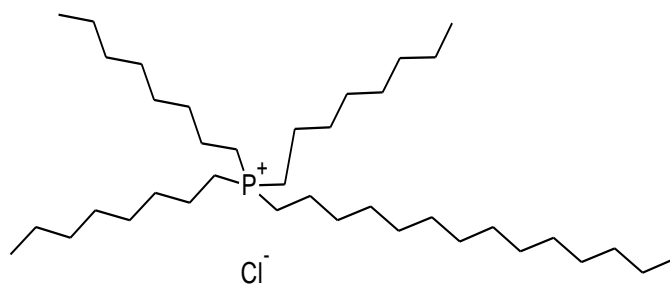


Fig 4-28 Structure of $[P_{8,8,8,14}]Cl$

$[P_{8,8,8,14}]Cl$; $\delta_H(400\text{ MHz; }CDCl_3) = 2.36$ (t, 8H, CH_2P), 1.65(m, 8H, CH_2CH_2P), 1.23 (br, 52H, CH_2), 0.86 (t, 12H, CH_3CH_2).

Elemental analysis: % actual C, 72.51; H, 12.64. $C_{38}H_{80}PCl$ % theoretical C, 72.36; H, 12.82. mass fraction of water 389×10^{-6} .

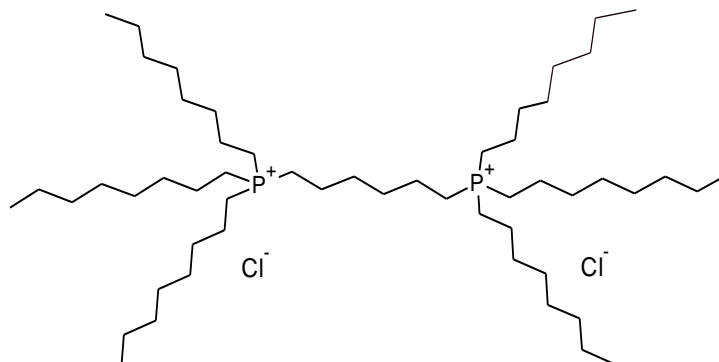


Fig 4-29 Structure of $[P_{8,8,8}C_6P_{8,8,8}]Cl_2$

$[P_{8,8,8}C_6P_{8,8,8}]Cl_2$; $\delta_H(400\text{ MHz; }CDCl_3) = 2.30-2.42$ (br, 16H, CH_2CH_2P), 2.1-2.25 (br, 52H, CH_2), 1.35-1.55 (br, 16H, CH_2CH_2P), 1.21 (m, 12H, CH_3CH_2), 0.79 (t, 18H, CH_3CH_2).

Elemental analysis: % actual C, 72.21; H, 12.75. $C_{54}H_{114}P_2Cl_2$ % theoretical C, 72.34; H, 12.84 mass fraction of water 530×10^{-6} .

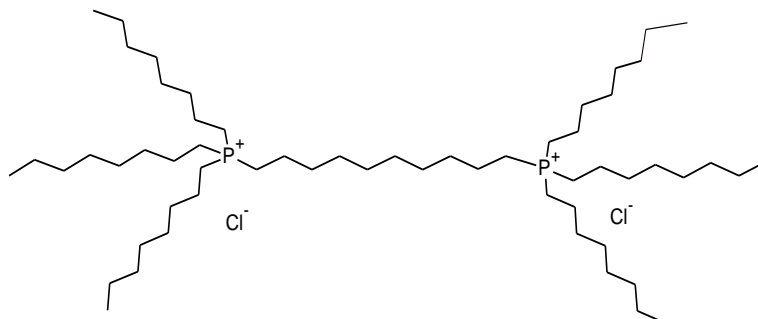


Fig 4-30 Structure of $[P_{8,8,8}C_{10}P_{8,8,8}]Cl_2$

[P_{8,8,8}C₁₀P_{8,8,8}]Cl₂; δ_{H} (400 MHz; CDCl₃): = 2.25-2.40 (br, 16H, CH₂CH₂P), 2.0-2.08 (br, 60H, CH₂), 1.30-1.60 (br, 16H, CH₂CH₂P), 1.15 (m, 12H, CH₃CH₂), 0.74 (t, 18H, CH₃CH₂).

Elemental analysis: % actual C, 73.01; H, 12.85. C₅₈H₁₂₂P₂Cl₂ % theoretical C, 73.12; H, 12.93 mass fraction of water 553×10⁻⁶.

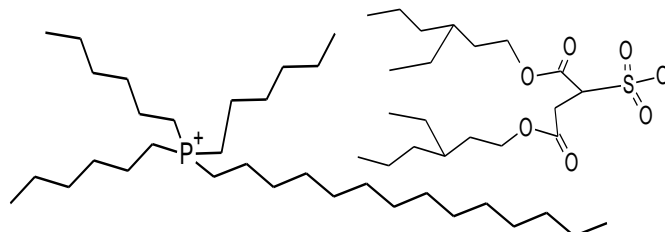


Fig 4-31 Structure of [P_{6,6,6,14}]DOSS

[P_{6,6,6,14}]DOSS; δ_{H} (400 MHz; CDCl₃): = 5.10 (s, 1H, CO-CH), 3.90-4.20 (br, 4H, CH₂-O), 3.10 (t, 2H, CH₂COO), 2.2-2.3 (br, 8H, CH₂-P), 1.26-1.41 (br, 64H, CH₂), 0.89 (t, 24H, CH₃). FTIR-ATR ν_{max} /cm⁻¹: 2923 and 2854 (C-H), 1230 and 1033 (SO₃), 1731 (C=O), 1159 (C-O-C).

Elemental analysis: % actual C, 68.23; H, 11.57; S, 3.47. C₅₂H₁₁₅O₇PS % theoretical C, 68.98; H, 11.69; S, 3.54 mass fraction of water 127×10⁻⁶, mass fraction of chloride 69×10⁻⁶.

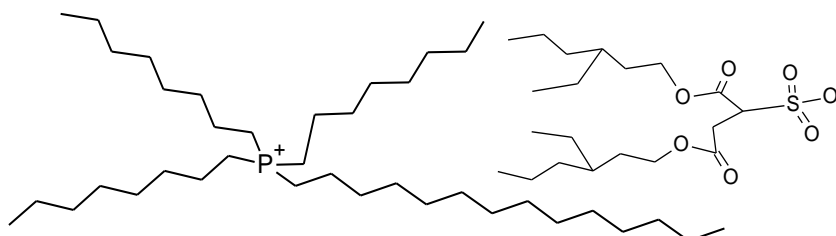


Fig 4-32 Structure of [P_{8,8,8,14}]DOSS

[P_{8,8,8,14}]DOSS; δ_{H} (400 MHz; CDCl₃): = 3.96 (s, 1H, CO-CH), 3.25-4.20 (br, 4H, 4H, CH₂-O), 2.35 (t, 2H, CH₂COO), 1.66 (br, 8H, CH₂-P), 1.29 (br, 76H, CH₂), 0.88 (t, 24H, CH₃). ¹³C NMR (75 MHz; CDCl₃) = 171.73, 169.13, 77.01, 66.96, 61.92, 38.53, 34.32, 31.73, 30.08, 28.99, 22.59, 21.78, 18.93, 14.02, 10.84. FTIR-ATR ν_{max} /cm⁻¹: 2923 and 2854 (C-H), 1220 and 1033 (SO₃), 1733 (C=O), 1155 (C-O-C).

Elemental analysis: % actual C, 68.65; H, 11.87; S, 3.49. C₅₈H₁₁₇O₇PS % theoretical C, 68.98; H, 11.69; S, 3.54 mass fraction of water 121×10⁻⁶, mass fraction of chloride 41×10⁻⁶.

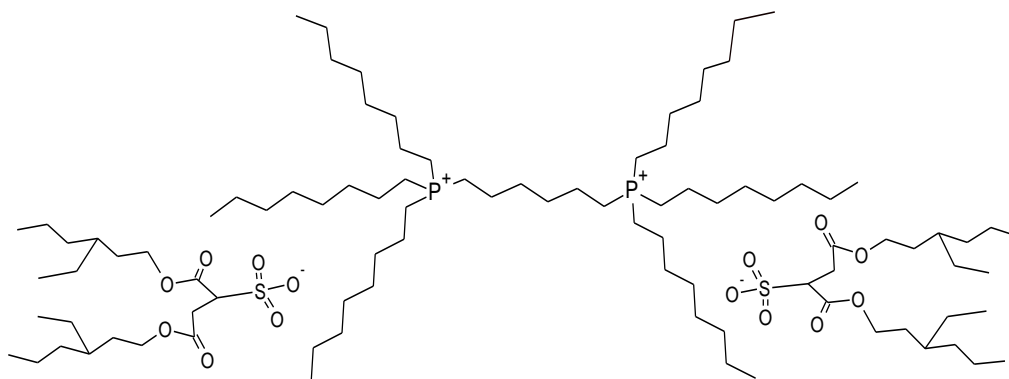


Fig 4-33 Structure of $[P_{8,8,8}C_6P_{8,8,8}]DOSS_2$

$[P_{8,8,8}C_6P_{8,8,8}]DOSS$; $\delta_H(400\text{ MHz}; CDCl_3)$: = 7.26 (m, 2H, CO-CH), 4.15 (br, 8H, CH_2 -O), 3.34 (m, 4H, CH_2 COO), 2.76 (t, 16H, CH_2 -P), 2.18 (br, 8H, CH_2), 1.25 (br, 108H, CH_2), 0.84 (t, 42H, CH_3). ^{13}C NMR (75 MHz; $CDCl_3$) = 171.66, 169.34, 77.00, 67.10, 38.65, 31.70, 30.26, 28.94, 3.42, 22.58, 21.88, 19.24, 14.01, 10.82. FTIR-ATR ν_{max}/cm^{-1} : 2923 and 2856(C-H), 1222 and 1033 (SO_3), 1731 (C=O), 1155 (C-O-C). Elemental analysis: % actual C, 67.73; H, 11.28; S, 3.72. $C_{94}H_{188}O_{14}P_2S_2$ % theoretical C, 67.66; H, 11.36; S, 3.84 mass fraction of water 142×10^{-6} , mass fraction of chloride 59×10^{-6} .

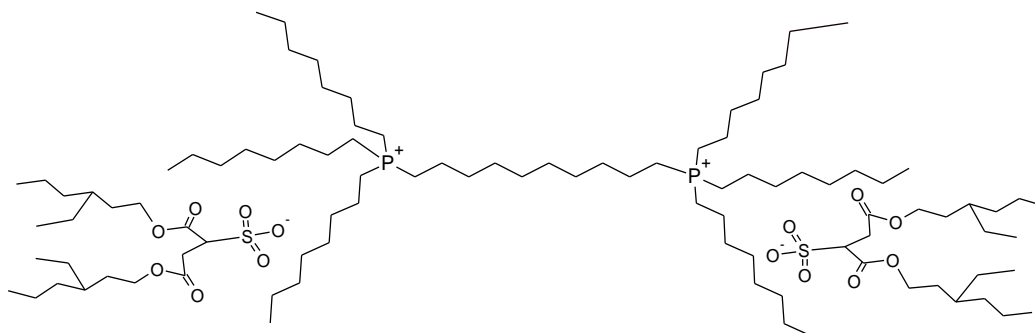


Fig 4-34 Structure of $[P_{8,8,8}C_{10}P_{8,8,8}]DOSS_2$

$[P_{8,8,8}C_{10}P_{8,8,8}]DOSS$; $\delta_H(400\text{ MHz}; CDCl_3)$: = 7.20 (m, 2H, CO-CH), 3.99 (br, 8H, CH_2 -O), 3.14 (m, 4H, CH_2 COO), 2.22 (t, 16H, CH_2 -P), 1.42 (br, 8H, CH_2), 1.19 (br, 116H, CH_2), 0.81 (t, 42H, CH_3). FTIR-ATR ν_{max}/cm^{-1} : 2925 and 2856 (C-H), 1218 and 1033 (SO_3), 1731 (C=O), 1157 (C-O-C). Elemental analysis: % actual C, 68.39; H, 11.59; S, 3.65. $C_{98}H_{196}O_{14}P_2S_2$ % theoretical C, 68.25; H, 11.45; S, 3.72 mass fraction of water 136×10^{-6} , mass fraction of chloride 74×10^{-6} .

The imidazolium cation, as for any aromatic system, generates two magnetically shielding cones above and below its molecular plane, classically seen as caused by an electronic current circulating around the π -orbitals, on both sides of the aromatic ring. A proton penetrating into these cones will have an NMR signal moving to higher field. The ^1H NMR spectra of the imidazolium-based ILs showed the C-2 characteristic resonance at high field (7.81-9.99 ppm) due to the acidic proton in the C-2 of imidazolium ring and the other ring protons observed between 6.83-8.29 ppm. This might be due to the relatively strong electron withdrawing effect of the nitrile group incorporated to the imidazolium ring which increases the acidity of the acidic protons in the C-2 of imidazolium ring and the other protons in the C-4 and C-5.

The most noteworthy feature of the ^1H NMR spectra of the imidazolium salts is the characteristic resonance for the acidic proton in the 2-position. In $[\text{C}_2\text{CN C}_n\text{im}]\text{X}$ RTILs this proton is observed between 9.24 – 9.82 ppm (for $[\text{C}_2\text{CN C}_n\text{im}]\text{Br}$), 7.92-9.99 ppm (for $[\text{C}_2\text{CN C}_n\text{im}]\text{Cl}$), 9.95 – 9.96 ppm (for $[\text{C}_2\text{CN C}_n\text{im}]\text{DOSS}$), 7.81 – 7.77 ppm (for $[\text{C}_2\text{CN C}_n\text{im}]\text{DSS}$), 9.93 – 9.03 ppm (for $[\text{C}_2\text{CN C}_n\text{im}]\text{SBA}$), 8.98 – 9.01 ppm (for $[\text{C}_2\text{CN C}_n\text{im}]\text{BS}$) and 8.94 – 8.06 ppm (for $[\text{C}_2\text{CN C}_n\text{im}]\text{TFMS}$) but no clear trends are present. It is noteworthy that H-D exchange takes place at the acidic 2-position in all the ionic liquids described, and is fastest where the alkyl chain is shortest and the protons interact most strongly with the anion. The chemical shifts of the imidazolium protons in the C-2, C-4 and C-5 are most influenced by such variables as the concentration, structure of the ionic liquid, nature of deuterated solvent and temperature [191].

It is supposed that with concentration increase, the imidazolium cations progressively form ions pairs with the anions, which stack as the neutral aromatic systems do. Thus, the chemical shift displacement with concentration can be analyzed in terms of two effects: H-bonding leading to higher shifts and ring stacking leading to lower shifts. The extreme case is that of the CH_3 protons of the ethyl group. Being unable to H-bond, they are only affected by ring stacking. For the other protons, both effects can be observed, depending on the nature of the anion and on its concentration [192]. With the most basic anions, the influence of concentration is in part or completely opposite for protons in the C-2 and C-4 which can be rationalized based

on the top-to-bottom structure. It can be assumed that the stacking will take place the closest to that model for the most tightly bound ion-pairs, which means for the most basic anions. With a concentration increase, the proton in the C-2 entering the shielding cone of the neighboring imidazolium moves to lower shifts while the protons in the C-4 and C-5, pointing outside, remain only influenced by H-bonding strengthening [192].

The ionic interactions present in neat ILs will be affected by the addition of molecular solvents. Depending on the dielectric constants of the molecular solvents, more or less effective ion solvation should be observed leading to changes in the NMR spectra of the ionic liquid [193]. The influence of the concentration is more complex. It is expected that a concentration increase will displace the equilibrium to the right and thus lead to a chemical shift increase. This trend is observed for the protons in the C-2 signal only with the most basic anions (DOSS, DDS) and at low concentration [194].

The alkyl protons adjacent to the nitrile group also exchange with deuterium, but at a considerably slower rate. It is possible that the slight differences in the molecular geometry are caused by the different hydrogen bond networks arising from the different anions and different side chains. Hydrogen bonds between the hydrogen bond acceptor usually from the counteranions and the H atoms in the imidazolium ring are the most frequently observed interactions, and in most cases they are the strongest. However, the strength of the hydrogen bond is largely dependent on the nature of the counteranion.

Sulfonate based anions that have strong electron withdrawing groups such as trifluoromethane and carbonyl, hence the C-2 of the imidazolium cation resonate downfield compared to benzene sulfonate and dodecylsulfate. In addition, hydrogen bonding would produce a downfield shift [195]. H-bonding in imidazolium ring depends on the basicity of anion. C-2 proton is less electron rich than C-4 and C-5 because it is attached to carbon in between two electronegative nitrogen atoms. So C-2 proton is more prone for H-bonding with counter anion than others. Increase in the length of alkyl chain resulted in the different shift between C-4 and C-5 protons [24].

The chemical shifts of the imidazolium ring protons are anion- and concentration-dependent [196].

The ^{13}C NMR chemical shifts of the carbonyl carbon move to higher field by the hydrogen bonding. The chemical shift of the carbonyl carbon of the [C₂CN Bim]DOSS RTILs is 168.56 ppm and the chemical shift was shifted to 169.22, 169.31 and 169.37 ppm for the analogous RTILs incorporating hexyl, octyl and decyl alkyl chains respectively. When the imidazolium cation forms a hydrogen bond the chemical shifts of the ring protons move to a lower field. The decrease of alkyl chain length caused a slight movement of the chemical shift of imidazolium ring protons to the lower field so there is little hydrogen bond formation. This different finding showed that the imidazolium cation formed weaker hydrogen bonding with the carbonyl carbon as the alkyl chain increase. It is well known that hydrogen bonding causes the proton chemical shift to move to lower field. It has also been noticed that the shifts of the imidazolium ring protons depend on the concentration of the solvent used and on the anion.

The FTIR spectra of the present imidazolium-based ILs show the characteristic absorption bands of the nitrile group in the range from 2235 to 2265 cm^{-1} , exhibit C-H bond at 3080 to 3145 cm^{-1} and weaker C-H bonds stretches from 2854 to 2933 cm^{-1} , which are similar to that reported for other nitrile-functionalized ILs [41, 106, 197]. In addition, characteristic absorption peaks for the $-\text{SO}_3^-$ group in the regions from 1180-1250 cm^{-1} and 1020-1170 cm^{-1} were also observed. The ILs incorporating the DOSS anion showed strong peak at 1710-1730 cm^{-1} which is due to the presence of the C=O group. Moreover and as shown in Fig 4-35, the larger the sulfonate based anions, the weaker the CN peak. Allyl and 2-hydroxyethyl imidazolium ILs contains stretches at 3050-3100 cm^{-1} and 3428 cm^{-1} that correspond to =C-H and OH vibrations respectively while the C=C stretch was observed at 1645 cm^{-1} . The ILs incorporating the SBA anion show characteristic absorption bands of the OH group at 3405-3420 cm^{-1} .

The water content value of the present ILs is comparable with the other ILs [16]. Since the present synthesized RTILs incorporating halide anion are highly hygroscopic in nature compared to the other anions their water content was high

comparable to the other anions. The water content and halide content of the present ILs are reported along with the characterization results due to their strong effect on the thermophysical properties [100].

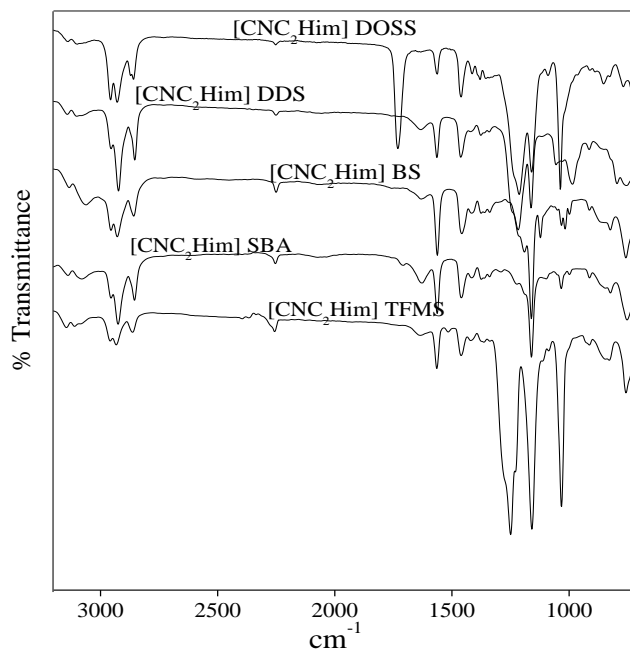


Fig 4-35 FTIR spectra of [CNC₂Him]DOSS, [CNC₂Him]DDS, [CNC₂Him]BS, [CNC₂Him]SBA and [CNC₂Him]TFMS

4.2 Thermophysical properties

4.2.1 Density

Information on solvent density values is particularly used in fluid flow calculations, for the design of liquid/liquid two phase mixer settler units, as a fundamental data for developing equations of state (the main tool used for thermophysical properties prediction for process design purposes, and solution theories for ILs), for liquid metering applications or for the design of different types of equipment such as condensers, separation trains, or even storage vessels [124].

The experimental densities of the synthesized ILs are shown in appendix A (Table A-1 to Table A- 10). The effect of the possessing different anions on the liquid density of imidazolium-based ILs incorporating sulfonate-based anions is shown in

Fig 4-36 to Fig 4-39. The densities of the imidazolium-based ILs are highest when paired with the TFMS anion followed by SBA and then by the BS anion. The lowest densities were observed with the DOSS anion.

These results showed that the increase of the anion molecular weight does not directly correspond to the rise in the density values for the present ILs and a similar behavior for other imidazolium – based ILs was observed by Sánchez and Gardas [198] for imidazolium cations, where the increase of the liquid density does not directly correspond to a rise in the molecular weight of the anion.

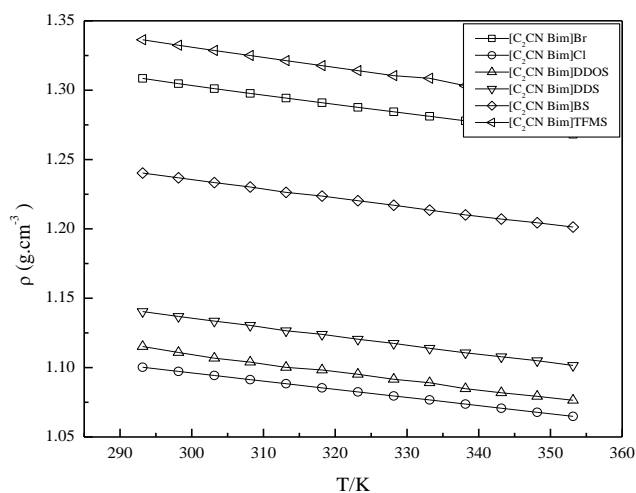


Fig 4-36 Densities ρ ($\text{g}\cdot\text{cm}^{-3}$) of $[\text{C}_2\text{CN Bim}]$ ILs as a function of temperature with a linear correlation of the data

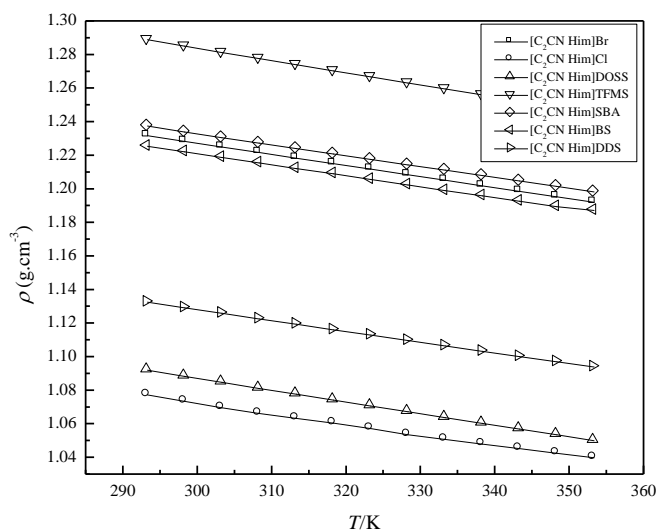


Fig 4-37 Densities ρ ($\text{g}\cdot\text{cm}^{-3}$) of $[\text{C}_2\text{CN Him}]$ ILs as a function of temperature with a linear correlation of the data

These lower densities of DOSS and DDS anions might be due to the presence of a long alkyl chains compared to the other anions which prohibits the formation of tight molecular assemblies leading to a lower density as reported by Benjamin, H. *et al.*[119]. In general the density decreases as the alkyl chain length of the anion increases [199]. Moreover, the lower density of the DOSS anion can also be explained by the large free volume and the weak localized charge which decreases the possibility of a strong ion pairing with the imidazolium cation resulting in a lower density.

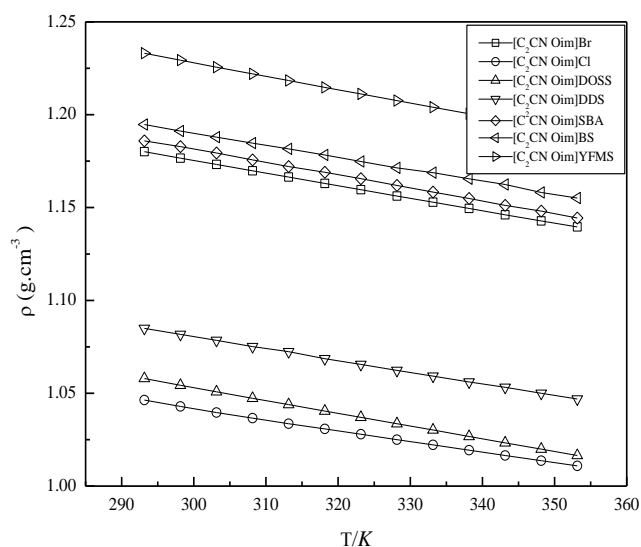


Fig 4-38 Densities ρ ($\text{g}\cdot\text{cm}^{-3}$) of $[\text{C}_2\text{CN Oim}]$ ILs as a function of temperature with a linear correlation of the data

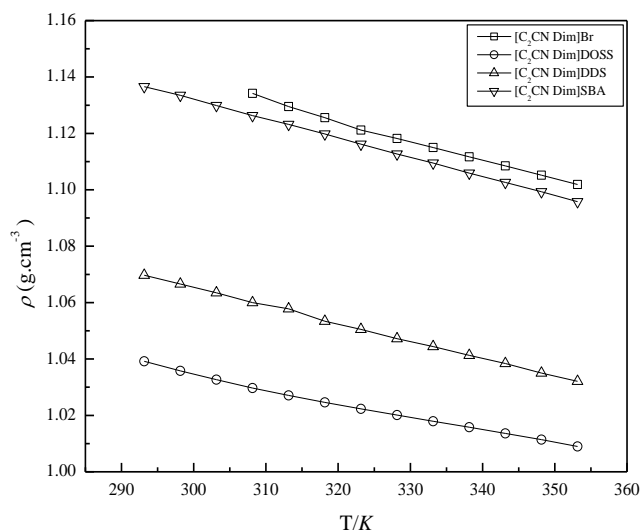


Fig 4-39 Densities ρ ($\text{g}\cdot\text{cm}^{-3}$) of $[\text{C}_2\text{CN Dim}]$ ILs as a function of temperature with a linear correlation of the data

The influence of the different synthesized cations on the density of the ILs incorporating the DOSS anion is shown in Fig 4-40. The densities of the ILs with dual functionalized cations are highest followed by imidazolium-based nitrile functionalized ILs and then by the monocationic phosphonium-based ILs. The lowest densities were observed with the dicationic phosphonium-based ILs. Moreover, the density of the IL with the same anion decreases when the alkyl chain length on the cation increases. The densities of the imidazolium-based ILs incorporating the allyl, benzyl and 2-hydroxyethyl are higher compared to those containing just the alkyl substituent. This observation is in agreement with an anticipated density of a phenyl moiety as compared to methylene groups [191].

Addition of $-\text{CH}_2-$ groups to the alkyl chain of cation decreases the density while the larger hydrophilic anions increase the density of the IL. This may be due to strong molecular attraction and strong hydrogen bonding which increases molecular agglomeration [24].

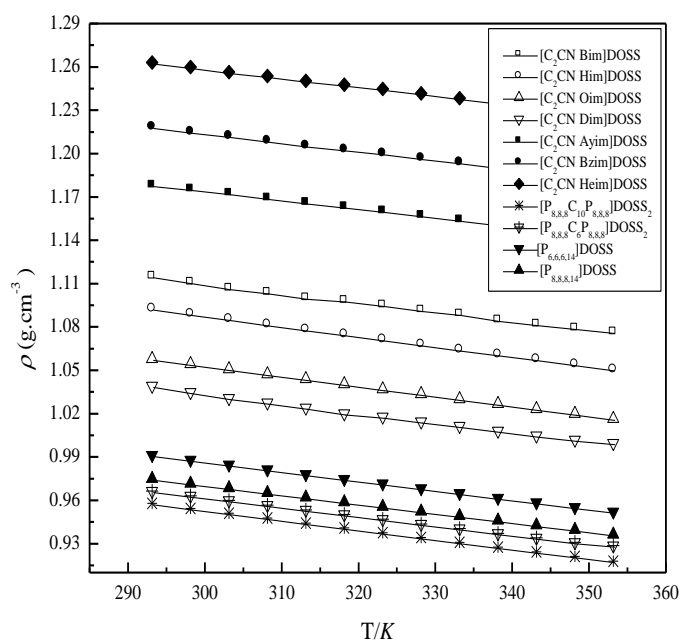


Fig 4-40 Densities ρ ($\text{g}\cdot\text{cm}^{-3}$) of imidazolium and phosphonium-based ILs incorporating DOSS anion as a function of temperature

The densities of $[\text{C}_2\text{CN C}_n\text{im}]\text{Br}$ series of ILs are in good agreement with that calculated using Ye and Shreeve method [200]; the calculated density values at

298.15 K are 1.2991, 1.2281 and 1.1780 $\text{g}\cdot\text{cm}^{-3}$ for $[\text{C}_2\text{CNBim}]\text{Br}$, $[\text{C}_2\text{CN Him}]\text{Br}$ and $[\text{C}_2\text{CN Oim}]\text{Br}$ respectively when compared with the present values of 1.2947, 1.2290 and 1.1766 $\text{g}\cdot\text{cm}^{-3}$ respectively. In addition the calculated density values at 298.15 K are 1.1021, 1.0621 and 1.0247 $\text{g}\cdot\text{cm}^{-3}$ for $[\text{C}_2\text{CNBim}]\text{Cl}$, $[\text{C}_2\text{CN Him}]\text{Cl}$ and $[\text{C}_2\text{CN Oim}]\text{Cl}$, respectively when compared with the present values of 1.0973, 1.0741 and 1.0427 $\text{g}\cdot\text{cm}^{-3}$, respectively.

The density values are found to increase after the incorporation of a nitrile group due to the nature of structural arrangement of cation and anion in the IL molecule which may be due to the strong dipole moment of the nitrile group [106]. The densities of the present synthesized ILs are lower compared to the other nitrile-functionalized ILs reported by Zhao *et al.* [41] (the densities of $[\text{C}_2\text{CN Mim}]\text{BF}_4$, $[\text{C}_3\text{CN Mim}]\text{BF}_4$ and $[\text{C}_4\text{CN Mim}]\text{Cl}$ are 2.15, 1.87 and 1.61 $\text{g}\cdot\text{cm}^{-3}$ respectively) and Zhang *et al.* [106] (the densities of $[\text{C}_3\text{CN Mim}]\text{BF}_4$ and $[\text{C}_3\text{CN Mim}]\text{NTf}_2$ are 1.319 and 1.519 $\text{g}\cdot\text{cm}^{-3}$ respectively). These results might be due to the presence of a long alkyl chains (butyl, hexyl, octyl and decyl) compared to the other nitrile-functionalized ILs [41, 106]. In general the density decreases as the alkyl chain length increases [199]. The densities of the present ILs are lower compared to those of the pyrrolidinium-based nitrile functionalized ILs, for 1-cyanoalkyl-1-methylpyrrolidinium bistriflimide ($[\text{C}_1\text{C}_n\text{CN Pyr}]\text{NTf}_2$, $n=1, 2, 3, 5$) ILs the densities are in the range from 1.157- 1.435 $\text{g}\cdot\text{cm}^{-3}$ [201]. The lower densities when compared to the other nitrile-functionalized ILs are due to the presence of large anions, more-and long alkyl chain of the cations (butyl and decyl). This causes a bigger free volume which decreases the density. Also the presence of more $-\text{CH}_2-$ function reduces the overall density; this is the same for large phosphonium ILs.

As shown in Fig 4-41 to Fig 4-46, the same effect of the cation on density was observed for the $[\text{C}_2\text{CN C}_n\text{im}]\text{Cl}$, $[\text{C}_2\text{CN C}_n\text{im}]\text{DDS}$, $[\text{C}_2\text{CN C}_n\text{im}]\text{SBA}$, $[\text{C}_2\text{CN C}_n\text{im}]\text{BS}$, $[\text{C}_2\text{CN C}_n\text{im}]\text{TFMS}$ and $[\text{C}_2\text{CN C}_n\text{im}]\text{Br}$ ILs, density decreases with increases of the alkyl chain length of the cation.

As expected, the density values decrease almost linearly with increasing temperature. This linear behaviour is common to ILs in general and is a consequence of the large temperature difference between their working temperature range and their

(inaccessible and therefore hypothetical) critical temperatures (the temperature at/above which vapor of the substance cannot be liquefy, regardless of the pressure applied) [102]. This is a reflection of the large liquid range of the IL since these ILs are liquids at room temperature having melting points less than $-40\text{ }^{\circ}\text{C}$, negligible vapor pressure with critical temperatures greater than $800\text{ }^{\circ}\text{C}$. Then the increase of volume with increasing temperature will occur during this large range.

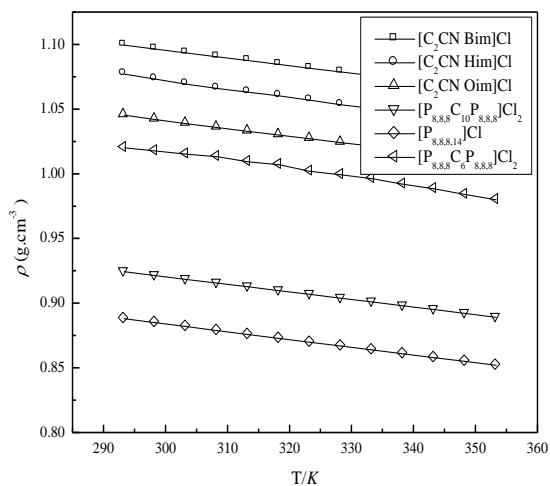


Fig 4-41 Densities $\rho\text{ (g.cm}^{-3}\text{)}$ of chloride-based ILs as a function of temperature

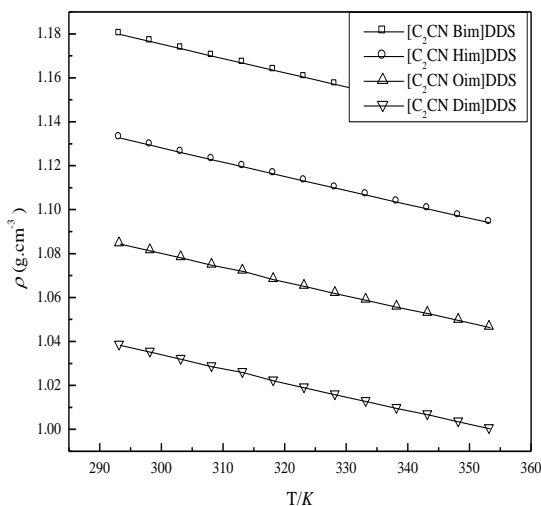


Fig 4-42 Densities $\rho\text{ (g.cm}^{-3}\text{)}$ of $[\text{C}_2\text{CN C}_n\text{im}]\text{DDS}$ ILs as a function of temperature

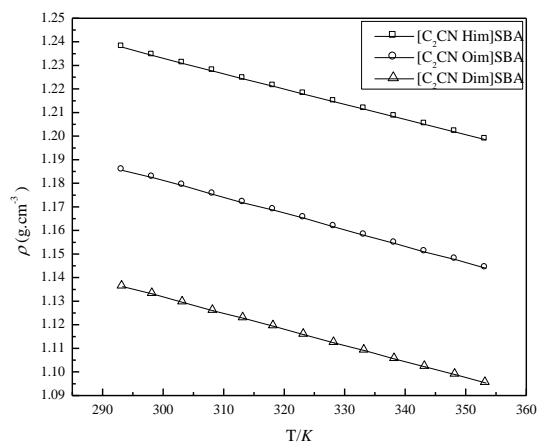


Fig 4-43 Densities ρ ($\text{g}\cdot\text{cm}^{-3}$) of $[\text{C}_2\text{CN C}_n\text{im}]\text{SBA}$ ILs as a function of temperature

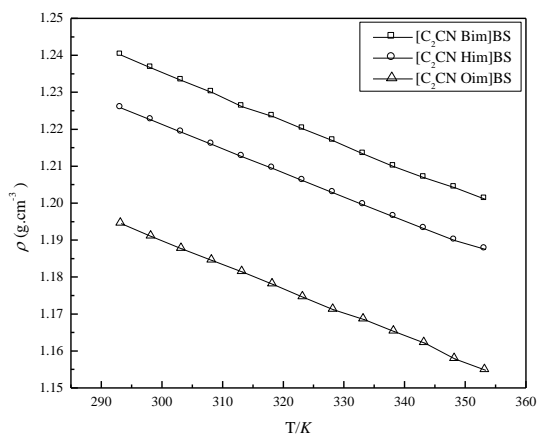


Fig 4-44 Densities ρ ($\text{g}\cdot\text{cm}^{-3}$) of $[\text{C}_2\text{CN C}_n\text{im}]\text{BS}$ ILs as a function of temperature

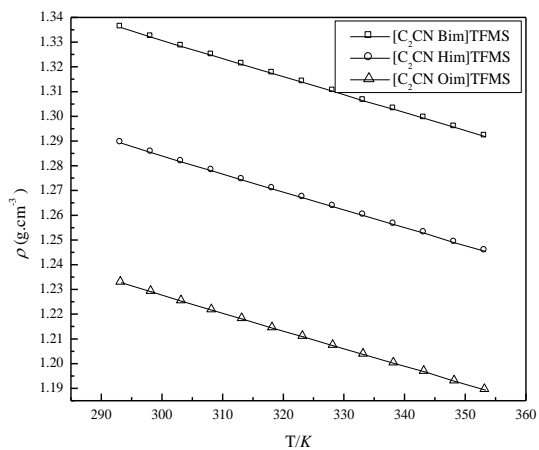


Fig 4-45 Densities ρ ($\text{g}\cdot\text{cm}^{-3}$) of $[\text{C}_2\text{CN C}_n\text{im}]\text{TFMS}$ ILs as a function of temperature

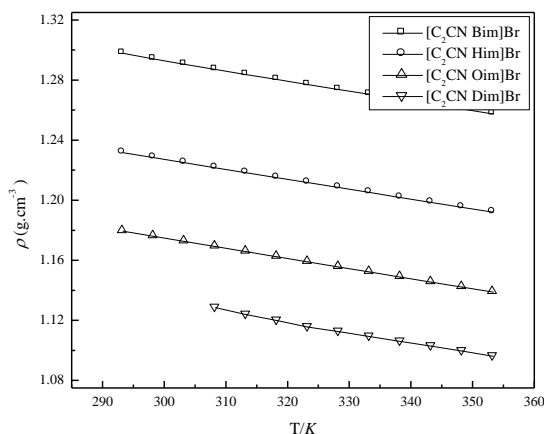


Fig 4-46 Densities ρ ($\text{g}\cdot\text{cm}^{-3}$) of $[\text{C}_2\text{CN C}_n\text{im}]\text{Br}$ ILs as a function of temperature

The measured density of the $[\text{P}_{6,6,6,14}]\text{DOSS}$ is in agreement with the published values for $[\text{P}_{6,6,6,14}]\text{NTf}_2$ and $[\text{P}_{6,6,6,14}]\text{OTf}$ [102], The densities of $[\text{P}_{6,6,6,14}]\text{NTf}_2$ and $[\text{P}_{6,6,6,14}]\text{OTf}$ are 1.0654 and $0.9823 \text{ g}\cdot\text{cm}^{-3}$ respectively which indicates that the effect of the DOSS anion on density is similar to that for NTf_2 and OTf anions. The density of the present IL is lower compared to the phosphonium ILs with short alkyl chain, the density of $[\text{P}_{2,2,2,8}]\text{NTf}_2$ and $[\text{P}_{2,2,2,12}]\text{NTf}_2$ are 1.26 , 1.21 and $1.61 \text{ g}\cdot\text{cm}^{-3}$ [102] respectively which results from the increases of free volume due to the long alkyl chain.

As shown in Fig 4-40, the densities of the phosphonium-based ILs decreased with increasing alkyl chain length and also with increasing length of the hydrocarbon linkage chain; density of $[\text{P}_{8,8,8}\text{C}_6\text{P}_{8,8,8}]_2$ ILs is greater than that of $[\text{P}_{8,8,8}\text{C}_{10}\text{P}_{8,8,8}]_2$ ILs. The decrease in density with increasing spacer alkyl chain length has been reported for a large series of DCILs [50]. Moreover, the density of the present DCILs is lower compared to the phosphonium-based monocationic ILs.

The effect of the length of the alkyl chain of the imidazolium cation on the molar volume of the IL is plotted in Fig 4-47. The positive change in the molar volume caused by the addition of $-\text{CH}_2-$ groups is on average ($17.9 \text{ cm}^3\cdot\text{mol}^{-1}$). It agrees with the values calculated by Gardas *et al.* [104] ($33.88 \text{ cm}^3\cdot\text{mol}^{-1}$) and Gomez de Azevedo [202] ($34.56 \text{ cm}^3\cdot\text{mol}^{-1}$) each for two $-\text{CH}_2-$ groups. The difference between the molar volumes of two ILs belonging to each family and having the same anion

yields approximately the same value that corresponds to the difference in the molar volume contributions between the [C₂CN Bim]X, [C₂CN Him]X, [C₂CN Oim]X, and [C₂CN Dim]X. The plots clearly show almost linear, anion-independent, correlations between the molar volume (V_m) and number of carbon atoms in the alkyl chain (n_C). These trends are also reported by Tariq, M. *et al.*[102].

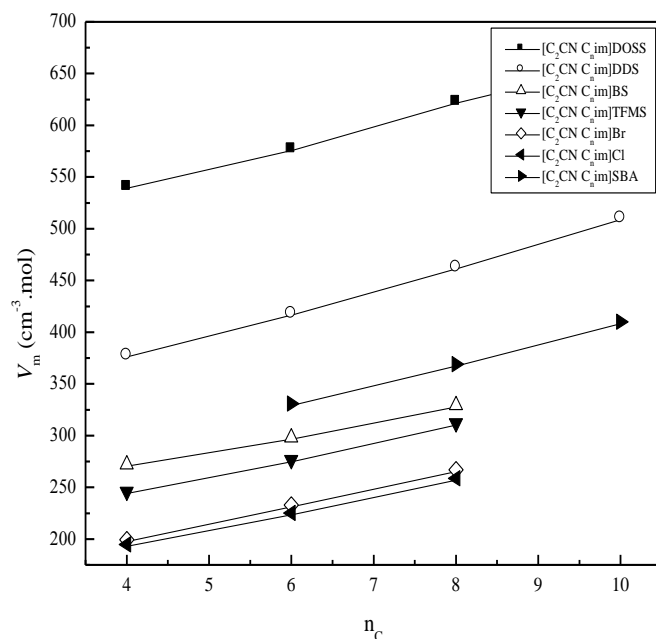


Fig 4-47 Plot of Molar volumes (V_m) versus the number of carbon (n_C) in the alkyl chains of the [C₂CN C_nim]X ILs

The present experimental results on density could be represented by the following empirical equation as a function of temperature [127, 182].

$$\rho / (g \cdot cm^{-3}) = A_0 + A_1 T \quad 4-1$$

where ρ and T are density and absolute temperature respectively, A_0 and A_1 are correlation coefficients. The correlation coefficients are estimated using linear regression analysis and the values are reported in

Table A- 11 of appendix A together with the standard deviations (SD). The standard deviations were calculated by applying the following expression [127]:

$$SD = \sqrt{\frac{\sum_j^{n_{DAT}} (Z_{exp} - Z_{cal})^2}{n_{DAT}}} \quad 4-2$$

where n_{DAT} is the number of experimental points, Z_{exp} and Z_{cal} are the experimental and calculated values respectively.

The extended of Ye and Shreeve's group contribution method for estimation of ILs densities proposed by Gardas, *et al.* [200] was used to predict densities of the synthesized ILs for a wide range of temperatures and pressures. The densities at temperatures 298.15, 313.15 and 343.15 K and pressures 1, 5, 10, 15 and 20 bars were estimated using the following equation:

$$\rho = \frac{M}{N_A V(a + bT + cP)} \quad 4-3$$

where ρ is density ($\text{g}\cdot\text{cm}^{-3}$), M is molar mass ($\text{g}\cdot\text{mol}^{-1}$), N_A is Avogadro's number, V is molecular volume (\AA^3), T is temperature (K) and P is pressure (bar). The constants a , b and c were proposed by Gardas, *et al.* [200] after analyzing 800 data points with mean percent deviation 0.45 % and 0.49 % for imidazolium and phosphonium-based ILs respectively; ($a = 0.8005$, $b = 6.652 \times 10^{-4} \text{ K}^{-1}$, $c = -5.919 \times 10^{-4} \text{ MPa}^{-1}$). It is important to know the effect of pressure on the densities of ILs since they contain some cavities (free volume) in their structure and also for better understanding of its role in their solubility behavior at high pressure.

The predicted densities for the present ILs are presented in Table A-12, Table A-13 and Table A-14 in Appendix A. The effect of pressure on the densities of the studied ILs is shown in Fig 4-48 and Fig 4-49. The results show that the density values increase almost linearly with increasing pressure. The linear correlation between pressure and density can be used to estimate the thermal compressibility (k_T). Compressibility is a universal phenomenon, of a significant importance where all substances are compressible, some more compressible than others. The compressibility of materials must be considered in engineering applications when changes in dimension due to pressure are expected.

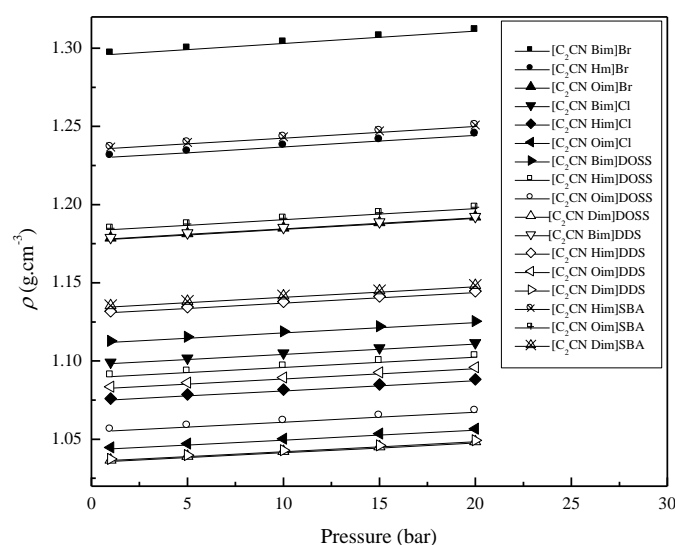


Fig 4-48 Effect of pressure on the densities of $[C_2CN C_nim]Br$, $[C_2CN C_nim]Cl$, $[C_2CN C_nim]DOSS$, $[C_2CN C_nim]DDS$ and $[C_2CN C_nim]SBA$ ILs at 298.15 K

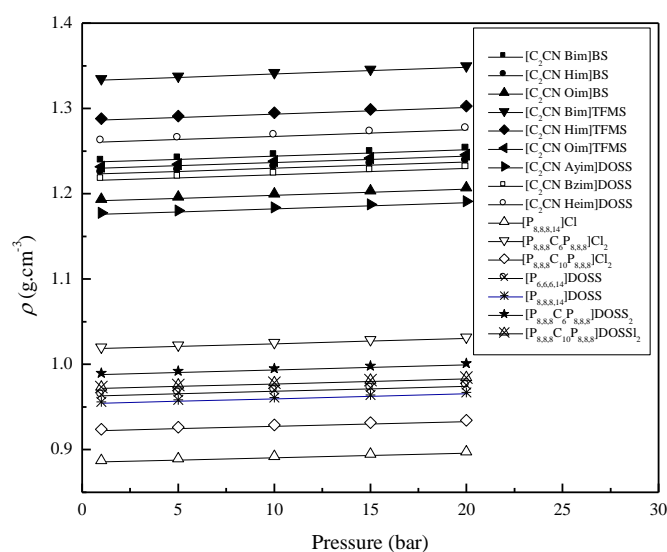


Fig 4-49 Effect of pressure on the densities of $[C_2CN C_nim]BS$, $[C_2CN C_nim]TFMS$, $[C_2CN Ayim]DOSS$, $[C_2CN Bzim]DOSS$, $[C_2CN Heim]DOSS$, $[P_{6,6,6,14}]DOSS$, $[P_{8,8,8,14}]X$ and $[P_{8,8,8}C_nP_{8,8,8}]X_2$ ILs at 298.15 K.

4.2.2 Viscosity

Viscosity is an important physical property for a number of processes. It determines the force and energy required to transfer and mix the IL with other substances and

appears in many dimensionless groups used in mass- and heat-transfer correlations. The applications that occur at high temperatures and/or pressures require reliable and accurate experimental data and mathematical models. This is especially pertinent for engineering applications as hydraulic fluids. ILs cover a wide range of viscosity [108].

The experimental viscosity values of the synthesized ILs are shown in Table A-15 to Table A-24 in Appendix A. High viscosity is a characteristic of most ILs. However the high thermal stability exhibited by ILs allows for applications at higher temperatures where the viscosity is reduced. Previous studies showed that the viscosity of ILs is largely controlled by hydrogen bonding, van der Waals forces, molecular weight and mobility [24]. The high viscosity for various ILs compared to molecular solvents was attributed to enhanced van der Waals forces relative to the hydrogen bonding [191].

The influence of anion on viscosity for the studied ILs is shown in Fig 4-51 to Fig 4-54. The measured viscosities are higher for the IL with DOSS anion among the sulfonate based anions, while it was the lowest for IL with TFMS anion. The ILs [C₂CN C_nim]TFMS shows the lowest viscosity of the [C₂CN C_nim]-based ILs investigated in this work. This can be explained by the incapability of the TFMS-anion to interact by hydrogen bonding and a randomized aggregation of ions caused by a low anionic basicity. More basic anions lead to tighter ion pairing of the cation with the anion, which also increases the intermolecular forces like hydrogen bonding [119]. Sulfonate groups can attract positively charged species to reduce the average transport of cations. The basicity of the anions incorporating sulfonate group varied depending on the alkyl chains and functional groups attached to the anion. As shown in Fig 4-50, The TFMS anion incorporate with withdrawing group (CF₃) which result in decreasing the negative charge of the SO₃⁻ group and hence decrease the basicity. The DOSS anion incorporates with donating groups (alkyl chains) which increase the negative charge of the SO₃⁻ group and hence increase the basicity. Moreover, the DOSS anions incorporates two alkyl chains while DDS incorporates one alkyl chain which results in higher basicity of the SO₃⁻ group for DOSS anion compared to that for DDS anion [203].

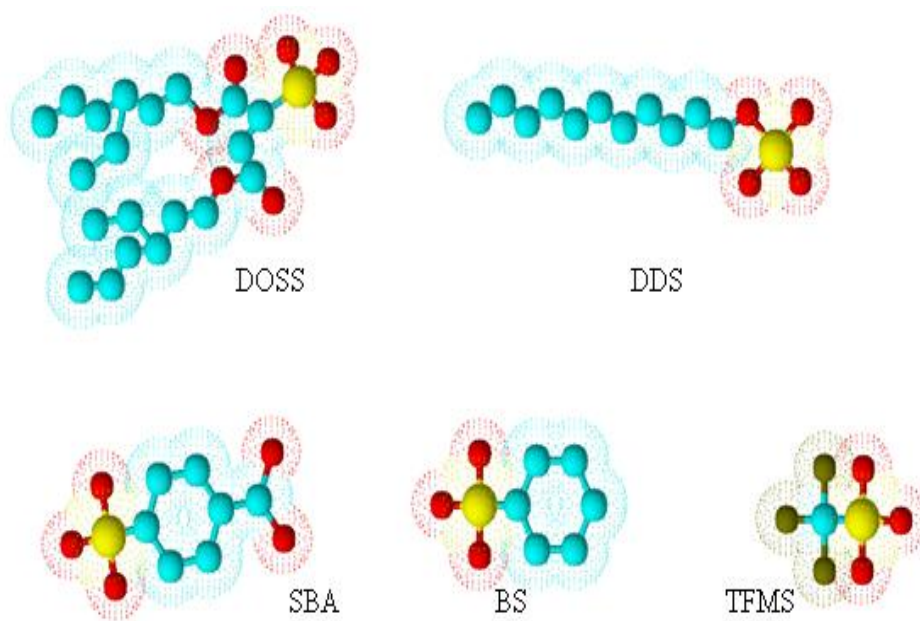


Fig 4-50 Structures of DOSS, DDS, SBA, BS and TFMS anions

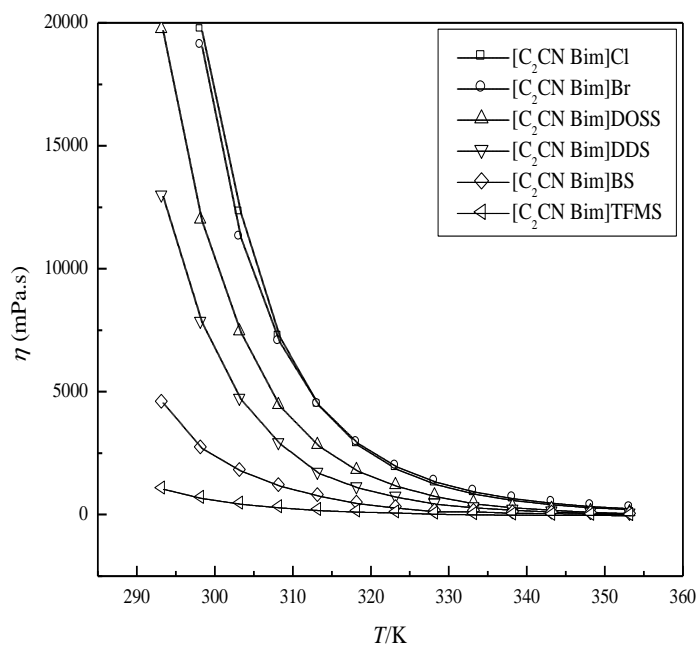


Fig 4-51 Viscosities as a function of temperature for [C₂CN Bim]X

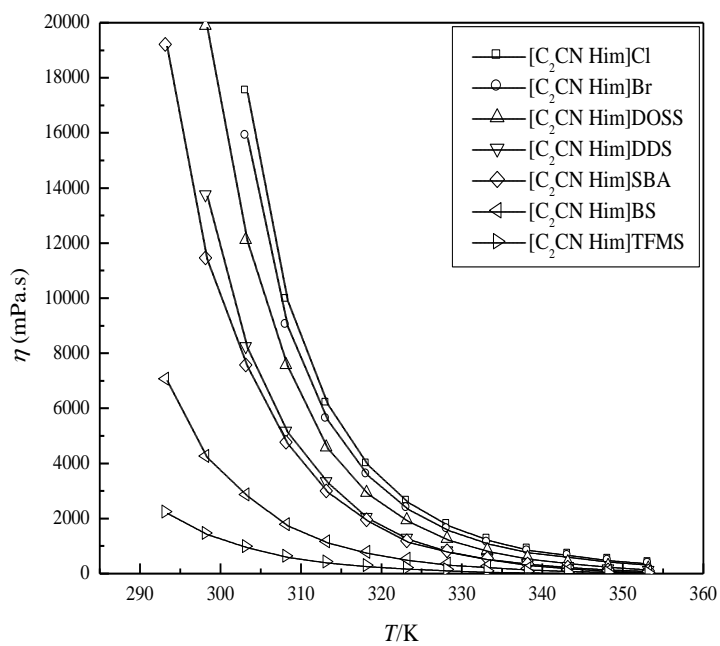


Fig 4-52 Viscosities as a function of temperature for $[C_2CN\ Him]X$

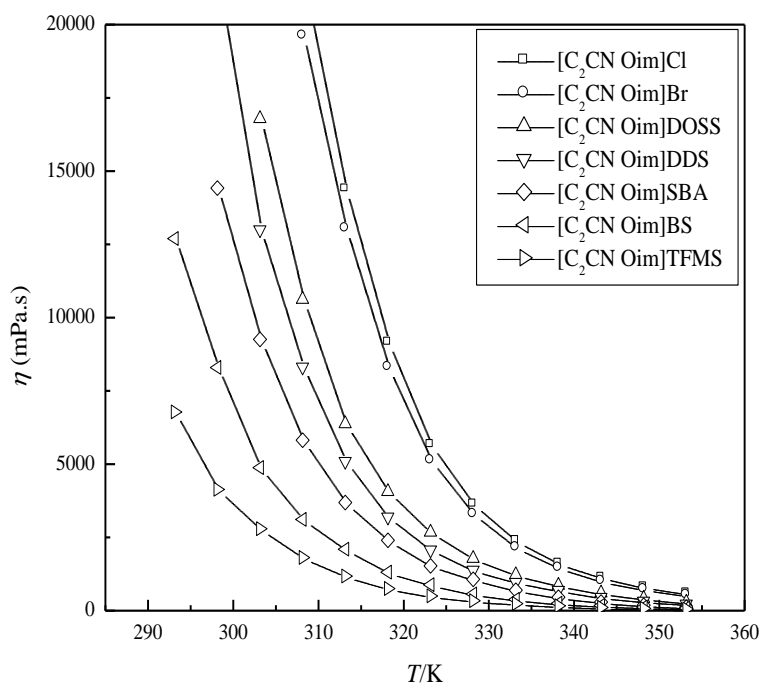


Fig 4-53 Viscosities as a function of temperature for $[C_2CN\ Oim]X$

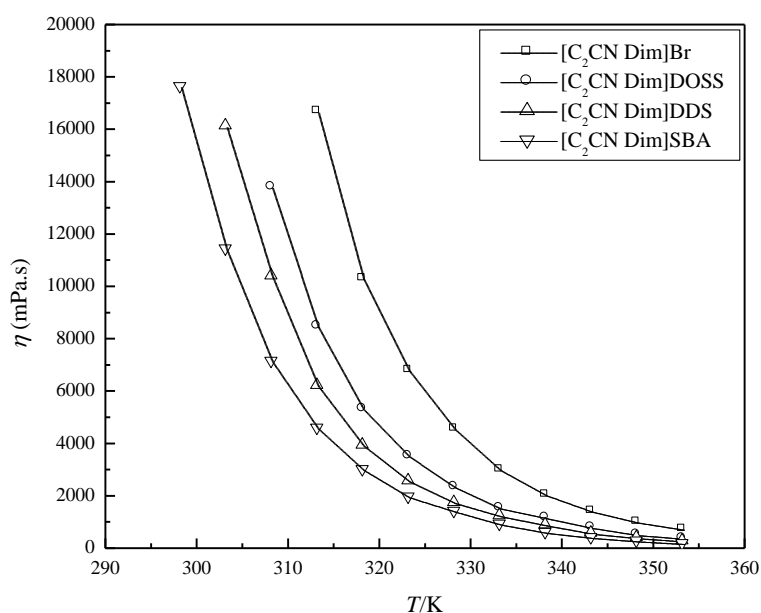


Fig 4-54 Viscosities as a function of temperature for [C₂CN Dim]X

The increased volumes of the anions here (trifluoromethanesulfonate excepted) lead to higher viscosities through reductions in ion mobility [67]. In addition, the high viscosity can also be ascribed to increased electrostatic interactions between the cation and anion. The [C₂CN Dim]DOSS IL showed highest viscosity since it possesses the largest anions with a values while [C₂CN Bim]TFMS showed lowest viscosity.

The viscosity values of the synthesized imidazolium-based ILs are higher than those of the corresponding ILs without nitrile group, which could be due to the high electron mobility around the nitrile group [106].

The viscosity values increase as the alkyl chains increases as observed by Tokuda *et al.* [111]. Even though the viscosities are high, the effect of shear rate on viscosities was investigated. ILs is classified as either Newtonian fluid or a thixotropic fluid. For the present ILs the shear rate has no difference in the viscosity but longer alkyl chains, (*e.g.*, [C_nMim]BF₄ where n ≥ 12) show non-Newtonian behavior [92]. The present ILs are classified as Newtonian fluid since n = 4, 6, 8, 10 (where n is the number of carbon atoms).

The viscosities of these nitrile-functionalized ILs with sulfonate anions are much higher compared with the reported imidazolium-based nitrile-functionalized ILs. For [C₂CN MIm]BF₄, [C₃CN Mim]BF₄ and [C₄CN Mim]Cl the viscosities are 65.5, 352 and 5222 mPa.s respectively [41, 106]. Moreover, the viscosities of the present synthesized ILs are higher compared to the other pyridinium-based nitrile-functionalized ILs (for [C₁C_nCNPyr]NTf₂ (n=1, 2, 3, 5 where n is the number of carbon atoms) the viscosities are in the range (345 to 540) cP) as reported by Nockeman and coworkers [201]. The imidazolium cations and sulfonate anions are joined together by a hydrogen bonding network [65] which resulted in increased viscosity. Low anion weight and low basicity (for less basic anion, the van der Waals forces dominates over the H-bonding due to better charge delocalization and this will reduce the viscosity of the IL) are necessary to obtain IL with low viscosity [191].

The viscosity increases with increasing molecular weight or alkyl chain [113] as shown in Fig 4-55. The high viscosities of the [P_{6,6,6,14}]DOSS and [P_{8,8,8,14}]DOSS ILs when compared to [P_{6,6,6,14}]NTf₂ and [P_{6,6,6,14}]OTf is due to the long alkyl chain of the DOSS anion. It is accomplished by increasing the electrostatic interaction between the cation and anion. Further the higher viscosity of the present phosphonium-based ILs when compared to [P_{2,2,2,8}]NTf₂ and [P_{2,2,2,2}]NTf₂ is attribute to the increased Van der Waals interactions of the long alkyl chains from both the phosphonium cations and the DOSS anion. The large volume of the DOSS anion causes low ion mobility and hence low viscosity [67].

Increasing the alkyl chain length has two contradictory effects: increase the electron donation into the cationic centre which decreases the electrostatic interaction between the cation and anion and hence viscosity is reduced. However increases the alkyl chain length also causes the Van der Waal's interactions to increase and viscosity to increase.

The viscosity values of the present DCILs are much higher and is comparable to phosphonium-based monocationic ILs (Fig 4-55); the viscosities of [P_{6,6,6,14}]NTf₂, [P_{8,8,8,8}]NTf₂ and [P_{8,8,8,8}] dithiomalenitrile is 450, 418 and 5590 mPa.s respectively [114]. The viscosity values increases as the spacer alkyl chain length increases and the

result is in agreement with that observed by Tokuda *et al.*[111]. The high viscosity of the DCILs was attributed to an increase in van der Waals forces, hydrogen bonding between cationic protons and anionic halides and the symmetry of the cations and anions [92].

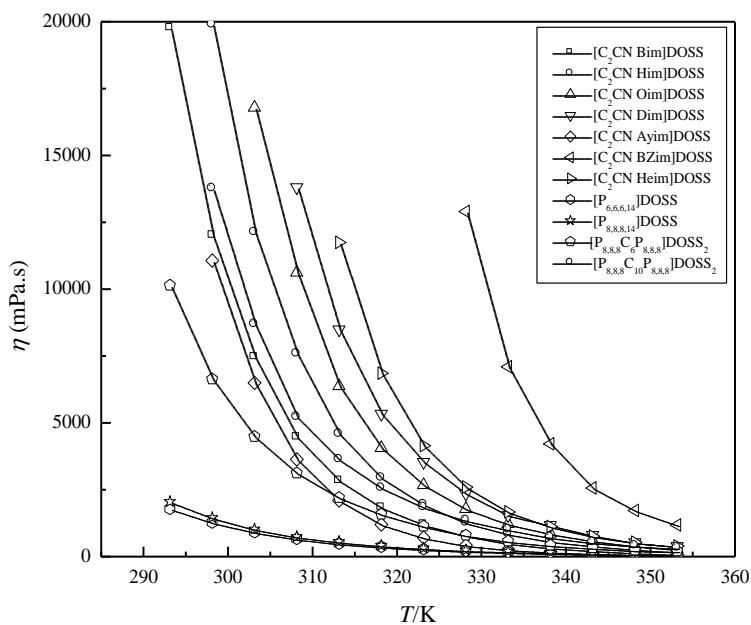


Fig 4-55 Viscosities for the DOSS-based ILs as a function of temperature

The influence of temperature on viscosity for the studied ILs is shown in Fig 4-51 to Fig 4-55. As can be observed, a rise in temperature caused a significant reduction in the viscosities of the synthesized ILs. An increase in temperature diminishes the strength of interactions between the cation and anion and should result in a lower viscosity [191]. These results suggest that slow mass-transfer processes occur in ILs at room temperatures due to high viscosity of ILs will become accelerated at elevated temperatures.

As can be observed, a rise in temperature caused a significant reduction in the viscosities of the present synthesized ILs. However, as shown in Fig 4-55 and in Table A-15 to Table A-24 in Appendix A, the viscosity values of the ILs show functional group and alkyl chain length dependency [119], and an addition of

functional group or increasing alkyl chain length has been found to give higher viscosity value.

Variation of the viscosity with temperature provides information on the structure of the ILs [133]. The temperature dependence of viscosity was studied for all of the synthesized ILs over the temperature range 293.15-353.15 K and the plots (Fig 4-56 to Fig 4-60) were fitted with the logarithmic form of the Arrhenius equation (4-4).

$$\ln \eta = \ln \eta_{\infty} + \frac{E_{\eta}}{RT} \quad 4-4$$

where η is the viscosity, η_{∞} is the viscosity at infinite temperature, E_{η} activation energy for viscous flow, R is universal gas constant and T is temperature in Kelvin. The activation energies for viscous flow (E_{η}) and the viscosities at infinite temperature (η_{∞}) were calculated from the slopes and intercepts (respectively) of the Arrhenius plots (Fig 4-56 to Fig 4-60). Table A-25 shows the Arrhenius parameters obtained from the Arrhenius plots together with the standard deviations (SD). The standard deviations were calculated using equation 4-2.

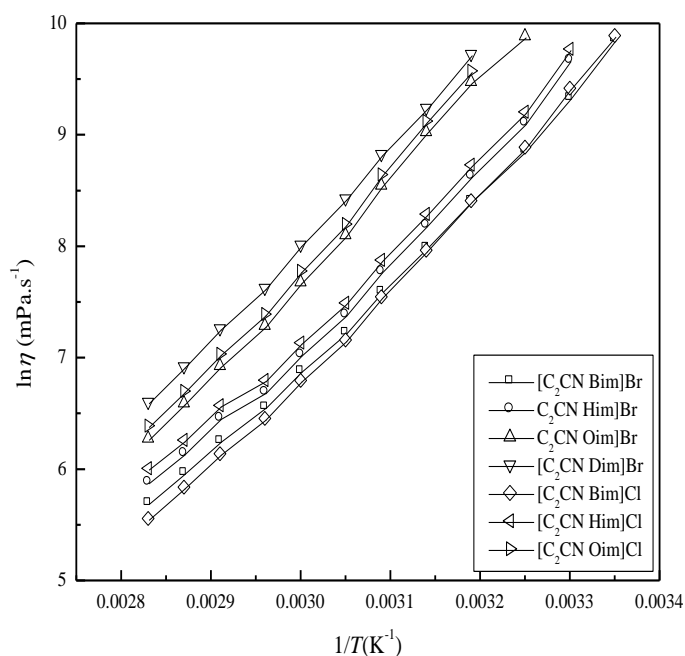


Fig 4-56 Arrhenius plot of viscosity for $[C_2CN C_n m]Br$ and $[C_2CN C_n m]Cl$ ILs

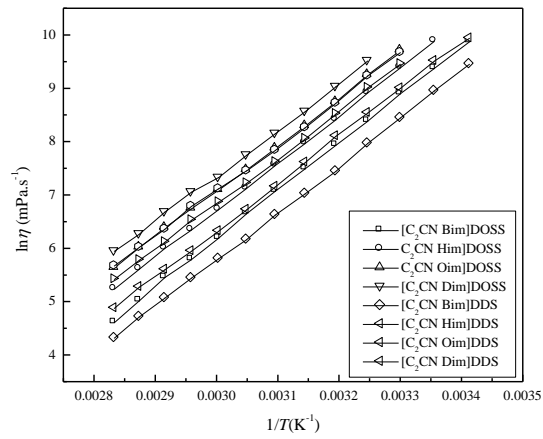


Fig 4-57 Arrhenius plot of viscosity for $[C_2CN C_n m]DOSS$ and $[C_2CN C_n m]DDS$ ILs

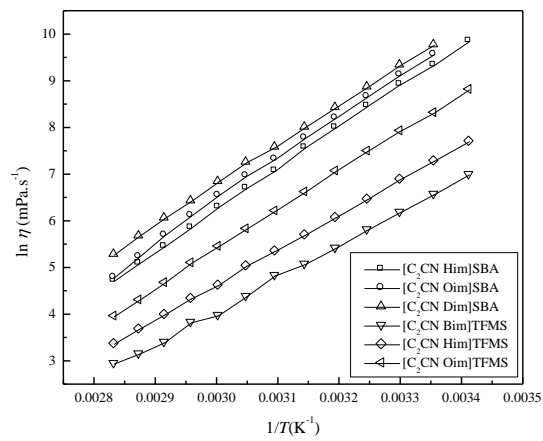


Fig 4-58 Arrhenius plot of viscosity for $[C_2CN C_n m]SBA$ and $[C_2CN C_n m]TFMS$ ILs

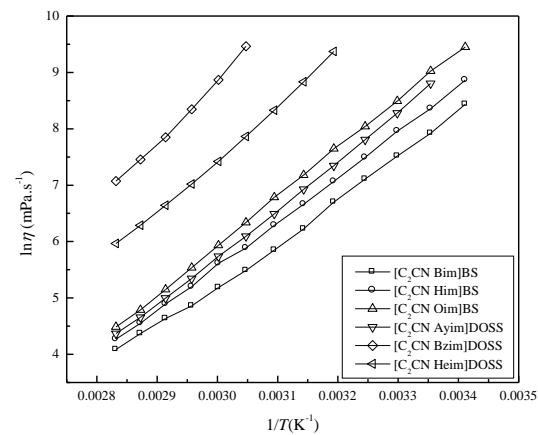


Fig 4-59 Arrhenius plot of viscosity for $[C_2CN C_n m]BS$ and dual functionalized ILs

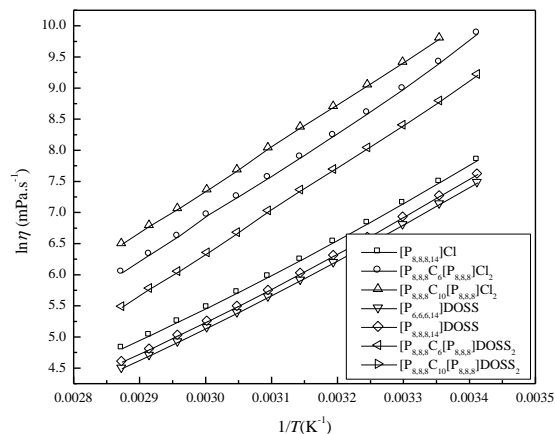


Fig 4-60 Arrhenius plot of viscosity for phosphonium-based ILs

The activation energy for viscous flow (E_η) gives an estimation of the level of energy required by the ions to move freely inside the IL. The value of E_η can be correlated with structural information about the ILs. The larger the value of E_η , the harder it is for the ions to move freely inside the IL. That might be due to either physical size or more numerous or stronger interactions in the IL (and hence more order) [109]. The viscosity at infinite temperature (η_∞) is an indication of the magnitude of the constitutive ions structures effect on the viscosity of the ILs [109, 133]. At infinite temperature, interactions which contribute to viscosity at room temperature in ILs are no longer effective and the viscosity (η_∞) is governed only by the geometric structure of the ions in the IL. So the value of η_∞ is representative of a structural contribution of the ions to the viscosity [109].

The activation energies (E_η) are higher for the dual functionalized imidazolium-based ILs while it was the lowest for phosphonium-based ILs. The activation energy is higher for the dual functionalized ILs than for the nitrile functionalized IL, suggesting that for the constitutive ions of the dual functionalized ILs is more difficult to pass each other in comparison with the nitrile functionalized. The energy barrier for the dual functionalized ILs ions, which must be surpassed, could become higher as a result of attaching two functionalized chains to the imidazolium cation. The present ILs showed lower activation energies compared to that for other ILs reported by Sánchez, *et al.* [133], (the activation energies of [Bmim]BF₄ and [Amim]BF₄ are (33.53 and 49.18)·10³ KJ.mol⁻¹). Furthermore, these ILs except [C₂CN C_nim]TFMS

show higher activation energies compared to [Bmmim]BF₄, [Bmim]PF₆ and [Bmim]CF₃SO₃ ILs that have activation energies in the range of 21-26.17 KJ.mol⁻¹ [109].

The viscosities at infinite temperatures (η_{∞}) are higher for the phosphonium-based ILs followed by the nitrile functionalized IL while it was the lowest for the dual functionalized imidazolium-based ILs. These results suggest that the structural contribution of the phosphonium-based ILs ions to the viscosity is greater than the other studied ILs. This might be due to the large number of alkyl chains of the phosphonium-based ILs. It is accomplished by increasing the electrostatic interaction between the cation and anion and also the Van der Waal's interactions between the alkyl chains.

4.2.3 Refractive index

The refractive index is related to the excess molar refraction which is used in the least squares energy relationships (LSERs) as a predictor of solute distribution [50]. The relation between the refraction index and the polarizability constitute a measure of the importance of the dispersion forces to the cohesion of the liquid (solvents with a large index of refraction should be capable of enjoying strong dispersion forces). Also the values of refractive index are regarded as a measure of the relative extent of the polar domains in the IL [102].

The measured data of the refractive indices of the present RTILs are presented in Table A-26 to Table A- 35 in Appendix A. The results suggested that cation type, the functional group, alkyl chain length of cation and type of the anion has a large effect on the refractive index values. The refractive index values of the present nitrile functionalized ILs are in good agreement with that reported by Zhang, *et al.* [106] for the other nitrile functionalized ILs; for [C₃CN Mim]NTf₂ and [C₃CN Mim]BF₄, [C₂CN Bim]Br and [C₂CN Oim]Br the refractive index are (1.4398, 1.4349, 1.54540 and 1.51473) respectively. Moreover, the refractive indices of these nitrile-functionalized ILs with sulfonate anions are much higher compared to [C₁C_nCNPyR]Tf₂N ILs where the reported refractive indices are in the range from

(1.4305 to 1.4365) [201]. The results show that the present ILs has higher values of refractive index than those of the corresponding ILs without nitrile group, which could be due to the high electron mobility around the nitrile group [106]. The effect of different anions used in the refractive index values was shown in Fig 4-61. Among the studied anions, TFMS shows the highest refractive index value while DOSS shows the lowest value. This may be attributed to the lower density of the DOSS anion.

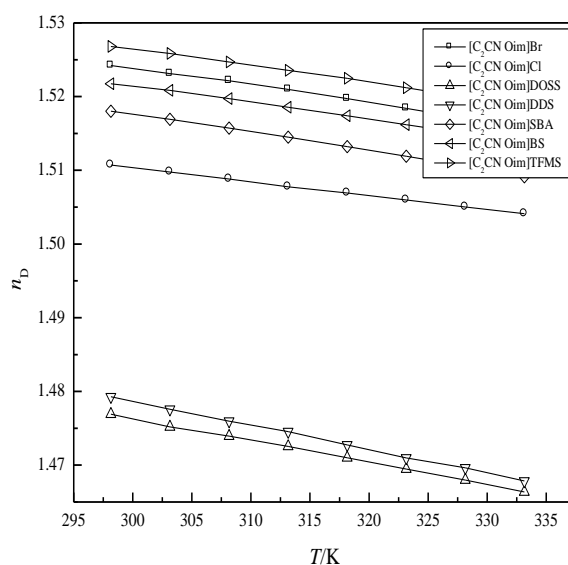


Fig 4-61 Experimental values of refractive index n_D , against T for $[C_2CN Oim]$ -based ILs

The measured refractive index values in the temperature range from (298.15 to 333.15) K for $[P_{6,6,6,14}]DOSS$ show that the refractive index values of this IL is in agreement with other trihexyltetradecylphosphonium ILs, the refractive index of $[P_{6,6,6,14}]NTf_2$ and $[P_{6,6,6,14}]OTf$ is 1.4587 and 1.4585 as reported by Tariq *et al.*[102]. The refractive index for $[P_{8,8,8,14}]Cl$ is greater than that of $[P_{8,8,8,14}]DOSS$ which have refractive index value lower than that for $[P_{6,6,6,14}]DOSS$ IL. These results indicate that the anion and alkyl chain length of the cation have a great effect on the refractive index. Moreover, the refractive indices of the present DCILs decrease with increasing the spacer alkyl chain length.

The effect of different cations in the refractive index values is shown in Fig 4-62. When comparing the refractive indices of the synthesized phosphonium-based ILs with their analogous imidazolium-based ILs, it was found that the phosphonium-based ILs have a slightly lower refractive index. This finding indicates that the phosphonium cation plays a role in the refractive index of an ILs which might be due to the large number of alkyl chains of the phosphonium-based ILs.

Experimental results for the temperature dependency of the refractive indices, n_D , for the synthesized ILs are shown in Fig 4-62 to Fig 4-66. Refractive indices values for each of the studied ILs decrease almost linearly with increasing temperature as in density.

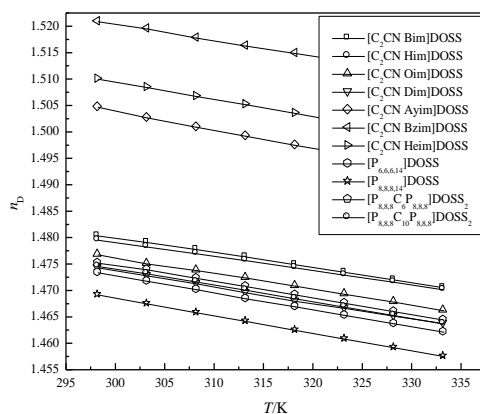


Fig 4-62 Experimental values of refractive index n_D , against T for imidazolium and phosphonium-based ILs incorporating DOSS anion

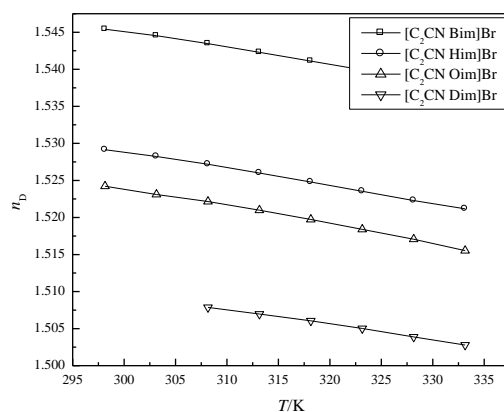


Fig 4-63 Experimental values of refractive index n_D , against T for [C₂CN C_nim]Br

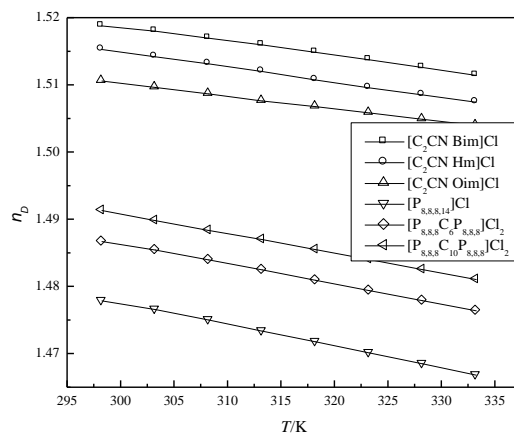


Fig 4-64 Experimental values of refractive index n_D , against T for the ILs incorporating chloride anion

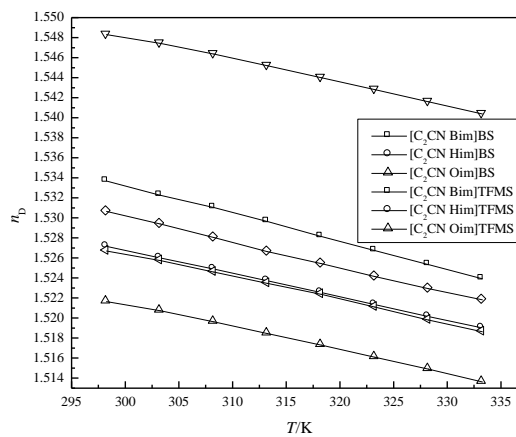


Fig 4-65 Experimental values of refractive index n_D , against T for $[C_2CN C_{nim}]BS$ and $[C_2CN C_{nim}]TFMS$

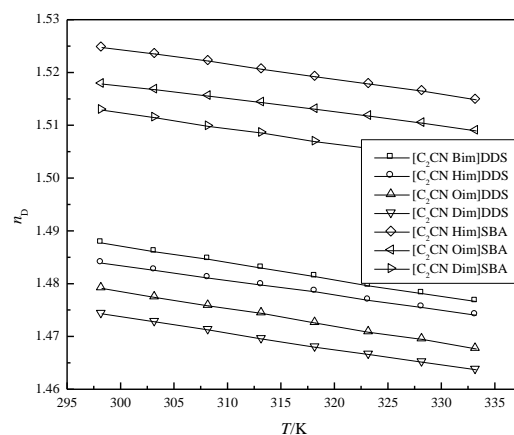


Fig 4-66 Experimental values of refractive index n_D , against T for $[C_2CN C_{nim}]DDS$ and $[C_2CN C_{nim}]SBA$

The measured refractive indices for the present ILs were correlated as a function of temperature T using the following form of equation [94, 182]:

$$n_D = A_2 + A_3T \quad 4-5$$

The coefficients A_2 and A_3 are estimated using the method of least squares and are listed in Table A- 36 together with the standard deviations (SD). The standard deviations were calculated using equation 4-2.

4.2.4 Thermal stability

Thermal stability of ILs is of practical importance for various applications. For CO₂ capture it is important for the determination of the process conditions. The effects of anion, cation and alkyl chain were studied and the results were reported in term of start temperatures for weight loss (T_{start}) and onset temperatures (T_{onset}). As shown in Fig 4-67 and Fig 4-68, the onset temperatures of these ILs are affected by the type of the cation, the anion and the size of the alkyl chain of the cation [204]; the decomposition temperature decreases as the alkyl chain increases which may due to the increase of the reactivity.

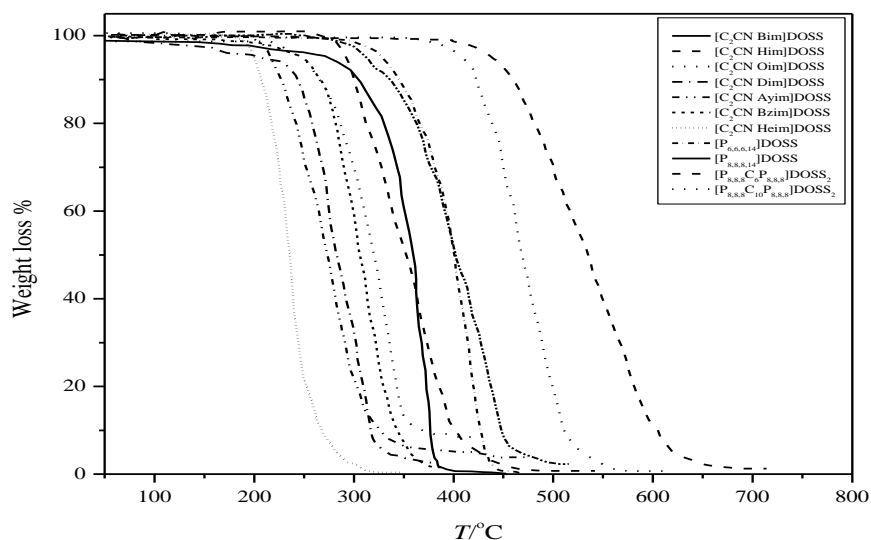


Fig 4-67 Thermogravimetric traces of imidazolium and phosphonium - based ILs incorporating DOSS anion

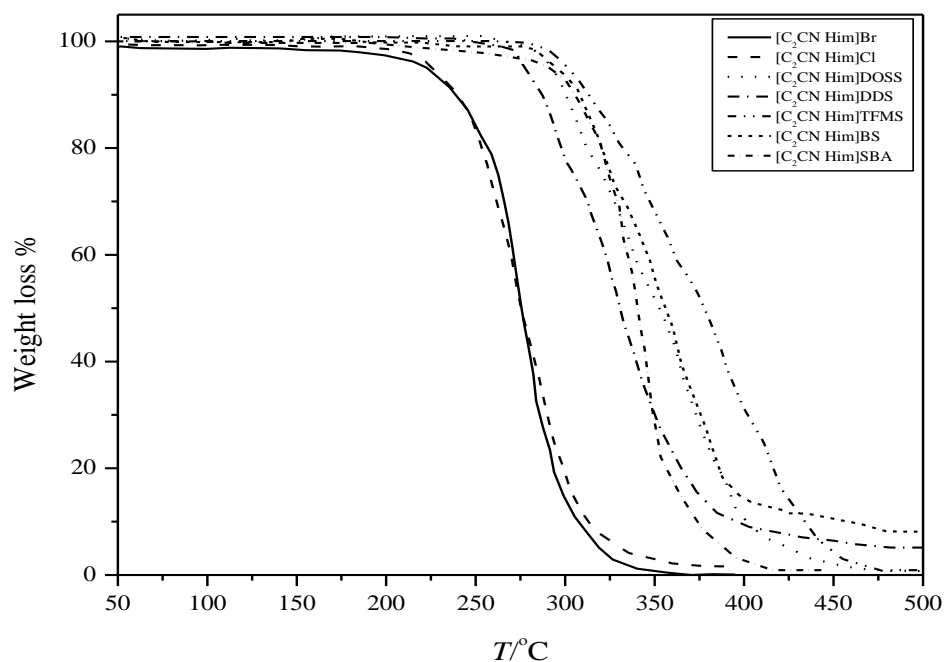


Fig 4-68 Thermogravimetric traces of [C₂CN Him]-based ILs

Also the T_d of ILs with incorporation of a CN group decreased remarkably in comparison with the corresponding ILs without a CN group (T_d of [C₄Mim]Cl, [C₆Mim]Cl and [C₈Mim]Cl is (254, 253 and 243) °C respectively) [92]. However, the incorporation of a CN group made the ILs more reactive than the ILs without a CN group [106].

The decomposition temperatures of the present nitrile functionalized ILs incorporating sulfonate –based anions are high compared with that reported for other nitrile functionalized ILs; for [C₃CN Mim]Cl the T_d is (254.9) °C [106], as a result of replacing the basic, reactive chloride with more stable anions. The thermal stability of the TFMS containing ILs is the highest due to the extremely stable anion (Fig 4-68). This might be due to the high chemical and thermal stability of the C-F bond. The thermogravimetric traces of the ILs incorporating DDS, SBA, BS and TFMS, Cl and Br anions are shown in Fig 4-69 to Fig 4-72. Moreover, the thermal stability of the ILs with DOSS, DDS, SBA, BS and TFMS anions were high in comparison with the corresponding ILs with bromide anion which due to the high reactivity of the bromide anion.

The start and onset temperatures of the studied ILs are presented in Table 4-2. Thermal stability studies of the dual functionalized imidazolium-based ILs incorporating nitrile functionality with allyl, benzyl or 2-hydroxyethyl functionalities shows that these ILs begin to decompose at temperatures lower than that for their analogous incorporating only nitrile functionality (Fig 4-67). However, the incorporation of a two functional group made the ILs more reactive than the ILs with one functional group. The results show that the thermogravimetric decreases of the benzyl substituted imidazolium compound took place at much higher temperatures than those of the other imidazolium-based dual functionalized ILs, revealing the relatively high thermal stability of the benzyl-substituted imidazolium-based compound. The π -electrons in the benzyl group might be associated with the d orbital interactions. These interactions seem likely to give a significant increase in the bond strength, thereby resulting in the high thermal stability. Similar results have been reported [205].

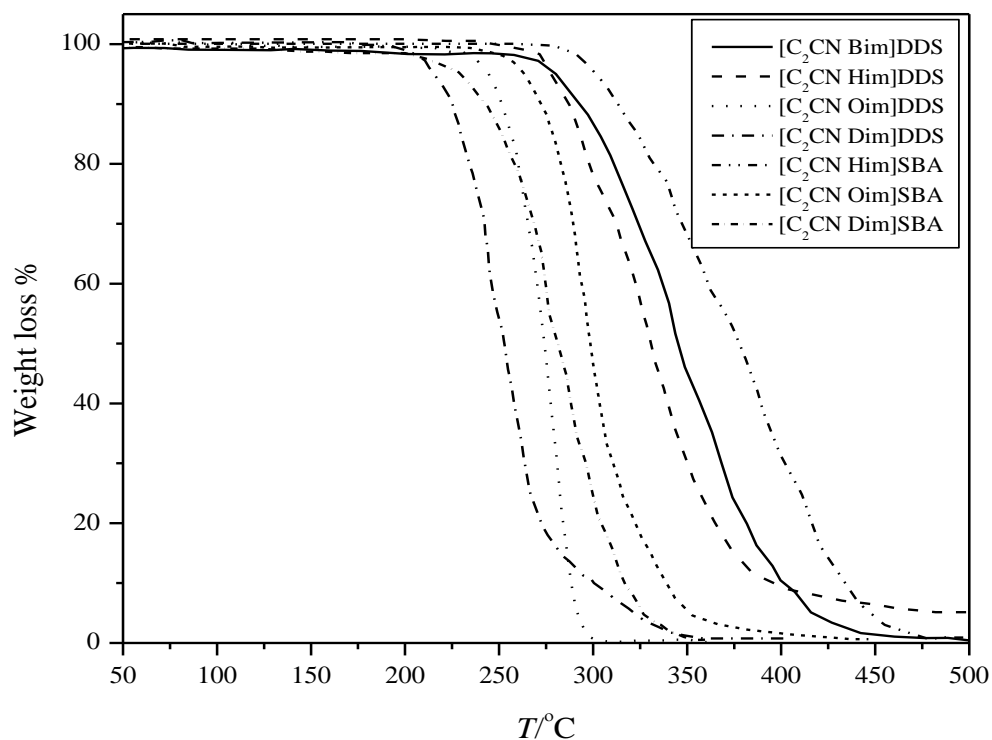


Fig 4-69 Thermogravimetric traces of [C₂CN C_nim]DDS and [C₂CN C_nim]SBA ILs

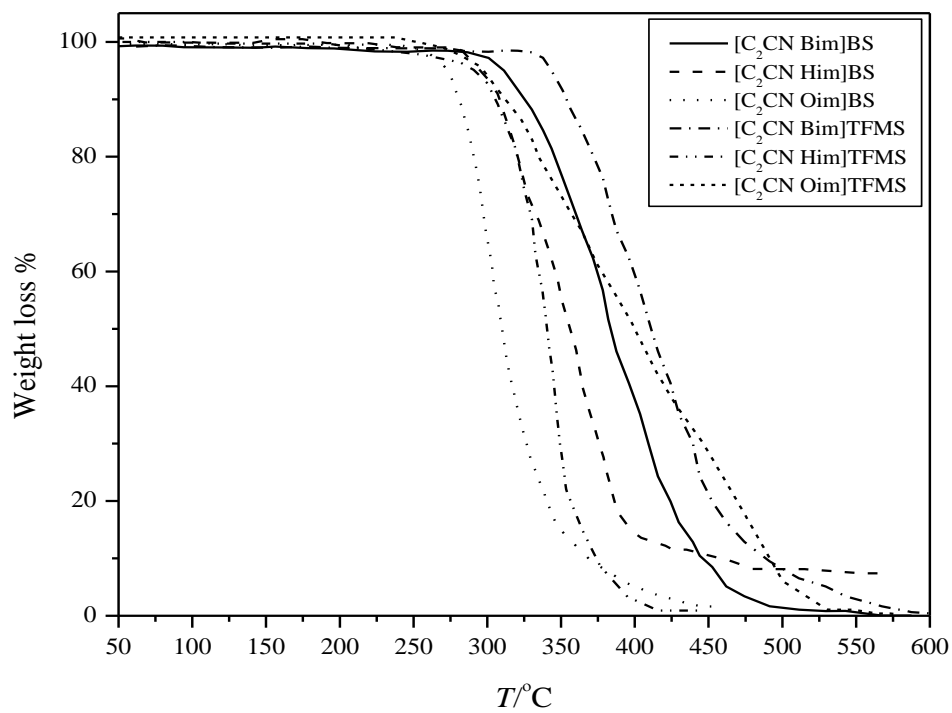


Fig 4-70 Thermogravimetric traces of $[C_2CN C_n im]BS$ and $[C_2CN C_n im]TFMS$ ILs

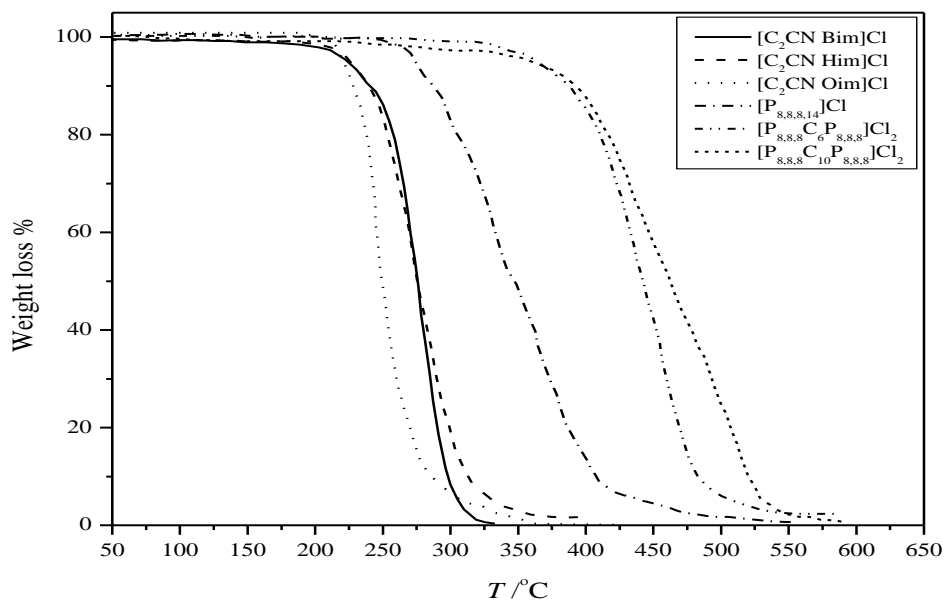


Fig 4-71 Thermogravimetric traces of $[C_2CN C_n im]Cl$ ILs

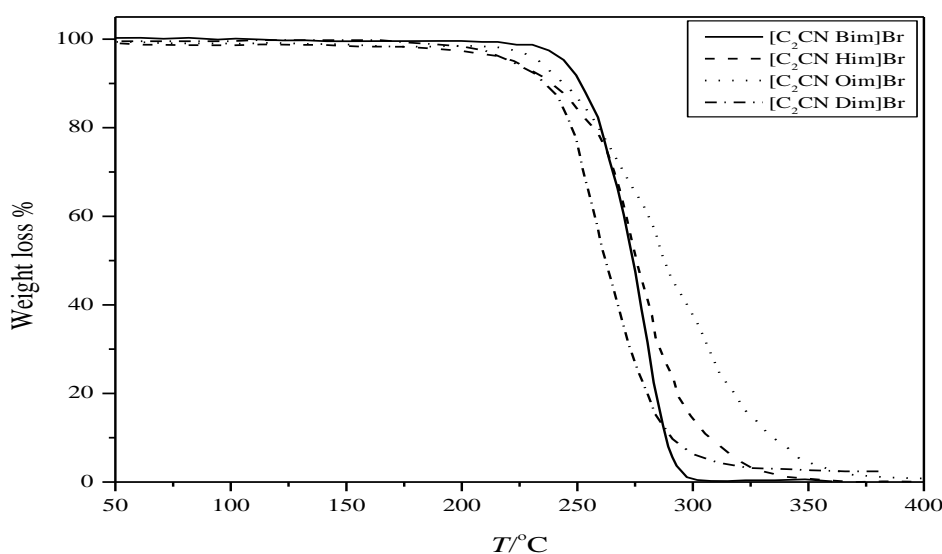


Fig 4-72 Thermogravimetric traces of $[C_2CN C_n\text{im}]Br$

Decomposition of imidazolium salts is attributed to decomposition of cation as facilitated by the anion which itself becomes transformed. Pyrolysis of imidazolium salts yielded volatile degradation products such as 1-substituted imidazoles and alkylated anions and the degradation pathway was identified as elimination of the N-substituent, which is essentially the reverse substitution synthesis reaction. Nucleophilicity of anion and the ability of cation to undergo alkyl migration or elimination reaction have a significant influence on thermal stability of ionic liquids [123].

The start and onset temperatures of the phosphonium-based ILs are also affected slightly by the size of the alkyl chain of the cation (Fig 4-67). The decomposition temperatures of the present phosphonium-based ILs are lower compared to other phosphonium ILs with short alkyl chain, for $[P_{2,2,2,8}]NTf_2$ and $[P_{2,2,2,12}]NTf_2$ are 400 and 380 °C respectively [113]. Decomposition temperatures of the DCILs are affected slightly by the spacer alkyl chain length; the decomposition temperature decreases as the spacer alkyl chain length increases as reported by Jared L. *et al.* [51] for DCILs. This might be due to the increase of the reactivity with the increase of the alkyl chain length. The measured decomposition temperatures values of the present ILs are comparable to other DCILs reported by Guiqin, Y. *et al.* [50]. The TGA data reported

showed only a dynamic property of IL where the IL is heated for a short period of time, which is not representative for the application in which longer heating time is required [206].

Table 4-2 Start and onset temperatures of the studied ILs

Cations \ Anions	[C ₂ CN Bim]		[C ₂ CN Him]		[C ₂ CN Oim]		[C ₂ CN Dim]	
	<i>T</i> _{start} (°C)	<i>T</i> _{onset} (°C)	<i>T</i> _{start} (°C)	<i>T</i> _{onset} (°C)	<i>T</i> _{start} (°C)	<i>T</i> _{onset} (°C)	<i>T</i> _{start} (°C)	<i>T</i> _{onset} (°C)
Br	218	253	211	245	194	240	191	238
Cl	205	247	194	239	191	229	-	-
DOSS	291	307	263	293	257	274	250	261
DDS	279	297	265	285	238	259	235	246
SBA	-	-	268	302	249	288	255	273
BS	298	312	271	308	256	291	-	-
TFMS	304	328	288	316	261	296	-	-
	[C ₂ CN Ayim]		[C ₂ CN Bzim]		[C ₂ CN Heim]			
DOSS	199	228	205	241	203	219	-	-
	[P _{6,6,6,14}]		[P _{8,8,8,14}]		[P _{8,8,8} C ₆ P _{8,8,8}]		[P _{8,8,8} C ₁₀ P _{8,8,8}]	
Cl	-	-	236	297	378	395	354	381
DOSS	294	368	283	341	389	446	371	426

As general the residue of the TGA results might be due to the impurities in the studied RTILs. Most of the ionic liquids synthesized are fully water-miscible at room temperature, which makes it difficult to free them from bromide and chloride impurities. Clearly, all ionic liquids made by metathesis from the corresponding sodium salt have high halide contents. The sources of impurities in RTILs were studied and it was concluded that the high halide content is due to unreacted starting material [100].

4.3 Derived thermodynamic properties

Thermodynamic considerations are essential to understand the stability and behaviour of molten materials.

4.3.1 Thermal expansion coefficient

The expansion of materials must be considered in engineering applications when changes in dimension due to temperature are expected. The changes in the liquid volume with temperature were evaluated using the thermal expansion coefficient. Since the temperature-density relationship for ILs is linear, density values as a function of temperature were used to calculate the thermal expansion coefficient. The thermal expansion coefficients (α_p), also known as volume expansivity, as a function of temperature at atmospheric pressure was estimated using the following equation [207].

$$\alpha_p(\text{K}^{-1}) = -(1/\rho)(\partial\rho/\partial T)_p = -(A_1)/(A_0 + A_1T) \quad 4-6$$

where, α_p is thermal expansion coefficient in K^{-1} , ρ is the density, A_0 and A_1 are the fitting parameters of equation 4-1. Estimates of isothermal expansion, α_p , made from experimental densities are presented in Table A- 37 and Table A- 41 in Appendix A. The thermal expansion coefficients of these ILs do not appreciably change with temperature for the range 293.15 to 353.15 K studied in the present work. The studied ILs show weak temperature dependency for the thermal expansion coefficient, $\alpha = 4.89 \times 10^{-4}$ to $7.31 \times 10^{-4} \text{ K}^{-1}$, which are higher than those of high-temperature molten salts, but are, noticeably smaller than those for molecular organic liquids. Also these values are similar to that reported for imidazolium-, pyridinium-, phosphonium- and ammonium – based ILs (5.0×10^{-4} to 6.5×10^{-4}) K^{-1} [94]. ILs having shorter alkyl chain on cation possess a lower expansion coefficient compared with those having longer alkyl chain. This is associated with the coiling of the chain. Moreover, the large cation size of the IL reduces the electrostatic interactions and facilitates the molecular enlargement. The phosphonium-based ILs shown higher expansion coefficients compare to the imidazolium-based ILs. In addition, the dual

functionalized ILs shows the lowest expansion coefficients. This might be due to the large number of the alkyl chains of the phosphonium-based ILs.

4.3.2 Lattice energy

Lattice energy is an important quantity in assessing the stability of an ionic material (the energy required to remove the ions from their positions in the crystal structure to infinite separation)[99]. The strength of the bond between the ions of opposite charge in an ionic compound therefore depends on the charges on the ions and the distance between the centers of the ions when they pack to form a crystal. An estimate of the strength of the bonds in an ionic compound can be obtained by measuring the lattice energy of the compound.

Lattice energy of IL is the surface excess energy which is reliant on the interaction energy between ions. The low crystal energy is the underlying reason for forming the IL at room temperatures [97]. Lattice energies of ILs were estimated according to Glasser theory [99] using the following equation:

$$U_{POT} = 1981.2(\rho/M)^{1/3} + 103.8 \quad 4-7$$

where U_{POT} is the lattice energy in $\text{kJ}\cdot\text{mol}^{-1}$. The results presented in Table 4-3 show that lattice energies of ILs are much less than that of inorganic fused salts; the minimal lattice energy (U_{POT}) among alkali chlorides is $602.5 \text{ kJ}\cdot\text{mol}^{-1}$ [97]. The results indicate that the lattice energies for the synthesized ILs (except $[\text{C}_2\text{CN C}_n\text{im}]\text{Br}$) are lower than that of the other ILs (for $[\text{C}_n\text{Mim}]\text{alanine}$ and $[\text{C}_n\text{Mim}]\text{glycine}$ (where $n=2-6$), ranging from 421 to 456 and 429 to 469 $\text{kJ}\cdot\text{mol}^{-1}$ respectively [97]. Also, these values are lower than that reported by W. Guan; for $[\text{C}_n\text{Mim}]\text{Gly}$ and $[\text{C}_n\text{Mim}]\text{Glu}$ the lattice energies are in the range of 410 to 450 $\text{kJ}\cdot\text{mol}^{-1}$ [125]. The results of the lattice energy for the present RTILs show that the lattice energy was found to decrease as the anion volume increase and also decrease with increasing alkyl chain length of the cation.

4.3.3 Molar refraction

The molar refractions are often considered as a measure of the hard-core molecular volume [102, 130], consequently was used to calculate the molar free volume (V_f) (unoccupied part of the molar volume of a substance [83]) of the present ILs. The molar refraction R_M values for present ILs were estimated using the Lorentz–Lorenz relationship [102], this equation takes the form shown as in equation 4-8.

$$R_M = \frac{N_A \alpha_e}{3\epsilon_0} = V_m \left(\frac{n_D^2 - 1}{n_D^2 + 2} \right) \quad 4-8$$

where, R_M is the molar refraction in $\text{cm}^3 \cdot \text{mol}^{-1}$, N_A is the Avogadro's number in mol^{-1} , α_e is mean molecular polarizability (electronic polarizability), ϵ_0 is the permittivity of free space, V_m is the molar volume in $\text{cm}^3 \cdot \text{mol}^{-1}$ and n_D is refractive index. The molar refraction for the studied RTILs are presented in Table A- 42 to Table A- 45 in Appendix A.

The molar free volumes for the synthesized ILs was calculated from the molar volume and molar refraction and the results are presented in Table 4-4. The molar free volumes for the synthesized imidazolium-based ILs are decreasing following the order $[\text{C}_2\text{CN C}_n\text{im}]\text{DOSS}$, $[\text{C}_2\text{CN C}_n\text{im}]\text{DDS}$, $[\text{C}_2\text{CN C}_n\text{im}]\text{SBA}$, $[\text{C}_2\text{CN C}_n\text{im}]\text{BS}$ and $[\text{C}_2\text{CN C}_n\text{im}]\text{TFMS}$.

$[\text{C}_2\text{CN C}_n\text{im}]\text{DOSS}$ shows very high molar refraction while the other ILs in this study show comparable values when compared with the values (47.93 to 121.73) $\text{cm}^3 \cdot \text{mol}^{-1}$ reported for the ILs $[\text{C}_n\text{mim}]\text{X}$ (where $n = 2$ to 14, $\text{X} = \text{NTf}_2$, PF_6 , BF_4 , OAc , MeSO_4) [102]. For the phosphonium-based ILs the molar free volume increases with increase of the alkyl chain length and alkyl chain spacer. Refractive indices of the present ILs decrease as the molar free volume increases, this behavior is in good agreement with that reported in literature (the larger the reduced molar free volume the smaller its refractive index is)[119], for other ILs.

Table 4-3 Molar volume (V_m), Molecular volume ($V_{molecular}$), molar standard entropy (S^0) and lattice energy (U_{POT}) of the studied ILs.

ILs	V_m ($\text{cm}^3 \cdot \text{mol}^{-1}$)	$V_{molecular}$ (nm^3)	S^0 $\text{JK}^{-1} \cdot \text{mol}^{-1}$	U_{POT} kJmol^{-1}
[C ₂ CN Bim]Br	199.4	0.331	442.23	443.52
[C ₂ CN Him]Br	232.9	0.387	511.53	426.41
[C ₂ CN Oim]Br	267.1	0.444	582.34	412.01
[C ₂ CN Bim]Cl	194.8	0.323	432.63	420.62
[C ₂ CN Him]Cl	225.1	0.374	495.39	344.76
[C ₂ CN Oim]Cl	258.7	0.430	565.00	338.81
[C ₂ CN Bim]DOSS	540.8	0.898	1148.98	347.48
[C ₂ CN Him]DOSS	577.5	0.959	1224.81	342.22
[C ₂ CN Oim]DOSS	623.1	1.035	1319.24	336.26
[C ₂ CN Dim]DOSS	662.0	1.099	1399.65	331.62
[C ₂ CN Bim]DDS	377.8	0.627	811.46	378.40
[C ₂ CN Him]DDS	418.4	0.695	895.52	369.22
[C ₂ CN Oim]DDS	462.9	0.769	987.72	360.43
[C ₂ CN Dim]DDS	510.6	0.848	1086.44	352.19
[C ₂ CN Him]SBA	330.9	0.549	714.35	390.80
[C ₂ CN Oim]SBA	369.1	0.613	793.43	380.54
[C ₂ CN Dim]SBA	409.9	0.681	877.90	371.05
[C ₂ CN Bim]BS	272.0	0.452	592.54	410.14
[C ₂ CN Him]BS	298.1	0.495	646.51	400.95
[C ₂ CN Oim]BS	329.6	0.547	711.66	391.18
[C ₂ CN Bim]TFMS	245.7	0.408	537.99	420.72
[C ₂ CN Him]TFMS	276.4	0.459	601.63	408.51
[C ₂ CN Oim]TFMS	311.9	0.518	675.06	396.50
[C ₂ CN Ayim]DOSS	504.2	0.837	1073.22	353.23
[C ₂ CN Bzim]DOSS	540.5	0.898	1148.29	347.53
[C ₂ CN Heim]DOSS	484.8	0.805	1032.90	356.52
[P _{8,8,8,14}]Cl	681.3	1.131	1439.64	329.45
[P _{8,8,8} C ₆ P _{8,8,8}]Cl ₂	880.1	1.461	1851.10	311.01
[P _{8,8,8} C ₁₀ P _{8,8,8}]Cl ₂	1032.7	1.715	2167.00	300.26
[P _{6,6,6,14}]DOSS	964.1	1.601	2025.07	304.81
[P _{8,8,8,14}]DOSS	1060.9	1.762	2225.43	298.51
[P _{8,8,8} C ₆ P _{8,8,8}]DOSS ₂	1734.9	2.881	3620.46	269.09
[P _{8,8,8} C ₁₀ P _{8,8,8}]DOSS ₂	1822.1	3.026	3801.05	266.41

4.3.4 Standard molar entropy

It is useful to be able to estimate standard entropy data for several reasons. First, there is a paucity of standard entropy data for inorganic materials in standard thermochemical tables. Second, experimental determination of absolute entropy, S^0 , by calorimetry is both a lengthy and nontrivial procedure; such measurements are no longer fashionable science and, for this reason, increasing reliance has to be placed on estimation techniques for standard entropy data [98, 208]. Furthermore, as temperature rises and energy gained the molten salts lose their order correlation and becomes reduced to disorder. These increases in disorder are observed as changes in the structures of the material concerned, accompanied by enthalpy increases resulting from the altered interactions, and are described by increases in entropy.

Glasser and Jenkins [98] used the following equation to estimate the standard molar entropy for ILs:

$$S^0 = 1246.5(V_m) + 29.5 \quad 4-9$$

where S^0 is the standard entropy at 298.15 K in $\text{J.K}^{-1}.\text{mol}^{-1}$, V_m is the molecular volume in nm^3 . The standard entropies for the synthesized ILs were estimated using equation 4-9 and the results are presented in Table 4-3. The present RTILs show a high values compare with the other ILs; for $[\text{C}_n\text{Mim}]$ alanine and $[\text{C}_n\text{Mim}]$ glycine; where $n=2-6$, the standard entropy ranges from 396.9 to 535.8 $\text{J.K}^{-1}.\text{mol}^{-1}$ and from 360.2 to 498.8 $\text{J.K}^{-1}.\text{mol}^{-1}$ respectively [25, 97].

Table 4-4 Molar free volumes (V_f) of the synthesized ILs

IL	V_f ($\text{cm}^3 \cdot \text{mol}^{-1}$)	IL	V_f ($\text{cm}^3 \cdot \text{mol}^{-1}$)
[C ₂ CN Bim]Br	136.3	[C ₂ CN Bim]DOSS	387.1
[C ₂ CN Him]Br	161.0	[C ₂ CN Him]DOSS	413.7
[C ₂ CN Oim]Br	186.6	[C ₂ CN Oim]DOSS	447.1
[C ₂ CN Bim]Cl	135.7	[C ₂ CN Dim]DOSS	475.2
[C ₂ CN Him]Cl	157.2	[C ₂ CN Bim]DDS	269.0
[C ₂ CN Oim]Cl	181.8	[C ₂ CN Him]DDS	298.7
[C ₂ CN Bim]BS	187.5	[C ₂ CN Oim]DDS	331.6
[C ₂ CN Him]BS	206.4	[C ₂ CN Dim]DDS	367.0
[C ₂ CN Oim]BS	229.1	[C ₂ CN Ayim]DOSS	353.4
[C ₂ CN Him]SBA	229.5	[C ₂ CN Bzim]DOSS	380.2
[C ₂ CN Oim]SBA	257.2	[C ₂ CN Heim]DOSS	337.1
[C ₂ CN Dim]SBA	286.7	[P _{8,8,8,14}]Cl	488.4
[C ₂ CN Bim]TFMS	169.2	[P _{8,8,8} C ₆ P _{8,8,8}]Cl ₂	627.0
[C ₂ CN Him]TFMS	190.9	[P _{8,8,8} C ₁₀ P _{8,8,8}]Cl ₂	733.4
[C ₂ CN Oim]TFMS	216.0	[P _{8,8,8} C ₆ P _{8,8,8}]DOSS ₂	1232.0
[P _{6,6,6,14}]DOSS	691.2	[P _{8,8,8} C ₁₀ P _{8,8,8}]DOSS ₂	1309.6
[P _{8,8,8,14}]DOSS	755.9		

CHAPTER 5

CARBON DIOXIDE SOLUBILITY

5.1 Introduction

ILs possess obvious advantages over traditional solvents when considering user safety and environmental impact [209]. Under many conditions, ILs have negligible vapor pressures, are largely inflammable, and exhibit thermal and chemical stabilities [64]. The most useful feature of ILs is the ability to tailor their chemistry and properties in a variety of ways. ILs can be synthesized as custom or “task-specific” solvents with functional groups presenting a seemingly infinite number of opportunities to design solvents with enhanced physical properties, improved interaction with solutes and matched to individual solutes of interest.

Separations of liquids or gases are just one area where the design of IL solvents is of great utility and importance [209]. Understanding of gas solubilities in ILs is important for future process development using ILs because many reactions and separations involve permanent or condensable gases [210]. Moreover, understanding CO₂ solubility in ILs is of great importance for the development of systems for separation of CO₂ from other gases [210].

The experimental solubility of CO₂ in all the studied ILs was performed using the gravimetric method. The gravimetric method is commonly used for absorption of gases onto solids by measuring the change in weight of the sample upon absorption. This technique is rarely used for absorption of gases in liquids because any loss of the liquid due to evaporation affects the final weight of the sample. However, due to the nonvolatile nature of the ILs, the gravimetric technique is attempted to determine the gas solubility [61].

Using the magnetic suspension balance (MSB) to measure gas solubility has several advantages. Ensuring that equilibrium has been reached is an utmost important step when measuring gas solubility. The MBS allows the user to monitor the mass change as time progresses; as equilibrium is reached, the mass change will draw near zero. Once the mass no longer changes, the sample is at equilibrium. Ensuring the initial liquid has been fully degassed prior to the measurement is also an important factor in order to determine how much gas is dissolved in the sample during the solubility measurement. Again, the ability to monitor the mass change as time progresses allows the user to ensure that the mass has stopped decreasing during the degassing step (equilibrium is reached) before proceeding to the solubility measurement [61].

5.2 Effect of the ILs anions on CO₂ solubility

The solubility of a gas is governed by a combination of factors namely; polarizability of the gas, the dispersion forces and the interactions between the gas and the solvent. The relative influence of each of these factors differs with the nature of the gas and the solvent involved. Several studies reported that CO₂ solubility in ILs depends primarily on the strength of interaction of CO₂ with the anion [211]. In this study we made a comparison between different ILs with same cation and different anions to see their affinity to absorb CO₂. Five ILs with same cation ([C₂CN Him]) and five different anions (DOSS, DDS, TFMS, SBA and BS) were used to study the effect of these anions on CO₂ solubility.

The CO₂ solubility in [C₂CN Him] cation incorporating DOSS, DDS, TFMS, SBA and BS anions at temperature 298.15 K and pressures 1, 5, 10, 15 and 20 bar are measured and the time-dependence of CO₂ uptake by the studied ILs is reported in Table B- 1 to Table B- 4 in Appendix B and shown in Fig 5-1 to Fig 5-5 in terms of mol fraction (x_{CO_2}) versus time. The results showed that TFMS and BS anions based ILs reached equilibrium in shorter time compared to the other anions. This may be due to the lower viscosities of these anions. The gas diffusion in IL depends on the IL's viscosity; where the increase of the viscosity of IL results in greater diffusion

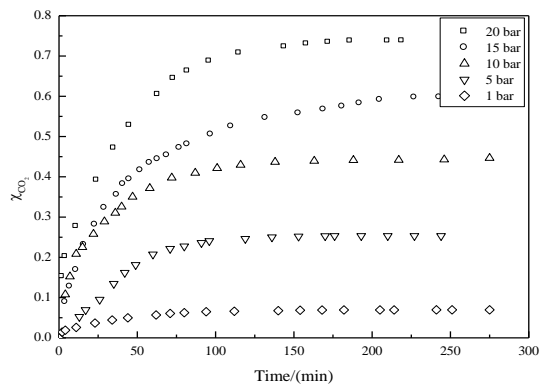


Fig 5-1 CO₂ solubility in [C₂CN Him]DOSS as a function of time at 298.15 K

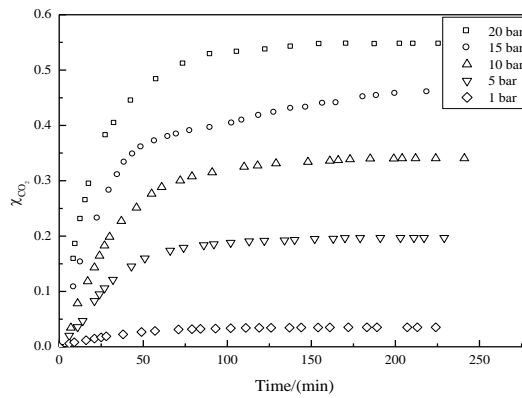


Fig 5-2 CO₂ solubility in [C₂CN Him]TFMS as a function of time at 298.15 K

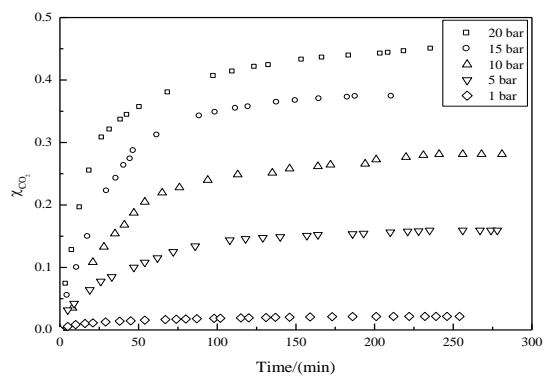


Fig 5-3 CO₂ solubility in [C₂CN Him]DDS as a function of time at 298.15 K

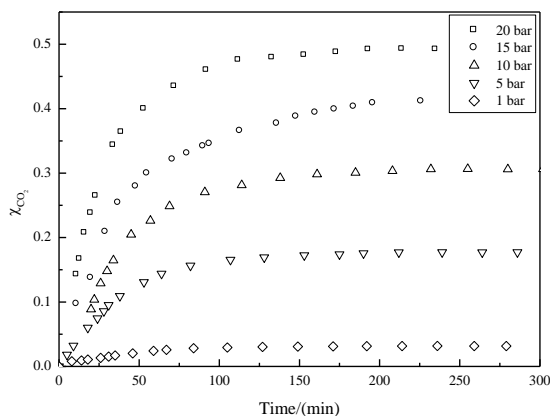


Fig 5-4 CO₂ solubility in [C₂CN Him]SBA as a function of time at 298.15 K

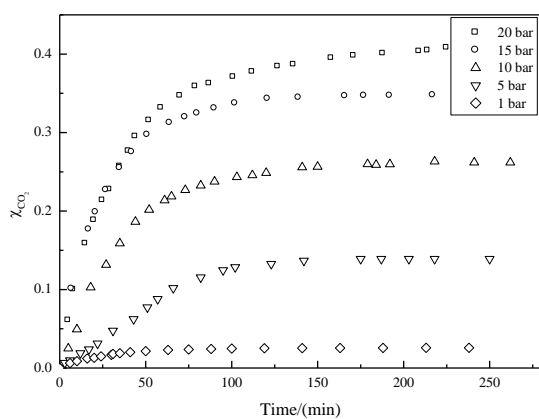


Fig 5-5 CO₂ solubility in [C₂CN Him]BS as a function of time at 298.15 K

versus time. This increased the time required to reach equilibrium [61]. The viscosities of the studied ILs are moderately high, so the diffusion of gas into these ILs can be slow.

The time required for the five ILs to reach the equilibrium is greater than that for the ILs incorporating the amine functionality (180 min) [61] and also greater than that reported for non functionalized imidazolium-based ILs (90 – 180 min) [165, 168] but lower than that reported for [emim]NTf₂ (1800 – 2400 min) and [bmim]NTf₂ (2160 - 2880 min) [61].

The solubility of CO₂ increases with increasing pressure for all five ILs, as expected (increased pressure will force the gas into the IL). The solubility of a gas is

defined as the concentration of the dissolved gas in equilibrium with the substance in the gaseous state. At equilibrium, the rate at which solute gas molecules escape the solution equals the rate at which the gas molecules reenter the solution. An increase in pressure results in more molecules of gas striking the surface of the liquid and entering the solution in a given time. The solution eventually reaches a new equilibrium when the concentration of gas dissolved in the solvent is high enough that the rate of gas molecules escaping the solution again equals the rate of gas molecules entering the solution [212].

The results showed that the CO₂ solubility is dependent on the choice of the anion which is in agreement with reported literature (the effect of the anion on the solubility of CO₂ in the ILs was investigated experimentally. The solubility of CO₂ in the IL was higher for the ILs with lower anion polarity) [213]. The isotherms for the effect of the anion on the solubility of CO₂ in [C₂CN Him]-based ILs at 298.15 K are shown in Fig 5-6 and presented in Table 5-1. The gas solubilities appear linear as a function of the pressure but exhibited a nonlinear trend as the pressure increased for all the studied ILs.

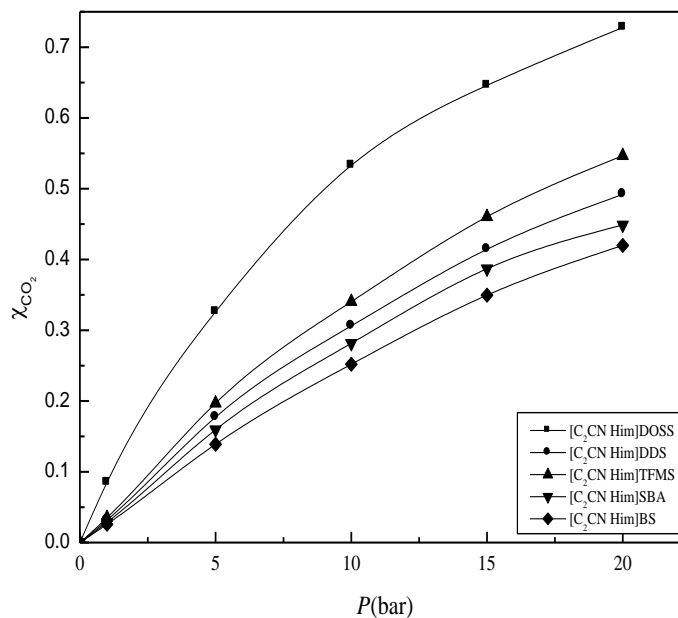


Fig 5-6 CO₂ solubility in [C₂CN Him]-based ILs incorporating DOSS, DDS, TFMS, SBA and BS anions at 298.15 K.

The IL with the DOSS anion has a considerably higher affinity for CO₂ compared with the ILs incorporating DDS, TFMS, SBA and BS anions. The DOSS anion has several features that are known to enhance a molecule's CO₂-philicity and lead to good solubility of CO₂; carbonyl and sulfonyl functionalities, long alkyl chains and branched alkyl chains [82]. In addition, another major factor that affects the capacity of CO₂ solubility is the molar free volume of the IL. In general, the larger the molecular size of the anion, the larger the free volume in which CO₂ can occupy [214]. The molar free volume of the IL exerted a more pronounced effect than the anion basicity which is one of the key factors in determining the CO₂ solubility in ILs.

Table 5-1 Experimental solubility data for CO₂ in [C₂CN C_nmim]X at 298 K

Pressure (bar)	CO ₂ mol fraction				
	[C ₂ CNHim] DDS	[C ₂ CNHim] TFMS	[C ₂ CNHim] SBA	[C ₂ CNHim] BS	[C ₂ CNHim] DOSS
1±0.01	0.021673	0.035242	0.031718	0.025789	0.069501
5±0.01	0.159438	0.196824	0.177141	0.139046	0.253262
10±0.03	0.281268	0.340454	0.306288	0.261962	0.446553
15±0.04	0.378069	0.460321	0.414288	0.349617	0.598146
20±0.05	0.448793	0.546700	0.492030	0.410599	0.737900
	g CO ₂ / g IL				
1±0.01	0.002	0.005	0.004	0.003	0.005
5±0.01	0.018	0.030	0.023	0.019	0.024
10±0.03	0.036	0.064	0.048	0.043	0.056
15±0.04	0.057	0.106	0.076	0.065	0.104
20±0.05	0.076	0.149	0.104	0.084	0.197

Moreover, DOSS anion has a known low toxicity [215] and is not likely to be as environmentally persistent as fluorinated ILs, while maintaining good capacity for CO₂ solubility. The [N_{4,4,4,4}] IL incorporating DOSS anion showed a good capacity for CO₂ and is higher than [Hmim]NTf₂ at the high pressures [82].

The relatively high solubility of CO₂ in the TFMS-based IL compared to the DDS, SBA, and BS-based ILs may be due to the greater interactions between CO₂ and the fluoroalkyl substituents on the TFMS anion [211, 216]. Two types of interactions are

known: one is the acid-base interaction between CO₂ and the anion in ILs, and the other is between CO₂ and fluorine in the anion [8]. In fact, CO₂ solubility increases with increasing number of CF₃ groups in the anion [8]. The fluorinated compounds has a high stability and low reactivity which gives them many excellent properties, but these also lead them to being poorly biodegradable and persistent in the environment [156].

The relatively high solubility of CO₂ in IL with SBA anion compared to those with DDS and BS anions is associated with the presence of carbonyl functionality. This enhances a molecule's CO₂-philicity and lead to good solubility of CO₂. Moreover the relatively high solubility capacity of CO₂ in DDS-based IL compared to BS-based IL is due to the long alkyl chain of the DDS anion which results in the increases of the van der Waals-type interactions between the gas and the liquid.

5.3 Effect of the ILs cations on CO₂ solubility

The influence of the IL cation on the CO₂ solubility is studied by comparing the solubility into ILs formed with a similar anion and different cation structures. According to the structural features the studied ILs was classified into three categories: imidazolium-based nitrile functionalized ILs, imidazolium-based dual functionalized ILs and phosphonium-based ILs.

5.3.1 Imidazolium-based nitrile functionalized ILs

The CO₂ solubility in [C₂CNC_nim]DOSS are measured. The chain length substituted on the imidazolium is varied while the side-chain linking the CN group is constant. These cations were chosen because when the side-chain linking the CN group is smaller, moieties may have weak hydrogen bond interactions. Presumably the interaction of the π -system with the anion is weaker than conventional hydrogen bonds. It reduces the number of hydrogen bonds between the anion and cation [217]. Moreover, as the side-chain linking the CN group decreases the viscosity is decreased and also the melting point which results in a RTIL. The alkyl chain was chosen to vary from butyl

to decyl since the other alkyl chains normally produce ILs with high melting point (some times greater than 100 °C) [217]. In addition, one can significantly minimize the strong ion-to-ion interactions by increasing the length of the alkyl group on the imidazolium cation [52].

The CO₂ solubility in DOSS-based ILs with [C₂CNBim], [C₂CNHim], [C₂CNOim] and [C₂CNDim] cations at temperature 298.15 K and pressures 1, 5, 10, 15 and 20 bar are measured. The time-dependence of CO₂ uptake by the studied ILs is reported in Table B- 5 to Table B- 8 in Appendix B and shown in Fig 5-1 and Fig 5-7 to Fig 5-9.

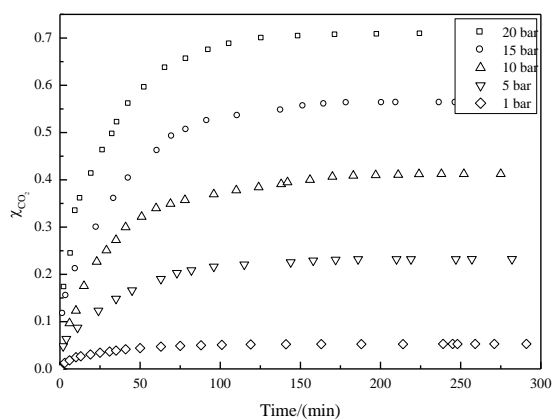


Fig 5-7 CO₂ solubility in [C₂CNBim]DOSS ILs as a function of time at 298.15 K

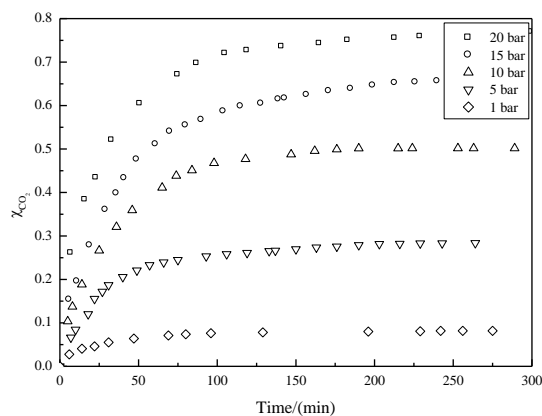


Fig 5-8 CO₂ solubility in [C₂CNOim]DOSS ILs as a function of time at 298.15 K

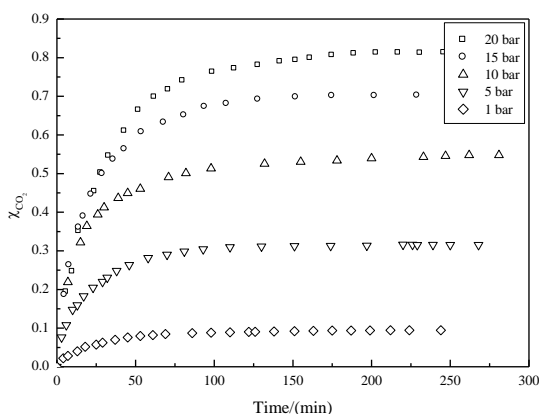


Fig 5-9 CO₂ solubility in [C₂CNDim]DOSS ILs as a function of time at 298.15 K

The time required for these ILs to reach the equilibrium is lower than that reported for [emim]NTf₂ (1800 - 2400 min) and [Bmim]NTf₂ (2160 - 2880 min) [61] but greater than that for the non functionalized imidazolium-based ILs (90 to 180 min) [61, 165, 168]. These results are a reflection of the high viscosity of these ILs. The CO₂ solubility in these ILs increases with increasing pressure (if the pressure is increased, the gas molecules are "forced" into the solution since this will best relieve the pressure that has been applied).

The isotherm for the solubility of CO₂ in terms of mol fraction for the ILs [C₂CNBim]DOSS, [C₂CNHim]DOSS, [C₂CNOim]DOSS and [C₂CNDim]DOSS is presented in Table 5-2 and shown in Fig 5-10.

In general, the CO₂ solubility increases with an increase in the alkyl chain length ([C₂CNBim] < [C₂CNHim] < [C₂CNOim] < [C₂CNDim]). As expected the larger free volume originating from the longer alkyl chain of the cation makes the CO₂ more soluble in IL with long alkyl chain. In addition, the alkyl group increases the dispersion forces of the cation for better interaction with CO₂ [147]. The difference in solubility with increasing alkyl chain length is increasing as the alkyl chain length increases (difference mol fraction between [C₂CNBim]-[C₂CNHim], [C₂CNHim]-[C₂CNOim] and [C₂CNOim]- [C₂CNDim] is 0.0259, 0.0314 and 0.0438,

respectively). The increase of the solubility values with an increase in the alkyl chain length becomes more apparent at higher pressures [61].

Table 5-2 Experimental solubility data for CO₂ in [C₂CN C_nim]DOSS at 298 K

Pressure (bar)	CO ₂ mol fraction			
	[C ₂ CN Dim] DOSS	[C ₂ CN Oim] DOSS	[C ₂ CN Him] DOSS	[C ₂ CN Bim] DOSS
1±0.01	0.094573	0.0815654	0.069501	0.052812
5±0.01	0.315421	0.2836155	0.253262	0.232191
10±0.03	0.547694	0.5017694	0.446553	0.412384
15±0.04	0.702002	0.6571002	0.598146	0.562400
20±0.05	0.813029	0.76926	0.737900	0.711993
	g CO ₂ /g IL			
1±0.01	0.00671	0.00595	0.00523	0.00408
5±0.01	0.02960	0.02652	0.02373	0.02215
10±0.03	0.07778	0.06745	0.05645	0.05139
15±0.04	0.15132	0.12835	0.10414	0.09412
20±0.05	0.27932	0.22329	0.19698	0.18104

However, the CO₂ solubility in these ILs does not increase linearly with the length of the alkyl chain in the cation, its augmentation being more important as the alkyl chain length increase as shown in Fig 5-10. Opposite trend was observed for the conventional ILs; the augmentation being less important for alkyl chains larger than 8 carbon atoms [142]. The increase trend of CO₂ solubility in the [C₂CNBim]DOSS, [C₂CNHim]DOSS, [C₂CNOim]DOSS and [C₂CNDim]DOSS ILs may be due to the increase of the molar volume and the presence of the CN group in the side chain of the ILs (the presence of the CN group completely changes the architecture of the hydrogen bonding network of these ILs; differences in the molecular geometry are caused by the different hydrogen bond networks arising from the different side chains) [41]. Moreover, the extent of intermolecular hydrogen bonding revealed from the solid-state structural studies indicates that the nitrile functionalized ILs can be described as polymeric supermolecular networks [41]. In addition, the large volume of the anion results in a weaker interaction of the π -system with the anion compared

to the conventional hydrogen bonds which increase the possibility of the van der Waals-type interactions between the CO₂ and the cation and anion.

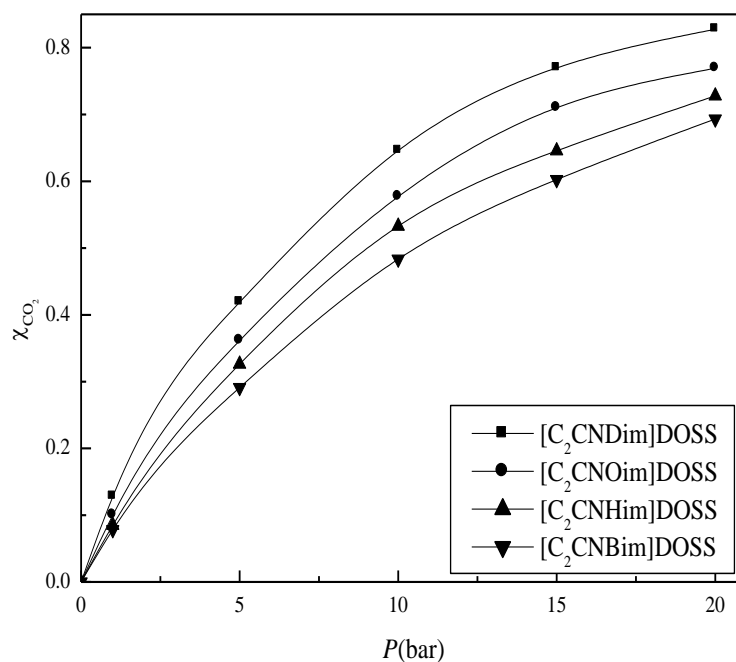


Fig 5-10 Solubility of CO₂ in [C₂CNC_nim]DOSS ILs at 298.15 K as a function of pressure

5.3.2 Imidazolium-based dual functionalized ILs

Even though the functionality is used to improve the CO₂ solubility in ILs, dual functionalized-based ILs have received less attention than functionalized-based ILs. Allyl, hydroxyl and benzyl functional groups can be easily introduced into imidazole ring systems using the quaternization method. They are often liquids and some of them less viscous than their saturated counterparts [217]. The incorporation of a second functional group increases the possibility of the interaction between the π -system and the CO₂. Moreover, these ILs were studied to compare the effect of the second functional group on the CO₂ solubility in ILs compared to conventional and functionalized ILs. The solubility of CO₂ in [C₂CNHeim]DOSS, [C₂CNBzim]DOSS and [C₂CNAyim]DOSS at temperature 298.15 K and pressures 1, 5, 10, 15 and 20 bar are measured and the time-dependence of CO₂ uptake by the studied ILs is reported in Table B-9 to Table B-11 in Appendix B and shown in Fig 5-11 to Fig 5-13.

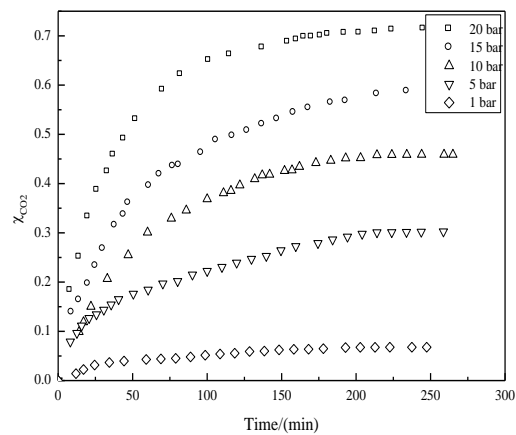


Fig 5-11 CO₂ solubility in [C₂CN Heim]DOSS as a function of time at 298.15 K

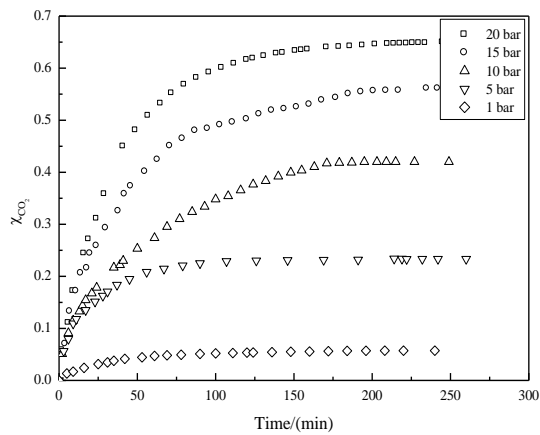


Fig 5-12 CO₂ solubility in [C₂CN Bzeim]DOSS as a function of time at 298.15 K

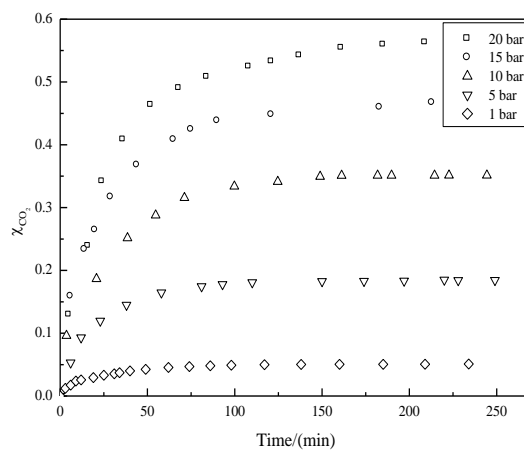


Fig 5-13 CO₂ solubility in [C₂CN Ayim]DOSS as a function of time at 298.15 K

The results showed that the time required for [C₂CNAyim]DOSS to reach the equilibrium (209 min) is less than that for the [C₂CNHeim]DOSS (256 min), [C₂CNBzim]DOSS (245 min) ILs. This result may be due to the effect of the high viscosity of these ILs. The CO₂ solubility in these ILs increases with increasing pressure as expected. Although these ILs has high viscosity, the time required for the CO₂ uptake to reach the equilibrium was comparable to [C₂CNC_nim]DOSS. The solubility of CO₂ in functionalized RTILs needed considerably more time reaching equilibrium at each pressure, especially for the some amine containing ionic liquids, where for some samples more than 2880 min was required [133].

A comparison between the CO₂ solubility capacities in [C₂CNHeim]DOSS, [C₂CNBzim]DOSS and [C₂CNAyim]DOSS ILs is reported in Table 5-3 and presented in Fig 5-14.

Table 5-3 Experimental solubility data for CO₂ in imidazolium-based dual functionalized ILs at 298 K

Pressure (bar)	CO ₂ (mol fraction)		
	[C ₂ CN Heim]DOSS	[C ₂ CN Bzim]DOSS	[C ₂ CN Ayim]DOSS
1±0.01	0.067732	0.057215	0.051040
5±0.01	0.274114	0.233279	0.184390
10±0.03	0.458762	0.420099	0.351240
15±0.04	0.593422	0.560760	0.468310
20±0.05	0.715072	0.650137	0.563873
	g CO ₂ /g IL		
1±0.01	0.00523	0.00407	0.00399
5±0.01	0.02721	0.02038	0.01678
10±0.03	0.06107	0.04853	0.04019
15±0.04	0.10516	0.08552	0.06538
20±0.05	0.18083	0.12448	0.09597

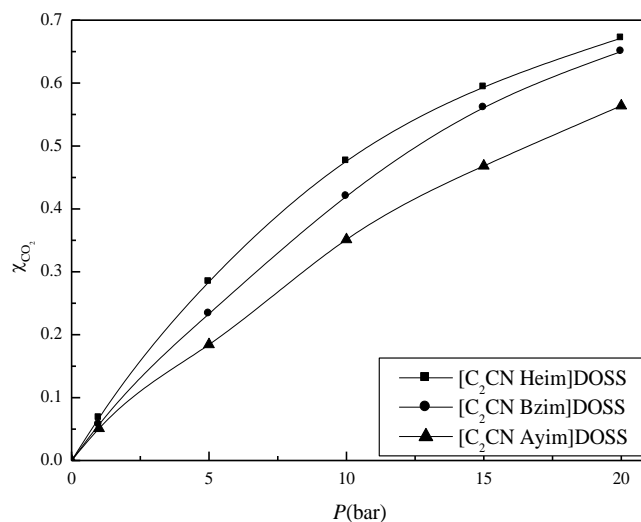


Fig 5-14 Solubility of CO₂ in imidazolium-based dual functionalized ILs at 298.15 K as a function of pressure

The [C₂CNHeim]DOSS IL shows highest CO₂ solubility followed by [C₂CNBzim]DOSS while the [C₂CNAyim]DOSS IL shows the lowest value. The differences between these ILs are due to the effects of the hydroxyl, benzyl and allyl functionalities. The high CO₂ solubility in the [C₂CNHeim]DOSS IL may be due to the increases of the hydrogen bonding between the gas and the liquid as a result of the presence of the hydroxyl group. The greater CO₂ solubility in [C₂CNBzim]DOSS compare to [C₂CNAyim]DOSS may be due to the greater number of π-electrons which increases the interaction with the CO₂.

It is well-known that the CO₂ molecule can act both as proton acceptor or electron donor according to the nature of the solvent, forming electron donor–acceptor (EDA) complexes. The interactions between CO₂ and carbonyl groups, ester groups, hydroxyl groups, ether groups with ILs have been investigated. While these interactions observed by spectroscopic techniques are of relevance for an understanding of the solvation of CO₂ in nonvolatile solvents, they are inadequate to fully explain its solubility or the deviations to the ideal behavior on these systems [218]. These observations shouldn't come entirely as a surprise since the non ideality of a solution and its impact on the solubility of a given solute depend not only on the solute–solvent interactions, but on a delicate balance between the solute–solute, solute–solvent, and solvent–solvent interactions. Moreover, in systems of nonvolatile solvents, these solvents present in general a large molar volume, and the

solute–solvent size and shape asymmetries will generate important entropic and free volume contributions to the non ideality of the system with significant impact on the CO₂ solubility on these systems [218].

5.3.3 Phosponium-based ILs

Phosponium ILs have been available in a large scale for about ten years and their utility as a solvent medium has gained interest over the last couple of years as evident by the number of review articles and industrial use [206]. Compared to the other ILs, the remarkable features of phosponium ILs are their chemical, thermal and electrochemical stabilities [206] and also some phosponium ionic liquids exhibit lower melting points and lower viscosities which are practical advantages for various applications [113, 219]. Phosponium ILs have received less attention than imidazolium systems [217]. Compared with the popular imidazolium-based ILs, phosponium ILs are known to possess some rather interesting, and often advantageous properties such as; lower density and lack of an acidic proton [51, 120].

The CO₂ solubility in the phosponium-based ILs incorporating DOSS anion at temperature 298.15 K and pressures 1, 5, 10, 15 and 20 bar are measured and the time-dependence of CO₂ uptake by the studied ILs is reported in Table B- 12 to Table B- 15 in Appendix B and shown in Fig 5-15 to Fig 5-18 in term of mol fraction (x_{CO_2}) versus time.

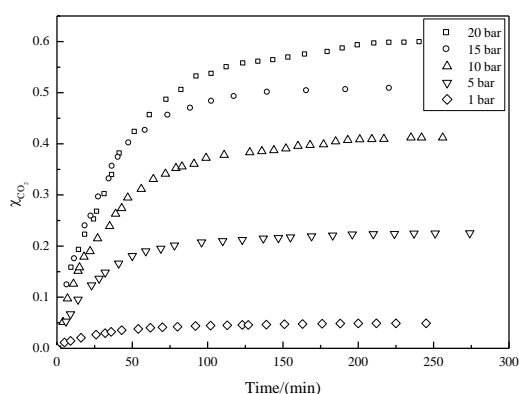


Fig 5-15 CO₂ solubility in [P_{6,6,6,14}]DOSS as a function of time at 298.15 K

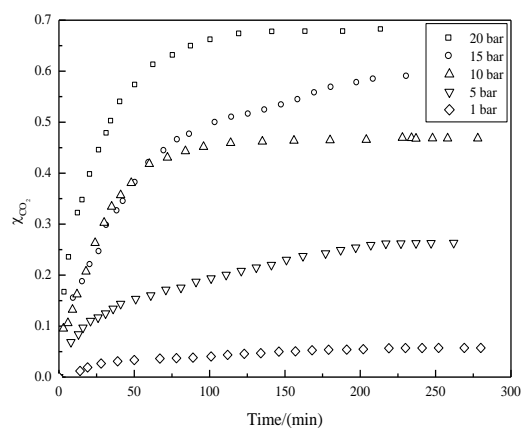


Fig 5-16 CO₂ solubility in [P_{8,8,8,14}]DOSS as a function of time at 298.15 K

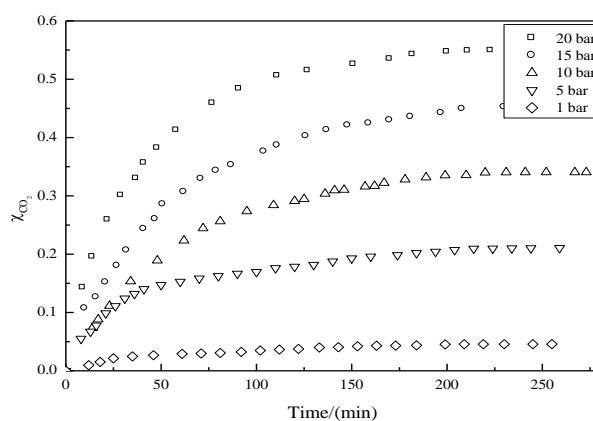


Fig 5-17 CO₂ solubility in [P_{8,8,8}C₆ P_{8,8,8}]DOSS₂ as a function of time at 298.15 K

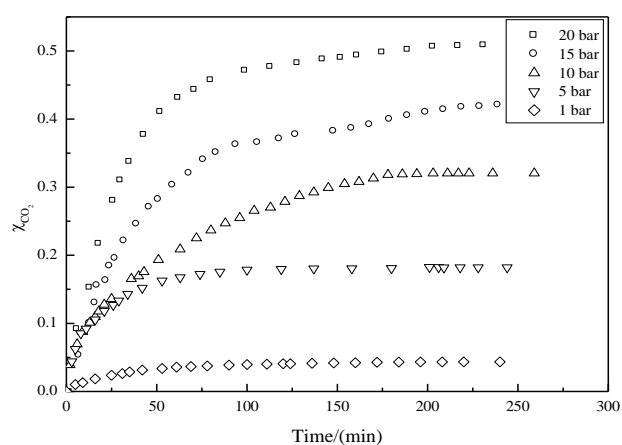


Fig 5-18 CO₂ solubility in [P_{8,8,8}C₁₀ P_{8,8,8}]DOSS₂ as a function of time at 298.15 K

Although these ILs has different viscosities, the time required for the CO₂ uptake to reach the equilibrium was comparable to [C₂CNC_nim]DOSS ILs. Moreover, no significant difference in the CO₂ uptake time between the monocationic and dicationic ILs. The time required for these ILs to reach the equilibrium is greater than that for the ILs incorporating the amine functionality (180 min) [61] and also greater than that reported for non functionalized imidazolium-based ILs (90 to 180 min) [165, 168] but lower that that reported for [emim][NTf₂] (1800-2400 hr) and for [bmim][NTf₂] (2160 – 2880 min) [61].

The effect of the phosphonium cation type in the CO₂ solubility in term of mol fraction for the ILs [P_{8,8,8,14}]DOSS, [P_{6,6,6,14}]DOSS, [P_{8,8,8}C₆P_{8,8,8}]DOSS₂ and [P_{8,8,8}C₁₀P_{8,8,8}]DOSS₂ is reported in Table 5-4 and presented in Fig 5-19.

Table 5-4 Experimental solubility data for CO₂ in phosphonium-based ILs at 298 K

Pressure (bar)	CO ₂ (mol fraction)			
	[P _{8,8,8,14}] DOSS	[P _{6,6,6,14}] DOSS	[P _{8,8,8} C ₁₀ P _{8,8,8}] DOSS ₂	[P _{8,8,8} C ₆ P _{8,8,8}] DOSS ₂
1±0.01	0.057215	0.048914	0.043483	0.045772
5±0.01	0.263374	0.225211	0.182001	0.210662
10±0.03	0.438105	0.384121	0.320463	0.340560
15±0.04	0.573422	0.510946	0.420511	0.458078
20±0.05	0.685009	0.599670	0.510930	0.556110
	g CO ₂ /g IL			
1±0.01	0.00264	0.00244	0.00113	0.00123
5±0.01	0.01554	0.01377	0.00553	0.00685
10±0.03	0.03388	0.02955	0.01172	0.01326
15±0.04	0.05841	0.04951	0.01803	0.02170
20±0.05	0.09450	0.07098	0.02596	0.03216

In general, the monocationic-based phosphonium ILs shows higher CO₂ solubility compared to the dicationic-based phosphonium ILs. For the monocationic-based phosphonium ILs, the CO₂ solubility was higher in [P_{8,8,8,14}]DOSS compared [P_{6,6,6,14}]DOSS, which is due to the increases of the alkyl chain length. As expected the larger free volume originating from the longer alkyl chain of the cation makes the

CO₂ more soluble in IL with long alkyl chain. This trend is similar to that for the imidazolium-based ILs. However the dicationic-based phosphonium ILs has a grater free volume compare to the monocationic-based phosphonium ILs studied, the CO₂ solubility in these ILs was lower. This result is a consequence of the extremely high viscosity of the dicationic-based phosphonium ILs compare to the monocationic-based phosphonium ILs (the viscosities of [P_{8,8,8,14}]DOSS and [P_{6,6,6,14}]DOSS is 1795 and 2051 mPa.s while for [P_{8,8,8}C₆P_{8,8,8}]DOSS₂ and [P_{8,8,8}C₁₀P_{8,8,8}]DOSS₂) is 16188 and 18767 mPa.s respectively. Moreover, the CO₂ solubility in these ILs decreases with the increase of the spacer alkyl chain length.

The strength of the interactions cannot be solely responsible for the solubility of CO₂ in ionic liquids as reported in some studies [157, 218, 220] and also the free volume. In addition, the ambient pressure molar volumes increase with increasing chain length, this effect diminishes with higher amounts of dissolved CO₂ and the molar volumes of each IL becomes very similar [147]. At these pressures, the IL consists of greater than 70% mole of CO₂ and thus the properties are better correlated with CO₂ than the ambient pressure IL properties. The solubilities of CO₂ in the present ILs increased rapidly to about 0.3 to 0.4 in mole fraction for pressures up to 10 bar, but towards higher pressures, the increasing rates slowed down and the solubility finally leveled off. The fast solubility increase in the low-pressure range may be due to the Henry's sorption in the inter-ion space. The cations of ILs are normally bulkier than the corresponding anions and provide inter-ion spaces where CO₂ can squeeze in. As the openings between cation and anion of the IL are large, CO₂ molecules can easily enter into that space. However, these openings are continuously filled with CO₂ molecules with increasing pressure. Eventually, the spaces are filled up, leaving no more room for CO₂ molecules to get in. To let more CO₂ molecules enter into the IL, it is necessary for the inter-ion space to be expanded. As this expansion requires energy, only small amounts of CO₂ can penetrate into the IL. This is why ILs show that particular leveling off solubility behavior

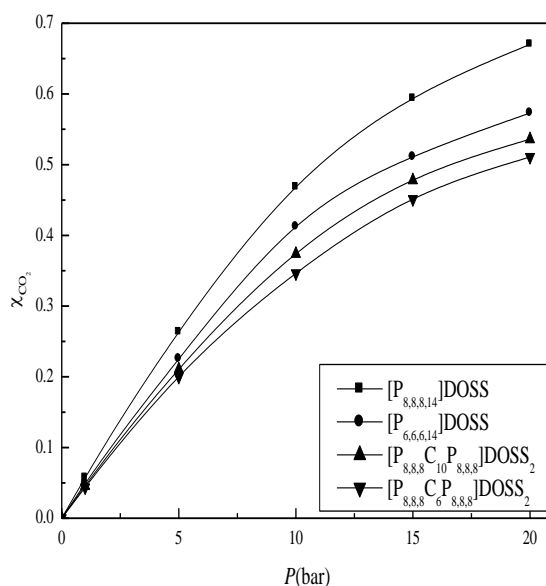


Fig 5-19 Solubility of CO₂ in phosphonium-based ILs at 298.15 K as a function of pressure

The influence of the IL cation on the CO₂ solubility is studied by comparing the solubility into ILs formed with DOSS anion and different cation structures. The CO₂ solubility results showed that the [C₂CNDim]DOSS, [C₂CNHeim]DOSS and [P_{8,8,8,14}]DOSS ILs have a higher solubility capacity among the studied imidazolium-based nitrile functionalized ILs, imidazolium-based dual functionalized ILs and phosphonium-based ILs. The effect of the cation type in the CO₂ solubility in terms of mol fraction for these three ILs is presented in Fig 5-20. The [C₂CNDim]DOSS IL shows the highest CO₂ solubility followed by [C₂CNHeim]DOSS while the [P_{8,8,8,14}]DOSS IL shows the lowest value. The results show that the CO₂ solubility capacity is greater for the imidazolium-based ILs than phosphonium-based ILs. Moreover, the CO₂ solubility was higher when the nitrile-imidazolium ILs incorporated with the decyl alkyl chain compared to the hydroxyl functional group. The greater CO₂ solubility in the [C₂CNDim]DOSS IL may be due to the weaker inter-ion interaction forces between the cation and anion (large cation size) which contribute to providing larger free volume. It plays a significant role in attaining high values of CO₂ solubility. In addition, the weak interaction forces between the cation and anion increases the van der Waals-type interactions between the gas and the liquid. The high CO₂ solubility in the [C₂CNHeim]DOSS compared to [P_{8,8,8,14}]DOSS

IL due to the presence of the hydroxyl group which increases the ability to attract the electron-poor carbon atom of CO₂ towards electronegative atoms (oxygen) [12].

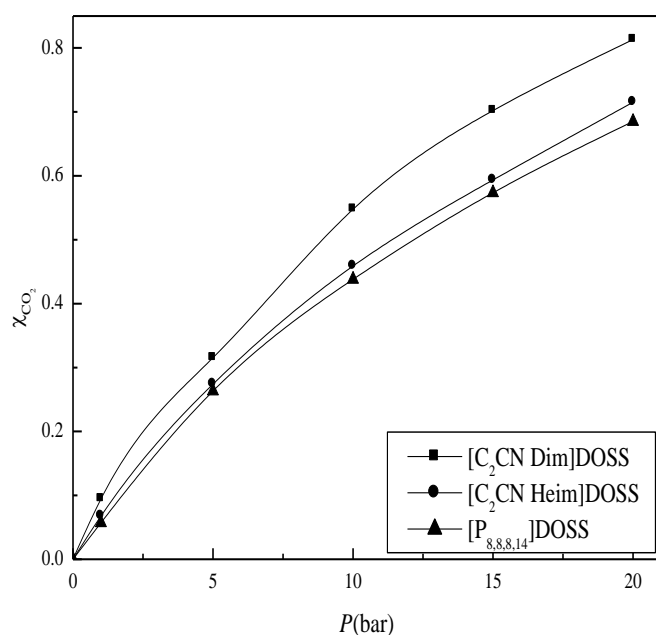


Fig 5-20 Solubility of CO₂ in [C₂CN Dim]DOSS, [C₂CN Heim]DOSS and [P_{8,8,8,14}]DOSS ILs at 298.15 K as a function of pressure

The most striking result from this analysis is that, in spite of the major differences in the chemical nature of the solvents investigated and of the interactions of their molecules in pure state, the non ideality of the absorption of CO₂ in solution in the composition range studied is remarkably lower than could be anticipated and, in most cases, is essentially driven by entropic effects. Moreover, as has been noticed before by other authors, this analysis on the non ideality of these systems also stresses that there is no direct relationship between the stability of the EDA complex formed between the CO₂ and a given solvent and the non ideality of CO₂ on this solvent. These two observations combined suggest that, by increasing the size difference between the CO₂ and the solvent, incorporating of functional groups the solubility must increase as the entropic contribution to the solution non ideality increases [218]. Seki et al. [220] in a recent work show that, although the interactions of CO₂ with BF₄ and PF₆ anion-based ILs are stronger than those with the NTf₂, the solubility of CO₂ on these ILs is larger than in the former, and thus the interactions alone are not enough to provide a full explanation for the CO₂ sorption. They recognize that “the

strong Lewis acid–base interactions between the ILs and the dissolved CO₂ is not the only effect on the solubility of CO₂”.

5.4 Thermodynamic parameters

The knowledge and understanding of the thermodynamic properties and equilibrium solubility behavior for any new IL allows for the development and optimization of the separation processes. The thermodynamic properties yield information about the strength of interaction between the liquid and dissolved gas and give indication of the level of ordering that takes place in the liquid/gas mixture [173]. The experimental data of the CO₂ solubility in the studied ILs was used to determine Henry’s law constant. The knowledge of Henry’s law constant for CO₂ in the studied ILs allows for the calculation of the solution thermodynamic properties namely the Gibbs free energy, enthalpy and entropy [81, 173].

5.4.1 Henry’s constant

The gas solubility in liquid is often reported using Henry law constant. Henry’s law constant relates the equilibrium mole fraction of substance in the liquid phase to its partial pressure in the gas phase [221]. Henry’s law states that at a constant temperature, the amount of a given gas dissolved in a given type and volume of liquid is directly proportional to the partial pressure of the gas in equilibrium with that liquid [222]. There are several forms of Henry's Law, each of which defines the constant (k_H) differently and requires different dimensional units. In particular, the "concentration" of the solute in solution may be expressed as a mole fraction or as a molality.

The gas solubility decreases as temperature increases and pressure decreases for all standard ILs. Assuming ideal conditions, the gas solubility can be expressed in terms of a Henry’s law constant. At equilibrium conditions and infinite dilution the Henry’s law constant is estimated from the solubility in terms of mole fraction (x). The ILs have a very low or negligible vapour pressure and therefore the gas phase is

considered to be the pure gas solute [4, 165]. The fugacity coefficient is assumed equal to unity and Henry's law constant (k_H) is determined using the following equation [9, 61, 143, 223]:

$$k_H = \lim_{x \rightarrow 0} \left(\frac{P_{CO_2}}{x} \right) \quad 5-1$$

where P is the partial pressure of the gas and $k_H(T)$ will have units of pressure and is inversely proportional to the mole fraction of gas in the liquid (x). For gases that behave nearly ideally, the solubility is linearly related to the pressure. Therefore, the Henry's law constant can be found by calculating the linear slope of the data.

The CO₂ gas exhibits a nonlinear trend as the CO₂ pressure is increased for all the studied RTILs as shown in Fig 5-21 to Fig 5-24 (the curves begin to flatten out, indicating that the IL is beginning to approach its maximum, pressure-independent capacity for CO₂ [39]) so the Henry's law constant can be found by fitting a second-order polynomial to the data and calculating the limiting slope as the solubility approaches zero [61, 81]. Accordingly, equation 5-2 was used to model the experimental values [224] with a correlation coefficient (R^2) greater than 0.996.

$$k_H = ax^2 + bx + c \quad 5-2$$

The Henry's law constant at infinite dilution (k_H) was calculated from equation 5-1 as follows:

$$k_H = \lim_{x \rightarrow 0} \left(\frac{P_{CO_2}}{x} \right) = b \quad 5-3$$

The Henry's law constants for all the studied ILs and the correlation coefficients of the polynomial equation (equation 5-2) are presented in Table 5-5. The Henry's law constant value is an indication of the gas solubility in the solvent; the decrease of the value is an indication of the increases of gas solubility in the solvent. In addition, Henry's law constants can be used to classify whether the absorption is of physical or chemical type. Usually, a small value of Henry's law constants less than 3 MPa at 298 K would be the case of a chemical absorption for CO₂ into ILs [181].

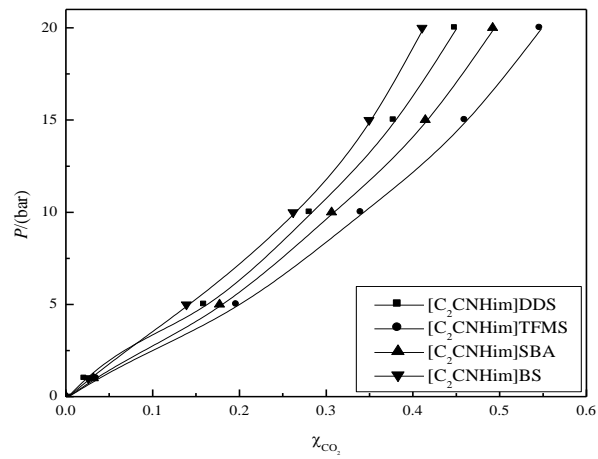


Fig 5-21 Solubility of CO₂ in [C₂CNHim]-based ILs as a function of pressure

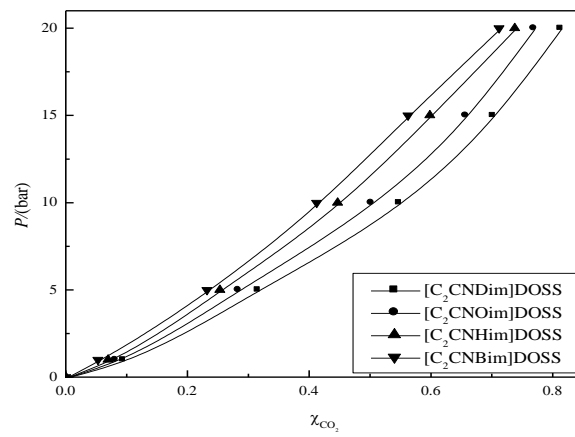


Fig 5-22 Solubility of CO₂ in [C₂CNC_nim]DOSS ILs as a function of pressure

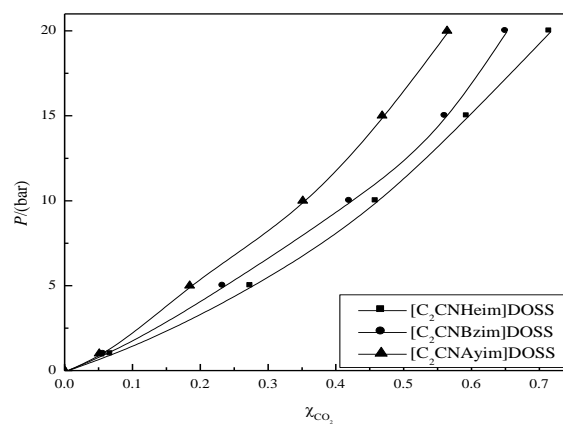


Fig 5-23 Solubility of CO₂ in dual functionalized-based ILs as a function of pressure

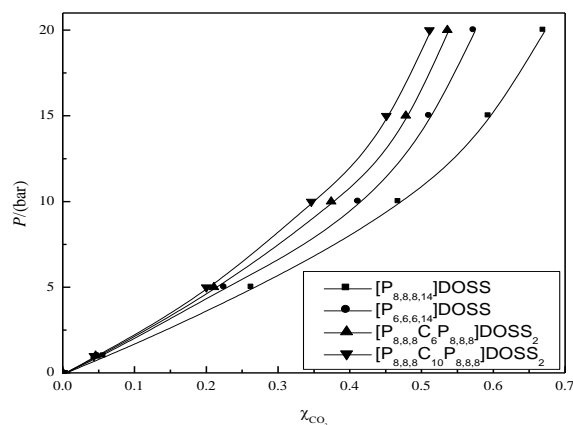


Fig 5-24 Solubility of CO₂ in phosphonium-based ILs as a function of pressure

These solubility behaviors are more clearly understood in terms of the thermodynamic excess functions (excess Gibbs, excess enthalpy, and excess entropy *TSE* energies); sufficiently negative values in excess Gibbs usually indicate some chemical complex formations; the heat of mixing (or excess enthalpy) is more negative than *TSE*. A minimum in excess Gibbs occurs around 50 mol % of the CO₂ + IL system, suggesting the 1:1 complex formation, whereas excess Gibbs minimum around 33 mol % of CO₂ in indicates the 1:2 (CO₂: IL) complex formation [122].

As shown in Table 5-5, the DOSS-based IL shows the lower value compared to the other anions. The [C₂CDim]DOSS, [C₂C Heim]DOSS and [P_{8,8,8,14}]DOSS show the lower values among the three categories. Moreover, [C₂CDim]DOSS shows the lower value among all the studied ILs. The effect of temperature in the solubility of CO₂ in the [C₂CNDim]DOSS, [C₂CNHeim]DOSS and [P_{8,8,8,14}]DOSS ILs was studied and the results are shown in Fig 5-25 and reported in Table 5-6 and Table 5-7. Henry's law constants for these ILs are estimated using equation 5-3 and the results are presented in Table 5-5.

The CO₂ solubility decreases with the increasing temperature, which is in accordance with the results found in most cases of gas dissolution into liquid [181]. Increased temperature causes an increase in kinetic energy. The higher kinetic energy causes more motion in molecules which break intermolecular bonds and escape from solution. In addition, this may be due to the decrease in the inter-ion space as the ions

become active with the increased kinetic energy and are more irregularly distributed. The effect of temperature is important for the study of the thermodynamic properties.

Table 5-5 Henry's law constant and correlation coefficients for the studied ILs

Property	[C ₂ CNHim] DDS	[C ₂ CNHim] SBA	[C ₂ CNHim] BS	[C ₂ CHim] TFMS
k_H (298 K)	20.07	18.93	22.09	17.02
R^2	0.998	0.999	0.997	0.999
	[C ₂ CNBim] DOSS	[C ₂ CNHim] DOSS	[C ₂ CNOim] DOSS	[P _{6,6,6,14}] DOSS
k_H (298 K)	19.21	15.79	10.16	13.33
R^2	0.999	0.999	0.998	0.999
	[C ₂ CNBzim] DOSS	[C ₂ CNAyim] DOSS	[P _{8,8,8} C ₆ P _{8,8,8}]DOSS ₂	[P _{8,8,8} C ₁₀ P _{8,8,8}]DOSS ₂
k_H (298 K)	14.64	19.13	17.47	19.17
R^2	0.997	0.998	0.999	0.999
	[C ₂ C Dim] DOSS	[C ₂ CNHeim] DOSS	[P _{8,8,8,14}] DOSS	
k_H (298 K)	7.45	11.40	11.62	
R^2	0.998	0.999	0.999	
k_H (313 K)	10.56	30.01	31.88	
R^2	0.998	0.999	0.999	
k_H (343 K)	19.11	43.09	48.02	
R^2	0.998	0.999	0.999	

Moreover, Henry's law constant as an indication of the gas solubility in the solvent was applied to study the effect of temperature on the CO₂ solubility capacity of these ILs. The experimental solubility data for [C₂CN Dim]DOSS, [C₂CN Heim]DOSS and [P_{8,8,8,14}]DOSS at 313 and 343 K are reported in Table 5-6 and Table 5-7 and also plotted in Fig 5-25. Henry's law constants for these ILs are estimated using equation 5-3 and the results are presented in Table 5-5.

Table 5-6 Experimental solubility data for CO₂ in [C₂CN Dim]DOSS, [C₂CN Heim]DOSS and [P_{8,8,8,14}]DOSS at 313 K

Pressure (bar)	CO ₂ (mol fraction)		
	[C ₂ CN Dim]DOSS	[C ₂ CN Heim]DOSS	[P _{8,8,8,14}]DOSS
1±0.01	0.066739	0.025730	0.024222
5±0.01	0.222589	0.104131	0.098029
10±0.03	0.386501	0.174275	0.164063
15±0.04	0.495395	0.225430	0.212220
20±0.05	0.573745	0.271642	0.255724
	gCO ₂ /g IL		
1±0.01	0.00459	0.00170	0.00159
5±0.01	0.01839	0.00747	0.00698
10±0.03	0.04047	0.01356	0.01261
15±0.04	0.06306	0.01869	0.01730
20±0.05	0.08646	0.02396	0.02207

Table 5-7 Experimental solubility data for CO₂ in [C₂CN Dim]DOSS, [C₂CN Heim]DOSS and [P_{8,8,8,14}]DOSS at 343 K

Pressure (bar)	CO ₂ (mol fraction)		
	[C ₂ CN Dim]DOSS	[C ₂ CN Heim]DOSS	[P _{8,8,8,14}]DOSS
1±0.01	0.036888	0.017921	0.016081
5±0.01	0.123028	0.072527	0.065078
10±0.03	0.213624	0.121383	0.108917
15±0.04	0.273811	0.157012	0.140887
20±0.05	0.317116	0.189199	0.169768
	gCO ₂ /g IL		
1±0.01	0.00246	0.00117	0.00105
5±0.01	0.00901	0.00502	0.00447
10±0.03	0.01745	0.00887	0.00785
15±0.04	0.02422	0.01196	0.01053
20±0.05	0.02983	0.01499	0.01313

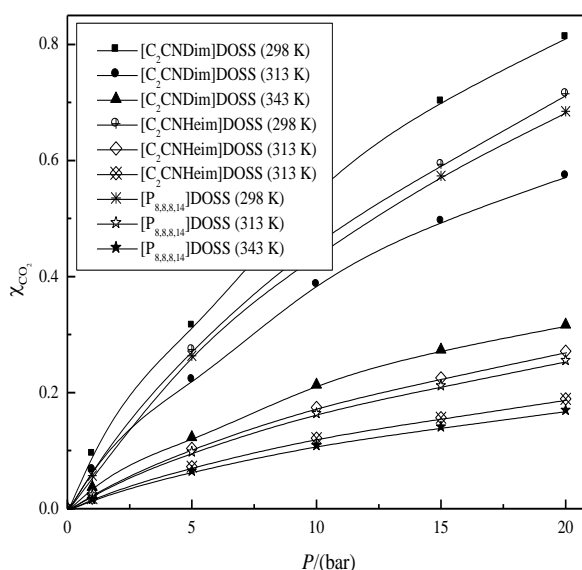


Fig 5-25 Solubility of CO₂ in [C₂CNDim]DOSS, [C₂CNHeim]DOSS and [P_{8,8,8,14}]DOSS ILs at different temperatures

5.4.2 Enthalpy, entropy and Gibbs free energy

Standard enthalpy (ΔH^0), entropy (ΔS^0) and Gibbs free energy (ΔG^0) of gas dissolution can be estimated by considering the effect of temperature on gas solubility [173, 223]. The dependence of the measured solubility with temperature is related to the thermodynamic properties of solvation. At infinite dilution, low pressure, the Henry constant (K_H) can be used to describe the thermodynamic solution properties [39]. The standard enthalpy (ΔH^0), entropy (ΔS^0) and Gibbs free energy (ΔG^0) of the gas solubility can be estimated from the calculated Henry constants.

The standard Gibbs free energy of solution of a gas (ΔG^0) was calculated from the Henry's Law constant (k_H) using equation 5-4, where P^0 is a standard pressure, the value of which is taken to be 1.01325 bar [223].

$$\Delta G^0 = -RT \ln \left(\frac{P^0}{k_H} \right) \quad 5-4$$

In certain cases the standard heat of solution of a gas (ΔH°) may be treated as a constant (for small temperature change) and can be related to the Henry's law constant at infinite dilution using the linear equation:

$$\ln k_H = \ln k_0 + \frac{\Delta H^0}{RT} \quad 5-5$$

However, there are other cases (for relatively wide temperature ranges) in which ΔH^0 is temperature dependent and, therefore, is not a constant. For the latter cases, ΔH^0 may be estimated obtained from equation 5-6 [223].

$$\frac{\Delta H^0}{R} = \left(\frac{\partial \ln k_H}{\partial (1/T)} \right) \quad 5-6$$

The change in molar enthalpy upon gas solubility is obtained by plotting the natural logarithm of the calculated Henry constant ($\ln k_H$) versus the reciprocal of absolute temperature ($1/T$) and the curve was fitted with the following equation [223]:

$$\ln k_H = A + \frac{B}{T} + \frac{C}{T^2} \quad 5-7$$

where, A , B and C are correlation coefficients. The correlation coefficients are estimated using linear regression analysis and the values are reported in Table B- 16 in Appendix B. Combination of equation 5-65-7 5-7 was used to estimate the standard enthalpy using the following equation [223]:

$$\Delta H^0 = R \left(B + \frac{2C}{T} \right) \quad 5-8$$

The standard entropy was calculated using the following equation [223]:

$$\Delta S^0 = \left(\frac{\Delta H^0 - \Delta G^0}{T} \right) \quad 5-9$$

The standard enthalpy (ΔH^0), entropy (ΔS^0) and Gibbs free energy (ΔG^0) of the solution of the CO₂ in the [C₂CNDim]DOSS, [C₂CNHeim]DOSS and [P_{8,8,8,14}]DOSS at different studied temperatures are given in Table 5-8.

As indicated above, based on the relationship given in equation 5-3 and the data presented in Table 5-5, the increase in k_H with increasing T corresponds with a decrease in the mole fraction (x) of CO_2 solubility in the ILs. The positive values of ΔG^0 indicate that the solubility of CO_2 in $[\text{C}_2\text{CNDim}]\text{DOSS}$, $[\text{C}_2\text{CNHeim}]\text{DOSS}$ and $[\text{P}_{8,8,8,14}]\text{DOSS}$ is a non-spontaneous process [223] in the temperature range 298–343 K. However, the negative values of ΔH^0 indicate that CO_2 still dissolves in (associates with [223]) the ILs in the specified temperature range, the magnitude of ΔH^0 decreases from that for moderately strong acid-base bonds at 298 K to that for weak acid-base bonds at 343 K for $[\text{C}_2\text{CNHeim}]\text{DOSS}$ and $[\text{P}_{8,8,8,14}]\text{DOSS}$ ILs while $[\text{C}_2\text{CNDim}]\text{DOSS}$ shows a very small decreases. The partial molar change in enthalpy can be divided into two parts: the enthalpy of condensation of the pure gas and the partial enthalpy of mixing the condensed gas and liquid.

Table 5-8 Thermodynamic properties for the solution of CO_2 in selected ILs

Thermodynamic property	Temperature (K)	ILs		
		$[\text{C}_2\text{CN Dim}]\text{DOSS}$	$[\text{C}_2\text{CN Heim}]\text{DOSS}$	$[\text{P}_{8,8,8,14}]\text{DOSS}$
ΔG^0 ($\text{kJ}\cdot\text{mol}^{-1}$)	298	4.94	5.49	5.54
	313	6.10	8.82	8.98
	343	8.38	10.69	11.00
ΔH^0 ($\text{kJ}\cdot\text{mol}^{-1}$)	298	-12.85	-21.22	-14.45
	313	-12.82	-13.17	-7.27
	343	-12.77	-8.36	-2.98
ΔS^0 ($\text{J}\cdot\text{mol}^{-1}\cdot\text{K}^{-1}$)	298	-61.65	-97.85	-73.23
	313	-60.44	-70.25	-51.90
	343	-59.70	-55.57	-40.77

In general, the enthalpy of a liquid is lower than the enthalpy of a gas, which results in a negative change in enthalpy for gas condensation. Therefore, the magnitude and sign of the enthalpy of mixing will determine the sign and magnitude

of the overall partial enthalpy change for solvation. For higher solubility gas-liquid mixtures, the enthalpy of condensation dominates and results in an overall partial molar change in enthalpy that is negative [225]. In addition, a larger negative value for the enthalpy indicates stronger IL/CO₂ interactions [82] which indicate that [C₂CNHeim]DOSS has greater IL/CO₂ interactions compared to [C₂CNDim]DOSS and [P_{8,8,8,14}]DOSS but the affect of temperature on this interaction was lower for [C₂CNDim]DOSS. In addition, the negative enthalpies of solvation indicate an exothermal solvation process.

The increase of ΔG^0 with increasing T indicates that the CO₂ solution process consumes more energy with increasing temperature [223]. The solubility of CO₂ in [C₂CNHeim]DOSS and [P_{8,8,8,14}]DOSS ILs is associated with an unfavorable change [223] in entropy (ΔS^0) between 298 and 343 K while [C₂CNDim]DOSS shows a very small change. The negative values observed for the entropy of solvation can be explained by the structuring effect caused by the specific interactions between the solute and the charged centers of the IL. The increase of solubility being explained by the balance of the carbon dioxide-ionic liquid interactions (enthalpic term) and the structure of the solvent surrounding the solute (entropic term). It was stated (using molecular simulation) that the negative values for the entropy of solvation are attributed to the interactions between the solute and the charged centers of the ionic liquid [142].

The smaller change in enthalpy of absorption of the nitrile functionalized ionic liquids compared to that reported for the aqueous amine solvents indicates that less energy is required for the regeneration of the solvent and therefore the nitrile functionalized ionic liquids can potentially impact positively on the energy balance of the solvent recovery process.

5.5 Ideal CO₂/CH₄ Solubility Selectivity

The solubility of gas mixtures in ILs is really a key issue [226]. The measurement of the solubility of methane (CH₄) in IL is essential for using IL in such gas-separation processes since it is the main component of natural gas. The solubility of CH₄ in [C₂CNDim]DOSS was studied and the solubility measurement was performed in a

similar test condition as that used for CO₂ solubility. The solubility measurements were made using a single gas, so that the solubility selectivity that was calculated would be the ideal selectivity. Moreover, Henry's law constant was estimated using the same method mentioned above. The solubility selectivity was calculated from the inverse ratio of Henry's constants for the gas pair.

The nitrile functionality was chosen for this study due to its polar nature and large molar attraction constant relative to a methyl group. It has also been suggested, by analogy to CH₃CN, that the inclusion of a nitrile group(s) in a polymer or solvent may be useful for improving CO₂ solubility and selectivity. Lewis basic polar groups undergo acid-base interactions with the Lewis acidic (i.e., electron-deficient) carbon atom in CO₂ molecules. Furthermore, the chemical synthesis for tethering a nitrile-terminated alkyl unit to an imidazolium ring has been shown to be relatively simple. The molar selectivity toward CO₂ provided by the nitrile-functionalized RTILs was calculated based on the single gas absorption measurements for CO₂ and CH₄ as expressed in equation 5-10 [39].

$$S_{CO_2/CH_4} = \left[\frac{mol_{CO_2}/mol_{RTIL}}{mol_{CH_4}/mol_{RTIL}} \right] = \left(\frac{mol_{CO_2}}{mol_{CH_4}} \right) \quad 5-10$$

The solubility of CH₄ in [C₂CNDim]DOSS in term of mol fraction was found to be 4.29, 14.32, 21.97, 26.90 and 31.21 ×10⁻⁴ at pressures 1, 5, 10, 15 and 20 bars respectively (Fig 5-26).

The estimated Henry's law constant for CH₄ is 616.3 bar and the ideal CO₂/CH₄ solubility selectivity is 82.7. The result shows considerable increases in ideal CO₂/CH₄ solubility selectivity relative to the corresponding non functionalized imidazolium-based ILs (Fig 5-27). The high ratio of the solubility selectivity of this IL may have resulted from the inclusion of the nitrile group as it is known that it can improve the solubility selectivity [175]. In addition, the increased number of regions where the gas molecules absorb (functionality of the anion) increase the solubility of CO₂ compared to CH₄ which resulted in increases of the ideal CO₂/CH₄ solubility selectivity.

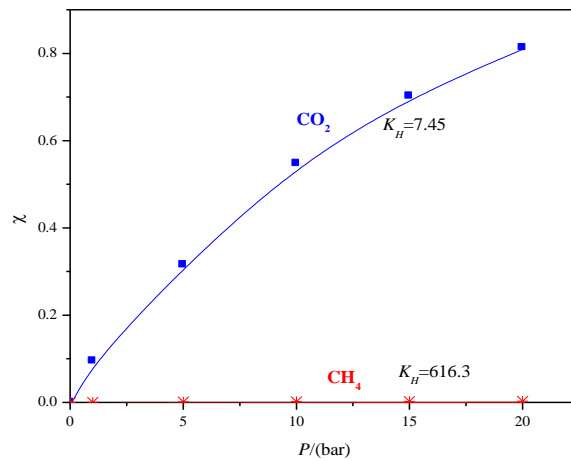


Fig 5-26 Solubility selectivity of [C₂CNDim]DOSS RTIL

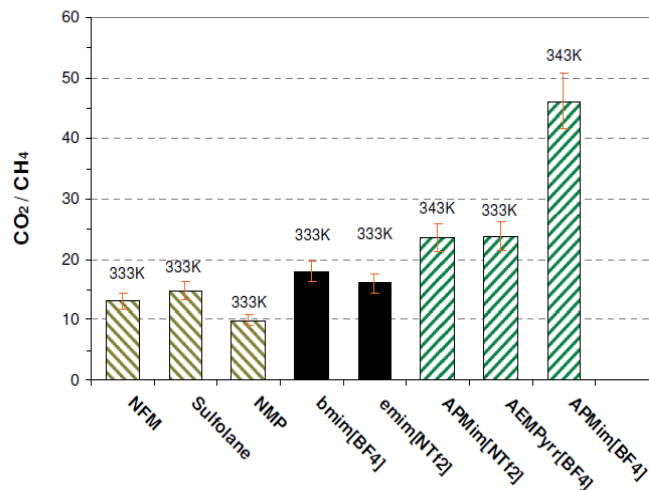


Fig 5-27 CO₂/CH₄ selectivity of physical solvents and ionic liquids at 10 bar. Selectivity at 333 K in physical solvents was taken from available literature: NFM from Rivas and Prausnitz, Sulfolane from Jou et al. and NMP from Murrieta-Guevara et al [39]

Physical solvents are preferably used when CO₂ is a large fraction of the gas stream. The selectivity towards CO₂ is similar for standard RTILs and better in the case of nitrile functionalized RTILs than that provided by traditional physical solvent used in separation of CO₂/CH₄.

The nitrile-functionalized RTILs explored in this work are direct analogues to the exhaustively studied. Thus, direct comparisons between the nitrile-terminated RTILs

presented here and the methyl-terminated RTIL analogues reported in literature facilitates interpretation of experimental results and correlation of structure-property effects. The solubility selectivity result showed substantial increases in ideal CO₂/CH₄ solubility selectivity relative to the analogous non functionalized n-alkyl-substituted RTILs resulted from the inclusion of the nitrile group. However, it was reported that the enhancement of CO₂/CH₄ selectivity is appreciably reduced as alkyl spacer length is extended, which follows the CO₂/CH₄ selectivity trend of the [H₃C-C_nmim]Tf₂N RTILs [175].

The CO₂/CH₄ selectivity calculated from single gas absorption is largely better for the nitrile functionalized IL compare to the non functionalized ILs (as shown in Fig 5-27). The highest selectivity obtained with non functionalized ILs ([APMim]BF₄) is around 47 while for the nitrile functionalized IL ([C₂CNDim]DOSS) is 82.7. Moreover, the CO₂/CH₄ selectivity for the nitrile functionalized IL ([C₂CNDim]DOSS was approximately four times higher than that of the [bmim]BF₄, [emim]NTf₂ and Sulfolane.

It is also worth discussing the bulk solubility results of RTILs used in this study. It was expected that the observed enhancements in selectivity would be accompanied with a fairly substantial tradeoff in bulk solubility as observed with the analogous n-alkyl-substituted RTILs. However, this does not seem to be the case for the [CNC₂Dim]DOSS. This attribute combined with the observed enhanced selectivity performance makes these functionalized RTILs better CO₂ separation solvents compared to their non functionalized alkyl analogues.

5.6 Recyclability of IL

Environmental considerations require the recovery of ILs after their use. ILs are quite expensive, and hence their recycling is also necessary due to economic reasons. Generally, recycling is based on the non-volatile nature of ILs and the solubility differences between ILs, organic compounds and water [39, 65]. The recyclability of [C₂CNDim]DOSS was evaluated at 20 bars. The recycling process was carried at 100 °C by desorption of the CO₂ through depressurization followed by evacuation to zero

bar. This process was continued until there was no further mass change of the sample then a new solubility measurement was made.

The same solubility measurement was performed in a similar test condition with the same IL. Here, regeneration tests were performed five times continuously, and we could see the regeneration performance of [C₂CNDim]DOSS as seen in Fig 5-28. The time required for one recycle of the IL was found to be 5-6 hrs. The CO₂ solubility in the recycled IL was plotted in Fig 5-28. The results reveal this IL can absorb CO₂ reversibly and efficiently. Moreover, the recyclability studies indicated that the CO₂ solubility capacity of the studied IL could be maintained for several cycles.

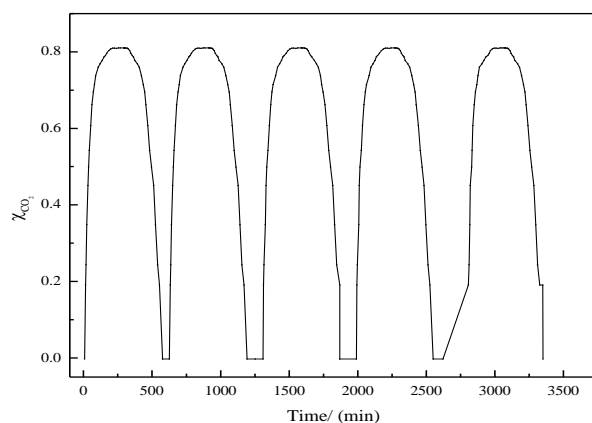


Fig 5-28 Solubility of CO₂ in recycled [C₂CNDim]DOSS

Most of the previous studies suggested that the high CO₂ solubility in RTILs resulted from weak Lewis acid/base complexation between CO₂ and the RTIL anion regulated by the available RTIL "free volume". Below, we first consider CO₂ solubility deviations from ideality to comment on if CO₂/RTIL complexation is the factor that dominates CO₂ solubility. The [C₂CN Dim]DOSS showed a higher CO₂ solubility capacity even more than that of the alkyl-fluoroalkyl-based ILs which has the highest CO₂ affinity. The solubility of CO₂ is commonly higher in ILs with fluoroalkyl groups in the anion (tris(trifluoromethylsulfonyl), and bis(trifluoromethylsulfonyl)imide, Tf₂N) and lower in ILs with non-fluorinated inorganic anions (nitrate, NO₃ and dicyanamide, DCA). The three ILs [C₂CNDim]DOSS, [C₂CNHeim]DOSS and [P_{8,8,8,14}]DOSS showed higher solubility

capacity compared to the ILs with fluoroalkyl groups in the anion which showed solubility capacity of 0.5 mol fraction [8].

The CO₂ solubility capacity of the [C₂CN C_nmim]DOSS ILs improved significantly by the incorporation of nitrile group and long alkyl chain on the imidazolium cation. The positive effect exerted by the long alkyl chain and nitrile functional group is counterbalanced by the viscosity increase with the substitution. On the contrary, the effect of the alkyl chain substitution was much more pronounced for [C₂CN Dim]DOSS. The solubility of carbon dioxide in derivatives of imidazolium-based ILs, in which the length of the alkyl chain attached to the nitrogen atom of the imidazolium ring varies (C₃mim, C₄mim, C₆mim, and C₈mim) and the octyl derivative is fluorinated (C₈F₁₃mim) were reported. They observed that Henry's constant for the studied ILs decrease gradually from 39 to 30 bar when the length of the alkyl side chain in the cation decreases.

The CO₂ solubility capacity of the [C₂CN C₂im]DOSS IL increased 15 % when the butyl group on the imidazolium ring was replaced by a decyl group and Henry's constant for these ILs decrease gradually from 19.21 to 7.45 bar. This is a rather surprising result because this increases is extremely high compared to the increases for the same replacement in the conventional ILs. This results is in agreement with the new direction in which suggested that the solubility of CO₂ in nonvolatile solvents is not driven exclusively or predominantly by the favorable interactions between the gas and the solvent [218].

The amine-appended functionalized IL was reported to be capable of reversibly capturing up to 1 mol of CO₂ per 2 mol of functionalized IL, a level more than 100 times greater than the physical CO₂ uptake in [Rmim]NTf₂ solvents at similar temperature and pressure conditions [14]. The experimental results showed that at pressure of 10 bar, 1 mol of the [C₂CNDim]DOSS, [C₂CNHeim]DOSS and [P_{8,8,8,14}]DOSS is capable to capture 0.75, 0.82 and 1.17 mol of CO₂, respectively.

The solubility capacity of [C₂CN Dim]DOSS at 1 bar is higher compared with the reported acetate-based ILs but lower than that for [N₂₂₂₂]Ala. For [Emim]CH₃COO, [Bmim][CH₃COO] and [N₂₂₂₂]Ala the mol fractions are 0.0942, 0.0842 and 0.0970

respectively [181]. Moreover, the results of the absorption of CO₂ by [P₄₄₄₃]Gly and [P₄₄₄₃]Ala show that the ratio of absorption is close to 1 mol of CO₂ per 1 mol of IL [172] which is also lower than that of [C₂CN Dim]DOSS.

The solubility selectivity of [C₂CN Dim]DOSS is higher compared to the conventional ILs. This results in agreement with that reported for other imidazolium-based ILs containing nitrile groups; the solubility selectivity for CO₂/CH₄ were 25-75 % greater than their [Rmim]NTf₂ analogues. It should be noted here that the CO₂ solubilities in these ILs are low compete with the alkanolamine process (Henry's law constant for the MEA-CO₂ system is 3.16 bar).

CHAPTER 6

CONCLUSIONS AND RECOMMENDATIONS

6.1 Conclusions

The study of the thermophysical properties of ILs is of great importance since it is related to the engineering components associated with a process. It is required for the validation and improvement of the property prediction methods, which can be later applied for molecular simulation, design and development of the commercial process [103103].

The density and viscosity of all ILs were measured in a temperature range of 293.15 to 353.15 K and at atmospheric pressure using a Stabinger viscometer. The density of the ILs shows linear decrease with increasing temperature. It was found that the densities of the imidazolium-based ILs are higher when paired with the TFMS anion followed by SBA, BS and then by DDS anion. The lowest densities were observed with the DOSS anion. These results showed that increasing of the anion molecular weight does not directly correspond to the rise of the density values. The density value decrease with increasing free volume (for the ILs incorporating the same anion). The present ILs showed lower densities compared to the other nitrile – functionalized ILs.

The densities of the imidazolium-based dual functionalized ILs are highest followed by imidazolium-based nitrile functionalized ILs and then by the dicationic phosphonium-based ILs. The lowest densities were observed with the monocationic phosphonium-based ILs. Moreover, the density of the IL with the same anion decreases with increasing the alkyl chain length on the cation. Addition of $-CH_2-$ groups to the alkyl chain of cation decreases the density while the larger hydrophilic

anions increase the density of the IL. Moreover, the density values increase after the incorporation of nitrile group. Densities of the synthesized ILs for a wide range of temperatures and pressures were estimated using the extended of Ye and Shreeve's group contribution method. The results show that the density values decreased almost linearly with increasing pressure.

The measured viscosities are higher for the ILs with DOSS anion, while it was the lowest for ILs with TFMS anion. The increased volumes of the anions here lead to higher viscosities. In addition, the viscosity values of the ILs show functional group and alkyl chain length dependencies. An addition of functional group or increasing alkyl chain length has been found to give higher viscosity values. The viscosity values of the present ILs are much higher compared with that reported for nitrile-functionalized ILs and for the corresponding ILs without nitrile group. The viscosity values of the present DCILs are much higher comparable to phosphonium-based monocationic ILs and these values increase as the spacer alkyl chain length increases.

The activation energy values (E_{η}) are higher for the dual functionalized ILs than for the nitrile functionalized ILs and the phosphonium-based ILs show the lowest values. The values of the viscosities at infinite temperatures (η_{∞}) reveal that the structural contribution of the phosphonium-based ILs ions to the viscosity is greater than the other studied ILs. It is observed that a rise in temperature caused a significant reduction in the viscosities of the present synthesized ILs.

ATAGO programmable digital refractometer was used to measure the refractive index of various ILs in a temperature range of 298.15 to 333.15 at atmospheric pressure. The refractive indices results reveal that the cation type, the functional group, alkyl chain length of cation and type of the anion have large effect on the refractive index values. The size and alkyl chain of the anion has a large effect on density and free volume.

The results show that the present ILs show higher values of refractive index than those of the corresponding ILs without nitrile group. Among the studied anions, TFMS shows the highest refractive index value while DOSS shows the lowest value. Moreover, the results indicated that the anion and alkyl chain length of the cation

have a great effect on the refractive index. The refractive indices of the DCILs decrease with increasing the spacer alkyl chain length.

Comparing the refractive index values of the synthesized ILs, the phosphonium-based ILs show a slightly greater values than their analogous imidazolium-based ILs which indicates that the phosphonium cation plays a role in the refractive index of an ILs. In addition, the refractive indices values for each of the studied ILs decrease almost linearly with increasing temperature.

The start temperatures for weight loss (T_{start}) and onset (T_{onset}) temperatures of the present synthesized ILs were determined using Perkin–Elmer analyzer. The (T_{start}) and (T_{onset}) of the synthesized ILs are affected mainly by the type of the anion and slightly by the size of the alkyl chain of the cation. The T_{onset} of ILs with incorporation of a CN group decreased remarkably in comparison with the corresponding ILs without a CN group.

The imidazolium-based dual functionalized ILs incorporating nitrile functionality show lower decomposition temperatures compared to their analogous incorporating only nitrile functionality. The (T_{start}) and (T_{onset}) of the phosphonium-based ILs are also affected slightly by the size of the alkyl chain of the cation and by the spacer alkyl chain length for the DCILs.

The changes in the liquid volume with temperature were evaluated using the thermal expansion coefficient and the results show weak temperature dependency for the thermal expansion coefficient. In addition, ILs having shorter alkyl chain on cation show less expansion coefficient while large cation size of the IL reduces the electrostatic interactions and facilitates more expansion. The phosphonium-based ILs shown higher expansion coefficients compared to the imidazolium-based ILs. In addition, the dual functionalized ILs shows the lowest expansion coefficients.

The molar refractions as a measure of the hard-core molecular volume was used to calculate the molar free volume (V_f). $[C_2CN\ C_nim]DOSS$ shows very high molar refraction while the other ILs in this study show comparable values when compared with the values reported for the ILs $[C_nmim]X$. The molar free volume decreases

with increase of the alkyl chain length and alkyl chain spacer of the DCILS. Refractive indices of the present ILs decrease as the molar free volume increases.

The estimated lattice energy values for the synthesized ILs are lower than that of the amino acid ILs. In addition, these values decrease with increasing the anion volume and alkyl chain length of the cation. The standard entropies for the synthesized ILs were estimated and the results show a high values compare with the amino acid ILs.

The solubility of CO₂ in ILs studied was measured using magnetic suspension balance (MSB). The results show that the high viscosity of ILs results in greater diffusion time and hence greater time will be required to reach equilibrium. TFMS and BS anions based ILs reach the equilibrium in short time compare to the other anions while the IL with the DOSS anion has a considerably higher affinity for CO₂ compared with the ILs incorporating DDS, TFMS, SBA and BS anions. The results reveal that in some cases, the molar free volume of the IL exerted a more pronounced effect than the anion basicity which is one of the key factors in determining the CO₂ solubility in ILs. Moreover, the interactions between the anion and cation affect the IL interaction with the CO₂.

The results reported for the CO₂ solubility in ILs indicated that the solubility increased with increasing the number of carbons of the alkyl chain of the cation and with incorporation of such functional groups. The results disclose that incorporation of the functional group along with the long alkyl chain in the same cation increases the CO₂ solubility greater than of each of them separately and makes the cation play an important role in the improving of the CO₂ solubility. The increase of the solubility with an increase in the alkyl chain length becomes more apparent at higher pressures. The CO₂ solubility in these ILs increases with increasing pressure.

The CO₂ solubility results showed that the [C₂CNDim]DOSS, [C₂CNHeim]DOSS and P_{8,8,8,14}]DOSS ILs has a higher solubility capacity among the studied imidazolium-based nitrile functionalized ILs, imidazolium-based dual functionalized ILs and phosphonium-based ILs respectively. Moreover, the CO₂ solubility was

higher when the nitrile-imidazolium ILs incorporated with the decyl alkyl chain compare to the other studied ILs.

The CO₂ gas exhibits a nonlinear trend as the CO₂ pressure increased for all the studied ILs. In addition, the CO₂ solubility decreases with the increasing temperature. The Henry's law constants were estimated by fitting a second-order polynomial to the data and calculating the limiting slope as the solubility approaches zero. Moreover, the effect of temperature in the solubility of CO₂ in the IL [C₂CNDim]DOSS was studied. [C₂CDim]DOSS shows the lower Henry's law constant value among all the studied ILs.

Standard enthalpy (ΔH^0), entropy (ΔS^0) and Gibbs free energy (ΔG^0) of gas dissolution were estimated by considering the effect of temperature on gas solubility. The results reveal that the solubility of CO₂ in [C₂CNDim]DOSS, [C₂CNHeim]DOSS and [P_{8,8,8,14}]DOSS is a non-spontaneous process and the negative values of ΔH^0 indicate that CO₂ still dissolves in this IL. Moreover, the results show that [C₂CNHeim]DOSS has greater IL/CO₂ interactions compared to other studied ILs.

The [C₂CNDim]DOSS IL shows a high CO₂/CH₄ solubility selectivity. A better selectivity towards CO₂ was achieved with the nitrile functionalized ionic liquids designed to facilitate the preferential absorption of CO₂. Moreover, the recyclability studies indicated that the CO₂ solubility capacity of the studied IL could be maintained for several cycles.

6.2 Recommendations

This work explores the thermophysical properties of a novel ILs and their potential application for CO₂ capture. The thermophysical properties of ILs and their capability to capture the CO₂ are depend on the choice of the cation and anion.

Functionalized ILs are promising materials for CO₂ separations and more research is desired to further their progress and strictly understand their capabilities. The high viscosity is one of the main impediments in using these ILs for CO₂ separation and measuring the solubility of gases into these compounds. Moreover, the scarcity of the

thermophysical properties of these materials at high temperatures and pressures is also hinders their use.

The following recommendations could be useful to improve the progress of using ILs for CO₂ capture by modifying the existing ILs to enhance their properties.

- Attempts should be made to utilize the opportunities to fine-tune physical and chemical properties of ILs by modifying the bonding network architecture of the ILs to design an IL with high CO₂ solubility capacity, CO₂/CH₄ selectivity and low viscosity to minimize the amount of solvent needed for CO₂ capture and to increase mass transfer. There is likely a most favorable structure that can increase the solubility capacity without drastically increasing the viscosity. In addition, the cost issues and environmental effects must be taken into account.
- Nitrile group, polyether and Oligo(ethylene glycol) alkyl chains present interesting functional groups for enhanced CO₂ interactions with functionalized RTILs. Moreover, anions incorporating carboxyl and sulfonyl functionality can be reduced consequences if released into the environment and also their cost is low compare to the fluorinated anions.
- The ILs incorporating dioctylsulfosuccinate anion has a high CO₂ solubility capacity but they are highly viscous. Using hexylsulfosuccinate or octylsulfosuccinate anions can reduce the viscosity while keeping similar functional group. Also the incorporation of polyether functionality will produce decrease the viscosity.
- Attempt should be made to more purify the ILs to improve the residue by using another solvent or by increase the number of washing times since these residues may affect the properties.
- To study the binary mixture of these ILs with acrylonitrile since it could reduce the viscosity while it has a good solubility capacity.
- Attempt should be made to more evaluate the time needed for each ionic liquid to achieve the equilibrium at the measured pressured, together with the operation conditions for regeneration and the effect of the number of regeneration cycles on the solubility capacity.

REFERENCES

- [1] R. S. Prabhakar, "Low Hydrocarbon Solubility Polymers: Plasticization-resistant Membranes for Carbon Dioxide Removal from Natural Gas," Ph.D, University of Texas, Austin, 2004.
- [2] O. E. Babiker, "Thermodynamics Properties Modeling of Aqueous Carbonate Electrolyte System for CO₂ Separation from Natural Gas," M.Sc., Chemical Engineering, Universiti Teknologi Petronas, Tronoh, 2010.
- [3] R. W. Baker, *Membrane technology and applications*. New York: Wiley, 2004.
- [4] A. Muhammad, "Thermophysical Properties and Solubility of CO₂/CH₄ in Aqueous Alkanolamine Solutions and Ionic Liquids," Ph.D, Chemical Engineering, Universiti Teknologi PETRONAS, Bandar Seri Iskandar, 2009.
- [5] EIA, "International Energy Outlook 2010, Energy Information Administration of the Department of Energy, U.S. Government, Washington, DC," 2010.
- [6] EIA. (2009). *Official Energy Statistics from U.S government, Energy and the Environment*. Available: http://tonto.eia.doe.gov/energyexplained/index.cfm?page=environment_how_ghg_affect_climate
- [7] Y. Liang, "Carbon Dioxide Capture From Flue Gas Using Regenerable Sodium-Based Sorbents," M.Sc., Chemical Engineering, Tsinghua University, 2003.

- [8] H. Lee, M. Cho, B. Lee, J. Palgunadi, H. Kim, and H. Kim, "Alkyl-fluoroalkylimidazolium-Based Ionic Liquids as Efficient CO₂ Absorbents," *Energy & Fuels*, pp. 525-541, 2010.
- [9] H. Yang, Z. Xu, M. Fan, R. Gupta, R. Slimane, A. Bland, and I. Wright, "Progress in carbon dioxide separation and capture: A review," *Journal of Environmental Sciences*, vol. 20, pp. 14-27, 2008.
- [10] L. A. Blanchard, "Ionic Liquids-Carbon Dioxide Systems: Phase Behavior, Solubilities and Extraction," Ph.D, Chemical Engineering, University of Notre Dame, Notre Dame, 2000.
- [11] R. Baker, "Future directions of membrane gas separation technology," *Ind. Eng. Chem. Res.*, vol. 41, pp. 1393-1411, 2002.
- [12] F. Karadas, M. Atilhan, and S. Aparicio, "Review on the Use of Ionic Liquids (ILs) as Alternative Fluids for CO₂ Capture and Natural Gas Sweetening," *Energy & Fuels*, vol. 24, pp. 5817-5828, 2010.
- [13] G. Yu, S. Zhang, X. Yao, J. Zhang, K. Dong, W. Dai, and R. Mori, "Design of task-specific ionic liquids for capturing CO₂: a molecular orbital study," *Ind. Eng. Chem. Res.*, vol. 45, pp. 2875-2880, 2006.
- [14] E. D. Bates, R. D. Mayton, I. Ntai, and J. H. Davis, "CO₂ capture by a task-specific ionic liquid," *J. Am. Chem. Soc.*, vol. 124, pp. 926-927, 2002.
- [15] J. Bara, D. Camper, D. Gin, and R. Noble, "Room-Temperature Ionic Liquids and Composite Materials: Platform Technologies for CO₂ Capture," *Accounts of chemical research*, vol. 43, pp. 152-159, 2009.
- [16] M. J. Earle and K. R. Seddon, "Ionic liquids. Green solvents for the future," *Pure Appl. Chem.*, vol. 72 pp. 1391-1398, 2000
- [17] I. Newington, J. M. Perez-Arlandis, and T. Welton, "Ionic liquids as Designer Solvents for Nucleophilic Aromatic Substitutions. ," *Org. Lett.*, vol. 25, pp. 5247-5250, 2007.

- [18] N. Plechkova and K. Seddon, "ChemInform Abstract: Applications of Ionic Liquids in the Chemical Industry," *ChemInform*, vol. 39, 2008.
- [19] Q. Li, "Approaches to Mimic Catalysis fo Hydrocarbon Cracking by Ionic Liquids and Zeolites: A mechanistic Study," Ph.D, Chemistry, University of Regina, Regina, 2006.
- [20] S. Abedin and F. Endres, "Ionic Liquids: The Link to High-Temperature Molten Salts?," *Accounts of chemical research*, vol. 40, pp. 1106-1113, 2007.
- [21] J. Wilkes and M. Zaworotko, "Air and water stable 1-ethyl-3-methylimidazolium based ionic liquids," *Chem. Commun.*, pp. 965-967, 1992.
- [22] J. N. C. Lopes, T. C. Cordeiro, J. M. S. S. Esperanca, H. J. R. Guedes, S. Huq, L. P. N. Rebelo, and K. R. Seddon, "Deviations from Ideality in Mixtures of Two Ionic Liquids Containing a Common Ion," *J. Phys. Chem. B* vol. 109 pp. 3519-3525, 2005.
- [23] M. G. Freire, P. J. Carvalho, A. M. Fernandes, I. M. Marrucho, A. J. Queimada, and J. A. P. Coutinho, "Surface tensions of imidazolium based ionic liquids: Anion, cation, temperature and water effect," *J. Colloid Interface Sci.*, vol. 314, pp. 621-630, 2007.
- [24] R. Rajagopal, "Novel Synthetic Methodologies: Study Of Unit Processes For Preparation Of Industrially Important Organic Chemicals," Ph.D, Chemical Industry, University of Mumbai, Pune, 2002.
- [25] J.-Z. Yang, Q.-G. Zhang, B. Wang, and J. Tong, "Study on the Properties of Amino Acid Ionic Liquid EMIGly " *J. Phys. Chem. B.*, vol. 110 pp. 22521-22524, 2006
- [26] K. Fukumoto, M. Yoshizawa, and H. Ohno, "Room temperature ionic liquids from 20 natural amino acids," *Journal of the American Chemical Society*, vol. 127, pp. 2398-2399, 2005.

- [27] X. Jiang, Y. Nie, C. Li, and Z. Wang, "Imidazolium-based alkylphosphate ionic liquids-A potential solvent for extractive desulfurization of fuel," *Fuel*, vol. 87, pp. 79-84, 2008.
- [28] P. Nockemann, B. Thijs, K. Driesen, C. R. Janssen, K. Van Hecke, L. Van Meervelt, S. Kossmann, B. Kirchner, and K. Binnemans, "Choline saccharinate and choline acesulfamate: Ionic liquids with low toxicities," *The Journal of Physical Chemistry B*, vol. 111, pp. 5254-5263, 2007.
- [29] D. Brégeon, J. Levillain, F. Guillen, J. C. Plaquevent, and A. C. Gaumont, "Thiazolinium and imidazolium chiral ionic liquids derived from natural amino acid derivatives," *Amino acids*, vol. 35, pp. 175-184, 2008.
- [30] T. P. Thuy Pham, C. W. Cho, and Y. S. Yun, "Environmental fate and toxicity of ionic liquids: A review," *Water Res.*, vol. 44, pp. 352-372, 2010.
- [31] T. Yamada, P. J. Lukac, T. Yu, and R. G. Weiss, "Reversible, room-temperature, chiral ionic liquids. Amidinium carbamates derived from amidines and amino-acid esters with carbon dioxide," *Chemistry of Materials*, vol. 19, pp. 4761-4768, 2007.
- [32] G. Keglevich, Z. Baan, I. Hermeecz, T. Novak, and I. L. Odinetz, "The Phosphorus Aspects of Green Chemistry: the Use of Quaternary Phosphonium Salts and 1, 3-Dialkylimidazolium Hexafluorophosphates in Organic Synthesis," *Curr. Org. Chem.*, vol. 11, pp. 107-126, 2007.
- [33] H. Ohno, "Functional design of ionic liquids," *Bulletin of the Chemical Society of Japan*, vol. 79, pp. 1665-1680, 2006.
- [34] Y. Y. Jiang, G. N. Wang, Z. Zheng, and Y. T. Wu, "Tetraalkylammonium amino acids as functionalized ionic liquids of low viscosity," *Chem. Commun.*, pp. 505-507, 2008.
- [35] A. E. Visser, R. P. Swatloski, W. M. Reichert, R. Mayton, S. Sheff, A. Wierzbicki, J. H. Davis, and R. D. Rogers, "Task-Specific Ionic Liquids for

- the Extraction of Metal Ions from Aqueous Solutions " *Chem. Commun.* , vol. 36, pp. 135-136, 2001.
- [36] S. Lee, "Functionalized imidazolium salts for task-specific ionic liquids and their applications," *Chem. Commun.*, pp. 1049-1063, 2006.
- [37] P. Wasserscheid, T. Welton, and E. Corporation, *Ionic liquids in synthesis* vol. 2: Wiley Online Library, 2003.
- [38] P. Nockemann, Thijs B. , Parac-Vogt, T.N. , Hecke, K.V. , Meervelt L.V. , Tinant, B. , Hartenbach, I. , Schleid T. , Ngan, V.T. , Nguyen, M.T. , Binnemans, K. , "Carboxyl-Functionalized Task-Specific Ionic Liquids for Solubilizing Metal Oxides," *Inorg. Chem.* , vol. 47 pp. 9987–9999, 2008.
- [39] L. M. G. Sánchez, "Functionalized Ionic Liquids: Absorption Solvents for Carbon Dioxide and Olefin Separation," Ph.D, Chemical Engineering, Eindhoven University of Technology, Eindhoven, 2008.
- [40] Z. Fei, Ang, W. H. , Zhao, D. , Scopelliti, R. , Zvereva, E. E. , Katsyuba, S.A. , Dyson, P.J. , "Revisiting Ether-Derivatized Imidazolium-Based Ionic Liquids," *J. Phys. Chem. B.* , vol. 111 pp. 10095–10108, 2007.
- [41] D. Zhao, Fei, Z. , Scopelliti, R. , Dyson, P. J., "Synthesis and Characterization of Ionic Liquids Incorporating the Nitrile Functionality," *Inorg. Chem.*, vol. 43, pp. 2197-2205, 2004.
- [42] Z. Fei, D. Zhao, D. Pieraccini, W. H. Ang, T. J. Geldbach, R. Scopelliti, C. Chiappe, and P. J. Dyson, "Development of Nitrile-Functionalized Ionic Liquids for C- C Coupling Reactions: Implication of Carbene and Nanoparticle Catalysts," *Organometallics*, vol. 26, pp. 1588-1598, 2007.
- [43] S. Zhang, Y. Chen, F. Li, X. Lu, W. Dai, and R. Mori, "Fixation and conversion of CO₂ using ionic liquids " *Catal. Today*, vol. 115 pp. 61–69, 2006

- [44] F. Dong, G. Kai, F. Zhenghao, Z. Xinli, and L. Zuliang, "A practical and efficient synthesis of quinoxaline derivatives catalyzed by task-specific ionic liquid," *Catal. Commun.*, vol. 9, pp. 317-320, 2008.
- [45] G. Drake, G. Kaplan, L. Hall, T. Hawkins, and J. Larue, "A new family of energetic ionic liquids 1-amino-3-alkyl-1, 2, 3-triazolium nitrates," *J. Chem. Crystallogr.*, vol. 37, pp. 15-23, 2007.
- [46] X.-M. Liu, Z.-X. Song, and H.-J. Wang, "Density Functional Theory Study on the -SO₃H Functionalized Acidic Ionic Liquids," *Struct. Chem.*, vol. 20 pp. 509-515, 2009
- [47] H. S. Schrekker, M. P. Stracke, C. M. L. Schrekker, and J. Dupont, "Ether-functionalized imidazolium hexafluorophosphate ionic liquids for improved water miscibilities," *Ind. Eng. Chem. Res.*, vol. 46, pp. 7389-7392, 2007.
- [48] J. M. Crosthwaite, M. J. Muldoon, J. N. K. Dixon, J. L. Anderson, and J. F. Brennecke, "Phase transition and decomposition temperatures, heat capacities and viscosities of pyridinium ionic liquids," *J. Chem. Thermodyn.*, vol. 37, pp. 559-568, 2005.
- [49] F. Mazille, Z. Fei, D. Kuang, D. Zhao, S. M. Zakeeruddin, M. Grätzel, and P. J. Dyson, "Influence of Ionic Liquids Bearing Functional Groups in Dye-Sensitized Solar Cells " *Inorg. Chem.*, vol. 45, pp. 1585-1590, 2006
- [50] G. Yua, S. Yana, F. Zhoub, X. Liub, W. Liub, and Y. Liang, "Synthesis of dicationic symmetrical and asymmetrical ionic liquids and their tribological properties as ultrathin films," *Tribology Letters*, vol. 25, pp. 197-205, 2007.
- [51] R. D. Jared L. Anderson, Arkady Ellern, Daniel W. Armstrong, "Structure and Properties of High Stability Geminal Dicationic Ionic Liquids," *J. Am. Chem. Soc.*, vol. 127, pp. 593-604, 2005.
- [52] R. P. Swatloski, "Ionic Liquids as Green Solvents: Enabling New Materials and Technologies," Ph.D, Chemistry Department, University of Alabama, Tuscaloosa, 2005.

- [53] M. J. Earle, C. M. Gordon, N. V. Plechkova, K. R. Seddon, and T. Welton, "Decolorization of ionic liquids for spectroscopy," *Anal. Chem.*, vol. 79, pp. 758-764, 2007.
- [54] R. Alleti, "Lewis Acid Catalysis in Organic Synthesis," Ph.D, Chemistry, Missouri-Rolla, 2007.
- [55] D. Zhao, M. Wu, Y. Kou, and E. Min, "Ionic liquids: applications in catalysis," *Catalysis Today*, vol. 74, pp. 157-189, 2002.
- [56] C. Ye, W. Liu, Y. Chen, and L. Yu, "Room-temperature ionic liquids: a novel versatile lubricant " *Chem. Commun.* , vol. 21 pp. 2244–2245, 2001.
- [57] C. Chiappe and D. Pieraccini, "Kinetic Study of the Addition of Trihalides to Unsaturated Compounds in Ionic Liquids. Evidence of a Remarkable Solvent Effect in the Reaction of ICl_2^- ," *J. Org. Chem.*, vol. 69 pp. 6059–6064, 2004.
- [58] T. Welton, "Room-temperature ionic liquids. Solvents for synthesis and catalysis," *Chem. Rev.*, vol. 99, pp. 2071-2084, 1999.
- [59] R. Rogers and K. Seddon, "CHEMISTRY: Ionic Liquids--Solvents of the Future?," *Science*, vol. 302, p. 792, 2003.
- [60] T. E. Sutto, H. C. De Long, and P. C. Trulove, "Physical Properties of Substituted Imidazolium Based Ionic Liquids Gel Electrolytes," *ZEITSCHRIFT FUR NATURFORSCHUNG A*, vol. 57, pp. 839-846, 2002.
- [61] M. W. Arshad and K. Thomsen, "CO₂ Capture Using Ionic Liquids," M.Sc., Department of Chemical and Biochemical Engineering, Technical University of Denmark, Copenhagen, 2009.
- [62] M. E. Kandil, K. N. Marsh, and A. R. H. Goodwin, "Measurement of the viscosity, density, and electrical conductivity of 1-hexyl-3-methylimidazolium bis (trifluorosulfonyl) imide at temperatures between (288 and 433) K and pressures below 50 MPa," *J. Chem. Eng. Data*, vol. 52, pp. 2382-2387, 2007.

- [63] M. Smiglak, W. Reichert, J. Holbrey, J. Wilkes, L. Sun, J. Thrasher, K. Kirichenko, S. Singh, A. Katritzky, and R. Rogers, "Combustible ionic liquids by design: is laboratory safety another ionic liquid myth?," *Chem. Commun.*, vol. 2006, pp. 2554-2556, 2006.
- [64] M. Earle, J. Esperança, M. Gilea, J. Lopes, L. Rebelo, J. Magee, K. Seddon, and J. Widegren, "The distillation and volatility of ionic liquids," *Nature*, vol. 439, pp. 831-834, 2006.
- [65] J. Kärkkäinen, "Preparation and Characterization Of Some Ionic Liquids And Their Use In The Dimerization Reaction Of 2-Methylpropene," Ph.D, Chemistry, University of Oulu, 2007.
- [66] J. Vila, P. Gines, J. M. Pico, C. Franjo, E. Jiménez, L. M. Varela, and O. Cabeza, "Temperature dependence of the electrical conductivity in EMIM-based ionic liquids:: Evidence of Vogel-Tamman-Fulcher behavior," *Fluid Phase Equilib.*, vol. 242, pp. 141-146, 2006.
- [67] M. Yao, M. Fan, Y. Liang, F. Zhou, and Y. Xia, "Imidazolium hexafluorophosphate ionic liquids as high temperature lubricants for steel-steel contacts," *Wear*, vol. 268 pp. 67-71, 2010.
- [68] Y. Zhong, H. Wang, and K. Diao, "Densities and excess volumes of binary mixtures of the ionic liquid 1-butyl-3-methylimidazolium hexafluorophosphate with aromatic compound at T = (298.15 to 313.15) K," *J. Chem. Thermodyn.*, vol. 39 pp. 291-296, 2007.
- [69] A. E. Jimenez, M. D. Bermudez, F. J. Carrion, and G. Martinez-Nicolas, "Room temperature ionic liquids as lubricant additives in steel-aluminium contacts: Influence of sliding velocity, normal load and temperature," *Wear*, vol. 261, pp. 347-359, 2006.
- [70] S. Dai, D. DePaoli, M. Dietz, J. Mays, J. McFarlane, and W. Steele, "Technical summaries on ionic liquids in chemical processing," *Prepared for the Chemical Industry Vision*, 2003.

- [71] J. Huddleston, H. Willauer, R. Swatloski, A. Visser, and R. Rogers, "Chem Commun 1998, 1765," *CrossRef, ChemPort*.
- [72] A. Visser, R. Swatloski, W. Reichert, S. Griffin, and R. Rogers, "Traditional Extractants in Nontraditional Solvents: Groups 1 and 2 Extraction by Crown Ethers in Room-Temperature Ionic Liquids[†]," *Ind. Eng. Chem. Res*, vol. 39, pp. 3596-3604, 2000.
- [73] A. E. Visser, R. P. Swatloski, W. M. Reichert, Rebecca Mayton, S. Sheff, A. Wierzbicki, J. H. Davis, and R. D. Rogers, "Task-Specific Ionic Liquids Incorporating Novel Cations for the Coordination and Extraction of Hg²⁺ and Cd²⁺: Synthesis, Characterization, and Extraction Studies," *Environ. Sci. Technol.*, vol. 36 pp. 2523-2529, 2002.
- [74] J. D. Holbrey, W. M. Reichert, R. P. Swatloski, G. A. Broker, W. R. Pitner, K. R. Seddon, and R. D. Rogers, "Efficient, halide free synthesis of new, low cost ionic liquids: 1, 3-dialkylimidazolium salts containing methyl-and ethyl-sulfate anions," *Green Chem.*, vol. 4, pp. 407-413, 2002.
- [75] W. Wang, S. Wang, H. Liu, and Z. Wang, "Desulfurization of gasoline by a new method of electrochemical catalytic oxidation," *Fuel*, vol. 86, pp. 2747-2753, 2007.
- [76] D. O'rear, L. Boudreau, M. Driver, and C. Munson, "Removal of mercaptans from hydrocarbon streams using ionic liquids," ed: WO Patent WO/2002/034,863, 2002.
- [77] Y. Pei, J. Wang, X. Xuan, J. Fan, and M. Fan, "Factors affecting ionic liquids based removal of anionic dyes from water," *Environ. Sci. Technol*, vol. 41, pp. 5090-5095, 2007.
- [78] A. Bradley, J. Hatter, M. Nieuwenhuyzen, W. Pitner, K. Seddon, and R. Thied, "Precipitation of a dioxouranium (VI) species from a room temperature ionic liquid medium," *Inorg. Chem.*, vol. 41, pp. 1692-1694, 2002.

- [79] D. Armstrong, L. He, and Y. Liu, "Examination of ionic liquids and their interaction with molecules, when used as stationary phases in gas chromatography," *Anal. Chem.*, vol. 71, pp. 3873-3876, 1999.
- [80] T. Jiang, Y. Gu, B. Liang, J. Li, Y. Shi, and Q. Ou, "Dynamically coating the capillary with 1-alkyl-3-methylimidazolium-based ionic liquids for separation of basic proteins by capillary electrophoresis," *Analytica Chimica Acta*, vol. 479, pp. 249-254, 2003.
- [81] J. Anthony, E. Maginn, and J. Brennecke, "Solubilities and thermodynamic properties of gases in the ionic liquid 1-n-butyl-3-methylimidazolium hexafluorophosphate," *J. Phys. Chem. B*, vol. 106, pp. 7315-7320, 2002.
- [82] M. Muldoon, S. Aki, J. Anderson, J. Dixon, and J. Brennecke, "Improving carbon dioxide solubility in ionic liquids," *J. Phys. Chem. B*, vol. 111, pp. 9001-9009, 2007.
- [83] A. N. Soriano, B. T. Doma Jr, and M. H. Li, "Measurements of the density and refractive index for 1-n-butyl-3-methylimidazolium-based ionic liquids," *J. Chem. Thermodyn.*, vol. 41, pp. 301-307, 2009.
- [84] Y. Seo, S. P. Kang, and W. Jang, "Structure and Composition Analysis of Natural Gas Hydrates: ^{13}C NMR Spectroscopic and Gas Uptake Measurements of Mixed Gas Hydrates," *The Journal of Physical Chemistry A*, vol. 113, pp. 9641-9649, 2009.
- [85] A. J. Kidnay, W. Parrish, and W. R. Parrish, *Fundamentals of natural gas processing* vol. 200: CRC, 2006.
- [86] R. T. Morrison and R. N. Boyd, "Organic Chemistry, 1987," *no month*, p. 637.
- [87] S. Gupta and J. D. Olson, "Industrial needs in physical properties," *Ind. Eng. Chem. Res.*, vol. 42, pp. 6359-6374, 2003.
- [88] M. Reinhard and A. Drefahl. (1999). *Handbook for Estimating Physicochemical Properties of Organic Compounds. 1.*

- [89] E. Hendriks, G. M. Kontogeorgis, R. Dohrn, J.-C. d. Hemptinne, I. G. Economou, L. F. Zilnik, and V. Vesovic, "Industrial Requirements for Thermodynamics and Transport Properties," *Ind. Eng. Chem. Res.*, vol. 49, pp. 11131–11141, 2010.
- [90] S. Zhang, N. Sun, X. He, X. Lu, and X. Zhang, "Physical properties of ionic liquids: database and evaluation," *J. Phys. Chem. Ref. Data*, vol. 35, p. 1475, 2006.
- [91] J. N. C. Lopes, T. C. Cordeiro, J. Esperança, H. J. R. Guedes, S. Huq, L. P. N. Rebelo, and K. R. Seddon, "Deviations from ideality in mixtures of two ionic liquids containing a common ion," *J. Phys. Chem. B*, vol. 109, pp. 3519-3525, 2005.
- [92] J. G. Huddleston, A. E. Visser, W. M. Reichert, H. D. Willauer, G. A. Broker, and R. D. Rogers, "Characterization and comparison of hydrophilic and hydrophobic room temperature ionic liquids incorporating the imidazolium cation," *Green Chem.*, vol. 3, pp. 156-164, 2001.
- [93] F. Kopecký, Ed., *Physics for Students of Pharmacy 1*. Bratislava, UK, 1999, p.^pp. Pages.
- [94] Z. Gu, Brennecke, J. F. , "Volume expansivities and isothermal compressibilities of Imidazolium and Pyridinium-based ionic liquids " *J. Chem. Eng. Data*, vol. 47 pp. 339-345, 2002.
- [95] J. Troncoso, C. Cerdeiriña, Y. Sanmamed, L. Romaní, and L. Rebelo, "Thermodynamic properties of imidazolium-based ionic liquids: densities, heat capacities, and enthalpies of fusion of [bmim]PF₆ and [bmim]NTf₂," *J. Chem. Eng. Data*, vol. 51, pp. 1856-1859, 2006.
- [96] A. B. Pereiro, F. Santamarta, E. Tojo, A. Rodríguez, and J. Tojo, "Temperature Dependence of Physical Properties of Ionic Liquid 1,3-Dimethylimidazolium Methyl Sulfate " *J. Chem. Eng. Data* vol. 51 pp. 952 – 954, 2006.

- [97] D. W. Fang, Guan, W., Tong, J., Wang, Z. W., Yang, J.Z. , "Study on Physicochemical Properties of Ionic Liquids Based on Alanine [C_nmim]Ala (n = 2,3,4,5,6)," *J. Phys. Chem. B.*, vol. 112 pp. 7499–7505, 2008.
- [98] L. Glasser and H. D. B. Jenkins, "Standard absolute entropies, S°298, from volume or density Part II. Organic liquids and solids," *Thermochim. Acta*, vol. 414, pp. 125-130, 2004.
- [99] L. Glasser, "Lattice and phase transition thermodynamics of ionic liquids " *Thermochim. Acta*, vol. 421, pp. 87–93, 2004.
- [100] K. R. Seddon, A. Stark, and M. J. Torres, "Influence of chloride, water, and organic solvents on the physical properties of ionic liquids," *Pure Appl. Chem*, vol. 72, pp. 2275-2287, 2000.
- [101] G. Singh and A. Kumar, "Ionic liquids: Physico-chemical, solvent properties and their applications in chemical processes," *Indian J. Chem.*, vol. 47A, pp. 495-503, 2008.
- [102] M. Tariq, P. A. S. Forte, M. F. Costa, J. N. Canongia, and L. P. N. Rebelo, "Densities and refractive indices of imidazolium- and phosphonium-based ionic liquids: Effect of temperature, alkyl chain length, and anion," *J. Chem. Thermodyn.*, vol. 41, pp. 790–798, 2009.
- [103] L. G. Sanchez, J. R. Espel, F. Onink, G. W. Meindersma, and A. B. Haan, "Density, viscosity, and surface tension of synthesis grade imidazolium, pyridinium, and pyrrolidinium based room temperature ionic liquids," *J. Chem. Eng. Data*, vol. 54, pp. 2803-2812, 2009.
- [104] R. L. Gardas, M. G. Freire, P. J. Carvalho, I. M. Marrucho, I. M. A. Fonseca, A. G. M. Ferreira, and J. A. P. Coutinho, "High-pressure densities and derived thermodynamic properties of imidazolium-based ionic liquids," *J. Chem. Eng. Data*, vol. 52, pp. 80-88, 2007.
- [105] J. S. Torrecilla, J. Palomar, J. n. Garcí, and F. Rodrí'guez, "Effect of Cationic and Anionic Chain Lengths on Volumetric, Transport, and Surface Properties

- of 1-Alkyl-3-methylimidazolium Alkylsulfate Ionic Liquids at (298.15 and 313.15) K," *J. Chem. Eng. Data*, vol. 54, pp. 1297-1301, 2009.
- [106] Q. Zhang, Z. Li, J. Zhang, S. Zhang, L. Zhu, J. Yang, X. Zhang, and Y. Deng, "Physicochemical Properties of Nitrile-Functionalized Ionic Liquids," *J. Phys. Chem. B*, vol. 111, pp. 2864-2872, 2007.
- [107] R. Bird, W. Stewart, and E. Lightfoot, "Transport Phenomena, Wiley, New York," 1960.
- [108] A. Ahosseini and A. M. Scurto, "Viscosity of imidazolium-based ionic liquids at elevated pressures: Cation and anion effects," *Int. J. Thermophys.*, vol. 29, pp. 1222-1243, 2008.
- [109] O. Okoturo and T. VanderNoot, "Temperature dependence of viscosity for room temperature ionic liquids," *Journal of Electroanalytical Chemistry*, vol. 568, pp. 167-181, 2004.
- [110] H. Tokuda, K. Hayamizu, K. Ishii, M. Susan, and M. Watanabe, "Physicochemical properties and structures of room temperature ionic liquids. 1. Variation of anionic species," *J. Phys. Chem. B*, vol. 108, pp. 16593-16600, 2004.
- [111] H. Tokuda, K. Hayamizu, K. Ishii, M. Susan, and M. Watanabe, "Physicochemical properties and structures of room temperature ionic liquids. 2. Variation of alkyl chain length in imidazolium cation," *J. Phys. Chem. B.*, vol. 109, pp. 6103-6110, 2005.
- [112] C. J. Bradaric, A. Downard, C. Kennedy, A. J. Robertson, and Y. Zhou, "Industrial preparation of phosphonium ionic liquids," *Green Chem.*, vol. 5, pp. 143-152, 2003.
- [113] K. Tsunashima and M. Sugiya, "Physical and electrochemical properties of low-viscosity phosphonium ionic liquids as potential electrolytes," *Electrochem. Commun.*, vol. 9, pp. 2353-2358, 2007.

- [114] R. E. Del Sesto, C. Corley, A. Robertson, and J. S. Wilkes, "Tetraalkylphosphonium-based ionic liquids," *J. Organomet. Chem.*, vol. 690, pp. 2536-2542, 2005.
- [115] H. Tokuda, K. Ishii, M. Susan, S. Tsuzuki, K. Hayamizu, and M. Watanabe, "Physicochemical properties and structures of room-temperature ionic liquids. 3. Variation of cationic structures," *J. Phys. Chem. B.*, vol. 110, pp. 2833-2839, 2006.
- [116] T. Payagala, J. Huang, Z. Breitbach, P. Sharma, and D. Armstrong, "Unsymmetrical dicationic ionic liquids: manipulation of physicochemical properties using specific structural architectures," *Chemistry of Materials*, vol. 19, pp. 5848-5850, 2007.
- [117] M. Deetlefs, K. Seddon, and M. Shara, "Predicting physical properties of ionic liquids," *Phys. Chem. Chem. Phys.*, vol. 8, pp. 642-649, 2006.
- [118] P. Brocos, Á. Piñeiro, R. Bravo, and A. Amigo, "Refractive indices, molar volumes and molar refractions of binary liquid mixtures: concepts and correlations," *Phys. Chem. Chem. Phys.*, vol. 5, pp. 550-557, 2003.
- [119] B. Hasse, J. Lehmann, D. Assenbaum, P. Wasserscheid, A. Leipertz, and A. P. Froba, "Viscosity, Interfacial Tension, Density, and Refractive Index of Ionic Liquids [EMIM][MeSO₃], [EMIM][MeOHPO₂], [EMIM][OcSO₄] and [BBIM][NTf₂] in Dependence on Temperature at Atmospheric Pressure," *J. Chem. Eng. Data*, vol. 54, pp. 2576-2583, 2009.
- [120] Z. S. Breitbach and D. W. Armstrong, "Characterization of phosphonium ionic liquids through a linear solvation energy relationship and their use as GLC stationary phases," *Anal. Bioanal. Chem.*, vol. 390, pp. 1605-1617, 2008.
- [121] H. L. Ngo, K. LeCompte, L. Hargens, and A. B. McEwen, "Thermal properties of imidazolium ionic liquids," *Thermochim. Acta.*, pp. 97-102, 2000.

- [122] M. Koel, "Physical and chemical properties of ionic liquids based on the dialkylimidazolium cation," *Proc. Estonian Acad. Sci. Chem.*, vol. 49, pp. 145–155, 2000.
- [123] V. Kamavaram and R. G. Reddy, "Thermal stabilities of di-alkylimidazolium chloride ionic liquids," *International Journal of Thermal Sciences*, vol. 47, pp. 773-777, 2008.
- [124] S. Aparicio, M. Atilhan, and F. Karadas, "Thermophysical Properties of Pure Ionic Liquids: Review of Present Situation," *Ind. Eng. Chem. Res.*, vol. 49, pp. 9580–9595, 2010.
- [125] W. Guan, J. Tong, S. P. Chen, Q. S. Liu, and S. L. Gao, "Density and Surface Tension of Amino Acid Ionic Liquid 1-Alkyl-3-methylimidazolium Glutamate," *J. Chem. Eng. Data*, pp. 639-646, 2010.
- [126] A. N. d. C. Carlos, E. Langaa, A. L. Moraisa, M. L. M. Lopesa, M. J. V. Lourenc, F. J. V. Santosa, M. S. C. S. Santosb, J. N. C. Lopesd, H. I. M. Veigad, M. Macatrãod, J. M. S. S. Esperanc, C. S. Marquese, L. P. N. Rebelod, and C. A. M. Afonsoe, "Studies on the density, heat capacity, surface tension and infinite dilution diffusion with the ionic liquids [C₄mim][NTf₂], [C₄mim][dca], [C₂mim][EtOSO₃] and [Aliquat][dca]," *Fluid Phase Equilibria*, vol. 294, pp. 157-179, 2010.
- [127] P. Kilaru, G. A. Baker, and P. Scovazzo, "Density and surface tension measurements of imidazolium-, quaternary phosphonium-, and ammonium-based room-temperature ionic liquids: data and correlations," *J. Chem. Eng. Data*, vol. 52, pp. 2306-2314, 2007.
- [128] A. B. Pereiro, H. I. M. Veiga, J. Esperança, and A. Rodríguez, "Effect of temperature on the physical properties of two ionic liquids," *J. Chem. Thermodyn.*, vol. 41, pp. 1419-1423, 2009.
- [129] I. Krossing, J. Slattery, C. Daguene, P. Dyson, A. Oleinikova, and H. Weingärtner, "Why are ionic liquids liquid? A simple explanation based on

- lattice and solvation energies," *J. Am. Chem. Soc.*, vol. 128, pp. 13427-13434, 2006.
- [130] T. Singh and A. Kumar, "Temperature Dependence of Physical Properties of Imidazolium Based Ionic Liquids: Internal Pressure and Molar Refraction," *J. Sol. Chem.*, vol. 38, pp. 1043-1053, 2009.
- [131] A. Kumar, "Estimates of Internal Pressure and Molar Refraction of Imidazolium Based Ionic Liquids as a Function of Temperature " *J. Sol. Chem.* , vol. 37 pp. 203–214, 2008
- [132] B. Gonza lez, N. Calvar, E. Go mez, E. A. Macedo, and A. Domi nquez, "Synthesis and Physical Properties of 1-Ethyl 3-methylpyridinium Ethylsulfate and Its Binary Mixtures with Ethanol and Water at Several Temperatures," *J. Chem. Eng. Data*, vol. 53, pp. 1824-1828, 2008.
- [133] L. M. Galán Sánchez, G. W. Meindersma, and A. B. De Haan, "Solvent properties of functionalized ionic liquids for CO₂ absorption," *Chem. Eng. Res. Des.*, vol. 85, pp. 31-39, 2007.
- [134] J. Kittel, R. Idem, D. Gelowitz, P. Tontiwachwuthikul, G. Parrain, and A. Bonneau, "Corrosion in MEA units for CO₂ capture: Pilot plant studies," *Energy Procedia*, vol. 1, pp. 791-797, 2009.
- [135] J. Anthony, S. Aki, E. Maginn, and J. Brennecke, "Feasibility of using ionic liquids for carbon dioxide capture," *International Journal of Environmental Technology and Management*, vol. 4, pp. 105-115, 2004.
- [136] A. H. Jalili, A. Mehdizadeh, M. Shokouhi, H. Sakhaeinia, and V. Taghikhani, "Solubility of CO₂ in 1-(2-hydroxyethyl)-3-methylimidazolium ionic liquids with different anions," *J. Chem. Thermodyn.* , vol. 42, pp. 787-791, 2010.
- [137] J. Kume an, Á. Kamps, D. Tuma, and G. Maurer, "Solubility of CO₂ in the ionic liquids [bmim][CH₃SO₄] and [bmim][PF₆]," *J. Chem. Eng. Data*, vol. 51, pp. 1802-1807, 2006.

- [138] D. Wappel, G. Gronald, R. Kalb, and J. Draxler, "Ionic liquids for post-combustion CO₂ absorption," *International Journal of Greenhouse Gas Control*, vol. 4, pp. 486-494, 2010.
- [139] G. Maurer and D. Tuma, "Gas Solubility (and Related High-Pressure Phenomena) in Systems with Ionic Liquids," in *Ionic Liquids: From Knowledge to Application* vol. 1030, A. C. Society, Ed., ed: ACS Publications, 2009, pp. 1-20.
- [140] L. Blanchard, D. Hancu, E. Beckman, and J. Brennecke, "Green processing using ionic liquids and CO₂," *Nature*, vol. 399, pp. 28-29, 1999.
- [141] J. E. Bara, "New Ionic Liquids and Ionic Liquid-Based Polymers and Liquid Crystals For Gas Separations," Ph.D, Chemical and Biological Engineering., University of Colorado, 2007.
- [142] D. Almantariotis, T. Gefflaut, A. Pa dua, J. Coxam, and M. Costa Gomes, "Effect of Fluorination and Size of the Alkyl Side-Chain on the Solubility of Carbon Dioxide in 1-Alkyl-3-methylimidazolium Bis (trifluoromethylsulfonyl) amide Ionic Liquids," *The Journal of Physical Chemistry B*, vol. 114, pp. 3608-3617, 2010.
- [143] C. Cadena, J. Anthony, J. Shah, T. Morrow, J. Brennecke, and E. Maginn, "Why is CO₂ so soluble in imidazolium-based ionic liquids?," *J. Am. Chem. Soc.*, vol. 126, pp. 5300-5308, 2004.
- [144] J. Huang and T. Ruether, "Why are Ionic Liquids Attractive for CO₂ Absorption? An Overview," *Australian Journal of Chemistry*, vol. 62, pp. 298-308, 2009.
- [145] R. Baltus, B. Culbertson, S. Dai, H. Luo, and D. DePaoli, "Low-pressure solubility of carbon dioxide in room-temperature ionic liquids measured with a quartz crystal microbalance," *J. Phys. Chem. B*, vol. 108, pp. 721-727, 2004.
- [146] A. Shariati and C. Peters, "High-pressure phase behavior of systems with ionic liquids:: Part III. The binary system carbon dioxide+ 1-hexyl-3-

- methylimidazolium hexafluorophosphate," *The Journal of Supercritical Fluids*, vol. 30, pp. 139-144, 2004.
- [147] W. Ren, B. Sensenich, and A. Scurto, "High-pressure phase equilibria of (carbon dioxide (CO₂) + n-alkyl-imidazolium bis (trifluoromethylsulfonyl) amide) ionic liquids," *The Journal of Chemical Thermodynamics*, vol. 42, pp. 305-311, 2010.
- [148] G. Hong, J. Jacquemin, M. Deetlefs, C. Hardacre, P. Husson, and M. Costa Gomes, "Solubility of carbon dioxide and ethane in three ionic liquids based on the bis {(trifluoromethyl) sulfonyl} imide anion," *Fluid Phase Equilibria*, vol. 257, pp. 27-34, 2007.
- [149] P. Kilaru and P. Scovazzo, "Correlations of Low-Pressure Carbon Dioxide and Hydrocarbon Solubilities in Imidazolium-, Phosphonium-, and Ammonium-Based Room-Temperature Ionic Liquids. Part 2. Using Activation Energy of Viscosity," *Ind. Eng. Chem. Res.*, vol. 47, pp. 910-919, 2008.
- [150] D. Kodama, M. Kanakubo, M. Kokubo, T. Ono, H. Kawanami, T. Yokoyama, H. Nanjo, and M. Kato, "CO₂ absorption properties of Brønsted acid-base ionic liquid composed of N, N-dimethylformamide and bis (trifluoromethanesulfonyl) amide," *The Journal of Supercritical Fluids*, vol. 52, pp. 189-192, 2010.
- [151] Z. Fenga, F. Cheng-Gangb, W. You-Tingb, W. Yuan-Taob, L. Ai-Mina, and Z. Zhi-Bingb, "Absorption of CO₂ in the aqueous solutions of functionalized ionic liquids," *Chemical Engineering Journal*, vol. 160 pp. 691–697, 2010.
- [152] J. Palgunadi, J. Kang, D. Nguyen, J. Kim, B. Min, S. Lee, H. Kim, and H. Kim, "Solubility of CO₂ in dialkylimidazolium dialkylphosphate ionic liquids," *Thermochimica Acta*, vol. 494, pp. 94-98, 2009.
- [153] P. Carvalho, V. Álvarez, I. Marrucho, M. Aznar, and J. Coutinho, "High carbon dioxide solubilities in trihexyltetradecylphosphonium-based ionic liquids," *The Journal of Supercritical Fluids*, vol. 52, pp. 258-265, 2010.

- [154] S. Zhang, Y. Chen, X. Rex, Y. Zhang, J. Zhang, and X. Zhang, "Solubility of CO₂ in sulfonate ionic liquids at high pressure," *J. Chem. Eng. Data*, vol. 50, pp. 230-233, 2005.
- [155] L. Ferguson and P. Scovazzo, "Solubility, diffusivity, and permeability of gases in phosphonium-based room temperature ionic liquids: data and correlations," *Ind. Eng. Chem. Res.*, vol. 46, pp. 1369-1374, 2007.
- [156] T. Sarbu, T. J. Styraneč, and E. J. Beckman, "Design and synthesis of low cost, sustainable CO₂-philes," *Industrial & Engineering Chemistry Research*, vol. 39, pp. 4678-4683, 2000.
- [157] S. Kazarian, B. Briscoe, and T. Welton, "Combining ionic liquids and supercritical fluids: in situ ATR-IR study of CO₂ dissolved in two ionic liquids at high pressures," *Chem. Commun.*, vol. 2000, pp. 2047-2048, 2000.
- [158] M. Kanakubo, T. Umecky, Y. Hiejima, T. Aizawa, H. Nanjo, and Y. Kameda, "Solution Structures of 1-Butyl-3-methylimidazolium Hexafluorophosphate Ionic Liquid Saturated with CO₂: Experimental Evidence of Specific Anion-CO₂ Interaction," *J. Phys. Chem. B*, vol. 109, pp. 13847-13850, 2005.
- [159] P. Scovazzo, J. Kieft, D. Finan, C. Koval, D. DuBois, and R. Noble, "Gas separations using non-hexafluorophosphate [PF₆]-anion supported ionic liquid membranes," *Journal of Membrane Science*, vol. 238, pp. 57-63, 2004.
- [160] A. Jalili, A. Mehdizadeh, M. Shokouhi, H. Sakhaeinia, and V. Taghikhani, "Solubility of CO₂ in 1-(2-hydroxyethyl)-3-methylimidazolium ionic liquids with different anions," *The Journal of Chemical Thermodynamics*, vol. 42, pp. 787-791, 2010.
- [161] S. Mahurin, J. Lee, G. Baker, H. Luo, and S. Dai, "Performance of nitrile-containing anions in task-specific ionic liquids for improved CO₂/N₂ separation," *Journal of Membrane Science*, vol. 353, pp. 177-183, 2010.

- [162] Y. Kim, W. Choi, J. Jang, K. Yoo, and C. Lee, "Solubility measurement and prediction of carbon dioxide in ionic liquids," *Fluid Phase Equilibria*, vol. 228, pp. 439-445, 2005.
- [163] D. Camper, C. Becker, C. Koval, and R. Noble, "Low pressure hydrocarbon solubility in room temperature ionic liquids containing imidazolium rings interpreted using regular solution theory," *Ind. Eng. Chem. Res.*, vol. 44, pp. 1928-1933, 2005.
- [164] J. Kumelan, D. Tuma, and G. Maurer, "Partial molar volumes of selected gases in some ionic liquids," *Fluid Phase Equilibria*, vol. 275, pp. 132-144, 2009.
- [165] J. L. Anthony, J. L. Anderson, E. J. Maginn, and J. F. Brennecke, "Anion effects on gas solubility in ionic liquids," *J. Phys. Chem. B*, vol. 109, pp. 6366-6374, 2005.
- [166] X. Yuan, S. Zhang, J. Liu, and X. Lu, "Solubilities of CO₂ in hydroxyl ammonium ionic liquids at elevated pressures," *Fluid Phase Equilibria*, vol. 257, pp. 195-200, 2007.
- [167] J. Bara, C. Gabriel, T. Carlisle, D. Camper, A. Finotello, D. Gin, and R. Noble, "Gas separations in fluoroalkyl-functionalized room-temperature ionic liquids using supported liquid membranes," *Chemical Engineering Journal*, vol. 147, pp. 43-50, 2009.
- [168] X. Zhang, Z. Liu, and W. Wang, "Screening of ionic liquids to capture CO₂ by COSMO RS and experiments," *AIChE Journal*, vol. 54, pp. 2717-2728, 2008.
- [169] J. Bara, C. Gabriel, S. Lessmann, T. Carlisle, A. Finotello, D. Gin, and R. Noble, "Enhanced CO₂ separation selectivity in oligo (ethylene glycol) functionalized room-temperature ionic liquids," *Ind. Eng. Chem. Res.*, vol. 46, pp. 5380-5386, 2007.
- [170] H. Xing, T. Wang, Z. Zhou, and Y. Dai, "Novel Brønsted-acidic ionic liquids for esterifications," *Ind. Eng. Chem. Res.*, vol. 44, pp. 4147-4150, 2005.

- [171] B. Gurkan, J. de la Fuente, E. Mindrup, L. Ficke, B. Goodrich, E. Price, W. Schneider, and J. Brennecke, "Equimolar CO₂ Absorption by Anion-Functionalized Ionic Liquids," *J. of the American Chem. Soci.*, vol. 132, pp. 2116-2117, 2010.
- [172] Y. Zhang, S. Zhang, X. Lu, Q. Zhou, W. Fan, and X. Zhang, "Dual Amino Functionalised Phosphonium Ionic Liquids for CO₂ Capture," *Chemistry–A European Journal*, vol. 15, pp. 3003-3011, 2009.
- [173] J. Huang, A. Riisager, R. Berg, and R. Fehrmann, "Tuning ionic liquids for high gas solubility and reversible gas sorption," *Journal of Molecular Catalysis A: Chemical*, vol. 279, pp. 170-176, 2008.
- [174] J. Zhang, Q. Zhang, B. Qiao, and Y. Deng, "Solubilities of the gaseous and liquid solutes and their thermodynamics of solubilization in the novel room-temperature ionic liquids at infinite dilution by gas chromatography," *J. Chem. Eng. Data*, vol. 52, pp. 2277-2283, 2007.
- [175] T. Carlisle, J. Bara, C. Gabriel, R. Noble, and D. Gin, "Interpretation of CO₂ solubility and selectivity in nitrile-functionalized room-temperature ionic liquids using a group contribution approach," *Industrial & Engineering Chemistry Research*, vol. 47, pp. 7005-7012, 2008.
- [176] Y. Hou and R. E. Baltus, "Experimental measurement of the solubility and diffusivity of CO₂ in room-temperature ionic liquids using a transient thin-liquid-film method," *Industrial & Engineering Chemistry Research*, vol. 46, pp. 8166-8175, 2007.
- [177] J. Jacquemin, P. Husson, V. Majer, and M. F. Costa Gomes, "Influence of the cation on the solubility of CO₂ and H₂ in ionic liquids based on the bis (trifluoromethylsulfonyl) imide anion," *J. of solution chem.*, vol. 36, pp. 967-979, 2007.
- [178] P. Scovazzo, D. Camper, J. Kieft, J. Poshusta, C. Koval, and R. Noble, "Regular solution theory and CO₂ gas solubility in room-temperature ionic

- liquids," *Industrial & Engineering Chemistry Research*, vol. 43, pp. 6855-6860, 2004.
- [179] A. L. Revelli, F. Mutelet, and J. N. Jaubert, "High Carbon Dioxide Solubilities in Imidazolium-Based Ionic Liquids and in Poly (ethylene glycol) Dimethyl Ether," *J. Phys. Chem. B*, pp. 897-907, 2010.
- [180] M. Shiflett, D. Drew, R. Cantini, and A. Yokozeki, "Carbon Dioxide Capture Using Ionic Liquid 1-Butyl-3-Methylimidazolium Acetate," *Energy & Fuels*, pp. 1652-1654.
- [181] G. Wang, W. Hou, F. Xiao, J. Geng, Y. Wu, and Z. Zhang, "Low-Viscosity Triethylbutylammonium Acetate as a Task-Specific Ionic Liquid for Reversible CO₂ Absorption," *Journal of Chemical & Engineering Data*, pp. 4467-4475.
- [182] A. K. Ziyada, C. D. Wilfred, M. A. Bustam, Z. Man, and T. Murugesan, "Thermophysical Properties of 1-Propyronitrile-3-alkylimidazolium Bromide Ionic Liquids at Temperatures from (293.15 to 353.15) K," *J. Chem. Eng. Data*, vol. 55, pp. 3886-3890, 2010.
- [183] K. N. Marsh, J. F. Brennecke, R. D. Chirico, M. Frenkel, A. Heintz, J. W. Magee, C. J. Peters, L. P. N. Rebelo, and K. R. Seddon, "Thermodynamic and Thermophysical Properties of The Reference Ionic Liquid: 1-Hexyl-3-methylimidazolium bis [(trifluoromethyl) sulfonyl] amide (Including Mixtures) Part 1. Experimental Methods and Results (IUPAC Technical Report)," *Pure and appl. chem.*, vol. 81, pp. 781-790, 2009.
- [184] J. Jacquemin, M. Anouti, and D. Lemordant, "Physico-Chemical Properties of Non-Newtonian Shear Thickening Diisopropyl-ethylammonium-Based Protic Ionic Liquids and Their Mixtures with Water and Acetonitrile," *J. Chem. Eng. Data*.

- [185] M. Nadeen, "A study on Enhanced Oil recovery by Surfactants for a Malaysian Sandstone Reser," Ph.D, Chemical Engineering, Universiti Teknologi PETRONAS, Bandar Seri Iskandar, 2007.
- [186] S. P. Ottiger, "Competitive Adsorption and Chromatography at Supercritical Conditions," Ph.D, Chemical Engineering, Zurich, 2008.
- [187] O. Talu, "Needs, status, techniques and problems with binary gas adsorption experiments," *Advances in Colloid and Interface Science*, vol. 76, pp. 227-269, 1998.
- [188] Y. Belmabkhout, M. Frere, and G. D. Weireld, "High-pressure adsorption measurements. A comparative study of the volumetric and gravimetric methods," *Measurement Science and Technology*, vol. 15, p. 848, 2004.
- [189] J. Keller and E. Robens, "A note on sorption measuring instruments," *Journal of Thermal Analysis and Calorimetry*, vol. 71, pp. 37-45, 2003.
- [190] C. H. Massen, E. Robens, J. A. Poullis, and T. Gast, *Thermochim. Acta*, vol. 82, p. 43, 1984.
- [191] S. V. Dzyuba, "Synthesis, Properties and Applications of Ionic Liquids," Ph.D, Chemistry, Texas Tech University, 2002.
- [192] P. B., A.-P. Dias, N. Papageorgiou, K. Kalyanasundaram, and M. G., "Hydrophobic, Highly Conductive Ambient-Temperature Molten Salts," *Inorg. Chem.*, vol. 35, pp. 1168-1178, 1996.
- [193] K. Nobuoka, S. Kitaoka, M. Iio, T. Harran, and Y. Ishikawa, "Solute-solvent interactions in imidazolium camphorsulfonate ionic liquids," *Physical Chemistry Chemical Physics*, vol. 9, pp. 5891-5896, 2007.
- [194] P. Bonhote, A. P. Dias, N. Papageorgiou, K. Kalyanasundaram, and M. Grätzel, "Hydrophobic, highly conductive ambient-temperature molten salts," *Inorganic chemistry*, vol. 35, pp. 1168-1178, 1996.

- [195] B. Cabovska, "Investigations of Separation Mechanisms in Capillary Electrophoresis and High Performance Liquid Chromatography," Ph.D, Chemistry, University of Cincinnati, 2003.
- [196] P. Bonhote, A. P. Dias, N. Papageorgiou, K. Kalyanasundaram, and M. Gratzel, "Hydrophobic, highly conductive ambient-temperature molten salts," *Inorg. Chem. Commun.*, vol. 35, pp. 1168–1178, 1996.
- [197] D. Zhao, Z. Fei, C. A. Ohlin, G. Laurency, and P. J. Dyson, "Dual-functionalised ionic liquids: synthesis and characterisation of imidazolium salts with a nitrile-functionalised anion," *Chem. Commun.*, vol. 2004, pp. 2500-2501, 2004.
- [198] R. L. Gardas, H. F. Costa, M. G. Freire, P. J. Carvalho, I. M. Marrucho, I. M. A. Fonseca, A. G. M. Ferreira, and J. A. P. Coutinho, "Densities and derived thermodynamic properties of imidazolium-, pyridinium-, pyrrolidinium-, and piperidinium-based ionic liquids," *J. Chem. Eng. Data*, vol. 53, pp. 805-811, 2008.
- [199] J. M. Crosthwaite, M. J. Muldoon, J. K. Dixon, J. L. Anderson, and J. F. Brennecke, "Phase transition and decomposition temperatures, heat capacities and viscosities of pyridinium ionic liquids," *J. Chem. Thermodyn.*, vol. 37 pp. 559-568, 2005.
- [200] R. L. Gardas and J. A. P. Coutinho, "Extension of the Ye and Shreeve group contribution method for density estimation of ionic liquids in a wide range of temperatures and pressures," *Fluid Phase Equilib.*, vol. 263, pp. 26-32, 2008.
- [201] P. Nockeman, M. Pellens, K. V. Hecke, L. V. Meervelt, J. Wouters, B. Thijs, E. Vanecht, T. N. Parac-Vogt, H. Mehdi, S. Schaltin, J. Fransaer, S. Zahn, B. Kirchner, and K. Binnemans, "Cobalt (II) Complexes of Nitrile Functionalized Ionic Liquids," *Chemistry—A European Journal*, vol. 16, pp. 1849-1858, 2010.

- [202] E. Gómez, N. Calvar, Á. Domínguez, and E. A. Macedo, "Synthesis and temperature dependence of physical properties of four pyridinium-based ionic liquids: Influence of the size of the cation," *J. Chem. Thermodyn.*, 2010.
- [203] J. Hou, Z. Zhang, and L. A. Madsen, "Cation/Anion Associations in Ionic Liquids Modulated by Hydration and Ionic Medium," *The Journal of Physical Chemistry B*, 2011.
- [204] N. M. Yunus, M. I. A. Mutalib, Z. Man, M. A. Bustam, and T. Murugesan, "Thermophysical properties of 1-alkylpyridinium bis(trifluoromethylsulfonyl)imide ionic liquids," *J. Chem. Thermodyn.*, vol. 42, pp. 491–495, 2010.
- [205] K. Tsunashima, E. Niwa, S. Kodama, M. Sugiya, and Y. Ono, "Thermal and Transport Properties of Ionic Liquids Based on Benzyl-Substituted Phosphonium Cations," *J. Phy. Chem. B*, vol. 113, pp. 15870-15874, 2009.
- [206] T. Ramnial, "The Chemistry of Imidazolium Salts and Phosphonium-Based Ionic Liquids," Ph.D, Chemistry, Simon Fraser, Burnaby, 2006.
- [207] A. B. Pereiro, H. I. M. Veiga, J. M. S. S. Esperança, and A. Rodríguez, "Effect of Temperature on the Physical Properties of two Ionic Liquids," *J. Chem. Thermodyn.*, vol. 41, pp. 1419-1423, 2009.
- [208] H. D. B. Jenkins and L. Glasser, "Standard absolute entropies, S°_{298} , from volume or density 1. Inorganic materials," *Inorg. Chem.*, vol. 42, pp. 8702-8708, 2003.
- [209] A. Finotello, J. E. Bara, S. Narayan, D. Camper, and R. D. Noble, "Ideal gas solubilities and solubility selectivities in a binary mixture of room-temperature ionic liquids," *J. Phys. Chem. B.*, vol. 112, pp. 2335-2339, 2008.
- [210] D. E. Camper, "Gas Solubility and Diffusion in Room Temperature Ionic Liquids with an Emphasis on Gas Separations," Ph.D, Chemical Engineering, University of Colorado, 2006.

- [211] J. M. Pringle, J. Golding, K. Baranyai, C. M. Forsyth, G. B. Deacon, J. L. Scott, and D. R. MacFarlane, "The effect of anion fluorination in ionic liquids—physical properties of a range of bis (methanesulfonyl) amide salts," *New J. Chem.*, vol. 27, pp. 1504-1510, 2003.
- [212] J. C. Kotz, P. Treichel, and J. R. Townsend, *Chemistry & chemical reactivity*: Brooks/Cole Pub Co, 2008.
- [213] S. N. V. K. Aki, B. R. Mellein, E. M. Saurer, and J. F. Brennecke, "High-pressure phase behavior of carbon dioxide with imidazolium-based ionic liquids," *The Journal of Physical Chemistry B*, vol. 108, pp. 20355-20365, 2004.
- [214] L. A. Blanchard, Z. Gu, and J. F. Brennecke, "High-pressure phase behavior of ionic liquid/CO₂ systems," *J. Phys. Chem. B.*, vol. 105, pp. 2437-2444, 2001.
- [215] J. H. Davis and P. A. Fox, "From curiosities to commodities: ionic liquids begin the transition," *Chem. Commun*, vol. 3, pp. 1209–1212, 2003.
- [216] W. Xu, E. I. Cooper, and C. A. Angell, "Ionic liquids: ion mobilities, glass temperatures, and fragilities," *The Journal of Physical Chemistry B*, vol. 107, pp. 6170-6178, 2003.
- [217] D. Zhao, "Design, synthesis and applications of functionalized ionic liquids," M.Sc., Chemistry, Xinan Petroleum University, Nanchong, China, 2007.
- [218] P. J. Carvalho and J. A. P. Coutinho, "On the nonideality of CO₂ solutions in ionic liquids and other low volatile solvents," *J. Phys. Chem. Letters*, vol. 1, pp. 774-780, 2010.
- [219] S. Kanematsu, K. Matsumoto, and R. Hagiwara, "Electrochemically stable fluorohydrogenate ionic liquids based on quaternary phosphonium cations," *Electrochem. Commun.*, vol. 11, pp. 1312-1315, 2009.

- [220] T. Seki, J. D. Grunwaldt, and A. Baiker, "In Situ Attenuated Total Reflection Infrared Spectroscopy of Imidazolium-Based Room-Temperature Ionic Liquids under "Supercritical" CO₂," *J. Phys. Chem. B.*, vol. 113, pp. 114-122, 2008.
- [221] A. Henni, P. Tontiwachwuthikul, and A. Chakma, "Solubilities of carbon dioxide in polyethylene glycol ethers," *The Canadian Journal of Chemical Engineering*, vol. 83, pp. 358-361, 2005.
- [222] Y. Xu, R. P. Schutte, and L. G. Hepler, "Solubilities of carbon dioxide, hydrogen sulfide and sulfur dioxide in physical solvents," *The Canadian Journal of Chemical Engineering*, vol. 70, pp. 569-573, 1992.
- [223] H. W. Pennline, D. R. Luebke, K. L. Jones, C. R. Myers, B. I. Morsi, Y. J. Heintz, and J. B. Ilconich, "Progress in carbon dioxide capture and separation research for gasification-based power generation point sources," *Fuel Processing Technology*, vol. 89, pp. 897-907, 2008.
- [224] M. Hasib-ur-Rahman, M. Siaj, and F. Larachi, "Ionic liquids for CO₂ capture-- Development and progress," *Chemical Engineering and Processing: Process Intensification*, vol. 49, pp. 313-322, 2010.
- [225] A. Finotello, J. E. Bara, D. Camper, and R. D. Noble, "Room-temperature ionic liquids: temperature dependence of gas solubility selectivity," *Industrial & Engineering Chemistry Research*, vol. 47, pp. 3453-3459, 2008.
- [226] J. L. Anderson, J. N. K. Dixon, and J. F. Brennecke, "Solubility of CO₂, CH₄, C₂H₆, C₂H₄, O₂, and N₂ in 1-Hexyl-3-methylpyridinium Bis (trifluoromethylsulfonyl) imide: Comparison to Other Ionic Liquids," *Accounts of chemical research*, vol. 40, pp. 1208-1216, 2007.

PUBLICATIONS

Journal Publications:

Published papers

- [1] A. K. Ziyada, C. D. Wilfred, M. A. Bustam, Z. Man, and T. Murugesan, "Thermophysical Properties of 1-Propyronitrile-3-alkylimidazolium Bromide Ionic Liquids at Temperatures from (293.15 to 353.15) K," *J. Chem. Eng. Data*, vol. 55, pp. 3886-3890, 2010.
- [2] A. K. Ziyada, M. A. Bustam, C. D. Wilfred, and T. Murugesan, "Densities, viscosities and refractive Indices of 1-hexyl-3-propanenitrile imidazolium Ionic Liquids Incorporated with Sulfonate –based Anions," *J. Chem. Eng. Data*, vol. 56, pp. 2343-2338, 2011.
- [3] A. K. Ziyada, M. A. Bustam, T. Murugesan, and C. D. Wilfred, "Effect of sulfonate-based anions on the physicochemical properties of 1-alkyl-3-propanenitrile imidazolium ionic liquids," *New J. Chem.*, vol. 35, pp. 1111-1116, 2011.
- [4] A. K. Ziyada, C. D. Wilfred, and M. A. Bustam, "Synthesis and Physiochemical Properties of Supramolecular Phosphonium–Based Symmetrical Dicationic Ionic Liquids," *J. Appl. Sci.*, vol. 11, pp. 1356-1360, 2011.
- [5] A. K. Ziyada, C. D. Wilfred, M. A. Bustam, Z. Man, and T. Murugesan, "Thermophysical Properties of trihexyltetradecylphosphonium dioctylsulfosuccinate ionic liquid," *J. Appl. Sci.*, vol. 11, pp. 1396-1400, 2011.

- [6] M. M. Taib, A. K. Ziyada, C. D. Wilfred, and T. Murugesan, "Thermophysical properties of 1-propyronitrile-3-hexylimidazolium bromide + methanol at temperatures (293.15 to 323.15)K," *Journal of Molecular Liquids*, vol. 158, pp. 101-104, 2011.
- [7] A. K. Ziyada, C. D. Wilfred, and T. Murugesan, "Densities, viscosities and refractive Indices of 1-hexyl-3-propanenitrile imidazolium chloride Ionic Liquids," *J. Phys. Chem. Liquid*, ID GPCH-2010-0096. 2010. (in press).
- [8] M. M. Taib, A. K. Ziyada, C. D. Wilfred, and T. Murugesan, "Volumetric Properties and Refractive Indices for the Binary Mixture of 1-Propyronitrile-3-hexylimidazolium Bromide + Ethanol at Temperatures (293.15 to 323.15)K," *Sol. Chem. J*, Accepted (April 2011).

Submitted papers

- [9] A. K. Ziyada, M. A. Bustam, and C. D. Wilfred, "Synthesis and Physiochemical Properties of Monocationic and Dicationic Phosphonium Ionic Liquids Incorporating Dioctylsulfosuccinate Anion," *Malaysian Journal of Chemistry*, (Submitted).
- [10] A. K. Ziyada, M. A. Bustam, C. D. Wilfred and T. Murugesan, "Densities, Viscosities and Refractive indices of 1-octyl-3-propanenitrile imidazolium-based Ionic Liquids: Effect of Temperature and Anion", *J. Chem. Thermodynamics*, (Submitted).
- [11] A. K. Ziyada, M. A. Bustam, and C. D. Wilfred and T. Murugesan, "Cation and Anion Sizes Influence in the Temperature Dependence of the Thermophysical Properties of Nitrile Functionalized Imidazolium-Based Ionic Liquids at Temperatures (293.15 to 353.15) K," *J. Chem. Eng. Data*"-(submitted).

- [12] N. Muhammad, Z. Mana, A. K. Ziyada, C. D. Wilfred, M. A. Bustam and T. Murugesan, "Thermophysical Properties of Dual Functionalized Imidazolium-based ionic liquids", " *J. Chem. Eng. Data*"-(submitted).

Conference Proceeding:

- [1] A. K. Ziyada, C. D. Welfrid, M. A. Bustam, and Z. Man, "Synthesis and Characterization of Imidazolium-Based Symmetrical Dicationic Ionic Liquids," in *22nd Symposium Of Malaysian Chemical Engineers*, Kuala Lumpur, 2008, pp. 875-880.
- [2] A. K. Ziyada, M. A. Bustam, C. D. Wilfred, and Z. Man, "Synthesis and Thermophysical Properties of Novel Phosphonium-Based Dicationic Ionic Liquids," in *Regional Conferenece on Ionic Liquids*, Kuala Lumpur-Malaysia, 2009, p. 43.
- [3] A. K. Ziyada, C. D. Wilfred, M. A. Bustam, Z. Man, and T. Murugesan, "Thermophysical Properties of trihexyltetradecylphosphonium dioctylsulfosuccinate ionic liquid," in *International Conference on Fundamental and Applied Sciences*, Kuala Lumpur-Malaysia, 2010.
- [4] A. K. Ziyada, C. D. Wilfred, and M. A. Bustam, "Synthesis and Physiochemical Properties of Supramoelcular Phosphonium-Based Symmetrical Dicationic Ionic Liquids," in *International Conference on Fundamental and Applied Sciences*, Kuala Lumpur-Malaysia, 2010.
- [5] A. K. Ziyada, M. A. Bustam, and C. D. Wilfred, "Synthesis and Thermophysical Characterization of Trioctyltetradecylphosphonium-Based Room Temperature Ionic Liquids," in *3rd International Conference For Young Chemists*, Penang-Malaysia, 2010.
- [6] A. K. Ziyada, C. D. Wilfred, and M. A. Bustama, "Synthesis and Physiochemical Properties of Monocationic and Dicationic Phosphonium Ionic

Liquids Incorporating Dioctylsulfosuccinate Anion," in *16th Malaysian Chemical Congress*, Kuala Lumpur-Malaysia, 2010.

- [7] C. D. Wilfred, M. A. Bustama, Z. Man and A. K. Ziyada, "Effect of alkyl chains of cation and anion on the thermophysical properties of propanenitrile imidazolium based ionic liquids" *Congress on Ionic Liquids; COIL*" Washington DC, USA, June, 2011.

APPENDIX A

Experimental data for characterization and thermophysical properties

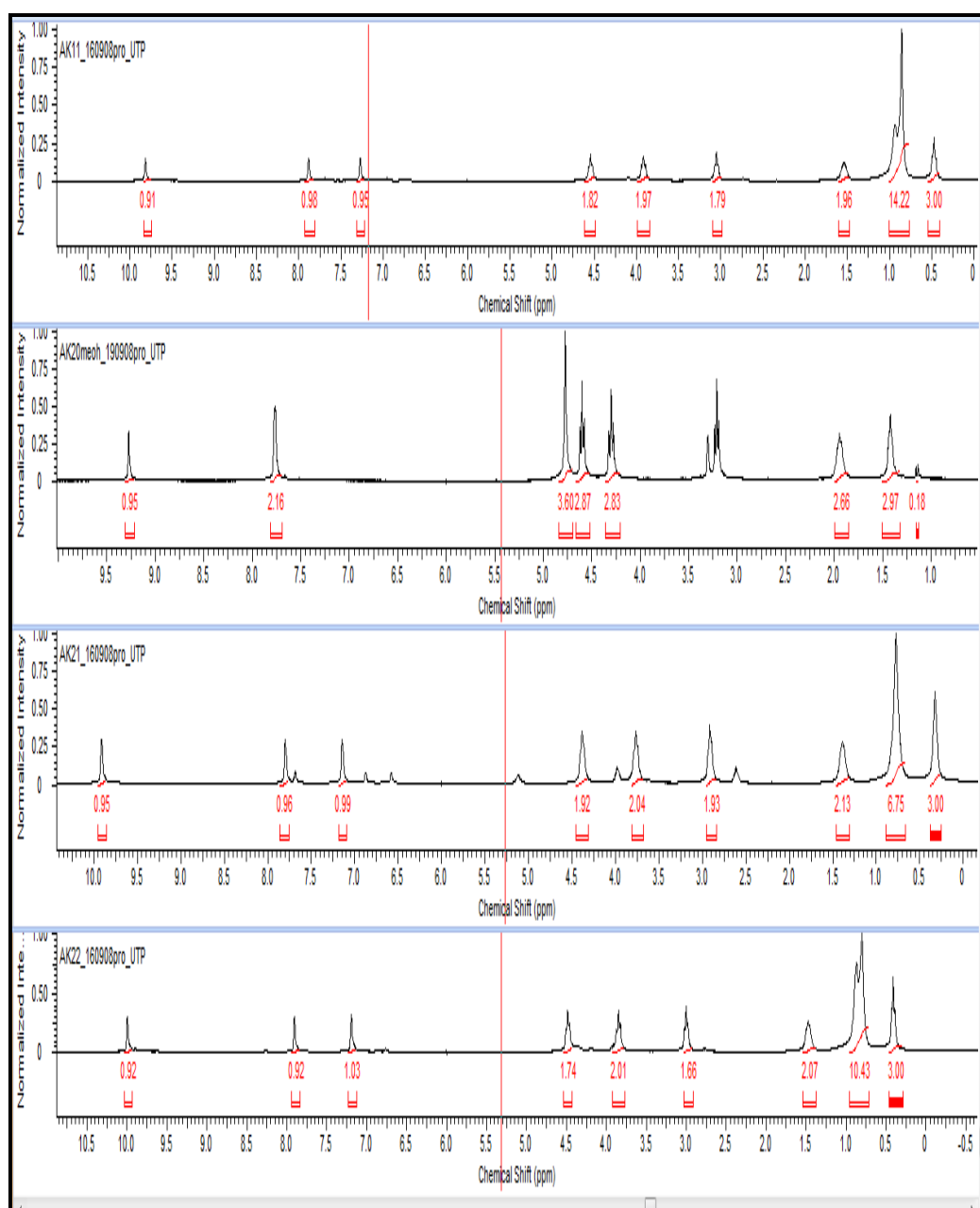


Fig A-1 ^1H NMR spectra for $[\text{C}_2\text{CN C}_n\text{im}]\text{Br}$ RTILs

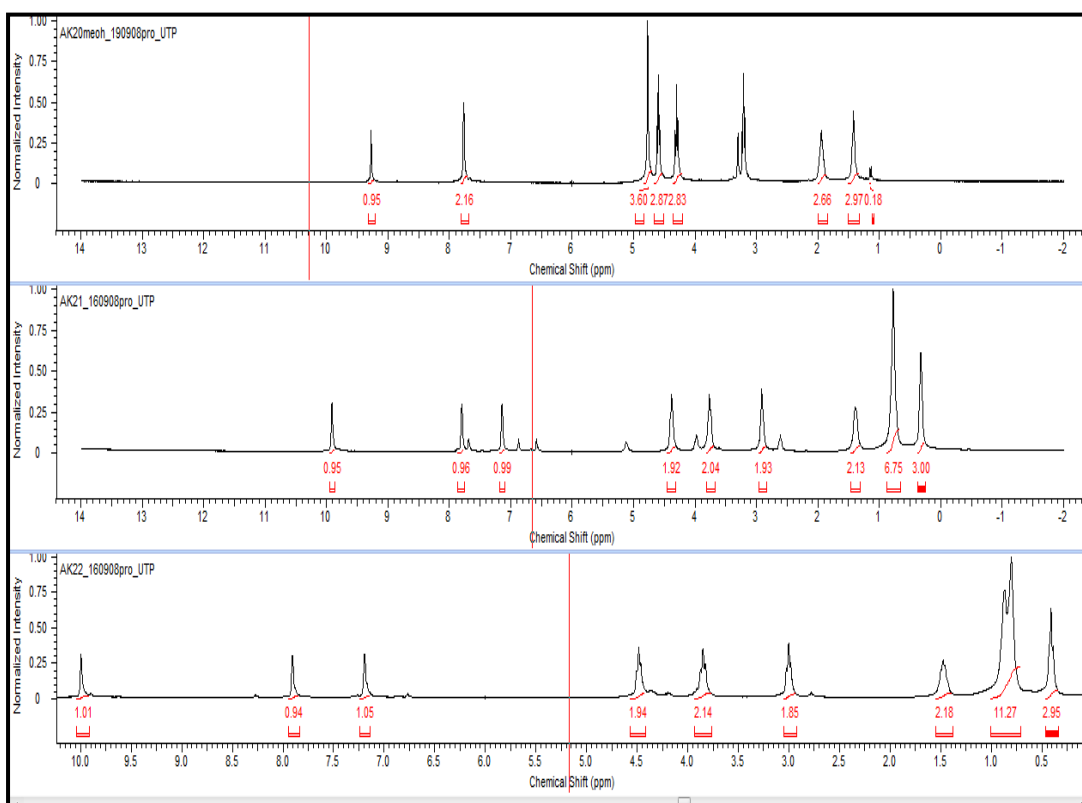


Fig A-2 ^1H NMR spectra for $[\text{C}_2\text{CN C}_n\text{im}]\text{Cl}$ RTILs

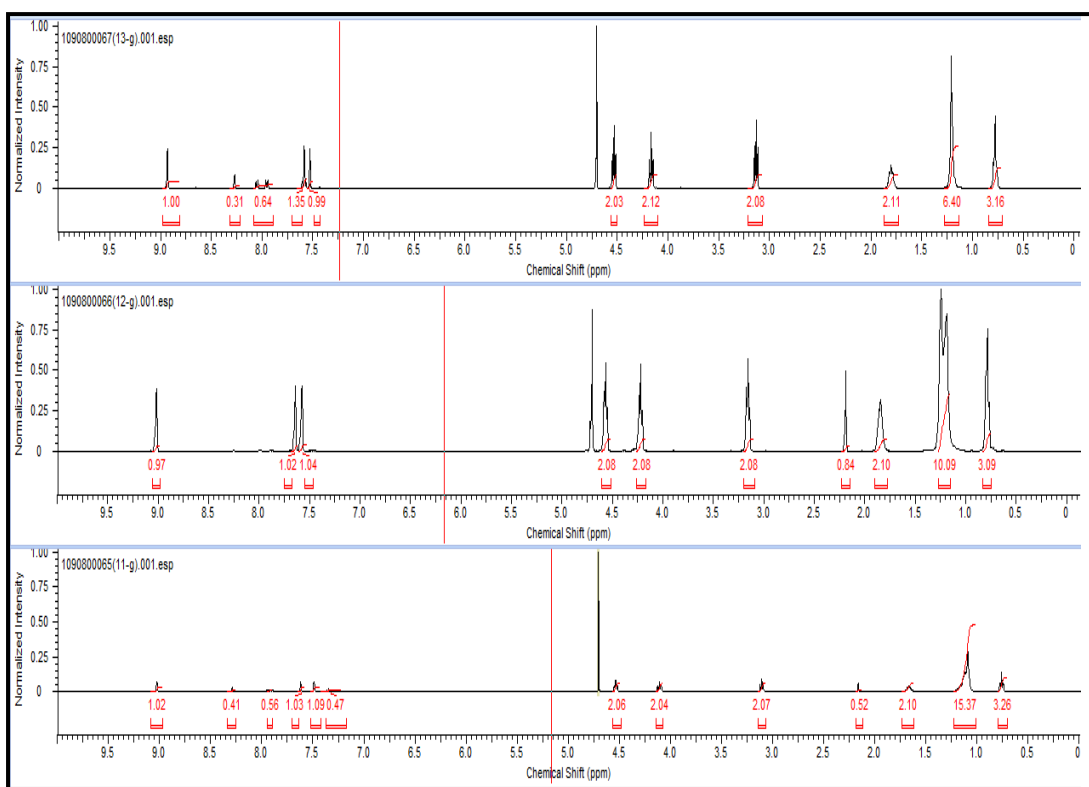


Fig A-3 ^1H NMR spectra for $[\text{C}_2\text{CN C}_n\text{im}]\text{SBA}$ RTILs

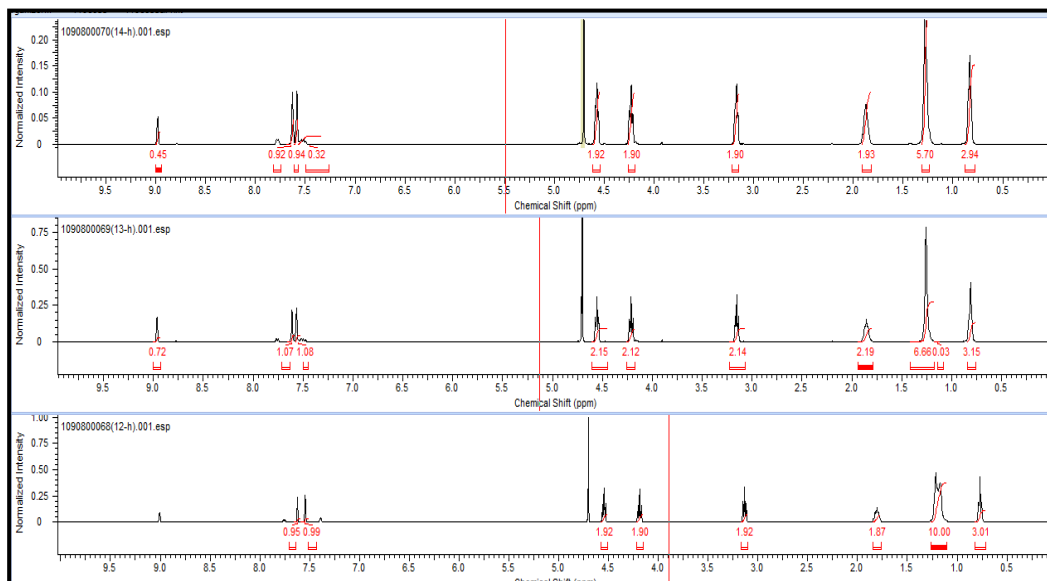


Fig A-4 ^1H NMR spectra for $[\text{C}_2\text{CN C}_n\text{im}]\text{BS}$ RTILs

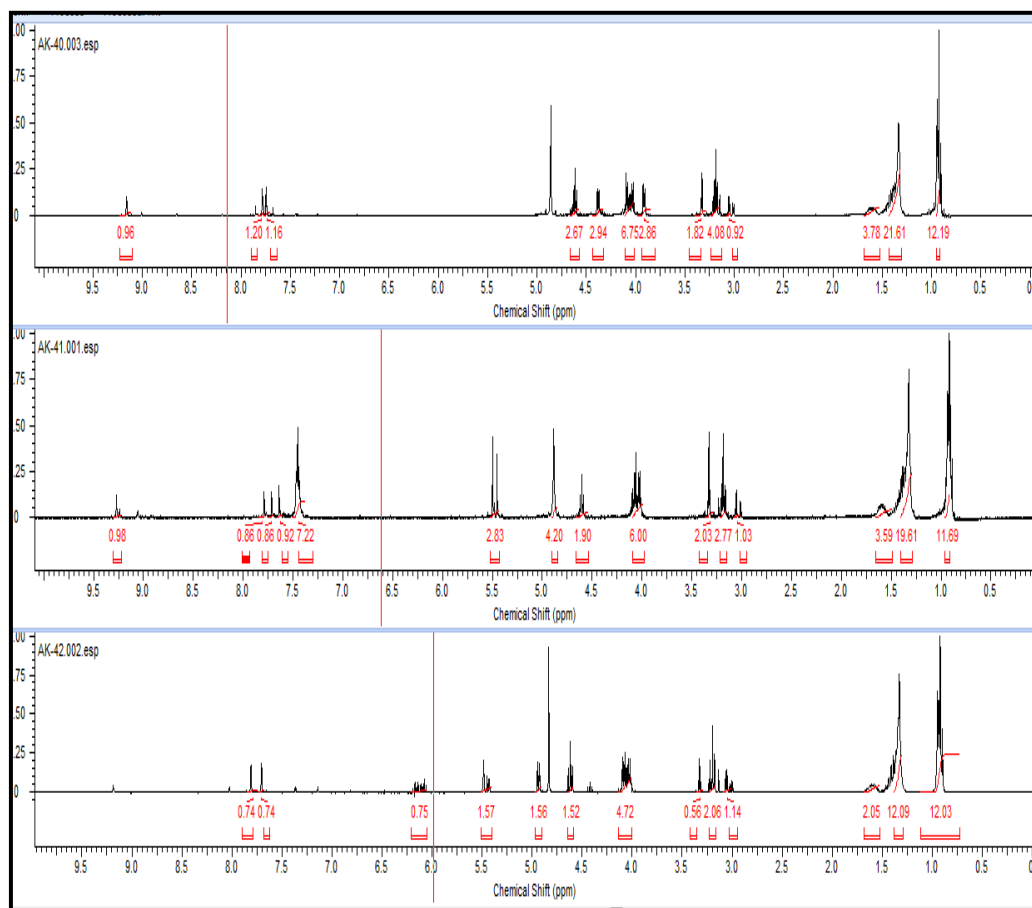


Fig A-5 ^1H NMR spectra for dual functionalized RTILs

Table A-1 Experimental densities ρ for [C₂CN C_nim]Br as a function of temperature.

T/K	$\rho/(\text{g}\cdot\text{cm}^{-3})$			
	[C ₂ CN Bim]Br	[C ₂ CN Him]Br	[C ₂ CN Oim]Br	[C ₂ CN Dim]Br
293.15	1.2985	1.2324	1.1801	-
298.15	1.2947	1.2290	1.1766	-
303.15	1.2911	1.2256	1.1732	-
308.15	1.2877	1.2223	1.1698	1.1292
313.15	1.2843	1.2190	1.1664	1.1245
318.15	1.281	1.2157	1.1630	1.1206
323.15	1.2776	1.2124	1.1596	1.1162
328.15	1.2744	1.2091	1.1562	1.1132
333.15	1.2712	1.2058	1.1529	1.110
338.15	1.2679	1.2025	1.1495	1.1067
343.15	1.2647	1.1992	1.1461	1.1035
348.15	1.2614	1.1959	1.1428	1.1002
353.15	1.2582	1.1927	1.1396	1.0969

Table A-2 Experimental densities for [C₂CN C_nim]Cl as a function of temperature

T/K	$\rho/(\text{g}\cdot\text{cm}^{-3})$		
	[C ₂ CN Bim]Cl	[C ₂ CN Him]Cl	[C ₂ CN Oim]Cl
293.15	1.1003	1.0770	1.0455
298.15	1.0973	1.0741	1.0427
303.15	1.0943	1.0708	1.0391
308.15	1.0913	1.0677	1.0364
313.15	1.0884	1.0653	1.0340
318.15	1.0854	1.0624	1.0310
323.15	1.0825	1.0594	1.0282
328.15	1.0796	1.0561	1.0247
333.15	1.0767	1.0533	1.0220
338.15	1.0737	1.0506	1.0191
343.15	1.0707	1.0474	1.0160
348.15	1.0678	1.0448	1.0134
353.15	1.0649	1.0416	1.0106

Table A- 3 Experimental densities for [C₂CNC_nim]DOSS as a function of temperature

T/K	$\rho/(\text{g}\cdot\text{cm}^{-3})$			
	[C ₂ CN Bim]	[C ₂ CN Him]	[C ₂ CN Oim]	[C ₂ CN Dim]
	DOSS	DOSS	DOSS	DOSS
293.15	1.1152	1.0927	1.0579	1.0392
298.15	1.1109	1.0890	1.0543	1.0348
303.15	1.1058	1.0854	1.0508	1.0307
308.15	1.1009	1.0818	1.0473	1.0277
313.15	1.0982	1.0783	1.0439	1.0241
318.15	1.0943	1.0748	1.0404	1.0202
323.15	1.0902	1.0713	1.0370	1.0178
328.15	1.0867	1.0679	1.0336	1.0145
333.15	1.0827	1.0644	1.0302	1.0114
338.15	1.0793	1.0610	1.0267	1.0081
343.15	1.0758	1.0576	1.0233	1.0048
348.15	1.0713	1.0542	1.0199	1.0019
353.15	1.0686	1.0507	1.0165	0.9997

Table A- 4 Experimental densities for [C₂CNC_nim]DDS as a function of temperature.

T/K	$\rho/(\text{g}\cdot\text{cm}^{-3})$			
	[C ₂ CN Bim]	[C ₂ CN Him]	[C ₂ CN Oim]	[C ₂ CN Dim]
	DDS	DDS	DDS	DDS
293.15	1.1404	1.1331	1.0849	1.0697
298.15	1.1369	1.1298	1.0817	1.0666
303.15	1.1335	1.1265	1.0785	1.0635
308.15	1.1304	1.1232	1.0751	1.0600
313.15	1.1266	1.1200	1.0724	1.0578
318.15	1.1240	1.1167	1.0686	1.0534
323.15	1.1205	1.1135	1.0655	1.0505
328.15	1.1175	1.1103	1.0623	1.0472
333.15	1.1139	1.1071	1.0592	1.0444
338.15	1.1107	1.1039	1.0561	1.0413
343.15	1.1078	1.1008	1.0532	1.0384
348.15	1.1050	1.0976	1.0500	1.0350
353.15	1.1016	1.0946	1.0469	1.0321

Table A- 5 Experimental densities for [C₂CN C_nim]SBA as a function of temperature.

T/K	$\rho/(\text{g}\cdot\text{cm}^{-3})$		
	[C ₂ CN Him]SBA	[C ₂ CN Oim] SBA	[C ₂ CN Dim] SBA
293.15	1.2381	1.1859	1.1366
298.15	1.2346	1.1828	1.1335
303.15	1.2312	1.1794	1.1299
308.15	1.2280	1.1757	1.1263
313.15	1.2247	1.1721	1.1232
318.15	1.2215	1.1690	1.1198
323.15	1.2182	1.1656	1.1162
328.15	1.2150	1.1619	1.1127
333.15	1.2118	1.1583	1.1095
338.15	1.2086	1.1549	1.1059
343.15	1.2054	1.1512	1.1026
348.15	1.2021	1.1481	1.0993
353.15	1.1989	1.1444	1.0958

Table A- 6 Experimental densities for [C₂CN C_nim]BS as a function of temperature

T/K	$\rho/(\text{g}\cdot\text{cm}^{-3})$		
	[C ₂ CN Bim]BS	[C ₂ CN Him]BS	[C ₂ CN Oim]BS
293.15	1.2403	1.2260	1.1947
298.15	1.2368	1.2227	1.1912
303.15	1.2334	1.2194	1.1879
308.15	1.2302	1.2161	1.1847
313.15	1.2263	1.2128	1.1816
318.15	1.2237	1.2096	1.1783
323.15	1.2203	1.2063	1.1748
328.15	1.2171	1.2030	1.1714
333.15	1.2135	1.1997	1.1688
338.15	1.2101	1.1965	1.1655
343.15	1.2071	1.1933	1.1624
348.15	1.2044	1.1901	1.1581
353.15	1.2013	1.1878	1.1551

Table A- 7 Experimental densities for [C₂CN C_nim]TFMS as a function of temperature

T/K	$\rho/(\text{g}\cdot\text{cm}^{-3})$		
	[C ₂ CN Bim]TFMS	[C ₂ CN Him]TFMS	[C ₂ CN Oim]TFMS
293.15	1.3363	1.2896	1.2331
298.15	1.3324	1.2857	1.2294
303.15	1.3286	1.2819	1.2256
308.15	1.3250	1.2783	1.2220
313.15	1.3213	1.2746	1.2184
318.15	1.3177	1.2710	1.2147
323.15	1.3141	1.2674	1.2112
328.15	1.3105	1.2638	1.2076
333.15	1.3086	1.2602	1.2040
338.15	1.3032	1.2566	1.2005
343.15	1.2996	1.2531	1.1971
348.15	1.2959	1.2492	1.1932
353.15	1.2922	1.2458	1.1897

Table A- 8 Experimental densities for dual functionalized imidazolium-based ILs as function of temperature

T/K	$\rho/(\text{g}\cdot\text{cm}^{-3})$		
	[C ₂ CN Ayim]DOSS	[C ₂ CN Bzim]DOSS	[C ₂ CN Heim]DOSS
293.15	1.1782	1.2184	1.2631
298.15	1.1755	1.2152	1.2599
303.15	1.1727	1.2123	1.2565
308.15	1.1693	1.2089	1.2537
313.15	1.1661	1.2056	1.2504
318.15	1.1632	1.2029	1.2476
323.15	1.1604	1.2002	1.2447
328.15	1.1573	1.1968	1.2416
333.15	1.1541	1.1939	1.2384
338.15	1.151	1.1907	1.2353
343.15	1.1482	1.1878	1.2325
348.15	1.1451	1.1846	1.2296
353.15	1.1423	1.1821	1.2270

Table A- 9 Experimental densities for $[P_{8,8,8,14}]Cl$ and $[P_{8,8,8} C_n P_{8,8,8}]Cl_2$ as a function of temperature

T/K	$\rho/(g \cdot cm^{-3})$		
	$[P_{8,8,8,14}]Cl$	$[P_{8,8,8} C_6 P_{8,8,8}]Cl_2$	$[P_{8,8,8} C_{10} P_{8,8,8}]Cl_2$
293.15	1.0211	0.9252	0.8889
298.15	1.0185	0.9223	0.8858
303.15	1.0161	0.9193	0.8828
308.15	1.0142	0.9164	0.8797
313.15	1.0103	0.9135	0.8767
318.15	1.0079	0.9106	0.8736
323.15	1.0028	0.9077	0.8706
328.15	1.0001	0.9047	0.8677
333.15	0.9971	0.9018	0.8647
338.15	0.9928	0.8989	0.8617
343.15	0.9893	0.8960	0.8588
348.15	0.9849	0.8930	0.8558
353.15	0.9808	0.8900	0.8529

Table A- 10 Experimental densities for $[P_{8,8,8,14}]DOSS$, $[P_{6,6,6,14}]DOSS$ and $[P_{8,8,8} C_n P_{8,8,8}]DOSS_2$ as a function of temperature.

T/K	$\rho/(g \cdot cm^{-3})$			
	$[P_{6,6,6,14}]DOSS$	$[P_{8,8,8,14}]DOSS$	$[P_{8,8,8} C_6 P_{8,8,8}]DOSS_2$	$[P_{8,8,8} C_{10} P_{8,8,8}]DOSS_2$
293.15	0.9914	0.9750	0.9664	0.9579
298.15	0.9880	0.9717	0.9631	0.9544
303.15	0.9847	0.9685	0.9599	0.9511
308.15	0.9814	0.9652	0.9566	0.9477
313.15	0.9781	0.9620	0.9534	0.9443
318.15	0.9748	0.9588	0.9502	0.9409
323.15	0.9716	0.9556	0.9469	0.9376
328.15	0.9683	0.9524	0.9436	0.9342
333.15	0.9650	0.9492	0.9404	0.9309
338.15	0.9617	0.9460	0.9372	0.9277
343.15	0.9585	0.9427	0.9341	0.9244
348.15	0.9552	0.9396	0.9309	0.9212
353.15	0.9521	0.9364	0.9287	0.9179

Table A- 11 Fitting parameters of density and standard deviations (*SD*) calculated using equation 4-2.

ILs	Fitting parameters		SD·10 ³	R ²
	A ₀	A ₁		
[C ₂ CN Bim]Br	1.49313	-0.00067	1.31	0.9996
[C ₂ CN Him]Br	1.42610	-0.00067	2.85	0.9999
[C ₂ CN Oim]Br	1.37811	-0.00066	5.16	0.9999
[C ₂ CN Bim]Cl	1.27300	-0.00060	0.20	0.9999
[C ₂ CN Him]Cl	1.25830	-0.00060	0.60	0.99750
[C ₂ CN Oim]Cl	1.21680	-0.00060	1.30	0.9994
[C ₂ CN Bim]DOSS	1.33969	-0.00077	0.71	0.9976
[C ₂ CN Him]DOSS	1.29672	-0.00070	0.97	0.9999
[C ₂ CN Oim]DOSS	1.25950	-0.00069	0.54	0.9999
[C ₂ CN Dim]DOSS	1.22936	-0.00065	1.42	0.9969
[C ₂ CN Bim]DDS	1.36853	-0.00064	0.90	0.9999
[C ₂ CN Him]DDS	1.32133	-0.00064	0.90	0.9999
[C ₂ CN Oim]DDS	1.27076	-0.00063	1.47	0.9997
[C ₂ CN Dim]DDS	1.22466	-0.00063	1.47	0.9997
[C ₂ CN Him]SBA	1.42833	-0.00065	0.11	0.9999
[C ₂ CN Oim]SBA	1.38990	-0.00069	1.53	0.9998
[C ₂ CN Dim]SBA	1.33667	-0.00068	0.69	0.9999
[C ₂ CN Bim]BS	1.43117	-0.00065	0.84	0.9993
[C ₂ CN Him]BS	1.41528	-0.00065	1.21	0.9995
[C ₂ CN Oim]BS	1.38632	-0.00065	1.34	0.9994
[C ₂ CN Bim]TFMS	1.55029	-0.00073	0.31	0.9999
[C ₂ CN Him]TFMS	1.50242	-0.00073	0.97	0.9999
[C ₂ CN Oim]TFMS	1.44415	-0.00072	0.24	0.9999
[C ₂ CN Ayim]DOSS	1.35564	-0.00060	1.50	0.9998
[C ₂ CN Bzim]DOSS	1.39629	-0.00061	0.81	0.9996
[C ₂ CN Heim]DOSS	1.43970	-0.00060	1.19	0.9996
[P _{8,8,8,14}]Cl	1.06460	-0.0006	0.10	0.9999
[P _{8,8,8} C ₆ P _{8,8,8}]Cl ₂	1.24050	-0.00074	1.95	0.9818
[P _{8,8,8} C ₁₀ P _{8,8,8}]Cl ₂	1.09681	-0.00059	1.50	0.9999
[P _{6,6,6,14}]DOSS	1.15342	-0.00064	0.51	0.9995
[P _{8,8,8,14}]DOSS	1.15301	-0.00067	1.22	0.9999
[P _{8,8,8} C ₆ P _{8,8,8}]DOSS ₂	1.18339	-0.00066	1.49	0.9997
[P _{8,8,8} C ₁₀ P _{8,8,8}]DOSS ₂	1.16333	-0.00064	0.89	0.9997

Table A-12 Predicted densities of the imidazolium and phosphonium-based ILs at 298.15 K

IL	Pressure				
	1 bar	5 bar	10 bar	15 bar	20 bar
[C ₂ CN Bim]Br	1.29699	1.30007	1.30394	1.30784	1.31176
[C ₂ CN Him]Br	1.23117	1.23410	1.23778	1.24148	1.24520
[C ₂ CN Oim]Br	1.17868	1.18148	1.18500	1.18854	1.19211
[C ₂ CN Bim]Cl	1.09924	1.10185	1.10513	1.10844	1.11176
[C ₂ CN Him]Cl	1.07600	1.07855	1.08177	1.08500	1.08826
[C ₂ CN Oim]Cl	1.04474	1.04723	1.05035	1.05349	1.05665
[C ₂ CN Bim]DOSS	1.11286	1.11551	1.11883	1.12218	1.12554
[C ₂ CN Him]DOSS	1.09092	1.09352	1.09678	1.10005	1.10335
[C ₂ CN Oim]DOSS	1.05616	1.05867	1.06183	1.06500	1.06820
[C ₂ CN Dim]DOSS	1.03663	1.03909	1.04219	1.04530	1.04844
[C ₂ CN Bim]DDS	1.17908	1.18188	1.18540	1.18895	1.19251
[C ₂ CN Him]DDS	1.13179	1.13449	1.13787	1.14127	1.14469
[C ₂ CN Oim]DDS	1.08361	1.08619	1.08942	1.09268	1.09596
[C ₂ CN Dim]DDS	1.03743	1.03989	1.04299	1.04611	1.04925
[C ₂ CN Him]SBA	1.23678	1.23972	1.24342	1.24713	1.25087
[C ₂ CN Oim]SBA	1.18489	1.18771	1.19125	1.19481	1.19839
[C ₂ CN Dim]SBA	1.13550	1.13820	1.14159	1.14501	1.14844
[C ₂ CN Bim]BS	1.23898	1.24193	1.24563	1.24935	1.25310
[C ₂ CN Him]BS	1.22486	1.22777	1.23143	1.23511	1.23882
[C ₂ CN Oim]BS	1.19330	1.19614	1.19971	1.20329	1.20690
[C ₂ CN Bim]TFMS	1.33475	1.33793	1.34191	1.34593	1.34996
[C ₂ CN Him]TFMS	1.28797	1.29103	1.29488	1.29875	1.30265
[C ₂ CN Oim]TFMS	1.23157	1.23450	1.23818	1.24188	1.24560
[C ₂ CN Ayim]DOSS	1.17758	1.18038	1.18389	1.18743	1.19099
[C ₂ CN Bzim]DOSS	1.21735	1.22024	1.22388	1.22754	1.23122
[C ₂ CN Heim]DOSS	1.26212	1.26513	1.26890	1.27269	1.27651
[P _{8,8,8,14}]Cl	0.88736	0.88947	0.89212	0.89479	0.89747
[P _{8,8,8} C ₆ P _{8,8,8}]Cl ₂	1.02030	1.02272	1.02577	1.02884	1.03192
[P _{8,8,8} C ₁₀ P _{8,8,8}]Cl ₂	0.92393	0.92613	0.92889	0.93166	0.93446
[P _{6,6,6,14}]DOSS	0.96480	0.96709	0.96998	0.97288	0.97579
[P _{8,8,8,14}]DOSS	0.95609	0.95836	0.96121	0.96409	0.96698
[P _{8,8,8} C ₆ P _{8,8,8}]DOSS ₂	0.98974	0.99210	0.99505	0.99803	1.00102
[P _{8,8,8} C ₁₀ P _{8,8,8}]DOSS ₂	0.97342	0.97573	0.97864	0.98156	0.98451

Table A-13 Predicted densities of the imidazolium and phosphonium-based ILs at 313.15 K

IL	Pressure				
	1 bar	5 bar	10 bar	15 bar	20 bar
[C ₂ CN Bim]Br	1.26719	1.27017	1.27392	1.27769	1.28148
[C ₂ CN Him]Br	1.20252	1.20535	1.20891	1.21249	1.21609
[C ₂ CN Oim]Br	1.15015	1.15286	1.15626	1.15968	1.16312
[C ₂ CN Dim]Br	1.10710	1.10971	1.11299	1.11628	1.11959
[C ₂ CN Bim]Cl	1.07368	1.07621	1.07938	1.08258	1.08579
[C ₂ CN Him]Cl	1.04918	1.05165	1.05475	1.05788	1.06102
[C ₂ CN Oim]Cl	1.01952	1.02192	1.02494	1.02797	1.03102
[C ₂ CN Bim]DOSS	1.08132	1.08386	1.08706	1.09028	1.09351
[C ₂ CN Him]DOSS	1.06257	1.06507	1.06821	1.07138	1.07456
[C ₂ CN Oim]DOSS	1.02855	1.03097	1.03401	1.03707	1.04015
[C ₂ CN Dim]DOSS	1.00951	1.01188	1.01487	1.01787	1.02089
[C ₂ CN Bim]DDS	1.15124	1.15395	1.15736	1.16078	1.16423
[C ₂ CN Him]DDS	1.10443	1.10703	1.11029	1.11358	1.11688
[C ₂ CN Oim]DDS	1.05682	1.05931	1.06243	1.06558	1.06874
[C ₂ CN Dim]DDS	1.01109	1.01347	1.01646	1.01947	1.02250
[C ₂ CN Him]SBA	1.20827	1.21112	1.21469	1.21829	1.22190
[C ₂ CN Oim]SBA	1.15610	1.15882	1.16224	1.16568	1.16914
[C ₂ CN Dim]SBA	1.10710	1.10971	1.11299	1.11628	1.11959
[C ₂ CN Bim]BS	1.21036	1.21321	1.21679	1.22039	1.22401
[C ₂ CN Him]BS	1.19647	1.19929	1.20283	1.20639	1.20997
[C ₂ CN Oim]BS	1.16523	1.16797	1.17142	1.17488	1.17837
[C ₂ CN Bim]TFMS	1.30339	1.30646	1.31032	1.31419	1.31809
[C ₂ CN Him]TFMS	1.25707	1.26003	1.26375	1.26749	1.27125
[C ₂ CN Oim]TFMS	1.20133	1.20416	1.20771	1.21129	1.21488
[C ₂ CN Ayim]DOSS	1.15094	1.15365	1.15706	1.16048	1.16393
[C ₂ CN Bzim]DOSS	1.19042	1.19322	1.19674	1.20029	1.20385
[C ₂ CN Heim]DOSS	1.23456	1.23746	1.24112	1.24479	1.24848
[P _{8,8,8,14}]Cl	0.86063	0.86266	0.86520	0.86776	0.87034
[P _{8,8,8} C ₆ P _{8,8,8}]Cl ₂	0.99195	0.99429	0.99722	1.00017	1.00314
[P _{8,8,8} C ₁₀ P _{8,8,8}]Cl ₂	0.89733	0.89944	0.90209	0.90476	0.90745
[P _{6,6,6,14}]DOSS	0.93918	0.94139	0.94417	0.94697	0.94978
[P _{8,8,8,14}]DOSS	0.92996	0.93215	0.93490	0.93767	0.94045
[P _{8,8,8} C ₆ P _{8,8,8}]DOSS ₂	0.96368	0.96595	0.96880	0.97167	0.97455
[P _{8,8,8} C ₁₀ P _{8,8,8}]DOSS ₂	0.94781	0.95004	0.95285	0.95567	0.95850

Table A-14 Predicted densities of the imidazolium and phosphonium-based ILs at 3438.15 K

IL	Pressure				
	1 bar	5 bar	10 bar	15 bar	20 bar
[C ₂ CN Bim]Br	1.23005	1.23289	1.23645	1.24004	1.24365
[C ₂ CN Him]Br	1.16634	1.16903	1.17242	1.17582	1.17924
[C ₂ CN Oim]Br	1.11470	1.11727	1.12050	1.12375	1.12702
[C ₂ CN Dim]Br	1.07326	1.07574	1.07885	1.08198	1.08513
[C ₂ CN Bim]Cl	1.04136	1.04377	1.04679	1.04982	1.05288
[C ₂ CN Him]Cl	1.01724	1.01959	1.02254	1.02551	1.02849
[C ₂ CN Oim]Cl	0.98865	0.99093	0.99380	0.99668	0.99958
[C ₂ CN Bim]DOSS	1.04632	1.04874	1.05177	1.05482	1.05789
[C ₂ CN Him]DOSS	1.02862	1.03100	1.03398	1.03698	1.04000
[C ₂ CN Oim]DOSS	0.99526	0.99756	1.00045	1.00335	1.00627
[C ₂ CN Dim]DOSS	0.97727	0.97952	0.98236	0.98521	0.98808
[C ₂ CN Bim]DDS	1.11655	1.11912	1.12236	1.12562	1.12889
[C ₂ CN Him]DDS	1.07064	1.07311	1.07621	1.07934	1.08248
[C ₂ CN Oim]DDS	1.02434	1.02671	1.02968	1.03267	1.03567
[C ₂ CN Dim]DDS	0.97951	0.98177	0.98461	0.98746	0.99034
[C ₂ CN Him]SBA	1.17237	1.17508	1.17848	1.18190	1.18534
[C ₂ CN Oim]SBA	1.11966	1.12224	1.12549	1.12875	1.13204
[C ₂ CN Dim]SBA	1.07239	1.07486	1.07797	1.08110	1.08425
[C ₂ CN Bim]BS	1.17403	1.17674	1.18014	1.18356	1.18701
[C ₂ CN Him]BS	1.16060	1.16328	1.16665	1.17003	1.17344
[C ₂ CN Oim]BS	1.13055	1.13316	1.13644	1.13974	1.14305
[C ₂ CN Bim]TFMS	1.26399	1.26691	1.27057	1.27426	1.27797
[C ₂ CN Him]TFMS	1.21877	1.22158	1.22511	1.22867	1.23224
[C ₂ CN Oim]TFMS	1.16430	1.16699	1.17036	1.17376	1.17718
[C ₂ CN Ayim]DOSS	1.11674	1.11932	1.12256	1.12581	1.12909
[C ₂ CN Bzim]DOSS	1.15525	1.15792	1.16127	1.16464	1.16803
[C ₂ CN Heim]DOSS	1.19873	1.20150	1.20497	1.20847	1.21199
[P _{8,8,8,14}]Cl	0.83527	0.83720	0.83962	0.84206	0.84451
[P _{8,8,8} C ₆ P _{8,8,8}]Cl ₂	0.95928	0.96149	0.96427	0.96707	0.96988
[P _{8,8,8} C ₁₀ P _{8,8,8}]Cl ₂	0.87145	0.87346	0.87599	0.87853	0.88109
[P _{6,6,6,14}]DOSS	0.90851	0.91060	0.91324	0.91589	0.91855
[P _{8,8,8,14}]DOSS	0.89907	0.90115	0.90375	0.90638	0.90901
[P _{8,8,8} C ₆ P _{8,8,8}]DOSS ₂	0.93224	0.93439	0.93709	0.93981	0.94255
[P _{8,8,8} C ₁₀ P _{8,8,8}]DOSS ₂	0.91687	0.91899	0.92165	0.92432	0.92701

Table A-15 Experimental viscosities data η , for $[\text{C}_2\text{CN C}_n\text{im}]\text{Br}$ as a function of temperature

T/K	$\eta/(\text{mPa}\cdot\text{s})$			
	$[\text{C}_2\text{CN Bim}]\text{Br}$	$[\text{C}_2\text{CN Him}]\text{Br}$	$[\text{C}_2\text{CN Oim}]\text{Br}$	$[\text{C}_2\text{CN Dim}]\text{Br}$
298.15	19103	-	-	-
303.15	11304	15893	-	-
308.15	7058	9030	19620	
313.15	4502	5610	13044	16702
318.15	2953	3602	8303	10315
323.15	1990	2380	5136	6813
328.15	1378	1618	3292	4574
333.15	976	1128	2160	3016
338.15	706	805	1460	2051
343.15	521	640	1020	1427
348.15	391	466	728	1015
353.15	298	359	530	737

Table A-16 Experimental viscosities data for $[\text{C}_2\text{CN C}_n\text{im}]\text{Cl}$ as a function of temperature

T/K	$\eta/(\text{mPa}\cdot\text{s})$		
	$[\text{C}_2\text{CN Bim}]\text{Cl}$	$[\text{C}_2\text{CN Him}]\text{Cl}$	$[\text{C}_2\text{CN Oim}]\text{Cl}$
298.15	19734	-	-
303.15	12317	17524	-
308.15	7262	9961	-
313.15	4492	6193	14385
318.15	2876	3980	9160
323.15	1896	2633	5670
328.15	1285	1794	3638
333.15	894	1254	2391
338.15	636	898	1619
343.15	463	715	1134
348.15	343	523	812
353.15	259	406	595

Table A-17 Experimental viscosities data for [C₂CN C_nim]DOSS as a function of temperature

T/K	η /(mPa.s)			
	[C ₂ CN Bim] DOSS	[C ₂ CN Him] DOSS	[C ₂ CN Oim] DOSS	[C ₂ CN Dim] DOSS
293.15	19758	-	-	-
298.15	12006	19896	-	-
303.15	7458	12117	16785	-
308.15	4462	7571	10624	13807
313.15	2843	4587	6375	8495
318.15	1829	2940	4059	5339
323.15	1203	1947	2673	3536
328.15	786	1265	1783	2355
333.15	497	848	1226	1548
338.15	333	579	866	1178
343.15	238	411	604	811
348.15	154	279	418	537
353.15	102	191	285	389

Table A-18 Experimental viscosities data for [C₂CN C_nim]DDS as a function of temperature

T/K	η /(mPa.s)			
	[C ₂ CN Bim] DDS	[C ₂ CN Him] DDS	[C ₂ CN Oim] DDS	[C ₂ CN Dim] DDS
293.15	13007	20997	-	-
298.15	7875	13770	-	-
303.15	4746	8253	12999	16145
308.15	2938	5185	8323	10417
313.15	1740	3355	5094	6231
318.15	1144	2051	3195	3951
323.15	768	1302	2071	2583
328.15	485	846	1391	1757
333.15	338	567	975	1252
338.15	235	390	695	904
343.15	162	275	461	588
348.15	114	199	330	418
353.15	76	134	230	296

Table A-19 Experimental viscosities data for [C₂CN C_nim]SBA as a function of temperature

T/K	η /(mPa.s)		
	[C ₂ CN Him]SBA	[C ₂ CN Oim] SBA	[C ₂ CN Dim] SBA
293.15	19212	-	-
298.15	11463	14420	17650
303.15	7578	9263	11449
308.15	4766	5821	7159
313.15	3001	3685	4606
318.15	1953	2405	3028
323.15	1190	1525	1977
328.15	821	1066	1431
333.15	547	702	944
338.15	352	455	623
343.15	236	299	431
348.15	164	188	294
353.15	113	121	198

Table A-20 Experimental viscosities data for [C₂CN C_nim]BS as a function of temperature

T/K	η /(mPa.s)		
	[C ₂ CN Bim]BS	[C ₂ CN Him]BS	[C ₂ CN Oim]BS
293.15	4612	4612	12693
298.15	2752	2752	8292
303.15	1806	1836	4880
308.15	1203	1223	3111
313.15	792	812	2098
318.15	505	505	1311
323.15	321	347	884
328.15	214	242	566
333.15	152	179	378
338.15	109	129	254
343.15	78	103	172
348.15	54	79	120
353.15	38	59	89

Table A-21 Experimental viscosities data for [C₂CN C_nim]TFMS as a function of temperature

<i>T</i> /K	η /(mPa.s)		
	[C ₂ CN Bim]TFMS	[C ₂ CN Him]TFMS	[C ₂ CN Oim]TFMS
293.15	1097	2244	6784
298.15	719	1470	4135
303.15	489	992	2799
308.15	336	649	1817
313.15	227	438	1182
318.15	161	302	753
323.15	119	214	503
328.15	85	155	342
333.15	61	103	236
338.15	46	77	165
343.15	35	55	108
348.15	25	40	75
353.15	19	29	53

Table A-22 Experimental viscosities data for dual functionalized imidazolium-based ILs as function of temperature.

<i>T</i> /K	η /(mPa.s)		
	[C ₂ CN Ayim]DOSS	[C ₂ CN Bzim]DOSS	[C ₂ CN HEim]DOSS
298.15	11070	-	-
303.15	6495	-	-
308.15	3635	-	-
313.15	2092	-	11744
318.15	1205	-	6856
323.15	711	-	4144
328.15	427	12904	2598
333.15	268	7095	1670
338.15	186	4212	1120
343.15	129	2564	768
348.15	90	1729	538
353.15	65	1180	390

Table A-23 Experimental viscosities data for $[P_{8,8,8,14}]Cl$ and $[P_{8,8,8} C_n P_{8,8,8}]Cl_2$ as a function of temperature.

T/K	$\eta/(mPa.s)$		
	$[P_{8,8,8,14}]Cl$	$[P_{8,8,8} C_6 P_{8,8,8}]Cl_2$	$[P_{8,8,8} C_{10} P_{8,8,8}]Cl_2$
293.15	2572	19705	-
298.15	1806	12349	18252
303.15	1285	8075	12344
308.15	932	5473	8580
313.15	689	3806	6058
318.15	517	2694	4364
323.15	395	1937	3119
328.15	306	1422	2194
333.15	241	1062	1591
338.15	191	754	1175
343.15	154	564	897
348.15	125	423	669
353.15	103	340	555

Table A-24 Experimental viscosities data for $[P_{8,8,8,14}]DOSS$, $[P_{6,6,6,14}]DOSS$ and $[P_{8,8,8} C_n P_{8,8,8}]DOSS_2$ as a function of temperature.

T/K	$\eta/(mPa.s)$			
	$[P_{6,6,6,14}]DOSS$	$[P_{8,8,8,14}]DOSS$	$[P_{8,8,8} C_6 P_{8,8,8}]DOSS_2$	$[P_{8,8,8} C_{10} P_{8,8,8}]DOSS_2$
293.15	1795	2051	10138	18767
298.15	1272	1447	6637	11761
303.15	912	1029	4489	7690
308.15	668	742	3120	5213
313.15	496	553	2203	3625
318.15	374	417	1587	2565
323.15	286	316	1134	1844
328.15	222	245	798	1355
333.15	174	193	578	1012
338.15	138	154	427	718
343.15	111	123	326	537
348.15	91	101	243	403
353.15	75	83	202	324

Table A-25 Arrhenius parameters obtained from plotting of $\ln\eta$ against $1/T$ and standard deviations (SD) calculated using equation 4-2.

ILs	η_{∞} ($\text{mPa}\cdot\text{s}^{-1} \times 10^{-3}$)	E_{η} ($\text{J}\cdot\text{mol}^{-1} \times 10^3$)	SD	R^2
[C ₂ CN Bim]Br	0.656	28.65	0.0292	0.9973
[C ₂ CN Him]Br	0.624	29.00	0.0390	0.9943
[C ₂ CN Oim]Br	0.260	32.16	0.0390	0.9943
[C ₂ CN Dim]Br	0.427	31.16	0.0093	0.9996
[C ₂ CN Bim]Cl	0.371	30.13	0.0305	0.9974
[C ₂ CN Him]Cl	0.699	28.82	0.0402	0.9939
[C ₂ CN Oim]Cl	0.281	32.07	0.0402	0.9939
[C ₂ CN Bim]DOSS	0.114	32.63	0.0116	0.9994
[C ₂ CN Him]DOSS	0.183	31.97	0.0083	0.9983
[C ₂ CN Oim]DOSS	0.285	31.19	0.0083	0.9983
[C ₂ CN Dim]DOSS	0.365	30.83	0.0155	0.999
[C ₂ CN Bim]DDS	0.128	31.84	0.0137	0.9996
[C ₂ CN Him]DDS	0.161	31.87	0.0143	0.9996
[C ₂ CN Oim]DDS	0.268	31.07	0.0143	0.9996
[C ₂ CN Dim]DDS	0.335	30.73	0.0166	0.9991
[C ₂ CN Him]SBA	0.140	32.12	0.0151	0.9995
[C ₂ CN Oim]SBA	0.124	32.69	0.0275	0.9982
[C ₂ CN Dim]SBA	0.281	30.84	0.0275	0.9982
[C ₂ CN Bim]BS	0.189	29.82	0.0130	0.9996
[C ₂ CN Him]BS	0.194	30.25	0.0146	0.9995
[C ₂ CN Oim]BS	0.161	31.33	0.0146	0.9995
[C ₂ CN Bim]TFMS	0.705	25.07	0.0083	0.9998
[C ₂ CN Him]TFMS	0.444	26.99	0.0078	0.9998
[C ₂ CN Oim]TFMS	0.193	30.22	0.0078	0.9998
[C ₂ CN Ayim]DOSS	0.019	36.97	0.0170	0.9995
[C ₂ CN Bzim]DOSS	0.026	39.98	0.0234	0.9956
[C ₂ CN Heim]DOSS	0.121	33.99	0.0234	0.9956
[P _{8,8,8,14}]Cl	7.928	20.03	0.0174	0.9984
[P _{8,8,8} C ₆ P _{8,8,8}]Cl ₂	2.322	25.16	0.0169	0.9991
[P _{8,8,8} C ₁₀ P _{8,8,8}]Cl ₂	3.534	24.54	0.0169	0.9991
[P _{6,6,6,14}]DOSS	7.464	19.80	0.0153	0.9987
[P _{8,8,8,14}]DOSS	7.333	19.98	0.0183	0.9984
[P _{8,8,8} C ₆ P _{8,8,8}]DOSS ₂	2.177	24.67	0.0183	0.9984
[P _{8,8,8} C ₁₀ P _{8,8,8}]DOSS ₂	2.273	25.16	0.0177	0.9991

Table A-26 Experimental refractive indices for [C₂CN C_nim]Br as a function of temperature

T/K	<i>n_D</i>			
	[C ₂ CN Bim]Br	[C ₂ CN Him]Br	[C ₂ CN Oim]Br	[C ₂ CN Dim]Br
298.15	1.54540	1.52914	1.52422	-
303.15	1.54454	1.52823	1.52311	-
308.15	1.54346	1.52719	1.52215	1.50786
313.15	1.54229	1.52600	1.52098	1.50696
318.15	1.54111	1.52479	1.51973	1.50606
323.15	1.53992	1.52354	1.51840	1.50502
328.15	1.53869	1.52229	1.51706	1.50388
333.15	1.53748	1.52117	1.51553	1.50279

Table A-27 Experimental refractive indices for [C₂CN C_nim]Cl as a function of temperature

T/K	<i>n_D</i>		
	[C ₂ CN Bim]Cl	[C ₂ CN Him]Cl	[C ₂ CN Oim]Cl
298.15	1.51893	1.51542	1.51072
303.15	1.51813	1.51434	1.50977
308.15	1.51710	1.51328	1.50881
313.15	1.51610	1.51213	1.50776
318.15	1.51500	1.51087	1.50691
323.15	1.51388	1.50970	1.50597
328.15	1.51272	1.50864	1.50502
333.15	1.51157	1.50756	1.50411

Table A-28 Experimental refractive indices for [C₂CN C_nim]DOSS as a function of temperature

T/K	<i>n_D</i>			
	[C ₂ CN Bim] DOSS	[C ₂ CN Him] DOSS	[C ₂ CN Oim] DOSS	[C ₂ CN Dim] DOSS
298.15	1.48048	1.47970	1.47692	1.47447
303.15	1.47926	1.47841	1.47518	1.47296
308.15	1.47792	1.47709	1.47393	1.47142
313.15	1.47653	1.47580	1.47253	1.46972
318.15	1.47504	1.47447	1.47099	1.46813
323.15	1.47361	1.47305	1.46946	1.46678
328.15	1.47216	1.47171	1.46798	1.46532
333.15	1.47070	1.47029	1.46636	1.46391

Table A-29 Experimental refractive indices for [C₂CN C_nim]DDS as a function of temperature

T/K	<i>n_D</i>			
	[C ₂ CN Bim] DDS	[C ₂ CN Him] DDS	[C ₂ CN Oim] DDS	[C ₂ CN Dim] DDS
298.15	1.48791	1.48409	1.47928	1.47610
303.15	1.48620	1.48269	1.47758	1.47476
308.15	1.48479	1.48125	1.47597	1.47345
313.15	1.48311	1.47991	1.47454	1.47203
318.15	1.48153	1.47863	1.47274	1.47055
323.15	1.47976	1.47702	1.47098	1.46909
328.15	1.47832	1.47566	1.46963	1.46761
333.15	1.47681	1.47422	1.46785	1.46601

Table A-30 Experimental refractive indices for [C₂CN C_nim]SBA as a function of temperature

T/K	<i>n_D</i>		
	[C ₂ CN Him]SBA	[C ₂ CN Oim] SBA	[C ₂ CN Dim] SBA
298.15	1.52493	1.51801	1.51306
303.15	1.52371	1.51692	1.51163
308.15	1.52236	1.51572	1.50998
313.15	1.52079	1.51450	1.50871
318.15	1.51936	1.51321	1.50706
323.15	1.51800	1.51191	1.50582
328.15	1.51666	1.51058	1.50450
333.15	1.51502	1.50912	1.50322

Table A-31 Experimental refractive indices for [C₂CN C_nim]BS as a function of temperature

T/K	<i>n_D</i>		
	[C ₂ CN Bim]BS	[C ₂ CN Him]BS	[C ₂ CN Oim]BS
298.15	1.53378	1.52726	1.52174
303.15	1.53237	1.52610	1.52084
308.15	1.53113	1.52499	1.51973
313.15	1.52975	1.52382	1.51856
318.15	1.52824	1.52266	1.51740
323.15	1.52684	1.52145	1.51619
328.15	1.52544	1.52025	1.51499
333.15	1.52403	1.51912	1.51373

Table A-32 Experimental refractive indices for [C₂CN C_nim]TFMS as a function of temperature

T/K	<i>n_D</i>		
	[C ₂ CN Bim]TFMS	[C ₂ CN Him]TFMS	[C ₂ CN Oim]TFMS
298.15	1.53523	1.53075	1.52679
303.15	1.53357	1.52951	1.52584
308.15	1.53216	1.52814	1.52470
313.15	1.53072	1.52673	1.52356
318.15	1.52925	1.52555	1.52248
323.15	1.52795	1.52424	1.52119
328.15	1.52652	1.52304	1.51991
333.15	1.52515	1.52193	1.51873

Table A-33 Experimental refractive indices for dual functionalized imidazolium-based ILs as function of temperature

T/K	<i>n_D</i>		
	[C ₂ CN Aim]DOSS	[C ₂ CN Bzim]DOSS	[C ₂ CN HEim]DOSS
298.15	1.51016	1.50484	1.52103
303.15	1.50858	1.50281	1.51968
308.15	1.50688	1.50107	1.51794
313.15	1.50532	1.49935	1.51641
318.15	1.50366	1.49762	1.51502
323.15	1.50199	1.49604	1.51357
328.15	1.50031	1.49443	1.51203
333.15	1.49837	1.49280	1.51039

Table A-34 Experimental refractive indices for [P_{8,8,8,14}]Cl and [P_{8,8,8} C_n P_{8,8,8}]Cl₂ as a function of temperature.

T/K	<i>n_D</i>		
	[P _{8,8,8,14}]Cl	[P _{8,8,8} C ₆ P _{8,8,8}]Cl ₂	[P _{8,8,8} C ₁₀ P _{8,8,8}]Cl ₂
298.15	1.47799	1.49144	1.48684
303.15	1.47671	1.48996	1.48556
308.15	1.47515	1.48849	1.48410
313.15	1.47350	1.48712	1.48263
318.15	1.47190	1.48564	1.48107
323.15	1.47024	1.48416	1.47954
328.15	1.46863	1.48266	1.47802
333.15	1.46695	1.48117	1.47652

Table A- 35 Experimental refractive indices n_D for [P_{8,8,8,14}]DOSS, [P_{6,6,6,14}]DOSS and [P_{8,8,8}C_nP_{8,8,8}]DOSS₂ as a function of temperature

T/K	n_D			
	[P _{6,6,6,14}] DOSS	[P _{8,8,8,14}] DOSS	[P _{8,8,8} C ₆ P _{8,8,8}] DOSS ₂	[P _{8,8,8} C ₁₀ P _{8,8,8}] DOSS ₂
298.15	1.47353	1.46934	1.47534	1.47472
303.15	1.47190	1.46763	1.47407	1.47332
308.15	1.47032	1.46595	1.47247	1.47176
313.15	1.46861	1.46431	1.47092	1.47020
318.15	1.46709	1.46264	1.46934	1.46861
323.15	1.46547	1.46098	1.46776	1.46701
328.15	1.46388	1.45936	1.46615	1.46542
333.15	1.46229	1.45769	1.46459	1.46386

Table A- 36 Fitting parameters of refractive indices (n_D) and standard deviations (SD) calculated using equation 4-3

ILs	Fitting parameters		SD·10 ³	R ²
	A ₂	A ₃		
[C ₂ CN Bim]Br	1.614128	-0.000230	0.14	0.9981
[C ₂ CN Him]Br	1.598682	-0.000233	0.20	0.9981
[C ₂ CN Oim]Br	1.588503	-0.000247	0.22	0.9956
[C ₂ CN Dim]Br	1.570713	-0.000204	0.16	0.9974
[C ₂ CN Bim]Cl	1.582564	-0.000213	0.15	0.9977
[C ₂ CN Him]Cl	1.583280	-0.000227	0.15	0.9995
[C ₂ CN Oim]Cl	1.567049	-0.000189	0.13	0.9979
[C ₂ CN Bim]DOSS	1.564681	-0.000282	0.10	0.9993
[C ₂ CN Him]DOSS	1.559855	-0.000269	0.13	0.9997
[C ₂ CN Oim]DOSS	1.565515	-0.000297	0.14	0.9992
[C ₂ CN Dim]DOSS	1.562092	-0.000288	0.10	0.9992
[C ₂ CN Bim]DDS	1.582838	-0.000319	0.18	0.9995
[C ₂ CN Him]DDS	1.568024	-0.000281	0.16	0.9996
[C ₂ CN Oim]DDS	1.576180	-0.000325	0.10	0.9994
[C ₂ CN Dim]DDS	1.565009	-0.000304	0.11	0.9991
[C ₂ CN Him]SBA	1.609636	-0.000284	0.14	0.9992
[C ₂ CN Oim]SBA	1.593899	-0.000254	0.11	0.9995
[C ₂ CN Dim]SBA	1.597176	-0.000283	0.20	0.9985
[C ₂ CN Bim]BS	1.617089	-0.000279	0.10	0.9997
[C ₂ CN Him]BS	1.596865	-0.000233	0.12	0.9996
[C ₂ CN Oim]BS	1.590873	-0.000231	0.12	0.9994
[C ₂ CN Bim]TFMS	1.620201	-0.000286	0.14	0.9993
[C ₂ CN Him]TFMS	1.606629	-0.000255	0.13	0.9991
[C ₂ CN Oim]TFMS	1.596311	-0.000233	0.17	0.9985
[C ₂ CN Ayim]DOSS	1.606091	-0.000340	0.20	0.9988
[C ₂ CN Bzim]DOSS	1.614882	-0.000351	0.09	0.9995
[C ₂ CN Heim]DOSS	1.611378	-0.000303	0.35	0.9994
[P _{8,8,8,14}]Cl	1.573349	-0.000319	0.11	0.9991
[P _{8,8,8} C ₆ P _{8,8,8}]Cl ₂	1.575864	-0.000298	0.08	0.9996
[P _{8,8,8} C ₁₀ P _{8,8,8}]Cl ₂	1.578665	-0.000293	0.15	0.9994
[P _{6,6,6,14}]DOSS	1.569232	-0.000321	0.04	0.9999
[P _{8,8,8,14}]DOSS	1.568313	-0.000332	0.04	0.9999
[P _{8,8,8} C ₆ P _{8,8,8}]DOSS ₂	1.568202	-0.000311	0.10	0.9994
[P _{8,8,8} C ₁₀ P _{8,8,8}]DOSS ₂	1.568086	-0.000313	0.09	0.9997

Table A- 37 Thermal expansion coefficients (α_p) for [C₂CN C_nim]Br and [C₂CN C_nim]Br as a function of temperature.

T/K	$\alpha_p \times 10^4 / (\text{K}^{-1})$						
	[C ₂ CN Bim]Br	[C ₂ CN Him]Br	[C ₂ CN Oim]Br	[C ₂ CN Dim]Br	[C ₂ CN Bim]Cl	[C ₂ CN Him]Cl	[C ₂ CN Oim]Cl
293.15	5.09	5.36	5.73	-	5.36	5.76	5.99
298.15	5.10	5.38	5.75	-	5.38	5.78	6.01
303.15	5.12	5.39	5.76	-	5.39	5.79	6.03
308.15	5.13	5.41	5.78	6.18	5.41	5.81	6.04
313.15	5.15	5.42	5.80	6.21	5.42	5.83	6.06
318.15	5.16	5.44	5.81	6.23	5.44	5.84	6.08
323.15	5.17	5.45	5.83	6.25	5.45	5.86	6.10
328.15	5.19	5.47	5.85	6.27	5.47	5.88	6.12
333.15	5.20	5.48	5.86	6.29	5.48	5.90	6.14
338.15	5.21	5.50	5.88	6.31	5.50	5.91	6.16
343.15	5.22	5.51	5.90	6.32	5.51	5.93	6.18
348.15	5.24	5.53	5.92	6.34	5.53	5.95	6.19
353.15	5.25	5.54	5.93	6.36	5.54	5.97	6.21

Table A- 38 Thermal expansion coefficients (α_p) for [C₂CN C_nim]DOSS and [C₂CN C_nim]BS as a function of temperature.

T/K	$\alpha_p \times 10^4 / (\text{K}^{-1})$						
	[C ₂ CN Bim]DOSS	[C ₂ CN Him]DOSS	[C ₂ CN Oim]DOSS	[C ₂ CN Dim]DOSS	[C ₂ CN Bim]BS	[C ₂ CN Him]BS	[C ₂ CN Oim]BS
293.15	6.26	6.41	6.53	6.91	5.24	5.31	5.44
298.15	6.28	6.43	6.55	6.94	5.25	5.32	5.45
303.15	6.30	6.45	6.57	6.96	5.27	5.34	5.47
308.15	6.32	6.48	6.59	6.98	5.28	5.35	5.48
313.15	6.34	6.50	6.61	7.01	5.29	5.36	5.50
318.15	6.36	6.52	6.63	7.03	5.31	5.38	5.51
323.15	6.38	6.54	6.66	7.06	5.32	5.39	5.53
328.15	6.40	6.56	6.68	7.08	5.34	5.41	5.54
333.15	6.42	6.58	6.70	7.11	5.35	5.42	5.56
338.15	6.44	6.60	6.72	7.13	5.37	5.44	5.57
343.15	6.46	6.63	6.75	7.16	5.38	5.45	5.59
348.15	6.48	6.65	6.77	7.19	5.39	5.47	5.60
353.15	6.50	6.67	6.79	7.21	5.41	5.48	5.62

Table A- 39 Thermal expansion coefficients (α_p) for [C₂CN C_nim]DDS and [C₂CN C_nim]SBA as a function of temperature.

T/K	$\alpha_p \times 10^4 / (\text{K}^{-1})$						
	[C ₂ CN Bim] DDS	[C ₂ CN Him] DDS	[C ₂ CN Oim] DDS	[C ₂ CN Dim] DDS	[C ₂ CN Bim]S BA	[C ₂ CN Him] SBA	[C ₂ CN Oim] SBA
	293.15	5.42	5.65	5.80	6.06	5.25	5.81
298.15	5.43	5.66	5.82	6.08	5.27	5.83	6.00
303.15	5.45	5.68	5.83	6.09	5.28	5.84	6.01
308.15	5.46	5.69	5.85	6.11	5.29	5.86	6.03
313.15	5.48	5.71	5.87	6.13	5.31	5.88	6.05
318.15	5.49	5.73	5.89	6.15	5.32	5.90	6.07
323.15	5.51	5.74	5.90	6.17	5.34	5.91	6.09
328.15	5.52	5.76	5.92	6.19	5.35	5.93	6.11
333.15	5.54	5.78	5.94	6.21	5.36	5.95	6.13
338.15	5.56	5.79	5.96	6.23	5.38	5.97	6.14
343.15	5.57	5.81	5.97	6.25	5.39	5.98	6.16
348.15	5.59	5.83	5.99	6.27	5.41	6.00	6.18
353.15	5.60	5.84	6.01	6.29	5.42	6.02	6.20

Table A- 40 Thermal expansion coefficients (α_p) [C₂CN C_nim]TFMS and dual functionalized ILs as a function of temperature.

T/K	$\alpha_p \times 10^4 / (\text{K}^{-1})$					
	[C ₂ CN Bim] TFMS	[C ₂ CN Him] TFMS	[C ₂ CN Oim] TFMS	[C ₂ CN Ayim] DOSS	[C ₂ CN Bzim] DOSS	[C ₂ CN Heim] DOSS
	293.15	5.46	5.67	5.84	5.09	5.01
298.15	5.48	5.68	5.86	5.10	5.02	4.76
303.15	5.49	5.70	5.87	5.11	5.04	4.77
308.15	5.51	5.71	5.89	5.12	5.05	4.78
313.15	5.52	5.73	5.91	5.14	5.06	4.79
318.15	5.54	5.75	5.93	5.15	5.07	4.80
323.15	5.55	5.76	5.94	5.16	5.09	4.82
328.15	5.57	5.78	5.96	5.18	5.10	4.83
333.15	5.58	5.80	5.98	5.19	5.11	4.84
338.15	5.60	5.81	6.00	5.20	5.13	4.85
343.15	5.62	5.83	6.01	5.22	5.14	4.86
348.15	5.63	5.85	6.03	5.23	5.15	4.87
353.15	5.65	5.87	6.05	5.25	5.17	4.89

Table A- 41 Thermal expansion coefficients (α_p) for [C₂CN C_nim]DDS and [C₂CN C_nim]SBA as a function of temperature.

T/K	$\alpha_p \times 10^4 / (\text{K}^{-1})$						
	[P _{8,8,8,14}] Cl	[P _{8,8,8} C ₆ P _{8,8,8}]Cl ₂	[P _{8,8,8} C ₁₀ P _{8,8,8}]Cl ₂	[P _{6,6,6,14}] DOSS	[P _{8,8,8,14}] DOSS	[P _{8,8,8} C ₆ P _{8,8,8}] DOSS ₂	[P _{8,8,8} C ₁₀ P _{8,8,8}] DOSS ₂
293.15	6.65	6.39	6.67	6.63	7.00	6.56	6.75
298.15	6.68	6.41	6.69	6.65	7.03	6.58	6.77
303.15	6.70	6.43	6.71	6.67	7.05	6.60	6.80
308.15	6.72	6.45	6.73	6.69	7.08	6.62	6.82
313.15	6.74	6.47	6.76	6.72	7.10	6.65	6.84
318.15	6.77	6.49	6.78	6.74	7.13	6.67	6.87
323.15	6.79	6.51	6.80	6.76	7.15	6.69	6.89
328.15	6.81	6.53	6.83	6.78	7.18	6.71	6.91
333.15	6.84	6.55	6.85	6.81	7.21	6.74	6.94
338.15	6.86	6.58	6.87	6.83	7.23	6.76	6.96
343.15	6.88	6.60	6.90	6.85	7.26	6.78	6.99
348.15	6.91	6.62	6.92	6.88	7.28	6.80	7.01
353.15	6.93	6.64	6.95	6.90	7.31	6.83	7.04

Table A- 42 Calculated values of molar refractions, R_M , for [C₂CN C_nim]Br and [C₂CN C_nim]Cl ILs as a function of temperature.

T/K	$R_M / (\text{cm}^3 \cdot \text{mol}^{-1})$						
	[C ₂ CN Bim]Br	[C ₂ CN Him]Br	[C ₂ CN Oim]Br	[C ₂ CN Dim]Br	[C ₂ CN Bim]Cl	[C ₂ CN Him]Cl	[C ₂ CN Oim]Cl
298.15	63.08	71.84	81.75	-	59.11	67.92	77.47
303.15	63.17	71.93	81.84	-	59.19	68.05	77.59
308.15	63.24	72.01	81.95	90.35	59.26	68.15	77.69
313.15	63.29	72.07	82.04	90.59	59.32	68.20	77.78
318.15	63.34	72.12	82.11	90.77	59.37	68.24	77.88
323.15	63.39	72.18	82.18	90.97	59.42	68.32	77.98
328.15	63.43	72.23	82.24	91.04	59.47	68.43	78.08
333.15	63.47	72.30	82.27	91.13	59.52	68.49	78.17

Table A- 43 Calculated values of molar refractions, R_M , for [C₂CN C_nim]DOSS and [C₂CN C_nim]BS ILs as a function of temperature.

T/K	$R_M / (\text{cm}^3 \cdot \text{mol}^{-1})$						
	[C ₂ CNB im]DOSS	[C ₂ CNH im]DOSS	[C ₂ CNO im]DOSS	[C ₂ CND im]DOSS	[C ₂ CB im]BS	[C ₂ CNH im]BS	[C ₂ CN Oim]BS
298.15	153.77	163.81	176.04	186.05	84.53	91.68	100.47
303.15	154.15	163.97	176.07	186.12	84.57	91.76	100.61
308.15	154.46	164.13	176.26	186.21	84.63	91.85	100.70
313.15	154.46	164.28	176.39	186.12	84.71	91.93	100.77
318.15	154.59	164.42	176.49	186.27	84.69	92.00	100.86
323.15	154.78	164.54	176.57	186.37	84.74	92.07	100.96
328.15	154.87	164.66	176.67	186.46	84.77	92.14	101.06
333.15	155.03	164.77	176.73	186.54	84.83	92.23	101.08

Table A- 44 Calculated values of molar refractions, R_M , for [C₂CN C_nim]DDS and [C₂CN C_nim]SBA ILs as a function of temperature.

T/K	$R_M / (\text{cm}^3 \cdot \text{mol}^{-1})$						
	[C ₂ CNB im]DDS	[C ₂ CNH im]DDS	[C ₂ CNO im]DDS	[C ₂ CND im]DDS	[C ₂ CB im]SBA	[C ₂ CNH im]SBA	[C ₂ CN Oim]SBA
298.15	108.83	119.72	131.34	139.86	101.39	111.84	123.21
303.15	108.81	119.77	131.33	139.93	101.47	111.96	123.31
308.15	108.84	119.82	131.37	140.07	101.51	112.10	123.37
313.15	108.82	119.88	131.36	139.99	101.53	112.22	123.45
318.15	108.82	119.96	131.40	140.20	101.56	112.28	123.48
323.15	108.78	119.96	131.36	140.21	101.61	112.37	123.63
328.15	108.80	120.01	131.43	140.27	101.66	112.48	123.74
333.15	108.81	120.04	131.39	140.24	101.65	112.55	123.83

Table A- 45 Calculated values of molar refractions, R_M , for [C₂CN C_nim]TFMS and dual functionalized ILs as a function of temperature.

T/K	$R_M / (\text{cm}^3 \cdot \text{mol}^{-1})$					
	[C ₂ CN Bim]TFMS	[C ₂ CN Him]TFMS	[C ₂ CN Oim]TFMS	[C ₂ CNAy im]DOSS	[C ₂ CBz im]DOSS	[C ₂ CNHe im]DOSS
298.15	78.07	85.48	95.85	150.85	160.28	147.70
303.15	78.19	85.57	96.00	150.83	160.11	147.68
308.15	78.28	85.62	96.11	150.82	160.09	147.63
313.15	78.36	85.68	96.22	150.82	160.06	147.63
318.15	78.43	85.76	96.35	150.80	159.95	147.62
323.15	78.50	85.83	96.43	150.74	159.89	147.62
328.15	78.57	85.91	96.51	150.72	159.88	147.61
333.15	78.54	86.00	96.62	150.64	159.83	147.60

APPENDIX B

Experimental solubility data for CO₂ in ILs

Table B- 1 Experimental solubility data for CO₂ in [C₂CN Him]DDS at 298 K

Time (min)	20bar χ	Time (min)	15bar χ	Time (min)	10bar χ	Time (min)	5bar χ	Time (min)	1bar χ
4	0.073241	5	0.054715	8	0.035213	5	0.031894	5	0.005621
13	0.195754	18	0.149135	28	0.132836	19	0.064197	16	0.010341
27	0.307323	36	0.242253	41	0.168103	33	0.085019	29	0.012783
39	0.335982	45	0.273256	54	0.204897	54	0.108054	45	0.014642
51	0.356297	62	0.311457	76	0.227840	72	0.125102	67	0.016726
69	0.379455	89	0.341903	94	0.239782	86	0.134172	74	0.017167
98	0.405862	99	0.347971	113	0.248730	108	0.143828	80	0.017599
110	0.413064	112	0.354194	135	0.251385	118	0.145919	87	0.017967
124	0.420453	120	0.356577	146	0.258040	129	0.147659	98	0.018540
133	0.423281	138	0.363968	164	0.261806	140	0.148935	102	0.018756
154	0.432054	150	0.366678	172	0.264360	157	0.150994	115	0.019306
167	0.435271	165	0.369496	194	0.265831	164	0.152411	120	0.019522
184	0.438617	183	0.371952	201	0.272691	186	0.153631	131	0.019889
204	0.441532	188	0.373099	220	0.276611	193	0.154469	137	0.020149
219	0.445385	211	0.373604	231	0.279715	210	0.156496	146	0.020424
236	0.449686	250	0.378821	241	0.281248	221	0.157782	173	0.021194
265	0.449566	251	0.378720	256	0.281259	228	0.158252	201	0.021603
279	0.448793	251	0.378069	268	0.281267	256	0.159418	222	0.021669
309	0.448793	278	0.378069	277	0.281267	267	0.159421	239	0.021672

Table B- 2 Experimental solubility data for CO₂ in [C₂CN Him]TFMS at 298 K

Time (min)	20bar χ	Time (min)	15bar χ	Time (min)	10bar χ	Time (min)	5bar χ	Time (min)	1bar χ
9	0.158209	9	0.107598	7	0.034275	6	0.020123	6	0.005770
13	0.230124	23	0.231808	17	0.118240	14	0.046665	16	0.011934
18	0.293835	35	0.310261	24	0.164486	24	0.095130	25	0.017033
33	0.403751	44	0.347533	30	0.198653	32	0.121235	38	0.022482
43	0.444068	57	0.371299	46	0.251335	51	0.159874	57	0.028593
58	0.482873	70	0.383640	61	0.288543	74	0.179132	79	0.031945
74	0.510821	78	0.389913	72	0.300388	86	0.183796	84	0.032365
90	0.528217	103	0.403562	91	0.314989	102	0.188088	102	0.033660
106	0.532280	109	0.408739	110	0.325048	113	0.190768	111	0.034100
123	0.536599	119	0.417394	118	0.327492	122	0.191632	119	0.034312
138	0.541604	128	0.423036	129	0.331344	134	0.192433	126	0.034403
155	0.546310	138	0.430119	148	0.334033	140	0.193187	137	0.034591
171	0.546896	147	0.432215	161	0.336173	152	0.194989	144	0.034852
188	0.546161	157	0.439328	166	0.337148	163	0.195342	154	0.034913
203	0.546700	181	0.451037	185	0.340078	179	0.196713	172	0.035217
211	0.546700	189	0.453287	199	0.340036	191	0.196894	183	0.035226
226	0.546700	200	0.457139	204	0.340443	203	0.196895	189	0.035255
256	0.546700	219	0.460059	212	0.340452	211	0.196896	207	0.035207
272	0.546700	233	0.460186	224	0.340453	217	0.196896	213	0.035241

Table B- 3 Experimental solubility data for CO₂ in [C₂CN Him]SBA at 298 K

Time (min)	20bar χ	Time (min)	15bar χ	Time (min)	10bar χ	Time (min)	5bar χ	Time (min)	1bar χ
11	0.142388	11	0.096838	20	0.088637	5	0.018111	8	0.007893
13	0.166612	20	0.137253	22	0.103716	9	0.032126	14	0.009179
16	0.207112	29	0.208627	26	0.128927	18	0.059984	18	0.010740
20	0.237811	37	0.253868	30	0.148037	24	0.074565	26	0.013351
23	0.264451	48	0.279235	34	0.164621	28	0.085617	31	0.015330
34	0.343375	55	0.299519	45	0.204547	31	0.095208	35	0.017047
39	0.363376	71	0.321145	57	0.226201	38	0.109112	46	0.020234
53	0.399661	80	0.330524	69	0.248789	53	0.130823	59	0.024096
72	0.434586	90	0.341440	91	0.270529	64	0.143886	67	0.025734
92	0.459739	94	0.345276	114	0.281249	82	0.156460	84	0.028153
112	0.475395	113	0.365426	138	0.292543	107	0.165416	105	0.029389
133	0.479052	136	0.376786	161	0.298210	128	0.169279	127	0.030294
173	0.487443	160	0.393807	185	0.300629	153	0.172469	149	0.030881
193	0.491679	172	0.398711	208	0.303433	175	0.173868	171	0.031132
214	0.492207	184	0.402979	232	0.306070	190	0.175490	192	0.031422
235	0.491845	196	0.408161	255	0.306398	212	0.177015	214	0.031695
254	0.492021	226	0.411206	280	0.305987	239	0.177054	236	0.031685
264	0.492028	274	0.414243	292	0.306198	248	0.177068	251	0.031699
282	0.492030	292	0.414253	299	0.306257	264	0.177096	259	0.031702

Table B- 4 Experimental solubility data for CO₂ in [C₂CN Him]BS at 298 K

Time (min)	20bar χ	Time (min)	15bar χ	Time (min)	10bar χ	Time (min)	5bar χ	Time (min)	1bar χ
5	0.060650	7	0.100837	5	0.024985	3	0.006451	6	0.006212
8	0.099919	17	0.176465	18	0.102694	6	0.009800	10	0.008784
15	0.158548	21	0.198325	27	0.131604	12	0.018850	16	0.012038
25	0.213551	27	0.226720	35	0.158898	17	0.023796	20	0.012995
29	0.227419	35	0.254735	52	0.201611	22	0.031149	24	0.014890
35	0.256774	42	0.274986	61	0.213697	31	0.047543	30	0.016679
52	0.315353	51	0.297139	65	0.218634	43	0.062321	31	0.017919
59	0.331470	64	0.312199	82	0.232602	51	0.077281	35	0.018810
79	0.358608	73	0.319454	90	0.237634	57	0.087932	41	0.020230
101	0.370683	80	0.324285	103	0.243322	66	0.101846	50	0.021470
112	0.377261	90	0.330845	112	0.245697	82	0.115482	63	0.022967
136	0.386592	102	0.337150	120	0.248684	95	0.124703	75	0.023656
158	0.394605	139	0.344317	141	0.255836	102	0.128532	88	0.024339
188	0.400599	166	0.346353	150	0.256395	123	0.132616	100	0.024803
209	0.403261	177	0.346750	179	0.259787	142	0.136756	119	0.025233
214	0.404504	192	0.346870	184	0.259036	175	0.138987	141	0.025381
225	0.407981	217	0.347502	192	0.259613	187	0.139012	163	0.025480
243	0.410572	231	0.350557	218	0.263189	203	0.139030	188	0.025619

Table B- 5 Experimental solubility data for CO₂ in [C₂CN Dim]DOSS at 298 K

Time (min)	20bar χ	Time (min)	15bar χ	Time (min)	10bar χ	Time (min)	5bar χ	Time (min)	1bar χ
6	0.193241	5	0.185929	7	0.219076	3	0.076193	4	0.022082
10	0.246207	8	0.262925	15	0.321774	6	0.107745	7	0.028135
14	0.350671	14	0.360329	19	0.364349	10	0.147660	13	0.040072
24	0.453431	17	0.388962	26	0.394079	13	0.159394	18	0.051814
28	0.501562	22	0.445669	30	0.412375	17	0.182632	25	0.057314
43	0.609963	29	0.499227	39	0.436781	23	0.204580	29	0.062333
52	0.664355	36	0.536337	45	0.449437	32	0.230714	45	0.075917
62	0.697997	54	0.607114	53	0.460718	38	0.248132	53	0.079761
80	0.740143	68	0.631874	71	0.49063	58	0.281712	69	0.084577
113	0.771535	81	0.650807	82	0.501004	70	0.290161	86	0.087119
128	0.780133	94	0.672850	98	0.513203	93	0.304226	110	0.089147
152	0.793176	128	0.691453	132	0.525303	110	0.309497	122	0.090222
161	0.798654	152	0.697560	155	0.530361	151	0.312530	138	0.091264
189	0.810104	175	0.700912	178	0.533612	174	0.312996	151	0.092100
203	0.812124	202	0.701001	200	0.539400	197	0.313567	163	0.092794
231	0.811923	229	0.701651	233	0.542940	226	0.316021	187	0.093844
246	0.813001	263	0.701090	247	0.545694	229	0.315137	199	0.094055
260	0.813028	278	0.702001	262	0.547604	250	0.315475	224	0.094448
283	0.813029	291	0.702002	281	0.547694	268	0.315421	244	0.094573

Table B- 6 Experimental solubility data for CO₂ in [C₂CN Oim]DOSS at 298 K

Time (min)	20bar χ	Time (min)	15bar χ	Time (min)	10bar χ	Time (min)	5bar χ	Time (min)	1bar χ
7	0.260965	6	0.153427	5	0.103610	7	0.066222	6	0.027670
16	0.383299	11	0.195481	8	0.137379	10	0.084373	14	0.040642
23	0.434016	19	0.278422	14	0.188207	18	0.120171	22	0.046019
33	0.520297	29	0.360010	25	0.266540	22	0.155386	31	0.055168
51	0.604161	36	0.398224	36	0.320681	27	0.171880	47	0.064060
75	0.670639	41	0.433098	46	0.359180	31	0.186932	69	0.071108
87	0.697036	61	0.510956	65	0.411206	40	0.205486	80	0.073907
105	0.719722	80	0.554503	74	0.438392	57	0.233019	96	0.076313
119	0.726724	90	0.567161	84	0.450867	75	0.244796	129	0.077997
141	0.735601	115	0.598245	98	0.467678	106	0.258213	154	0.079983
165	0.742880	128	0.604475	118	0.476989	119	0.260901	196	0.080068
183	0.750191	143	0.616470	147	0.487461	137	0.266079	202	0.080197
213	0.755134	157	0.624489	176	0.499154	150	0.269540	215	0.080339
229	0.758749	171	0.633466	190	0.501420	163	0.273415	229	0.080765
234	0.759903	199	0.646084	215	0.501563	190	0.278861	231	0.081032
249	0.761709	213	0.652037	224	0.501738	203	0.281430	242	0.081562
264	0.769224	226	0.653499	253	0.501766	229	0.283049	256	0.081563
279	0.769240	254	0.656232	263	0.501769	243	0.283241	263	0.081565
299	0.769260	278	0.657100	289	0.501769	264	0.283616	275	0.081565

Table B- 7 Experimental solubility data for CO₂ in [C₂CN Him]DOSS at 298 K

Time (min)	20bar χ	Time (min)	15bar χ	Time (min)	10bar χ	Time (min)	5bar χ	Time (min)	1bar χ
2	0.152369	4	0.089245	4	0.107561	13	0.05230	2	0.014351
4	0.202030	7	0.127325	7	0.152103	17	0.06934	4	0.019029
11	0.276776	11	0.168824	11	0.208452	26	0.09499	11	0.026069
24	0.391972	16	0.231285	15	0.225016	35	0.13453	23	0.036919
35	0.471592	29	0.323023	22	0.257821	42	0.16186	34	0.044418
45	0.528208	37	0.355480	29	0.288805	49	0.18129	44	0.049751
63	0.604717	52	0.416590	36	0.310273	60	0.20755	62	0.056957
73	0.644698	58	0.434896	40	0.325699	71	0.22127	71	0.060723
82	0.663043	63	0.443815	47	0.350288	80	0.22757	80	0.062450
96	0.687765	69	0.453565	58	0.371759	91	0.23605	94	0.064779
115	0.707787	97	0.505325	72	0.397692	96	0.24075	112	0.066069
144	0.722904	110	0.525395	87	0.409620	119	0.24604	140	0.067519
158	0.730082	132	0.546198	101	0.421444	136	0.25009	154	0.068631
172	0.734054	169	0.567218	116	0.429475	153	0.25194	168	0.069139
186	0.737386	192	0.582759	138	0.436916	170	0.25309	182	0.069453
210	0.737597	205	0.591079	163	0.439487	176	0.25316	205	0.069472
219	0.737853	227	0.596991	188	0.441198	193	0.25325	214	0.069497
247	0.737895	243	0.597769	217	0.441857	210	0.25326	241	0.069501
257	0.737899	263	0.598085	246	0.442662	227	0.25326	251	0.069501

Table B- 8 Experimental solubility data for CO₂ in [C₂CN Bim]DOSS at 298 K

Time (min)	20bar χ	Time (min)	15bar χ	Time (min)	10bar χ	Time (min)	5bar χ	Time (min)	1bar χ
3	0.171988	2	0.116130	6	0.096643	2	0.047945	3	0.012757
7	0.243210	4	0.153979	10	0.123132	4	0.063572	6	0.018040
10	0.333311	10	0.210949	15	0.175377	11	0.087092	10	0.024723
13	0.359797	23	0.298747	23	0.226769	24	0.123340	19	0.030579
20	0.412251	34	0.359430	29	0.250840	35	0.148393	25	0.034253
27	0.461794	43	0.402581	35	0.272806	45	0.166209	35	0.038629
33	0.496121	61	0.460893	41	0.299883	63	0.190283	50	0.044092
43	0.560104	70	0.491365	60	0.340065	73	0.202864	63	0.047168
53	0.594435	79	0.505347	69	0.349279	82	0.208636	88	0.049985
66	0.635902	92	0.524189	78	0.357252	96	0.216416	101	0.050938
93	0.673882	111	0.534625	110	0.377973	115	0.220724	119	0.051820
106	0.686723	138	0.546363	124	0.384182	144	0.225570	141	0.052125
126	0.698621	152	0.555363	138	0.390930	158	0.229286	163	0.052328
149	0.702731	165	0.559468	142	0.394920	172	0.230981	188	0.052406
172	0.705468	179	0.562008	156	0.400095	186	0.232029	214	0.052502
198	0.706520	201	0.562169	183	0.408960	210	0.232096	239	0.052963
251	0.711288	210	0.562365	197	0.410030	219	0.232177	245	0.052912
258	0.711588	237	0.562396	224	0.412157	247	0.232190	259	0.052811
285	0.711988	247	0.562399	252	0.412378	257	0.232191	271	0.052811

Table B- 9 Experimental solubility data for CO₂ in [C₂CN Heim]DOSS at 298 K

Time (min)	20bar χ	Time (min)	15bar χ	Time (min)	10bar χ	Time (min)	5bar χ	Time (min)	1bar χ
8	0.183413	9	0.138709	14	0.098934	8	0.079037	12	0.014203
14	0.251235	14	0.163531	17	0.118700	13	0.096561	17	0.022488
20	0.332891	20	0.196599	22	0.150224	16	0.111522	24	0.031631
26	0.386878	25	0.233109	33	0.206681	21	0.126679	34	0.036775
33	0.424511	30	0.267613	47	0.254827	26	0.134394	44	0.039643
44	0.491260	44	0.337022	76	0.329209	36	0.154291	69	0.043931
52	0.530495	47	0.360841	86	0.345566	41	0.165155	79	0.045204
70	0.590436	61	0.395547	100	0.368513	50	0.176150	89	0.047978
101	0.650556	77	0.435465	122	0.396719	82	0.201706	109	0.053972
115	0.662181	81	0.437942	132	0.409217	94	0.214949	119	0.055580
154	0.687790	106	0.488273	142	0.418268	110	0.230585	128	0.059162
160	0.692586	117	0.496908	152	0.425853	120	0.239255	138	0.059989
165	0.697681	127	0.507289	157	0.427279	130	0.246963	148	0.062388
176	0.700305	147	0.531056	162	0.434193	140	0.252967	158	0.063593
192	0.705723	168	0.553468	183	0.446776	160	0.272876	178	0.064813
202	0.706290	183	0.564220	193	0.451533	174	0.279037	193	0.067069
213	0.708722	193	0.567697	214	0.458052	194	0.292003	203	0.067486
224	0.712493	214	0.581914	234	0.458633	214	0.300995	213	0.067523
256	0.714903	250	0.591195	259	0.458757	244	0.302025	237	0.067656

Table B- 10 Experimental solubility data for CO₂ in [C₂CN Bzim]DOSS at 298 K

Time (min)	20bar χ	Time (min)	15bar χ	Time (min)	10bar χ	Time (min)	5bar χ	Time (min)	1bar χ
2	0.0582918	4	0.0699501	2	0.051085	3	0.0563505	5	0.0133592
9	0.1716205	11	0.1716205	9	0.1150136	9	0.1092067	16	0.0242428
16	0.2437664	14	0.2059446	13	0.1326713	11	0.1178847	25	0.0313468
24	0.310802	20	0.2437664	17	0.1543689	23	0.1513032	35	0.0377107
29	0.3579059	24	0.2584044	21	0.1674127	28	0.1625503	42	0.0414536
41	0.4494441	30	0.2925197	24	0.1784761	31	0.1706316	53	0.04449
57	0.508464	42	0.3579059	39	0.2219584	45	0.1947622	69	0.0482817
65	0.5319794	46	0.3729625	41	0.2300272	56	0.2083485	78	0.0493839
72	0.5516975	55	0.4010449	50	0.2534251	67	0.2145973	90	0.0510804
80	0.5680292	63	0.4239668	61	0.273779	79	0.2207921	100	0.0520905
96	0.5916238	79	0.4644686	77	0.3103871	107	0.2288978	120	0.0534954
104	0.6004788	87	0.4795956	85	0.3239352	126	0.2302443	124	0.0536774
124	0.6182291	111	0.4954721	108	0.3542997	146	0.231141	136	0.0543755
131	0.6231706	120	0.5018474	116	0.3654477	191	0.2319078	160	0.0556079
155	0.6343894	152	0.5248086	148	0.399555	214	0.2339465	172	0.0562559
171	0.6396792	168	0.5382049	163	0.4103642	219	0.233723	184	0.0567742
186	0.6419988	185	0.5503976	179	0.4183778	222	0.233069	196	0.0569016
202	0.6454921	201	0.5560316	195	0.4199801	232	0.2333672	208	0.0571009
245	0.6495566	242	0.5607565	227	0.420092	242	0.2333193	220	0.0571395

Table B- 11 Experimental solubility data for CO₂ in [C₂CN Ayim]DOSS at 298 K

Time (min)	20bar χ	Time (min)	15bar χ	Time (min)	10bar χ	Time (min)	5bar χ	Time (min)	1bar χ
5	0.129451	6	0.158870	4	0.096166	6	0.053182	3	0.012294
16	0.238920	14	0.233345	21	0.186579	12	0.093069	6	0.017385
19	0.298562	18	0.250982	29	0.216189	19	0.100032	9	0.023826
24	0.341726	20	0.264220	39	0.251427	23	0.119574	12	0.025719
36	0.408539	29	0.316746	55	0.287845	38	0.145030	19	0.029469
45	0.437813	38	0.343891	64	0.301182	42	0.149036	25	0.033010
52	0.463279	44	0.367801	71	0.315608	58	0.164656	31	0.035464
68	0.490100	65	0.408271	100	0.333893	81	0.174490	34	0.037227
84	0.508190	75	0.424342	125	0.341224	93	0.177815	40	0.040037
93	0.516328	81	0.429252	141	0.346249	104	0.179901	49	0.042491
108	0.524354	90	0.438152	149	0.349409	109	0.180896	62	0.045456
121	0.532721	121	0.447819	161	0.350995	153	0.182669	74	0.046819
133	0.539863	154	0.450351	175	0.351001	166	0.182779	86	0.048170
137	0.542172	183	0.459711	182	0.351096	174	0.182942	98	0.049088
154	0.547839	201	0.460345	188	0.351189	189	0.183109	117	0.049939
161	0.554327	213	0.467040	190	0.351218	197	0.183275	138	0.050233
185	0.559528	226	0.468296	214	0.351238	220	0.183985	160	0.050428
201	0.561097	231	0.468297	217	0.351239	225	0.184099	185	0.050504
209	0.562747	239	0.468298	223	0.351240	228	0.184193	209	0.050596

Table B- 12 Experimental solubility data for CO₂ in [P_{8,8,8,14}]DOSS at 298 K

Time (min)	20bar χ	Time (min)	15bar χ	Time (min)	10bar χ	Time (min)	5bar χ	Time (min)	1bar χ
4	0.165441	10	0.153871	3	0.095113	8	0.068804	14	0.011998
7	0.233952	16	0.186353	6	0.105990	13	0.084059	19	0.018996
16	0.346101	27	0.245311	12	0.162366	21	0.110277	39	0.031065
27	0.444216	39	0.325218	24	0.263036	31	0.124929	67	0.036304
32	0.477236	43	0.343702	30	0.302618	36	0.134314	78	0.037109
35	0.500962	51	0.380841	35	0.334239	41	0.143771	89	0.038185
41	0.538784	60	0.419555	41	0.356824	51	0.153342	101	0.040528
51	0.571808	87	0.475379	72	0.430618	81	0.175590	112	0.043546
63	0.611697	104	0.498247	84	0.443048	91	0.187118	123	0.045592
76	0.630043	115	0.508827	96	0.451491	101	0.193640	134	0.046950
88	0.648230	137	0.523073	135	0.462016	131	0.214987	146	0.049976
101	0.660583	148	0.533006	156	0.463815	141	0.220214	157	0.050674
120	0.672028	159	0.543106	180	0.464507	151	0.230081	168	0.052700
142	0.676255	170	0.556422	204	0.465354	177	0.242908	179	0.053719
164	0.676425	181	0.567535	228	0.469445	187	0.249156	202	0.054749
189	0.676590	198	0.576422	234	0.468996	207	0.259214	219	0.056654
214	0.680865	231	0.589138	237	0.467684	227	0.262191	230	0.057007
246	0.684268	253	0.591088	248	0.468282	237	0.262576	241	0.057038
260	0.685150	270	0.593220	258	0.468186	247	0.262920	269	0.057151

Table B- 13 Experimental solubility data for CO₂ in [P_{6,6,6,14}]DOSS at 298 K

Time (min)	20bar χ	Time (min)	15bar χ	Time (min)	10bar χ	Time (min)	5bar χ	Time (min)	1bar χ
10	0.156658	7	0.123071	4	0.051406	6	0.052585	5	0.011421
15	0.191392	12	0.174036	7	0.097342	9	0.066998	9	0.014551
25	0.251088	19	0.238510	14	0.151349	23	0.123388	26	0.026799
27	0.266380	23	0.257463	15	0.158251	28	0.136485	32	0.029643
37	0.337972	28	0.294999	22	0.189901	41	0.165983	43	0.035439
42	0.380051	35	0.330450	27	0.214973	50	0.180784	54	0.038035
52	0.422133	37	0.355014	35	0.238991	59	0.189939	62	0.040187
73	0.485340	41	0.372664	47	0.294728	78	0.201408	80	0.042219
93	0.530707	48	0.400799	64	0.330923	96	0.207461	92	0.043669
103	0.535994	59	0.425366	79	0.352455	110	0.209950	102	0.044532
134	0.559595	74	0.455039	83	0.355471	123	0.212290	113	0.044996
144	0.562528	89	0.468686	91	0.360622	147	0.215839	127	0.045889
165	0.573715	103	0.482216	111	0.378081	155	0.217330	139	0.046486
180	0.578609	118	0.491405	136	0.385410	169	0.219323	151	0.047154
190	0.585492	140	0.499919	160	0.395674	196	0.223068	176	0.048094
200	0.591645	166	0.502860	168	0.397553	210	0.223475	188	0.048537
211	0.595432	192	0.504818	185	0.404487	224	0.223977	200	0.048645
231	0.596978	221	0.507572	201	0.408628	237	0.224761	212	0.048816
251	0.598637	251	0.509305	235	0.412096	251	0.224913	225	0.048849

Table B- 14 Experimental solubility data for CO₂ in [P_{8,8,8}C₆P_{8,8,8}]DOSS₂ at 298 K

Time (min)	20bar χ	Time (min)	15bar χ	Time (min)	10bar χ	Time (min)	5bar χ	Time (min)	1bar χ
9	0.142640	10	0.107073	14	0.073443	8	0.055034	12	0.009598
14	0.195385	16	0.126234	17	0.088116	13	0.067235	18	0.015197
29	0.300874	27	0.179943	34	0.153429	21	0.098821	35	0.024852
41	0.356426	41	0.243325	62	0.223395	31	0.124100	61	0.029044
48	0.382052	47	0.260156	72	0.244386	36	0.132074	71	0.029688
77	0.459181	62	0.306792	95	0.273564	50	0.147227	92	0.032423
91	0.483699	71	0.329358	109	0.284109	60	0.152831	102	0.034837
111	0.505936	79	0.343241	120	0.291098	70	0.158371	112	0.036474
127	0.514976	87	0.352784	125	0.294502	80	0.162404	122	0.037560
151	0.525789	104	0.376157	136	0.303780	90	0.166497	133	0.039981
170	0.534893	111	0.386493	141	0.309511	100	0.169549	143	0.040539
182	0.542585	137	0.412844	157	0.316130	120	0.178666	153	0.042160
200	0.547130	148	0.420797	162	0.317188	130	0.181720	163	0.042975
211	0.548839	170	0.429677	178	0.328103	150	0.192840	173	0.043124
223	0.549280	181	0.435572	189	0.331662	160	0.196000	184	0.043799
235	0.551172	208	0.449126	210	0.335530	184	0.201898	199	0.045324
247	0.554104	230	0.452140	220	0.340032	204	0.207335	209	0.045606
270	0.555914	252	0.453660	241	0.340464	214	0.209582	230	0.045692
282	0.556110	269	0.456359	252	0.340545	234	0.210024	245	0.045721

Table B- 15 Experimental solubility data for CO₂ in [P_{8,8,8}C₁₀P_{8,8,8}]DOSS₂ at 298 K

Time (min)	20bar χ	Time (min)	15bar χ	Time (min)	10bar χ	Time (min)	5bar χ	Time (min)	1bar χ
6	0.091193	7	0.052814	2	0.038969	3	0.043964	5	0.010153
18	0.216488	16	0.129577	9	0.087736	8	0.085202	16	0.018424
30	0.309641	22	0.162584	16	0.109652	16	0.105381	31	0.026352
43	0.376562	27	0.195100	21	0.127707	26	0.126820	42	0.031505
52	0.410141	32	0.220858	25	0.136147	29	0.133125	53	0.033812
71	0.442632	46	0.270226	40	0.169316	42	0.151951	69	0.036694
80	0.456929	51	0.281594	43	0.175471	53	0.162551	78	0.037532
113	0.476309	68	0.320103	63	0.208846	74	0.172259	100	0.039589
128	0.481617	83	0.350683	80	0.236772	85	0.175542	111	0.040001
142	0.487423	106	0.365203	96	0.254840	100	0.178583	120	0.040656
152	0.489669	118	0.370495	104	0.265625	119	0.179634	124	0.040795
161	0.493051	127	0.376888	113	0.270270	137	0.180333	136	0.041325
175	0.497573	158	0.386174	129	0.287236	158	0.180602	148	0.041919
189	0.501317	168	0.391460	145	0.299170	180	0.180931	160	0.042262
203	0.506069	179	0.399205	162	0.307873	201	0.182522	172	0.042755
217	0.506993	199	0.409604	194	0.319473	206	0.182348	184	0.043148
231	0.508131	209	0.413519	203	0.320373	209	0.181837	196	0.043245
246	0.509911	239	0.420434	223	0.320454	218	0.182070	208	0.043397
260	0.510255	259	0.420486	236	0.320458	228	0.182033	220	0.043426

Table B- 16 Fitting parameters of equation 5-7

Coefficient	ILs		
	[C ₂ CN Dim]DOSS	[C ₂ CN Heim]DOSS	[P _{8,8,8,14}]DOSS
<i>A</i>	8.15	-2.09	-0.45
<i>B</i>	-1474	5024	5024
<i>C</i>	-10601	-1034151	-923067

Table B- 17 Experimental solubility data for CH₄ in [C₂ CN Dim]DOSS at 298 K

Time (min)	20bar χ	Time (min)	15bar χ	Time (min)	10bar χ	Time (min)	5bar χ	Time (min)	1bar χ
12	0.000365	8	0.000389	7	0.000265	11	0.073443	9	0.055034
19	0.000517	10	0.000456	12	0.000374	16	0.088116	12	0.067235
29	0.000786	15	0.000566	19	0.000513	23	0.111518	15	0.077652
39	0.000956	18	0.000650	21	0.000554	35	0.153429	20	0.098821
49	0.001051	20	0.000723	26	0.000635	47	0.189169	27	0.110936
56	0.001128	29	0.000939	32	0.000711	61	0.223395	30	0.124100
70	0.001209	34	0.000993	38	0.000764	72	0.244386	43	0.140150
81	0.001245	42	0.001093	40	0.000802	80	0.256530	51	0.147227
89	0.001286	57	0.001188	49	0.000862	97	0.273564	62	0.152831
92	0.001300	71	0.001257	59	0.000915	110	0.284109	82	0.162404
110	0.001376	88	0.001300	73	0.000979	121	0.291098	91	0.166497
135	0.001419	105	0.001310	90	0.001008	137	0.303780	103	0.169549
150	0.001459	121	0.001320	101	0.001037	146	0.310499	110	0.176056
161	0.001483	135	0.001333	119	0.001057	158	0.316130	129	0.181720
172	0.001501	157	0.001341	138	0.001075	179	0.328103	152	0.192840
185	0.001517	170	0.001343	166	0.001082	188	0.331662	160	0.196000
197	0.001537	188	0.001344	193	0.001086	197	0.335194	175	0.198429
228	0.001548	204	0.001344	207	0.001089	211	0.335530	184	0.201898
252	0.001549	213	0.001344	223	0.001092	229	0.340295	192	0.204332
271	0.001551	227	0.001345	239	0.001094	241	0.340464	203	0.207335
293	0.001554	253	0.001345	254	0.001096	253	0.340545	223	0.209716
301	0.001559	271	0.001345	266	0.001097	265	0.340556	242	0.210299
313	0.001560	290	0.001345	279	0.001099	274	0.340560	257	0.210662